Studies of spacetimes with spatial topologies $\mathbb{S}^3$ and $\mathbb{S}^1 \times \mathbb{S}^2$

Leon Escobar

a thesis submitted for the degree of

Doctor of Philosophy

at the University of Otago, Dunedin,

New Zealand.

December 23, 2015

Abstract

The purpose of this work is to introduce a new analytical and numerical approach to the treatment of the initial value problem for the vacuum Einstein field equations on spacetimes with spatial topologies $\mathbb{S}^3$ or $\mathbb{S}^1 \times \mathbb{S}^2$ and symmetry groups $\mathrm{U}(1)$ or $\mathrm{U}(1) \times \mathrm{U}(1)$. The general idea consists of taking advantage of the action of the symmetry group $\mathrm{U}(1)$ to rewrite those spacetimes as a principal fiber bundle, which is trivial for $\mathbb{S}^1 \times \mathbb{S}^2$ but not for $\mathbb{S}^3$. Thus, the initial value problem in four dimensions can be reduced to a three-dimensional initial value problem for a certain manifold with spatial topology $\mathbb{S}^2$. Furthermore, following the approach presented by Beyer et al. in [30], we avoid coordinate representations that suffer from coordinate singularities for $\mathbb{S}^2$ by expressing all the fields in terms of the spin-weighted spherical harmonics.

We use the generalized wave map formalism to reduce the vacuum Einstein field equations on a manifold with three spatial dimensions to a system of quasilinear wave equations in terms of generalized gauge source functions with well-defined spin-weights. As a result, thanks to the fully tensorial character of these equations, the system of evolution equations can be solved numerically using a $2+1$-pseudo-spectral approach based on a spin-weighted spherical harmonic transform [112]. In this work, however, we apply our infrastructure to the study of Gowdy symmetric spacetimes, where thanks to the symmetry group $\mathrm{U}(1) \times \mathrm{U}(1)$, the system of hyperbolic equations obtained from the vacuum Einstein field equations can be reduced to a $1+1$-system of partial differential equations. Therefore, we introduce an axial symmetric spin-weighted transform that provides an efficient treatment of axially symmetric functions in $\mathbb{S}^2$ by reducing the complexity of the general transform.

To analyse the consistency, accuracy, and feasibility of our numerical infrastructure, we reproduce an inhomogeneous cosmological solution of the vacuum Einstein field equations with spatial topology $\mathbb{S}^3$. In addition, we consider two applications of our infrastructure. In the first one, we numerically explore the behaviour of Gowdy $\mathbb{S}^1 \times \mathbb{S}^2$ spacetimes using our infrastructure. In particular, motivated by the works of Garfinkle [90] and Ståhl [183], we study the behaviour of some geometrical quantities to investigate the behaviour of those spacetimes when approach a future singularity. As a second application, we conduct a systematic investigation based on the previous research of Beyer [27, 28] on the non-linear instability of the Nariai spacetime and the asymptotic behaviour of its perturbations.

Acknowledgements

This thesis not only represents a lot of hours of work and cups of coffee, but also the culmination of a dream that began more than ten years ago. However, this would not have been possible without the help of many wonderful people who I want to devote a few words.

I want to begin by thanking to my family. Especially to my mother, my father and my dear nephew Juan Manuel, who was a child when I left him and he is now a teenager, for understanding that I had to be away from them for following my path. Also I want to thank to my dear cousin Diana who, since we were teenagers, has always offered me her valuable friendship and wise advice. Lastly, but the most important, I want to thank to my Canelita for always being at my side, not only during my PhD but also during my undergraduate and Master studies. Certainly, she is the reason that makes possible that I can take out all the courage, strength and determination that there are in my heart for following my dreams.

I want to express my sincere gratitude to all members of my beloved Department of Mathematics and Statistics at the University of Otago. In particular, I want to thank to Prof. Jöerg Frauendiener for being a great and wise leader who always promotes a nice and friendly atmosphere in the relativity group, which I had the honour of being part. Also I want to thank to my office mate and "relativity buddy" Chris Stevens, for all the interesting discussions (not always about science) and for his patience to help me to improve my English.

Finally, I want to give special thanks to my supervisor Dr. Florian Beyer. Thanks for give me the opportunity to be your student. Thanks for your endless kindness and patience to answer all my questions. Thanks for always encourage me to go beyond my limits. Thanks for your sincere friendship and for always believe in me, even when I was hesitant to do so. And lastly, thanks for not just being my supervisor, but also the older brother that I never had.

Contents

1 Introduction **1**

I Preliminaries **7**

2 Approach to the Einstein field equations **9**
2.1 The Einstein field equations . . . 10
2.2 Formulation of the Cauchy problem . . . 10
2.2.1 Cauchy surfaces . . . 10
2.2.2 The Cauchy problem . . . 11
2.3 Hyperbolicity and well-posedness . . . 12
2.4 Some formulations for the numerical solution of the EFE . . . 13
2.5 The idea of the generalized wave map formalism . . . 14
2.5.1 The general setting . . . 14
2.5.2 Constraint damping terms . . . 15
2.5.3 Gauge drivers . . . 16

3 Cosmological spacetimes **19**
3.1 Generalities on cosmological spacetimes . . . 19
3.2 Some fundamental issues for cosmological spacetimes . . . 21
3.2.1 The cosmic censorship conjecture . . . 21
3.2.2 The BKL-conjecture . . . 22
3.2.3 The cosmic no-hair conjecture . . . 22
3.3 Gowdy spacetimes . . . 23
3.3.1 General metric with group of motion $\mathrm{U}(1) \times \mathrm{U}(1)$ . . . 23
3.3.2 The case $\mathbb{T}^3$ . . . 24
3.3.3 The cases $\mathbb{S}^1 \times \mathbb{S}^2$ and $\mathbb{S}^3$ . . . 25

4 Symmetry reduction **27**
4.1 The space of orbits . . . 27
4.2 Induced tensor fields in S . . . 29
4.3 Relation between the geometry of M and S . . . 30
4.4 Geroch-Einstein system . . . 31
4.5 Reconstruction of the four-dimensional Kretschmann scalar . . . 33
4.6 Reconstruction of the four-dimensional metric . . . 33

5 Generalities of the manifold $\mathbb{S}^2$ **35**
5.1 Smooth frame on $\mathbb{S}^3$ . . . 35
5.2 Construction of a frame for $\mathbb{S}^2$ . . . 37
5.3 The spin-weighted spherical harmonics . . . 38
5.3.1 Wigner d-functions . . . 39
5.3.2 The spin-weighted spherical harmonics . . . 39
5.4 Tensor components in $\mathbb{S}^2$ . . . 42

II Analytical and numerical infrastructure **43**

6 U(1)-symmetric spacetimes with spatial topologies $\mathbb{S}^3$ or $\mathbb{S}^1 \times \mathbb{S}^2$ **45**
6.1 The symmetry reduction for U(1)-symmetric spacetimes . . . 45
6.2 Equations for the cases with spatial topology $\mathbb{S}^3$ or $\mathbb{S}^1 \times \mathbb{S}^2$ . . . 46
6.3 Evolution equations . . . 47
6.3.1 The wave map gauge . . . 48
6.3.2 The covariant generalized wave gauge in the case $\mathbb{R} \times \mathbb{S}^2$ . . . 50
6.4 Constraint equations . . . 51
6.4.1 Equivalence between the ADM and GWF constraints . . . 51
6.4.2 York-Lichnerowicz conformal decomposition on $\mathbb{S}^2$ . . . 53
6.4.3 Choosing initial data . . . 55
6.5 Reconstruction of the four-dimensional metric . . . 56

7 The pseudo-spectral implementation **57**
7.1 Method of lines . . . 57
7.2 Time integrator and convergence test . . . 58
7.3 The discrete Fourier transform . . . 59
7.4 Implementation of the spin-weighted transforms . . . 60
7.4.1 General description of the HWTs . . . 60
7.4.2 Axially symmetric spin-weighted transforms . . . 61
7.5 Choosing the optimal grid . . . 66
7.6 Code implementation of the AST . . . 67

III Applications to Gowdy spacetimes and their analysis **71**

8 Testing our implementation on a Gowdy spacetime $\mathbb{R} \times \mathbb{S}^3$ **73**
8.1 The class of smooth Gowdy symmetry generalized Taub-NUT solutions . . . 73
8.2 The family of exact solutions . . . 74
8.3 Choice of the gauge and initial data . . . 75
8.4 Possible numerical error sources . . . 76
8.5 Numerical evolutions in areal gauge . . . 77
8.6 Numerical evolutions in wave gauge . . . 80

9 Numerical studies of Gowdy spacetimes $\mathbb{R} \times \mathbb{S}^1 \times \mathbb{S}^2$ **83**
9.1 The general metric $\mathbb{S}^1 \times \mathbb{S}^2$ in areal gauge . . . 83
9.2 Symmetry reduction and choice of initial data . . . 84
9.3 Using a gauge driver . . . 85
9.4 Numerical studies . . . 86
9.4.1 Collapsing behaviour of the factors $\mathbb{S}^1$ and $\mathbb{S}^2$ . . . 86

9.4.2 Behaviour of the Kretschmann scalar . . . 87

10 Studies of Gowdy perturbations of the Nariai spacetime 89
10.1 The Nariai spacetime . . . 89
10.2 Perturbations . . . 90
10.3 Setting the Nariai gauge . . . 91
10.4 Construction of initial data . . . 93
10.4.1 Analytical initial data . . . 93
10.4.2 Numerical initial data . . . 94
10.5 Setting a stable evolution . . . 97
10.5.1 Evolution variables . . . 97
10.5.2 Constraint damping terms . . . 97
10.6 Perturbations of the Nariai spacetime . . . 99
10.6.1 Homogeneous perturbations . . . 99
10.6.2 Inhomogeneous perturbations . . . 101
10.7 Studies of the asymptotic behaviour . . . 105
10.7.1 Collapsing case . . . 105
10.7.2 Expanding case . . . 106

11 Discussion and future projects 111
11.1 Discussion of the analytical infrastructure . . . 111
11.2 Discussion of the numerical infrastructure . . . 112
11.3 Discussion of the applications . . . 113
11.4 Future projects . . . 115

Appendix A Tools of differential geometry 121
A.1 Differentiable manifolds . . . 121
A.2 Tensors, notation and conventions . . . 122
A.3 The metric tensor and the connection coefficients . . . 123
A.4 The Riemann and Ricci tensors . . . 124
A.5 Lie derivative and isometries . . . 124
A.6 Lie groups, Lie algebras and fiber bundles . . . 125

Bibliography 128

Chapter 1

Introduction

Motivation of this work

For thousands of years, astronomers have struggled with basic questions about the size and age of the universe. At the beginning of the twentieth century, the astronomer Edwin Hubble made a critical discovery that soon led to reasonable answers to these questions. Those measurements marked the first evidence that our universe is expanding. This discovery caused a profound revolution in our view of the universe, and understanding the source of its expansion is arguably the most dominant question in cosmology today [176].

In recent years, the standard cosmological model that emerges as a particular solution of the Einstein field equations has dramatically improved our understanding of the universe. It is built on several fundamental assumptions and principles; among them the so-called *cosmological principle* is particularly important. It states that our current universe is *homogeneous* and *isotropic*, that is, there is neither a preferred place nor direction, at least approximately on large scales. Although this model has been successful in explaining the majority of the current observations, such as the current expansion of the universe and the spectrum of the *cosmic microwave background* [121], it lacks of a fundamental justification. In fact, the theory of quantum mechanics [137] states that the early universe (just after the universe was born in the big bang) should have been extremely inhomogeneous and anisotropic due to quantum fluctuations that yield the creation of the fundamental particles and eventually to the formation of different kinds of matter distributions such as galaxies, stars or planets. Hence, fundamental questions arise about how such primordial inhomogeneities evolved and why they are essentially absent in the present universe on large scales that any consistent cosmological model must be able to answer.

One way to address this puzzle is by the assumption of an extremely short, but particularly violent, phase of expansion just after the big bang, called *inflation*. The basic idea is that during this phase initial inhomogeneities are effectively smoothed out, and from the point of view of any local observer, the universe rapidly becomes essentially homogeneous and isotropic. However, there is theoretical evidence [48, 100] that some assumptions of this model lead to significant drawbacks as important phenomena are ignored. In fact, it is conceivable that some inhomogeneities caused by quantum fluctuations would trigger the formation of primordial black holes [55] during the evolution of the universe. Therefore, if such phenomenon was better understood and taken into account, then we could obtain more general and realistic cosmological models.

In recent decades, there have been significant advances in this direction with a major interest in cosmological models with spherical topologies, that is, with spatial topology given by $\mathbb{S}^3$ or $\mathbb{S}^1 \times \mathbb{S}^2$. Some of the most relevant are the spherical Friedman-Robertson-Walker

models, Kottler-Schwarzschild-de Sitter models, the Bianchi IX and the Kantowski-Sachs models just to mention a few (for an extended list see [101, 184]). With the exception of a few particular cases, in general it is difficult to treat those spherical manifolds from both the numerical and analytic point of view. The main difficulty lies in the fact that the complete geometry of those manifolds cannot be covered by a single regular coordinate patch, and any coordinate description of a tensorial quantity inevitably breaks down somewhere. This problem is known in the literature as the *pole problem* because in standard polar coordinates for $\mathbb{S}^2$, these coordinate singularities appear at the poles. There are several approaches to deal with this issue (see for instance [26, 90] and references therein). Recently, Beyer et al. [29, 30] introduced a pseudo-spectral method to solve the initial value problem for fields in $\mathbb{S}^2$ as background. In particular, they have considered the $2+1$-Maxwell and $2+1$-Dirac equations as test applications. The crucial point consists in expressing the fields in terms of *spin-weighted spherical harmonics* which are a generalization of the well-known spherical harmonic (see for instance [148]) and form a complete basis for any function in $\mathbb{S}^2$. Mathematical concepts such as *spin-weight*, *eth-operators* and spin-weighted spherical harmonics will be discussed in detail in chapter 5.

In the context of general relativity, the $\mathbb{S}^2$ topology arises from studies of the Einstein field equations in several situations. For example, in the asymptotically flat setting, this topology emerges when the spatial manifold is written as the product $\mathbb{R}\times\mathbb{S}^2$ for addressing the spherical character of the far zone of the radiation field coming from an isolated source. On the other hand, in the cosmological setting the topology $\mathbb{S}^2$ arises when the original manifold has been reduced in accordance with the symmetry reduction procedure that will be explained in chapter 4. Examples of this procedure can be found in the work of Moncrief in [136] as well as in [32, 33]. Therefore, the main motivation for this work is to apply a similar analytic formalism and numerical infrastructure for dealing with tensor fields in $\mathbb{S}^2$ to the more complicated situation of the Einstein field equations.

Analytic approach to U(1)-symmetric spacetimes

The general idea of our approach consists of imposing the action of the symmetry group U(1) on spacetimes with spherical topology in order to write them as a principal fiber bundle that is trivial for $\mathbb{S}^1\times\mathbb{S}^2$, but not for $\mathbb{S}^3$. In order to take full advantage of the symmetry group action, the original four-dimensional problem can be reduced to a three-dimensional one by applying a symmetry reduction. In particular, it is known that the vacuum Einstein field equations with cosmological constant can be reduced to an equivalent system of equations in terms of a three-dimensional Lorentzian manifold coupled with two scalar fields. In fact, in chapter 6, we shall demonstrate that after the symmetry reduction procedure we end up with a three-dimensional manifold with topology $\mathbb{R}\times\mathbb{S}^2$. To our knowledge, this procedure was first performed for the vacuum case by Geroch in [92]. Later, this idea was implemented by Maeda et al. [131] in the context of the standard $3+1$-decomposition, making the problem suitable for numerical simulations. Nakamura et al. [140] extended the reduction to include general matter sources and to consider the case of a perfect fluid. Choptuik et al. [58] added a massless scalar field source without rotation, and later on a more general analysis including arbitrary sources and rotation was carried out by Rinne et al. [167, 168]. In this work we will restrict ourselves to the vacuum case because it displays many of the complicated and fundamental features that we want to address. However, we emphasize that our approach could be extended to the matter case. This will be done in a future project (see section 11.4).

The formulation of the initial value problem on the three-dimensional manifold with topology $\mathbb{R}\times\mathbb{S}^2$ is carried out by implementing the *generalized wave map formalism* [87],

which can be understood as a covariant version of the more familiar *generalized harmonic formalism*. To our knowledge, this formalism was first introduced by Friedrich [87] in order to generalize the original harmonic gauge considered in the pioneering work of Bruhat [79] on the proof of well-posedness of the initial value problem in general relativity. This formulation has gained considerable attention in the last decade due to the success of Pretorius [150] to perform (to my knowledge) the first binary black holes merging simulation by using this formulation. One of the reasons for his success consisted in the introduction of *constraint damping terms* into the evolution equations which, as will be discussed in section 2.5.2, enforce the decay of the numerical violation of the constraints along the evolution. This formulation, which evolves the spacetime metric directly, is considered nowadays as one of the most attractive methods for the numerical treatment of the initial value problem in general relativity. For this reason, we have decided to implement it for our numerical infrastructure. Using this approach, we will reduce the Einstein field equations to a coupled system of quasilinear wave equations for the metric components and constraints. The coordinates will be determined dynamically by means of the well-known gauge source functions. Even though these functions are in principle arbitrary, we shall demonstrate that due to the complexity of the topology of $\mathbb{S}^2$, they have to be chosen in such way that they satisfy certain conditions in order to be consistent with the generalized wave map formalism. To our knowledge, we are the first to combine the generalized wave map formalism with the spin-weight formalism and hence the first to show that this leads to completely regular evolution equations (no singular terms at the poles). We will devote chapter 6 to this issue.

Numerical approach

The numerical approach is based on the method of lines. Our choice for conducting the temporal discretization is the well-known Runge-Kutta-Fehlberg method. Spatial derivatives are calculated using the eth-operators [148] and the spin-weighted spherical harmonics transforms (forward and backward), which are obtained from the algorithm introduced by Huffenberger and Wandelt in [112] similarly as was used in [30]. As we will explain in chapter 7, the underlying functional transform is two-dimensional since it represents functions defined on the two-dimensional manifold $\mathbb{S}^2$ (in fact, a two-dimensional Fourier transform performs the basic work of this transform).

As a result, we will end up with pseudo-spectral $2+1$-infrastructure for solving the Einstein field equations for spacetimes with spatial topology $\mathbb{S}^3$ and $\mathbb{S}^1 \times \mathbb{S}^2$ and symmetry group U(1). However, in this thesis, we will restrict to use our numerical and analytical infrastructure to study a subclass of these spacetimes, namely *Gowdy symmetric spacetimes*. As will be summarized in chapter 3, the understanding of these scenarios constitute an active and rich area of investigation in both mathematical and numerical relativity; therefore, we believe that it is the perfect arena for beginning to apply our infrastructure. In Gowdy symmetric spacetimes, whose symmetry group is $\mathrm{U}(1) \times \mathrm{U}(1)$, there exist coordinates such that the Einstein field equations can be reduced to a $1+1$-system of partial differential equations due to all the fields in $\mathbb{S}^2$ will be invariant under rotations around an axis (when we consider $\mathbb{S}^2$ as the standard sub-manifold in $\mathbb{R}^3$), and will not depend on the azimuthal angle φ in standard polar coordinates. For treating such functions, that we will call from now on as *axial symmetric*, the two-dimensional transform is inefficient. Therefore, in this work we present a new efficient implementation of a one-dimensional variant of this transform which applies to axial symmetric functions in $\mathbb{S}^2$. The complexity $\mathcal{O}(L^3)$ of the general algorithm of Huffenberger and Wandelt is thereby reduced to the complexity $\mathcal{O}(L^2)$, where L is the band limit of the functions on $\mathbb{S}^2$ in terms of the spin-weighted spherical harmonics. Thus,

clearly, using this transform, which will be called *axially symmetric spin-weighted transform*, will allow us to optimize the pseudo-spectral implementation for the treatment of Gowdy spacetimes. We dedicate chapter 7.4.2 to explain the details of this new algorithm.

Applications to Gowdy symmetric spacetimes

As we previously mentioned, using our approach we can reduce the Einstein field equations into a coupled system of quasi-linear wave equations for the independent coordinate components of the metric. In this formalism, the coordinates are determined dynamically by means of the mentioned gauge source functions which, owing to the complexity of the $\mathbb{S}^2$ topology, have to be chosen such that it allows to treat $\mathbb{S}^2$ with a single polar coordinate chart. Thus, we obtain fully regular evolution and constraint equations where all singular terms induced by the singular coordinate chart are accounted for explicitly. This regularization has also been observed to work for the simpler equations considered in [29, 30], but we show here for first time that this also applies to the full Einstein field equations. This is discussed in detail in chapter 6. In addition, we carry out a judicious test of our numerical approach by reproducing a family of exact inhomogeneous solutions with spatial topology $\mathbb{S}^3$ that belong to the class of *smooth Gowdy-symmetric generalized Taub-NUT solutions* introduced by Beyer et al. in [32] and which was motivated by the early work of Moncrief [135] about generalizations of the Taub-NUT solution [188]. In this chapter, we explore the behaviour of the constraint for different gauges by choosing different gauge source functions. Further, we discuss the different error sources and how they arise in our implementation.

As a second application of our infrastructure, we conduct a study of singularities of Gowdy spacetimes with spatial topology $\mathbb{S}^1 \times \mathbb{S}^2$. It is well-known that in the last years there have been several investigations of Gowdy spacetime. However, from those, as is summarized in chapter 3, the most extensively studied by either analytical and numerical methods has been the case of $\mathbb{T}^3$ spatial topology. On the other hand, the other two cases have received less attention by the community because they exhibit some difficulties associated with the coordinate poles, where the action of the symmetry group degenerates, which significantly complicates their analysis. The reason lies in that for the $\mathbb{S}^1 \times \mathbb{S}^2$ and $\mathbb{S}^3$ cases, the Killing vectors generated by the action of the symmetry group $\mathrm{U}(1) \times \mathrm{U}(1)$ vanish at certain places (the poles), in contrast to the $\mathbb{T}^3$ case where the two Killing fields are nowhere vanishing. Thus, smoothness of the metric at the poles requires that the metric components behave in a particular way at these points. In other words, the smoothness conditions at the poles act as boundary conditions which are absent in the $\mathbb{T}^3$ case. In section 3.3, we summarize some of the most relevant facts about the Gowdy symmetric spacetimes.

It is expected that the behaviour for the cases $\mathbb{S}^1 \times \mathbb{S}^2$ and $\mathbb{S}^3$ should be similar to the $\mathbb{T}^3$ case at all points at the singularity except at the poles, since the action of the Gowdy symmetry group degenerates there. In fact, by means of analytical and numerical techniques Garfinkle [90] confirmed the above by showing that the $\mathbb{S}^1 \times \mathbb{S}^2$ case displays the same asymptotic velocity term dominated behaviour (except at the poles), which will be discussed in section 3.2.2, with the same sort of "spiky" features at isolated points as the $\mathbb{T}^3$ case. By spiky features we refer to spatial points where some metric components or geometric invariant quantities develop "sharp features" (or simply "sharps") in space the closer one approaches the singularity in time. Those receive the name of *spikes* and are divided into two classes, namely *false* and *true spikes*. The first class can be seen as "problems" due the chosen coordinates (without any geometrical meaning) causing that some metric components develop "sharps" in space near to the singularity. On the other hand, true spikes represent a localized change in the geometric behaviour of the solution at the singularity causing geometric

quantities like the *Kretschmann scalar* to develop sharps in space.

Spikes are mostly present in Gowdy spacetimes at the singularity; hence, a better understanding of those is needed in order to draw general conclusion about the behaviour of these cosmological models. An example of this is found in the analysis carried out by Ståhl [183] for Gowdy spacetimes $\mathbb{S}^1 \times \mathbb{S}^2$ and $\mathbb{S}^3$. Using *Fuchsian methods*, analogous to that done in [116] for the $\mathbb{T}^3$ case, he found that under some given conditions it can be shown that there exists a family of AVTD solutions for the cases $\mathbb{S}^1 \times \mathbb{S}^2$ and $\mathbb{S}^3$. However, because of smoothness conditions, the behaviour of those at the polar regions is still not well understood. Ståhl associates the complexity of analysing the dynamics of this sort of spacetimes near the polar regions with a possible emerging of spikes. In other words, Ståhl predicts that, in general, spikes should emerge at the poles; consequently, a direct treatment by Fuchsian methods is not enough for studying the behaviour at the singularities of those Gowdy spacetimes. Further, the nature of this possible polar spikes remains unclear. Motivated by the above, as a first application of our analytical and numerical infrastructure, in chapter 9 we numerically study the behaviour of Gowdy spacetimes $\mathbb{S}^1 \times \mathbb{S}^2$. In particular, we study the rising of spikes at the regions near the poles. However, since only true spikes have geometrical meaning, we will focus on studying those by means of the behaviour of the Kretschmann scalar. By doing so, we will show evidence that supports the claim that spikes are typical features at the singularity at the poles.

As a third application of our infrastructure, in chapter 10 we conduct a systematic investigation of a particular spatially homogeneous solution of the vacuum Einstein field equations with a positive cosmological constant called the *Nariai spacetime* [142]. This spacetime has become an object of special interest since Ginsparg and Perry [95] proved that it emerges as the extremal limit of Kottler-Schwarzschild–de Sitter spacetime [122], which can be interpreted as a static black hole immersed in a de Sitter universe, which is the maximally symmetric solution of the vacuum EFE with a positive cosmological constant that represents an expanding universe at an exponential rate. In other words, the Nariai spacetime can be interpreted as a de Sitter universe containing a black hole of maximal size, that is, the ratio of the black hole is equal to the cosmological horizon.

Thanks to its geometrical properties, the Nariai spacetime has been useful for modelling several situations. Among them, some works for modelling the quantum pair creation of black holes during the inflation epoch were carried out by Bousso and Hawking [42–44]. These cosmological models "at the borderline between inflation and gravitational collapse" were based on considering spherically symmetric perturbations of the Nariai spacetime. It was found that under certain conditions these models yield inflationary universes locally isometric to the de Sitter universe in agreement with the so-called *cosmic no-hair conjecture* [94, 106]. As we will explain in chapter 3, this conjecture states that generic (inhomogeneous and anisotropic) expanding solutions of the Einstein field equations with a positive cosmological constant approach to the *de Sitter spacetime* asymptotically, which is well-known to be homogeneous and isotropic. Although there is some support for this conjecture in some special situations [120, 160, 194], the general case remains unclear due to the complexity of the Einstein field equations. One of the most interesting features of the Nariai spacetime is that it is a particular case where the conjecture does not hold. Therefore, if this conjecture is assumed to be true, as it is usually expected, the Nariai solution should not be generic in a certain sense, and in particular, it should be unstable under arbitrary perturbations.

Motivated by the above, Beyer [27, 28] considered this question under a particular kind of perturbations, namely Gowdy symmetric perturbations. The basic idea of his approach consists of embedding the Nariai spacetime in a more general class of solutions that shares the same spatial topology, say $\mathbb{S}^1 \times \mathbb{S}^2$. The perturbations are defined as solutions of the

Einstein field equations whose initial data in some *Cauchy surface* are "close" to data in a Cauchy surface of the Nariai solution. The word "close" in this context means that the two data sets (Nariai and its perturbations) should not deviate "excessively" with respect to some suitable norm. Following this approach, the first work [27] was dedicated to study the instability of the Nariai solution under general homogeneous perturbations which gives rise to a parametric family of spatially homogeneous solutions, namely the *Kantowski-Sachs family*. The second work [28] was devoted to the investigation of spatially inhomogeneous perturbations. Here, the perturbations were defined in the Gowdy symmetric class with spatial topology $\mathbb{S}^1 \times \mathbb{S}^2$. Therefore, all the fields are invariant under translations along the manifold $\mathbb{S}^1$ by the action of the group U(1) and under rotations around the polar axis of $\mathbb{S}^2$. Based on a series of numerical experiments for different initial data sets, the expected instability of the Nariai solution under this sort of perturbations was confirmed. However, as is pointed out by the author, the underlying mechanism that triggers either the expanding or collapsing behaviour of the perturbed spacetime was not well understood. This is one of the questions that we address in chapter 10. We study the mechanism whereby Gowdy symmetric perturbations of the Nariai spacetime develop either an expanding or collapsing behaviour in order to obtain greater understanding of the instability of the Nariai spacetime. Additionally, we explore the asymptotic behaviour of the perturbations of the Nariai spacetime for both when the curvature blows up (the collapsing case) and when it tends to a constant value (the expanding case). In particular, the latter case is analysed in light of the CNH.

Organization of this work

This work is organized as follows. In the first part, called Preliminaries, we review the most relevant existing results and numerical techniques related to this work. These are mainly summarized in chapters 2 and 3. In addition, we provide all the necessary underlying mathematical background material on which our analytical and numerical method is based in chapters 4 and 5. Later in Part II, the analytical treatment for the initial value problem for U(1) symmetric spacetimes with spatial topologies $\mathbb{S}^3$ or $\mathbb{S}^1 \times \mathbb{S}^2$ is introduced in chapter 6, followed by a detailed discussion of the pseudo-spectral approach in chapter 7. In Part III, we present and analyse three applications of our infrastructure to Gowdy symmetric spacetimes. In particular, chapter 8 is devoted to reproducing an exact solution of the vacuum Einstein field equations with spatial topology $\mathbb{S}^3$ in order to test our infrastructure. In chapters 9 we focus on numerically studying the emerging of spikes near the polar regions for the case $\mathbb{S}^1 \times \mathbb{S}^2$ with zero cosmological constant. Later in 10, a situation with a positive cosmological constant is considered in order to study the non-linear stability of the Nariai spacetime. In chapter 11 we summarize the results obtained in this work and discuss some future projects. Since, the aim of this work is to be as self-contained as possible, in appendix A we have included a summary of some mathematical tools in differential geometry, such as fundamental definitions and conventions, that will be used in this work. We recommend the reader to have a "quick view" of this chapter in order to get familiar with the notation used in this thesis.

Part I

Preliminaries

Chapter 2

Approach to the Einstein field equations

The *Einstein field equations* (EFE) consist of a system of ten coupled, non-linear, partial differential equations (PDEs) in four dimensions, which are in general difficult to solve analytically. Because of this complexity, exact solutions of the EFE are only known in some particular cases such as spherical or axially symmetric solutions as well as homogeneous solutions. However, if one is interested in studying cases with little or no symmetry at all, it is very likely that finding an analytic solution of the EFE turn out to be an impossible task. In order to overcome this difficulty, researchers tried to solve the EFE using numerical techniques initiating in this way the field of the numerical relativity.

Numerical relativity appeared as an independent field of research in the 1960s with the pioneering efforts of Hahn and Lindquist [104], but it was not until in the 1970s when the first truly successful simulations were carried out by Smarr [180] and Eppley [75] in the context of collision of two black holes. However, at that time, the power of the available computers was very modest, and the simulations that could be performed were limited to some specific cases. This situation changed during the decades of the 1980s and 1990s with the appearance of better computers, which allowed researchers to tackle many different problems in general relativity such as rotating stars, black hole collisions, gravitational collapse, singularity structures, and the collisions of compact objects like neutron stars. A general introduction to numerical relativity can be found in [15, 124, 125] and more detailed discussion is available in the books [1, 16].

One of the essential difficulties in numerical relativity is to achieve long-term stable and accurate calculations. To do so, there have been proposed several ways to write the EFE which are mathematically equivalent. However, experience over the years has revealed that equivalent sets of evolution equations display different numerical stability. We devote this chapter to discussing some of the most relevant formulations that are used in numerical relativity. However, in order to provide a context for the discussion, we start the chapter by reviewing the formulation of the initial value, or simple Cauchy problem, in general relativity. In addition, we provide a brief discussion about hyperbolicity and stability, which are concepts that will play a fundamental role in the numerical solution of the Cauchy problem in general relativity. Then, in section 2.4, we discuss some of the most relevant formulations of the EFE used in numerical relativity. Moreover, we provide a discussion of the generalized harmonic formulation of the EFE [79] which corresponds to a particular case of the generalized wave map formalism [87]. The latter will be chosen for our numerical implementation and will be discussed in chapter 6. For some applications of the generalized harmonic formulation in

general relativity; see, for instance, [12, 127, 151, 152].

2.1 The Einstein field equations

In the theory of general relativity, we consider the spacetime as the set (M, g_{ab}), where M is a smooth real four dimensional manifold endowed with a Lorentzian metric g_{ab} of signature $(-,+,+,+)$, which is a solution of the EFE

$$G_{ab} + \Lambda g_{ab} = \kappa T_{ab} \, . \tag{2.1}$$

Here $G_{ab} := \mathcal{R}_{ab} - \frac{1}{2} g_{ab}\mathcal{R}$ is the Einstein tensor with $\mathcal{R}_{ab}$ being the Ricci tensor, κ a proportionality constant and Λ is the cosmological constant. Hereafter we shall choose units such that κ is equal to one. The gravitational field is measured by the curvature of the spacetime represented in terms of the Ricci tensor. The energy, momentum and stress of the matter content are represented by the symmetric energy-momentum (or stress-energy) tensor denoted by T_{ab}. All non-gravitational sources of energy and momentum in the spacetime contribute to T_{ab} like particles, fluids, fields, etc. Therefore, the EFE relate the geometry of spacetime with its matter content. For the particular case when there is no matter content, say the vacuum case, the EFE can be written in the shorter form

$$\mathcal{R}_{ab} = \Lambda g_{ab} \, . \tag{2.2}$$

This is the case that we will consider in this work. The equation is written in such a way that the space and time are treated in an equal manner. This covariance is very important (and quite elegant) from a theoretical point of view, but it does not allow us to think clearly about the evolution of any system described by the EFE. Thus, the first thing we need to do in order to rewrite the EFE as a Cauchy problem is to split the roles of space and time in a clear way. We devote the next section to the treatment of this issue.

2.2 Formulation of the Cauchy problem

2.2.1 Cauchy surfaces

A hypersurface Σ of the manifold M is the image set of a 3-dimensional manifold by the embedding $\Phi : \Sigma \to M$, where "embedding" means that Φ is a diffeomorphism, that is, an one-to-one mapping such that both Φ and Φ^{-1} are continuous. The induced metric on Σ is defined by (see [98])

$$h_{ab} = \Phi^* g_{ab} \, .$$

The hypersurface is said to be *spacelike* if the metric h_{ab} in Σ has signature $(+,+,+)$, *timelike* if the metric has signature $(-,+,+)$ and *null* if the metric has signature $(0,+,+)$. If the tangent vector field to a curve are timelike or null, the curve is a *causal curve*. A *Cauchy surface* is a spacelike hypersurface Σ in M such that each causal curve intersects Σ once and only once. Not all spacetimes admit a Cauchy surface. An example of these are spacetimes with closed timelike curves like the extensions of the Taub-NUT solution [144]. A spacetime (M, g_{ab}) that admits a Cauchy surface is said to be *globally hyperbolic*. An important consequence of this is that the spacetime can be foliated by a family of Cauchy surfaces (Σ_t) such that

$$M = \bigcup_{t \in \mathbb{R}} \Sigma_t \, .$$

By *foliation* or slicing, we mean that there exists a smooth scalar field τ on M which is regular (in the sense that its gradient never vanishes) such that each hypersurface is a level surface of this scalar field. Mathematically we write this as

$$\forall t \in \mathbb{R}, \quad \Sigma_t = \{p \in M \mid \tau(p) = t\} .$$

Since we assume that τ is a regular scalar field, the family member of hypersurfaces Σ_t do not intersect each other, that is, $\Sigma_t \cap \Sigma_{t'} = \emptyset$ for $t \neq t'$. The scalar function τ can be interpreted as a global time function.

2.2.2 The Cauchy problem

Let (M, g) be a 4-dimensional globally hyperbolic spacetime such that it can be foliated into Cauchy surfaces Σ_t parametrized by a global time function. In addition, let us consider a unit normal vector n^a to the Cauchy surfaces Σ_t. The spacetime metric g_{ab} induces a spatial metric h_{ab} on each Σ_t by means of the relation

$$h_{ab} = g_{ab} + n_a n_b . \tag{2.3}$$

Let t^a be a vector field on M satisfying $t^a \nabla_a t = 1$. The vector t^a can be decomposed into its normal and tangential parts to Σ_t by defining the *lapse function* α and the *shift vector* β^a respectively

$$\alpha := -t^a n_a, \qquad \beta_a := h_{ab} t^b . \tag{2.4}$$

We remark that these quantities cannot be considered as dynamical variables of the spacetime evolution since they represent the *gauge freedom* that fixes the coordinates in which the evolution equations are treated. On the other hand, we introduce the extrinsic curvature (or second fundamental form) as follows[1]

$$\mathcal{K}_{ab} := \frac{1}{2} \mathcal{L}_n \, h_{ab} . \tag{2.5}$$

The trace of this quantity $\mathcal{K} := \mathcal{K}^a{}_a$ is called the *extrinsic mean curvature* and can be interpreted as a measure of how much the Cauchy surface Σ_t changes along the vector field n^a. The EFE yield a system of ten second-order partial differential equations for the ten unknown metric components $g_{\mu\nu}$. From those ten equations, six determine the evolution of the metric components, while the remaining four represent conditions (or constraints) that must be satisfied during the evolution. The latter are extracted in view of the fact that $G_{ab} n^a$ does not contain second-order derivatives of the metric components $g_{\mu\nu}$. Using the Gauss-Codazzi and Codazzi-Mainardi equations (see [195]) these constraint equations can be written in the conventional form[2]

$$ {}^{(3)}R + \mathcal{K}^2 - \mathcal{K}_{ab}\mathcal{K}^{ab} - 2\Lambda = 2\rho, \tag{2.6}$$

$$ D_b(\mathcal{K}^{ba} - h^{ba}\mathcal{K}) = j^a, \tag{2.7}$$

where ${}^{(3)}R$ and $D_b = h_b{}^a \mathfrak{D}_a$ are the projected Ricci scalar and covariant derivative in some Σ_t, and $\rho := n_a n_b T^{ab}$, $j^a := h^a{}_b n_c T^{bc}$ correspond to the energy and momentum density respectively. Note that as a consequence of the Bianchi identities for the Ricci tensor we have $\mathfrak{D}^a G_{ab} = 0$. This fact guarantees that if the constraints are initially satisfied, they

[1] See section A.5.

[2] Note that as stated in section 2.1, we are using units such that $\kappa = 1$ in the EFE.

should be preserved during the whole evolution, i.e., the constraint propagates during the evolution. Hence, the solution obtained from the evolution equations corresponding to an arbitrary initial data set is a solution of the EFE; consequently, the given formulation of the Cauchy problem is *well-posed*. Here we want to point out that the concept of well-posedness of the Cauchy problem restricts its attention to only certain properties of the solutions like short-time existence, uniqueness and continuous dependence on the initial data. Thus, this is a necessary condition for the formulation of the initial value problem, otherwise one cannot expect to obtain reliable conclusions about solutions achieved numerically.

A Cauchy development (M, g_{ab}) of a given initial data is called *maximal global hyperbolic development* if there is no further Cauchy development of the same initial data set which is an extension of (M, g_{ab}). An important contribution by Choquet-Bruhat and Geroch [61] building on earlier work by Choquet-Bruhat [59] is the following theorem.

Theorem 2.2.1 *Let $(\Sigma, h_{ab}, \mathcal{K}_{ab})$ be a vacuum initial data set. Then there exists a unique (up to isometry) maximal Cauchy development of $(\Sigma, h_{ab}, \mathcal{K}_{ab})$.*

In fact, the authors proved this theorem for the case of $\Lambda = 0$ but it is straightforward to generalize their arguments (see [195]). An important consequence of this theorem is that for a given fixed initial data set, the maximal Cauchy development is an extension of all corresponding Cauchy developments. Hence, this result shows that the requirement for a formulation of the Cauchy problem of EFE to be well-posed discussed above can indeed be met.

2.3 Hyperbolicity and well-posedness

In what follows, we discuss briefly the notion of hyperbolicity, well-posedness and stability. We will provide definitions (most of them taken from [1]) that are necessary for the rest of this work. For a more extended discussion we refer the reader to the mentioned source as well as [157] and references therein. Let us begin by considering the following first-order system of evolution equations

$$\partial_t u + \Pi^i \, \partial_i u = s(u) \ , \tag{2.8}$$

where u is some n-dimensional vector-valued function of time and space, Π^i are $n \times n$ matrices, ∂_i denotes spatial derivatives for each spatial dimension and $s(u)$ is a source term that may depend on the components of u but *not* on their derivatives. The matrices Π^i are usually called characteristic matrices. Consider an arbitrary spatial unit vector σ_i and the matrix $P(\sigma_i) := \Pi^i \, \sigma_i$ known in the literature as the *principal symbol* of the system. It is said that the system is *strongly hyperbolic* if the principal symbol has real eigenvalues and a complete set of eigenvectors for all σ_i. If, on the other hand, Π^i has real eigenvalues but does not have a complete set of eigenvectors the system is said to be *weakly hyperbolic*. It can be always defined a matrix $H(\sigma_i)$ called symmetrizer [3]

$$H(\sigma_i) = \left(V^{-1}\right)^T V^{-1},$$

where V is the matrix of column eigenvectors of $P(\sigma_i)$. For the particular case when the symmetrizer is independent of σ_i, we say that the system is *symmetric hyperbolic*. Thus, symmetric hyperbolic systems are strongly hyperbolic but not in the other way around. However, in the case of one spatial dimension this distinction does not arise since the spatial unit vector σ_i turns in to a constant that does not affect the symmetrizer. In this work, this

[3] The super index T indicates matrix transposition.

case will be of particular relevance. In fact, for the particular situation that we will consider in section 10.3, all that we have to do in order to determine whether our system is symmetric hyperbolic is to check whether the matrix Π has a complete set of eigenvectors with all its eigenvalues real numbers.

A crucial property of symmetric hyperbolic systems is that it can be proved that they are *well-posed*, which means the following:

(i) There exists a local unique solution u of Eq. (2.8).

(ii) The solution u depends continuously on the initial data. In other words, small changes in the initial data will correspond to small changes in the solution.

The above can be expressed more formally as follows. A system of partial differential equations is called well-posed if we can define a norm $\|\cdot\|$ such that

$$\|u\| \leq \kappa e^{\alpha t} \|u_0\| \,, \tag{2.9}$$

where u_0 corresponds to the initial value of u with κ and α real constants. That is, the norm of the solution can be bounded by the same exponential than for all initial data. This indicates that the norm of u is bounded by a certain function, thus the system is *stable*.

2.4 Some formulations for the numerical solution of the EFE

There are several approaches for solving the EFE. The first was given by Arnowitt, Deser and Misner [11] with the purpose of constructing a canonical formulation of the EFE seeking the quantum nature of spacetime. Later in the late 1970s, this formulation was used by Smarr and York [181, 182] (with a slightly different notation). Hereafter, we refer to this formulation as the standard *ADM formulation*. This approach is based on splitting the EFE into constraint and evolution equations as described in section 2.2.2. Up to the middle of 1990s, the ADM formulation was the standard formulation in numerical relativity. This method allowed researchers to study several situations that had never been explored before, such as the formation of a naked singularity from collision-less particles [177], the critical behaviour for a black-hole formation [57] and the black-hole horizon dynamics [10] just to mention a few. Nevertheless, when scientists tried to make long-term simulations, they were often interrupted by unexplained blow-ups in the violation of the constraints. Initially, this was thought to be due to the lack of resolution, inappropriate gauge choice or the particular numerical scheme implemented. However, after the accumulation of some numerical experience, researchers noticed that the lack of stability in long-term numerical simulations can be related to the fact that the system of PDEs was only weakly hyperbolic. See, for instance, [1] for a detailed demonstration.

In the early 90's, Nakamura and Kojima [141] presented a reformulation of the ADM formulation based on a conformal transformation which improved the stability of the standard formulation. This new approach evolved over the following years until the late 90's when Baumgarte and Shapiro [14] compared it systematically with the ADM formulation in a series of spacetimes showing that the new formulation had far superior stability properties for all cases considered. Later, this formulation became the most popular until today. In fact, nowadays it is used by most large three-dimensional codes in numerical relativity. The more common version of this formulation is based on the work of Shibata and Nakamura [178] and is commonly known as the *BSSN formulation* (Baumgarte, Shapiro, Shibata and Nakamura).

In order to understand the superiority of the BSSN with respect to the ADM formulation, a series of numerical comparison tests has been conducted by several research groups around the world. In particular, Alcubierre et al. [2] found that one of the essential improvements of the BSSN formulation lies in the use of the momentum constraints in the equations. Later, Sarbach et al. [174] showed that the BSSN formulation is in fact strongly hyperbolic, so it is natural that it behaves better than the ADM formulation, which is only weakly hyperbolic.

Following the idea of hyperbolicty, several strongly hyperbolic formulations of the EFE have recently been proposed. We refer to them as *strongly hyperbolic formulations*. Some of the most relevant formulations nowadays are the Bona-Massó [38–40] formulation, the Frittelli-Reula formulation [89], the Kidder-Scheel-Teukolsky (KST) formulation [118], the Nagy-Ortiz-Reula (NOR) formulation [138], the Conformal formulation [83] and the *generalized wave map formalism* [87], which can be understood as a covariant version of the more familiar *generalized harmonic formalism* that was first introduced by Friedrich in order to generalize the original harmonic gauge considered in [79]. In particular, the latest formulation has gained considerable attention in the last decade due to the success of Pretorius [150] performing (to our knowledge) the first binary black-hole merging simulation by using this formulation. One of the reasons for his success consists of the implementation of "constraint damping terms" in the evolution equations, which, as we will discuss in more detail in section 2.5.2, enforce the decay of the numerical violation of the constraints along the evolution. This formulation that evolves the full four-dimensional spacetime metric, and is not directly based on the $3+1$-formalism, is considered nowadays as the most powerful contender for the BSSN. For this reason, we have decided to implement it in our numerical infrastructure.

2.5 The idea of the generalized wave map formalism

2.5.1 The general setting

Following the approach introduced by Friedrich [85], we can reduce the resulting PDE system from EFE into a coupled system of quasi-linear wave equations for the independent coordinate components of the metric. Later in section 6.3, we will apply this formalism to obtain general evolution equations for the particular manifold $\mathbb{R}\times\mathbb{S}^2$. For now, let us start by rewriting the components of the Ricci tensor as (see [88])[4]

$$R_{\mu\nu} = -\frac{1}{2}\, g^{\rho\sigma}\partial_\rho\partial_\sigma\, g_{\mu\nu} + \nabla_{(\mu}\Gamma_{\nu)} + \Upsilon_{\mu\nu}, \tag{2.10}$$

where the third term $\Upsilon_{\mu\nu}$ is a tensor which does not contain any second-order derivatives of the metric. Hereafter, we denote this third tensor by $\Upsilon_{\mu\nu}(g,\partial g)$ to indicate that it only depends on the metric components and its first derivatives. The terms Γ_μ denotes the *contracted connection coefficients* $\Gamma_\nu := g^{\mu\rho}\Gamma_{\nu\mu\rho}$ (see [184]). For the latter, it is assumed that it satisfies

$$\nabla_\mu\Gamma_\nu := \partial_\mu\Gamma_\nu - \Gamma^\rho{}_{\nu\mu}\Gamma_\rho,$$

which in other words means that the terms Γ_μ will be treated as covector components. Note that $\Gamma_{\nu\mu\rho}$ corresponds to the standard Christoffel symbols if we use a coordinate frame. However, as we will discuss in section 6.3, this will not be the case for our particular situation. To continue with the description of the generalized wave map formalism (GWF), let us note that the Ricci tensor considered as a differential operator acting on the metric is not hyperbolic because of the second-order derivatives of the metric contained in $\nabla_{(\mu}\Gamma_{\nu)}$. Thus,

[4] We have use ∂_ρ to denote general frame vectors.

the PDE theory for hyperbolic system cannot be used to guarantee well-posedness of the Cauchy problem. One way to overcome this problematic situation is by adding the so-called *gauge functions* F_μ, introduced by Friedrich in [85]. We start by defining a tensor field

$$\hat{R}_{ab} := R_{ab} + \nabla_{(a}\mathcal{D}_{b)}, \tag{2.11}$$

where the components of $\mathcal{D}_\nu$ are defined by

$$\mathcal{D}_\nu := F_\nu - \Gamma_\nu \, . \tag{2.12}$$

Thus, substituting this expression into Eq. (2.10), the components $R_{\mu\nu}$ of the Ricci tensor R_{ab} can be written as

$$\hat{R}_{\mu\nu} = -\frac{1}{2}\, h^{\rho\sigma}\partial_\rho\partial_\sigma h_{\mu\nu} + \nabla_{(\mu}\Gamma_{\nu)} + \Upsilon_{\mu\nu}(h, \partial h) + \nabla_{(\mu}\mathcal{D}_{\nu)}, \tag{2.13}$$

where the quantity $\mathcal{D}_a$ has to be a covector in order to preserve $R_{\mu\nu}$ as the components of a tensor. Later in section 6.3, we will come back to this delicate issue for our particular implementation in $\mathbb{R}\times\mathbb{S}^2$. Hereafter, we will refer to it as the *violation covector*. The functions F_μ are allowed to depend on the metric and the spacetime coordinates but not on the derivatives of the metric. Thus, if this is given, the Eq. (2.13) turns into a hyperbolic quasi-linear system for the metric components. In order to recover the original Ricci tensor, we set the violation covector $\mathcal{D}_a$ and its covariant derivative $\nabla_{(a}\mathcal{D}_{b)}$ equal to zero. Thus, these will be the constraint equations along the evolution. The gauge source functions and the initial data determine the coordinates by

$$\nabla_\nu\nabla^\nu x^\mu = -F^\mu.$$

The constraint equations are preserved since the evolution of $\mathcal{D}_a$ is driven by quasilinear wave equations known as the *subsidiary system* (see [162] for details)

$$\nabla_b\nabla^b\mathcal{D}_a + \mathcal{D}^b\nabla_{(b}\mathcal{D}_{a)} = 0. \tag{2.14}$$

This tensorial equation is obtained by substituting the modified Ricci tensor Eq. (2.13) into the EFE and using the divergence free property. Under the above consideration, the local Cauchy problem for the system Eq. (2.13) is well-posed; therefore, we can guarantee the existence and uniqueness of the solution and their continuous dependence on the initial data.

2.5.2 Constraint damping terms

Although hyperbolicity is a desirable property to guarantee the well-posedness of the system, it does not necessarily guarantee the stability of any numerical solution obtained from it. In fact, it may happen that in a hyperbolic formulation (see [179]) of the EFE, the error associated with the constraint violation may grow at a bounded rate. Furthermore, this error behaviour may not necessarily be due to the numerical algorithm itself, but to the hyperbolic formulation of the EFE admitting rapidly growing solutions. See the discussion in [152]. Therefore, it would be desirable if one could find a formulation of the EFE in which the submanifold of solutions, which also obeys the constraints, was an attractor. Clearly, this requires a mechanism for breaking the time-reversal symmetry of general relativity away from the constraint surface. Some mechanisms have been suggested that include dynamic adjusting of free parameters of the constraints (see for instance [190]) or adding derivatives of the constraints so that the system becomes mixed parabolic and hyperbolic [52]. In particular,

Brodbeck et al. [47] have suggested a general approach called λ-system to solve a system of evolution equations and constraints such that the constraint surface is an attractor. Later on, following this idea, Gundlach et al. [103] introduced the so called *constraint damping terms* into the EFE by adding to the Ricci tensor Eq. (2.13) the term

$$\kappa \left(\eta_{(a} \mathcal{D}_{b)} - g_{ab} \eta^c \mathcal{D}_c \right),$$

with η_a being a timelike vector and κ a constant. With this new term the subsidiary equation Eq. (6.11) takes the form

$$\nabla_b \nabla^b \mathcal{D}_a + \mathcal{D}^d \nabla_{(d} \mathcal{D}_{a)} = 2\kappa \nabla^c \eta_{(a} \mathcal{D}_{c)}. \tag{2.15}$$

They have shown by means of perturbations of the Minkowski spacetime that all the "short wave length" modes in the solutions of the subsidiary system Eq. (2.15) are damped at either the rate $e^{-\kappa t}$ or $e^{-\kappa t/2}$. In the last years, a good amount of numerical simulations have been successfully conducted using this approach (see for instance [128, 150]), which confirms its effectiveness for several situations.

Nevertheless, a complete understanding of how the "long wave length modes" solutions are damped (or not) for generic spacetimes is still missing. Due to the expanding (or collapsing) behaviour of most cosmological spacetimes, the "long wave length modes" are expected to be dominant during the evolution. Therefore, for our particular interests (cosmological spacetimes), we do not know whether or not adding constraint damping terms to the evolution equation will help to control the behaviour of the constraint. Later in section 10.5.2, we will address again this issue in the investigations of the non-linear instability of the Nariai spacetime.

2.5.3 Gauge drivers

One disadvantage of the GWF is that (to our knowledge) there is not a geometric description of the relationship between the regular gauge source functions and the resulting spacetime coordinates. One way to introduce a sort of criterion for the choice of such functions is by means of the well-known *lapse* and *shift* view of the coordinate freedom (see section 2.4). Using this, we can promote the regular gauge source functions to "system variables" by proposing evolution equations for them, usually called gauge drivers, depending on some prescribed lapse and shift. See, for instance, the formulation in [151]. Even though this approach has been useful for the numerical solution of the EFE in some complicated scenarios (see [150]), it may not be a good choice from a mathematical point of view. The reason lies in the fact that the resulting system of evolution equations (including the gauge drivers) may not be hyperbolic; hence, the setting of the Cauchy problem may not be well-posed any more. In order to determine the hyperbolicity of the system, one would have to analyse the resulting system of equations for the chosen gauge drivers with the particular choice of lapse and shift. Later in section 9.3 and section 10.3, we will appeal to this sort of method in order to keep the form of some metric components during the evolution. Some other (and more general) proposals for gauge drivers that preserve the hyperbolicity can be found in [127, 128].

On the other hand, a modified version of the GWF that uses precisely this idea of gauge drivers is the Z_4 formulation [36, 37] proposed by Bona et al. The main idea of this approach consists of combining the GWF with the standard ADM decomposition in order to turn the EFE into a system of ten non-linear evolution evolutions, i.e., the four elliptic constraint equations are transformed into evolution equations. To begin with, they start by writing the Ricci tensor as proposed in the GWF by Eq. (2.13). In this formulation they refer to

the violation covector D_a as Z_a (from whence we assume the name comes from). Then, by replacing the Ricci tensor in the EFE, followed by the standard ADM decomposition (see [16]), the evolution equations for the extrinsic curvature $\mathcal{K}$, the induced metric h_{ab} and the four components of the Z_a covector are obtained. The evolution equations for the components of Z_a now play the role of the Hamiltonian and momentum constraints which clearly are satisfied when the components of Z_a vanish. It is important to highlight that in order to obtain a strongly hyperbolic system, the slicing condition for the lapse function has to satisfy

$$(\partial_t - \mathcal{L}_\beta)\,\alpha = -\alpha^2\, f(\alpha)\, \left(\mathcal{K} - 2\alpha Z^0\right), \tag{2.16}$$

which is a generalization of the standard Bona–Masso slicing condition [39]. Then, provided that $f > 0$ this slicing condition yields the strongly hyperbolicity of the Z_4 formulation. Some current application of this formalism as well as some modifications (such as the Z_4c formulation) can be found in [3, 170, 197].

Chapter 3

Cosmological spacetimes

As mentioned in chapter 1, in this thesis we will focus on studying some cosmological spacetimes with certain symmetries. Therefore, we will provide some fundamental background about some of the most remarkable issues and discoveries concerning those kinds of spacetimes. We start this chapter by introducing the notion of cosmological spacetime. Then, based on a symmetry classification, we list some of the most relevant cosmological spacetimes in the literature. Later, we discuss relevant issues concerning current investigations on cosmological spacetimes like cosmic censorship, the BKL-conjecture and the cosmic no-hair conjecture. Since the aim of this work is to study Gowdy symmetry spacetimes, we devote the last section of this chapter to introducing them. We based the following discussion on the references [6, 24, 99, 155, 163, 193].

3.1 Generalities on cosmological spacetimes

We define a *cosmological spacetime* to any spacetime such that it can be foliated by a family of closed Cauchy surfaces Σ_t, that is, each Σ_t is a compact manifold (see section A.1) without a boundary. The cosmological spacetimes are usually classified depending on the dimension of the isometry group (or number of Killing vectors) acting on them[1]. In what follows we briefly mention some of the most relevant cosmological spacetimes in the literature.

Let us start by considering a vacuum maximally symmetric four-dimensional cosmological spacetime, that is, a spacetime endowed with ten Killing vectors which coincides with the dimension of the isometry group acting on it. For the case with a positive cosmological constant, this spacetime is known as the de Sitter spacetime, which has spatial topology $\mathbb{S}^3$ and constitutes the simplest inflationary solution obtained from the EFE. Other interesting cosmological spacetimes are the Friedmann-Lemaitre-Robertson-Walker spacetimes (FLRW), which are obtained in the case when the isometry group has dimension six. This symmetry group is assumed to act on spacelike hypersurfaces as opposed to the ten-dimensional case above which acts on space and time. Since six is the largest number of dimensions of a group acting on three-dimensional surfaces, this is the "maximal spacelike symmetry", which is also referred to as "spatially homogeneous and isotropic". For the non-vacuum case, the symmetries require that the matter fields are of perfect fluid type. The relevance of the FLRW models, at least for suitable matter fields, stems from the fact that they are the simplest parametrized models which have been successfully fitted to observational data [121].

One can show [130] that there cannot exist a five-dimensional isometry group acting on three-dimensional hypersurfaces transitively (see section A.6). Thus, we continue with the

[1] See section A.6 for a formal definition of isometry groups.

four-dimensional case. It turns out that there are two possibilities here. The first one arises when the isometry group has a three-dimensional subgroup that acts simply transitively on the spacelike Cauchy surfaces. This is called *Locally Rotationally Symmetric* or simply *LRS-Bianchi*. The second case is realized when the four-dimensional isometry group does not have such a three-dimensional subgroup. This is the so-called *Kantowski-Sachs* spacetime whose spacelike surfaces are topologically equivalent to the manifold with geometry $\mathbb{S}^1 \times \mathbb{S}^2$ [67,115].

If the isometry group is at least three-dimensional and the action of the group is transitive on the three-dimensional spacelike slices, which are usually called as homogeneous spacelike slices, we obtain the *Bianchi spacetimes*. These are classified in terms of the three-dimensional Lie algebras. See [193] for an introduction to the Bianchi classification and the definition of the Bianchi types I to IX (and the classes Bianchi-A and Bianchi-B). The relation of the allowed spatial topologies for (local) Bianchi isometry groups and the Thurston geometries can be found in [6, 102]. The theory of Bianchi spacetimes has been mainly developed in the recent years using dynamical system techniques, since the EFE can be reformulated in system of ordinary differential equations in these cases. For a review of the current state, we recommend [164] and references therein.

Let us now reduce the dimension of the isometry group further to two. Clearly, such spacetimes cannot be spatially homogeneous any more. However, we still assume that the orbits are subsets of spacelike Cauchy surfaces. In particular the Killing vector fields are assumed spacelike. Further, let us restrict to spacetimes under the global actions of the group $\mathrm{U}(1) \times \mathrm{U}(1)$. Spacetimes with such characteristics were discussed for the first time (to our knowledge) by Gowdy in [99]. Later on, some of his arguments and results were clarified and extended by Chrusciel in [63]. For the particular case when the tangent space orthogonal to the Killing vector fields is integrable we obtained the so-called *Gowdy spacetimes*. The assumption of a global smooth effective isometric $\mathrm{U}(1) \times \mathrm{U}(1)$ group action on a smooth connected three-manifold has the following implications (see references in [99]). Firstly, the associated Killing vector fields commute because the group action is Abelian. Secondly, the action is unique. It can be proved that the only admissible topologies for the spatial three-manifolds are equivalent to the three-torus $\mathbb{T}^3$, the three-sphere $\mathbb{S}^3$ (or lens spaces that are always included implicitly in the following discussions) and $\mathbb{S}^1 \times \mathbb{S}^2$. If $\mathrm{U}(1) \times \mathrm{U}(1)$ is a local isometry group, then further topologies are possible; for instance, see [187]. However, we will not consider those in this work. For the particular case where the Killing vectors can be chosen to be orthogonal everywhere is called as *polarized Gowdy spacetimes*. Since in this thesis we will focus on the study of Gowdy spacetimes, we will devote section 3.3 to introduce them.

Next, we decrease the dimension of the isometry group even further to reach the one-dimensional case. Most investigations about solutions of the EFE of this kind have been conducted for the particular case when the spatial isometry group is $\mathrm{U}(1)$. In this situation, the spacetime is usually treated by assuming that it is a $\mathrm{U}(1)$ bundle over a spatially compact $2+1$-dimensional spacetime. Finally, the most general class of spacetimes is given when there are no symmetries. Owing to spacetimes with symmetries should be considered as non-generic in the space of all solutions of EFE, real statements about the character of generic solutions cannot be made before this general class can be controlled. Unfortunately, the techniques, both on the rigorous analytical as on the numerical side, are not sufficient yet for such general studies. However, relevant techniques are progressing enormously so that there is hope for deeper understanding in the near future. One of them is the theorem about non-linear stability of the de Sitter spacetime by Friedrich [86]. This is restricted to the case of a positive cosmological constant. Similar theorems for scalar fields and matter models (Einstein-Vlasov models) have been proved by Ringström in [160,164]. Strong cosmic

censorship and the BKL-conjecture for spacetimes with a scalar field, which resembles a stiff fluid with its quiescent behaviour, have been studied, for instance, in [7]. Numerical investigations on those were carried out in [69] and in the vacuum case in [91].

3.2 Some fundamental issues for cosmological spacetimes

3.2.1 The cosmic censorship conjecture

Studies on cosmological solutions of the EFE have led to astonishing results about our Universe. In particular, observations indicate that there was an initial singularity, or big bang, in the distant past, and the simplest cosmological models like the Friedmann solutions, for reasonable matter fields, predict precisely this behaviour. However, the question of whether such curvature singularity may occur for generic solutions of the EFE is still open. The Hawking–Penrose singularity theorems [105] shed some light on this question. They predict incompleteness of causal geodesics and the existence of a singularity in a wide class of situations. However, the information about the geometric reasons for incompleteness that is provided by these theorems is limited and does not allow general conclusions to be drawn. For instance, it be possible that a globally hyperbolic spacetime is extensible to a non-globally hyperbolic region in which the geodesics are incomplete. In such a case, if the extension into the non-globally hyperbolic region is regular in an appropriate sense, there can be defined a *Cauchy horizon*. By this, we refer to the "region" that separates the globally hyperbolic "predictable" region from the non-globally hyperbolic rest, with the possibility of many kinds of pathologies like closed causal curves. An example of this kind is found for the well-known *Taub-NUT spacetime* [135, 162, 188]. More examples with this sort of behaviour are also known for the class of polarized Gowdy solutions; see, for instance, [65, 66]. If these pathological properties were "generic" among solutions of the EFE, Einstein's theory of general relativity would disagree with our fundamental beliefs about causality and deterministic laws of the nature. Then, it is natural to think that there must be a way to exclude these types of pathological solutions. This is precisely the concern of the *strong cosmic censorship* (SCC) which was first formulated (to our knowledge) by Chruściel [64] for the class of cosmological solutions in vacuum with arbitrary cosmological constant, based on the early ideas of Eardley et al. [134] and Penrose [147]. The following is a non-rigorous statement of the conjecture.

Conjecture 3.2.1 *Let Σ be a compact manifold of dimension 3. Then, for a generic vacuum initial data set (Σ, h, K), the corresponding maximal global hyperbolic development is inextensible.*

If this conjecture were true, it would imply that in generic situations, incompleteness of causal geodesics is indeed caused by a geometric singularity in some sense, while the pathologies like those encountered for the Taub-NUT spacetime only occur under special circumstances. At this stage, however, this conjecture has not been confirmed in general situations; see, for example, [162]. Additionally, in the presence of black holes, one might relax this conjecture and state that violations of global hyperbolicity are only allowed when they are inside the event horizon. This is the notion of the *weak cosmic censorship*. Weak cosmic censorship is usually considered in the case of asymptotically flat solutions, and one of the first rigorous results regarding it was obtained by Christodoulo [62], who proved the validity of this conjecture for the spherically symmetric case.

3.2.2 The BKL-conjecture

The BKL-conjecture is an attempt to describe the properties of gravitational singularities in general cases. Investigations in this direction were firstly carried out by Khalatnikov and Lifshitz (KL) [126], and later improved altogether with Belinsky in [17, 18] (BKL). A review and summary of the main results about this can be found in [20], while some recent numerical studies can be found in [69, 91]. Further, investigations into the direction of a precise formulation of the conjecture are given in [107]. This conjecture claims that generic singularities of solutions of EFE are spacelike and locally modelled by the family of the Mixmaster universes, which are spacetimes belonging to the class Bianchi IX, that it, one believes to find infinite sequences of *Kasner* epochs (spacetime of type Bianchi I) observable as oscillations when the spacetimes approached towards singularity. Each timelike world-line is assumed to decouple from all neighbouring world-lines and to behave as an individual "spatially homogeneous" spacetime. An important consequence of this concept (and also of the following concept of AVTD solutions) is that spatial derivatives are "negligible"at the singularity. This is usually referred as *silent singularities*. Furthermore, the BKL-authors suggested that "matter does not matter" at the singularity (excluding some special cases), that is, the details of the matter model are not important for the behaviour of the solution near the singularity. However, there are cases like stiff fluids, which can "stop" the BKL-like oscillations in such manner that the solution approaches towards, possibly point-wise dependent, the Kasner solution [70, 76]. However, in many of the special classes of solutions considered so far, even in vacuum, the solutions converge "only" to a point-wise dependent Kasner solution without oscillations. This behaviour is called in the literature *asymptotically velocity term dominated* (AVTD), a notion first introduced in [74] and later extended (and applied) in [114]. One of the reasons why it is important to determine whether a solution is AVTD type or not is due to Kichenassamy and Rendall [116]. Using Fuchsian methods they proved that for generic AVTD spacetimes (see for an introduction [155]), the Kretschmann scalar blows up at the singularity hence, generically, do not admit any extension.

3.2.3 The cosmic no-hair conjecture

Here we state the *cosmic no-hair conjecture* (CNH) which will play an important role in our investigation on the asymptotic behaviour of the Nariai spacetime in chapter 10. As far as we know, the notion of this conjecture was first introduced by Hawking et al. in [106]. The natural underlying question is whether in generic inflationary scenarios, cosmological solutions of the EFE converge locally to the de Sitter spacetime in the future. A more formal formulation of the conjecture is stated by Beyer in [27] as follows:

Conjecture 3.2.2 *Any generic future causal geodesically complete asymptotically future expanding cosmological solution of the vacuum EFE with positive cosmological constant is foliated by Cauchy surfaces which approach a homogeneous and isotropic foliation of the de-Sitter solution locally asymptotically to the future.*

Although there is some support for this conjecture in special situations, the general case remains unclear due to the complexity of the EFE. We point out that the precise definitions of "genericity" and "approach" are not fixed by the conjecture. Apart from this, it is often difficult to identify a foliation with the properties above for a given solution. In the spatially homogeneous case, there are geometrically preferred foliations and the analysis can be simplified. Indeed, there are several results in the literature that yield conditions for the spatially homogeneous spacetimes so that their foliations approach toward a foliation of the

de-Sitter solution. The first theorem in this direction was stated by Wald in [194] valid for all the Bianchi spacetimes with $\Lambda > 0$. Later on, cases with matter and scalar field content were considered in [9, 146, 154]. Some other results for the spatially homogeneous case can be found in [50, 56, 119, 120, 196]. On the other hand, fundamental results in this context of non-linear stability of the de-Sitter solution were proved in [86], which implies that the CNH may also apply to certain solutions without any symmetry assumptions.

3.3 Gowdy spacetimes

Since in this work we shall focus on numerically investigating some aspects of Gowdy symmetric spacetimes, we devote this section to providing a small introduction to this kind of solutions of the EFE as well as listing some of the most important known results about them.

3.3.1 General metric with group of motion $\mathrm{U}(1) \times \mathrm{U}(1)$

In order to construct a metric representation for the Gowdy spacetimes, we will use a global coordinate system from the isometry group and the properties of its trajectories. In those parts of the spacetime that contains no degenerate close trajectories, one can choose two of the spacelike coordinates to be the natural group coordinates. These coordinates are constructed by choosing a reference point on each trajectory, representing that point by the identity of the group and labelling any other point on the trajectory by the group parameters which connects it to the reference point. Then, the group parameters, say φ and ρ, can be taken to be values in $(0, 2\pi)$. Moreover, the vector fields generated by the effective action of the isometry group are respectively ∂^a_φ and ∂^a_ρ. Therefore, in those coordinates, we can write the general metric invariant under the group action $\mathrm{U}(1)\times\mathrm{U}(1)$ by assuming that the components of the metric will be all independent of φ and ρ, which is, in other words, demanding that ∂^a_φ and ∂^a_ρ are commuting Killing vectors. Let us now consider the twist parameters

$$c_1 := \epsilon_{abcd}\partial^a_\varphi\partial^b_\rho\mathfrak{D}^c\partial^d_\varphi\,, \quad c_2 := \epsilon_{abcd}\partial^a_\varphi\partial^b_\rho\mathfrak{D}^c\partial^d_\rho\,. \tag{3.1}$$

For a vacuum spacetime, these parameters are constant over the whole manifold (See [93]). For the particular case when they vanish, which is another assumption of the Gowdy symmetry, it can be proved (see [195]) that the two-dimensional subspace of the tangent space at each point can be expanded by the orthogonal vectors to the mentioned Killing vectors, that is, the two-dimensional subspace parametrized by the coordinates (φ, ρ) is integrable. On the other hand, because any regular two-dimensional metric is conformally flat, the coordinates θ and t can always be chosen so that the reference two-dimensional surface metric takes the form (see [99])

$$\mathcal{G}_{ab} = L^2 e^{2a(t,\theta)}\left(-\mathrm{d}t^2 + \mathrm{d}\theta^2\right), \tag{3.2}$$

where L is a constant that is included in order to make sure that all of the coordinates and metric functions are dimensionless. In what follows, we assume $L = 1$. In the literature such coordinates are called *isothermal*. Therefore, the invariance under the group action of $\mathrm{U}(1) \times \mathrm{U}(1)$ altogether with the assumption of $c_1 = c_2 = 0$, the general form of the four-dimensional Gowdy symmetric metrics is written (using the convention $(x^0, x^1, x^2, x^3) = (t, \theta, \varphi, \rho)$) as

$$g_{Gowdy} \;=\; e^{2a(t,\theta)}\left(-\mathrm{d}t^2 + \mathrm{d}\theta\right) + A\left((q_{22}\mathrm{d}\varphi + q_{23}\mathrm{d}\rho)^2 + (q_{32}\mathrm{d}\varphi + q_{33}\mathrm{d}\rho)^2\right),$$

where the matrix formed by the coefficients q_{mn} has unit determinant. The geometrical significance of this representation is that the area of the group orbit labelled by the coordinates t and θ is given by $4\pi L^2 A$. The function A (which depends on t and θ) is usually referred to as the *orbit areal function* or just *areal function*. The coefficients of the matrix q_{mn} can be parametrized in various ways. The parametrization that is used in most of the literature about Gowdy spacetimes is choosing $q_{22} = e^{P/2}$, $q_{23} = e^{P/2}Q$, $q_{33} = e^{-P/2}$ and $q_{32} = 0$, which yields the following metric form

$$g_{Gowdy} = e^{2a}\left(-\mathrm{d}t^2 + \mathrm{d}\theta^2\right) + A\,\left(e^{P}\left(\mathrm{d}\varphi + Q\mathrm{d}\rho\right)^2 + e^{-P}\mathrm{d}\rho^2\right). \tag{3.3}$$

Combining two components of the Einstein tensor yields the important relation

$$G_{11} - G_{00} = \left(\frac{\partial^2 A}{\partial\theta^2} - \frac{\partial^2 A}{\partial t^2}\right)/\left(L^2 e^{2a} A\right).$$

If the stress-energy tensor obeys the condition $T_{11} - T_{00} = 0$, then the areal function decouples and obeys the vibrating string equation (see [63])

$$\partial_{tt}A - \partial_{\theta\theta}A = 0,$$

where we have used the notation $\partial_{tt} = \partial^2/\partial t^2$ as similar with to the variable θ. By choosing a solution to this equation, one can link the arbitrary coordinates θ, t to the geometrically invariant orbit area. Different choices for A lead to different global spacetime structures we will see in the following.

3.3.2 The case $\mathbb{T}^3$

For this case, it is chosen $A = t$ with periodic boundary conditions at $\theta = 0$ and $\theta = 2\pi$. This spacetime is the "simplest" Gowdy model. In this case, the quantity a from the metric Eq. (3.3) is usually written in terms of a new variable λ where $a := -\ln t/4 + \lambda/2$. Then, the metric takes the well-known form

$$g_{\mathbb{T}^3} = t^{-1/2}\,e^{\lambda/2}\,\left(-\mathrm{d}t^2 + \mathrm{d}\theta^2\right) + t\left(e^{P}\left(\mathrm{d}\varphi + Q\mathrm{d}\rho\right)^2 + e^{-P}\mathrm{d}\rho^2\right). \tag{3.4}$$

In the vacuum case, the evolution equations obtained from the EFE are given by

$$\begin{aligned}
\partial_{tt}P + \frac{\partial_t P}{t} - \partial_{\theta\theta}P + \left(\partial_\theta Q^2 - \partial_t Q^2\right)e^{2P} &= 0,\\
\partial_{tt}Q + \frac{\partial_t Q}{t} - \partial_{\theta\theta}Q + 2\left(\partial_t P\,\partial_t Q - \partial_\theta P\,\partial_\theta Q\right)e^{2P} &= 0,
\end{aligned}$$

with the constraints

$$\partial_t\lambda = t\left(\,\partial_t P^2 + \partial_\theta P^2 + \left(\partial_\theta Q^2 - \partial_t Q^2\right)\,\right)e^{2P}, \tag{3.5}$$

$$\partial_\theta\lambda = 2t\left(\partial_t P\,\partial_\theta P + \partial_\theta Q\,\partial_t Q\,e^{2P}\right). \tag{3.6}$$

If the integral of the right-hand side of Eq. (3.6) vanishes due to the periodic conditions; see [163], the constraints decouple from the evolution equations because λ can be computed from P and Q. Hence, in an analytic analysis one can restrict the attention to the two semi-linear coupled wave equations for P and Q with arbitrary initial data subject only to that integral condition.
Moncrief, in [134], was able to prove global existence for solutions of these equations and

showed that there is a crushing singularity in the limit $t \to \infty$. Hence, the maximal Cauchy development of generic Gowdy data sets can be covered with the coordinates in which the metric Eq. (3.4) has been written. However, this does not exclude the possibility that there could be extensions beyond these coordinates. Geodesic completeness in the expanding time direction was proven in [158]. Thus, the main problem was to study the shrinking time direction and its extendibility.
In [66, 114], the polarized case $Q = 0$ where both Killing vectors can be chosen mutually orthogonal everywhere was studied. Indeed, their techniques can be also applied to all the other allowed spatial topologies, say $\mathbb{S}^3$ and $\mathbb{S}^1 \times \mathbb{S}^2$. Strong cosmic censorship, asymptotic velocity dominance (AVTD) (hence the BKL-conjecture) was confirmed in this class. Numerical studies by Berger et al. [19, 21] and references therein support the idea that general Gowdy spacetimes are AVTD.
On the other hand due to its complexity, the non-polarized $\mathbb{T}^3$ was first numerically investigated (to our knowledge) in [22] suggesting a non-oscillatory behaviour. In fact, it was suggested to be AVTD almost everywhere with *spiky features* as the exceptional points. These are formally defined in [156] in terms of the Kretschmann scalar. There are two distinct classes of spikes, namely *false spikes* and *true spikes*. The first class can be seem as local "problems" due to the chosen coordinates without any geometric meaning causing some metric components to blow up. On the other hand, true spikes represent a localized change in the geometric behaviour of the solution at the singularity causing a localized divergence of the Kretschmann scalar. In [159, 161], Ringström showed that generic Gowdy solutions may develop a finite number of false and true spikes with an AVTD in between, that is, in the open interval between two spike points spikes, the solutions are AVTD in a precise sense. Hence, spikes cannot accumulate somewhere thus the BKL-conjecture can be confirmed. Regarding the SCC conjecture, it was also proved that these solutions are geodesically complete in the expanding direction which confirms the SCC in this case.

3.3.3 The cases $\mathbb{S}^1 \times \mathbb{S}^2$ and $\mathbb{S}^3$

Case $\mathbb{S}^1 \times \mathbb{S}^2$

The metric for this case is obtained by choosing $A = \sin t \, \sin\theta$. A spacetime with spatial topology $\mathbb{S}^1 \times \mathbb{S}^2$ is expected to have a term proportional to $\sin^2\theta \mathrm{d}\rho^2$ near the rotation axes at $\theta = 0$ and π. In these coordinates, ρ plays the role of the rotation angle at each axis. Since the metric has the term $Ae^{-P}\mathrm{d}\rho^2 = \sin t \sin\theta \; e^{-P}\mathrm{d}\rho^2$, so we need to define a new variable that differs from P by a term proportional to $-\ln(\sin\theta)$. In addition are introduced the quantities W and λ defined by $P = W - \ln A$ and $a = \lambda/2 - W/2$ respectively. Using those, the spacetime metric takes the form

$$g_{\mathbb{S}^1\times\mathbb{S}^2} = e^{\lambda - W}\left(-\mathrm{d}t^2 + \mathrm{d}\theta^2\right) + e^{W}\left(\mathrm{d}\varphi + Q\mathrm{d}\rho\right)^2 + e^{-W}\sin^2 t \sin^2\theta \, \mathrm{d}\rho^2. \tag{3.7}$$

For this metric to be regular at the rotation axes, it is required that

$$e^{\lambda}|_{\sin\theta=0} = \sin^2 t + \lim_{\sin^2\theta\to 0}\frac{Q^2}{\sin^2\theta} \quad \Rightarrow \quad \lambda|_{\theta=0,\pi} = \ln\,\sin^2 t\,. \tag{3.8}$$

Additionally, this regularity condition requires Q to be zero at both axes. Moreover, for this metric to be differentiable at the axes (or poles of $\mathbb{S}^2$), Q must be a differentiable function on $\mathbb{S}^2$ so that its derivative with respect to θ must also vanish at the axes. Similarly, the function W must be differentiable on $\mathbb{S}^2$. Thus, the boundary conditions at the axes are

$$Q|_{\theta=0,\pi} = Q_\theta|_{\theta=0,\pi} = W_\theta|_{\theta=0,\pi} = 0. \tag{3.9}$$

Case $\mathbb{S}^3$

Similar to the previous case, we choose the areal function to be $A = \sin t \, \sin\theta$. A spacetime with constant time sections with $\mathbb{S}^3$ topology would have a metric with a rotation-axis term proportional to $\theta^2 \mathrm{d}\rho^2$ near $\theta = 0$ and another rotation axis term proportional to $(\pi - \theta)\mathrm{d}\varphi$ near $\theta = \pi$. In this case, the angles φ and ρ reverse roles at the two rotation axes. Therefore, similarly as in the previous case, the spacetime metric is expressed in terms of the quantities W and λ such that $P = W - \ln\tan(\theta/2) - \ln\tan(t/2)$ and $a = \lambda/2$. Using those, the metric takes the form

$$g_{\mathbb{S}^3} = e^{\lambda}\left(-\mathrm{d}t^2 + \mathrm{d}\theta^2\right) + 4\left(e^{W}\cos^2\frac{t}{2}\cos^2\frac{\theta}{2}\left(\mathrm{d}\varphi + Q\mathrm{d}\rho\right)^2 + e^{-W}\sin^2\frac{t}{2}\sin^2\frac{\theta}{2}\,\mathrm{d}\rho^2\right) .$$

Here, the regularity conditions at the poles for Q and W are exactly the same as for the case $\mathbb{S}^1 \times \mathbb{S}^2$. On the other hand, the regularity conditions for the function λ are

$$\lambda|_{\theta=0} = -W|_{\theta=0} + \ln\left(\frac{1-\cos t}{2}\right), \quad \lambda|_{\theta=\pi} = W|_{\theta=\pi} + \ln\left(\frac{1+\cos t}{2}\right).$$

Some facts about those spacetimes

There are some complete results given by Isenberg et al. [114] restricted to the polarized case ($Q = 0$). There, the AVTD behaviour and the SCC are confirmed. Additionally, as mentioned in chapter 1, Stahl [183] made a Fuchsian analysis analogous to [116] for these spacetimes in the general case and found that under certain conditions, it can be shown that there exist a family of AVTD solutions which will imply that the SCC in the shrinking direction. However, these results are not general, hence have to be considered as partial or incomplete. Some numerical investigations on the particular cases $\mathbb{S}^1 \times \mathbb{S}^2$ and $\mathbb{S}^3$ can be found in [24, 90]. On the other hand, by implementing the *soliton method*, (see for instance [109]), some partial analytical results were obtained for the general class of this spacetimes regarding the SCC. The first one was done by Hennig et al. [110] showing that the Gowdy spacetimes $\mathbb{S}^1 \times \mathbb{S}^2$ with a regular past Cauchy horizon develop a regular future horizon if and only if a particular quantity does not vanish. Later in [32], a similar result for a certain family of metric (smooth Gowdy-symmetric generalized Taub–NUT solutions) with spatial topology $\mathbb{S}^3$ was obtained by using the mentioned method altogether with Fuchsian methods. However, the nature of the singular behaviour is slightly different for both cases: In the first case, the curvature blows up along the entire future boundary, whereas for the second case the singularities are given just at isolated points of the future Cauchy horizon.

Finally, we want to mention that one of the most recent advances in this kind of spacetime that we are aware of, was carried out by Beyer et al. [33]. There, continuing with research initiated in [32], they derive a three-parametric family of exact solutions that contains the two-parametric Taub-NUT solution as a special case. Furthermore, for a special choice of these parameters, they showed that the spacetime contains a curvature singularity with directional behaviour that can be interpreted as a "true spike" analogous to the known results on the $\mathbb{T}^3$ case. For other parameter choices, the maximal globally hyperbolic region is singularity-free but may contain "false spikes".

Chapter 4

Symmetry reduction

Generally speaking, the existence of symmetry can be used to reduce the complexity of the EFE. This fact can be exploited in order to save computational resources when attempting a numerical solution. In this chapter, we shall see how the EFE for a four-dimensional spacetime M can be reduced into an equivalent system, that we call the Geroch-Einstein system, on a three-dimensional Lorentzian manifold S. As mentioned in chapter 1, this procedure was first introduced in vacuum spacetimes by Geroch in [92], and later extended in the context of numerical relativity in the works in [58, 131, 140], just to mention a few. Owing to the relevance of this approach in both our analytical and numerical infrastructure, we present a detailed discussion of it. We conduct the following discussion based on [84, 92, 166].

4.1 The space of orbits

Let us assume (M, g_{ab}) to be a spacetime under the effective action of a one-dimensional symmetry group. Then, there is an infinitesimal generator for the transformations which leaves the metric invariant (see section A.6), namely a Killing vector ξ^a. Furthermore, it is well-known that this vector field satisfies the following equations (see for instance [195])

$$\mathfrak{D}_{(a}\xi_{b)} = 0\,, \tag{4.1}$$

$$\mathfrak{D}_a\mathfrak{D}_b\xi_c = -\mathcal{R}_{bca}{}^{d}\xi_d. \tag{4.2}$$

Let us consider the orbits of the symmetry transformation. These are lines that split the entire spacetime into a set of lines. The Killing vector is tangent to those lines which can be considered integral curves of ξ^a. Next, we define *the space of orbits* S by considering the map

$$\pi : M \to S\,, \tag{4.3}$$

which assigns to each point in M the orbit that it lies on. Assuming this map is differentiable, it introduces a differential structure in S. Since ξ^a is tangent to the orbits and because π collapses each line in M to a point in S,

$$\pi_*\xi^a = 0. \tag{4.4}$$

Since S is a differentiable manifold, it can be defined a tensor algebra over its tangent bundle. Furthermore, since S is derived from M, it is possible to represent its tensor algebra in terms of the tensors algebra over M. To do so, let us consider a scalar field $\zeta : S \to R$. Then $\hat{\zeta} := \zeta \circ \pi : M \to \mathbb{R}$ is a scalar field on M which is constant along the symmetry lines, that is,

$$\xi^a\mathfrak{D}_a\hat{\zeta} = \mathcal{L}_\xi\hat{\zeta} = 0.$$

Inversely, every scalar field in M that is constant along the symmetry lines can be written as a scalar field in S combined with the projection map π. Next, consider a one-form α_a on S. Its pull-back $\hat{\alpha}_a = \pi^* \alpha_a$ is a one-form in M which satisfies the following two conditions:

$$\begin{aligned} \mathcal{L}_\xi \hat{\alpha}_a &= \mathcal{L}_{\xi^a} \pi^* \alpha_a = \pi^* \mathcal{L}_{\pi_* \xi^a} \alpha_a = 0, \\ \langle \pi^* \alpha_a, \xi^a \rangle &= \langle \alpha_a, \pi_* \xi^a \rangle = 0 \,. \end{aligned}$$

Conversely, every one-form in M satisfying these two conditions comes from a unique one-form in S. Next, we consider vector fields in S. Since the algebra of functions in S is represented by functions in M, which are constant along ξ^a, every vector field v^a in M defines a vector field in S provided that

$$\xi^a(\zeta) = 0 \implies \xi^a(v(\zeta)) = 0.$$

Note that when acting on scalars in S (represented on M), we obtain $v^a(\zeta) = (v^a + q\, \xi^a)(\zeta)$, so that the vectors v^a and $v^a + q\xi^a$ must be considered as "equivalent" for any function q in M. Thus, let $\{v^a\}$ be the equivalence class of v^a. It follows that

$$[\xi^a, v^b](\zeta) = \xi^a(v^b(\zeta)) - v^b(\xi^a(\zeta)) = 0,$$

when acting on scalar field in S. Therefore, the commutator will be in general

$$[\xi^a, v^a] = q\, \xi^a,$$

for some function q in M such that the commutator $[\xi^a, v^b]$ is equivalent to the zero vector field. We can always find a representative vector v^a in $\{v^a\}$ such that the commutator with ξ^a vanishes. These representatives are distinguished by scalars in S, that is, $\{v^a\} = \{v^a + \tilde{\psi}\, \xi^a\}$ for some $\tilde{\psi}$ that is constant along ξ^a. This implies that we can represent a vector field in S by an equivalence class of vector fields in M with the property

$$\mathcal{L}_{\xi^a} v^b = 0. \tag{4.5}$$

In order to find a unique representative vector, we have to impose the condition that ξ_a is spacelike, i.e.,

$$\tilde{\psi} := \xi_a \xi^a > 0. \tag{4.6}$$

Therefore, a unique representative vector v^a of the equivalence class $\{v^a\}$ can be fixed by requiring $v^a \xi_a = 0$.

Following similar arguments as above, it can be concluded that any tensor $T^{a\ldots}{}_{b\ldots}$ in S can be represented as a tensor in M subject to the following conditions

$$T^{a\ldots}{}_{b\ldots}\, \xi_a = 0 = T^{a\ldots}{}_{b\ldots}\, \xi^b, \tag{4.7}$$

$$\mathcal{L}_{\xi^c} T^{a\ldots}{}_{b\ldots} = 0. \tag{4.8}$$

In other words, the Lie derivative along the vector ξ^a as well as any other contraction with ξ^a or ξ_a vanishes. Finally, because of the tensor algebraic compositions (outer product, scalar multiplication and contractions) commutes with the map π, the entire tensor algebra in S is completely and uniquely mirrored by tensors in M subject to the previous two conditions.

4.2 Induced tensor fields in S

Next, we define the induced metric $\tilde{h}_{ab}$ in S, the projector operator $\tilde{h}^a{}_b$ from M to S and the volume element ε_{abc} compatible with $\tilde{h}_{ab}$ by

$$\tilde{h}_{ab} = g_{ab} - \frac{1}{\tilde{\psi}}\xi_a\xi_b \,, \tag{4.9}$$

$$\tilde{h}^a_b = \delta^a_b - \frac{1}{\tilde{\psi}}\xi^a\xi_b \,, \tag{4.10}$$

$$\varepsilon_{abc} = \frac{1}{\tilde{\psi}^{1/2}}\varepsilon_{abcd}\xi^d \,, \tag{4.11}$$

where ε_{abcd} is the antisymmetric Levi-Civita tensor (Eq. (A.5.4)) associated with g_{ab}. Evidently, all these fields are in S since they satisfy conditions Eqs. (4.7) and (4.8). To define the induced connection in S, let us consider the one-form α_a in S. Then, the covariant derivative in S is defined as

$$\tilde{D}_a\alpha_b = \tilde{h}_a{}^p\tilde{h}_b{}^q\mathfrak{D}_p\alpha_q \,, \tag{4.12}$$

i.e., the covariant derivative in M is projected to S by the action of $\tilde{h}_b{}^q$. Next, we define some other fields in S that will allow us to express the geometry of S in terms of field in M. To start with, let us consider $\tilde{\psi}$ being the *norm* of the Killing vector field Eq. (4.6). This scalar field is in S owing to

$$\xi^c\mathfrak{D}_c\tilde{\psi} = 2\xi^a\xi^c\mathfrak{D}_c\xi_a = 0.$$

On the other hand, we define the *twist* of the Killing vector ξ^a as

$$\Omega_a = \varepsilon_{abcd}\,\xi^b\mathfrak{D}^c\xi^d, \tag{4.13}$$

which is by construction, orthogonal to ξ^a. In virtue of the Frobenius theorem (see [195]), the vanishing of Ω_a is exactly the condition for the hypersurface orthogonality of the Killing vector to S. In what follows we list some properties of these quantities which will be used in the next section to relate the geometry of S and M. Next, we express the covariant derivative of ξ_a as the sum of two terms, one orthogonal to ξ_a and another term proportional to ξ_a. To do so, we make the ansatz

$$\mathfrak{D}_a\xi_b = \varepsilon_{abcd}\xi^c v^d + 2\xi_{[a}u_{b]} \,,$$

with v^a and u^a both orthogonal to ξ^a. Transvecting with ξ^b results in

$$\frac{1}{2}\mathfrak{D}_a\tilde{\psi} = -\tilde{\psi}u_b = \frac{1}{2}\tilde{D}_a\tilde{\psi}. \tag{4.14}$$

Skewing with ξ_c and taking the dual we obtain

$$\varepsilon^{dcab}\xi_c\mathfrak{D}_a\xi_b = -2\xi_c\left(\delta_p{}^d\delta_q{}^c - \delta_p{}^c\delta_q{}^d\right)\xi^p v^q = 2\tilde{\psi}v^d,$$

from where the covariant derivative of ξ can be written as

$$\mathfrak{D}_a\xi_b = \frac{1}{2\tilde{\psi}}\varepsilon_{abcd}\xi^c\Omega^d - \frac{1}{\tilde{\psi}}\xi_{[a}\tilde{D}_{b]}\tilde{\psi}. \tag{4.15}$$

Using the relation above, we obtain the useful formula (which will be used in the next section)

$$\begin{aligned}\mathfrak{D}_a\xi^c\mathfrak{D}_b\xi_c \;=\; & \frac{1}{4\tilde{\psi}}\Big(\tilde{D}_a\tilde{\psi}\tilde{D}_b\tilde{\psi} + \Omega_a\Omega_b - \tilde{h}_{ab}\Omega_c\Omega^c \\ & + \frac{1}{\tilde{\psi}}\,\xi_a\xi_b\tilde{D}_c\tilde{\psi}D^c\tilde{\psi} - 2\xi_{(b}\varepsilon_{a)cde}\,\xi^c\Omega^d D^e\tilde{\psi}\Big).\end{aligned} \tag{4.16}$$

Now, we list some relations for the one-form Ω_a. We start by writing its covariant derivative as

$$\mathfrak{D}_e\Omega_a = \varepsilon_{acdf}R_{eb}{}^{df}\xi^b\xi^c + \frac{1}{2\tilde{\psi}}\, g_{ae}\Omega^b\tilde{D}_b\tilde{\psi}\,.$$

On the other hand, we compute the divergence and curl of the twist in terms of the covariant derivative of S. To do so, noting that $\tilde{D}^a\Omega_a = \mathfrak{D}^a\Omega_a$, it can be obtained

$$\tilde{D}^a\Omega_a = \varepsilon_{abcd}\mathfrak{D}^a\xi^b\mathfrak{D}^c\xi^d + \varepsilon_{abcd}\xi^b\mathfrak{D}^a\mathfrak{D}^c\xi^d\,.$$

Finally, using Eq. (4.16) in the first term and Eq. (4.2) in the second term, we obtain

$$\tilde{D}^a\Omega_a = \frac{3}{2\tilde{\psi}}\Omega^b\tilde{D}_b\tilde{\psi}\,, \tag{4.17}$$

$$\tilde{D}_{[a}\Omega_{b]} = -\varepsilon_{abcd}\xi^c\mathcal{R}^d{}_e\xi^e. \tag{4.18}$$

4.3 Relation between the geometry of M and S

In this section, we express the components of the Riemann tensor $R_{abc}{}^d$ of M in terms of certain fields in S. These relations will expose the relation between the geometry of both manifolds, and will consequently allow us to "project" the EFE from the four dimensional manifold M to the space of orbits S.
To begin with, let us note that there are three parts of the Riemann tensor of M which will have to be treated differently. These are

$$\mathcal{R}_{\underline{abcd}}, \quad \mathcal{R}_{\underline{abc}d}\xi^d, \quad \mathcal{R}_{\underline{ab}cd}\xi^b\xi^d\,, \tag{4.19}$$

which thanks to the symmetry and antisymmetry properties listed in Eqs. (A.4.2), encode all the independent components of the Riemann tensor. The underlined indices indicate projection with $\tilde{h}_a{}^b$. Because these three parts are tensor fields in S, we will express them in terms of fields in S. Using the curvature identity for ξ^a, Eq. (4.2), and Eq. (4.16), we obtain

$$\begin{aligned}
-\mathcal{R}_{bcad}\xi^c\xi^d &= \xi^c\mathfrak{D}_a\mathfrak{D}_b\xi_c = \mathfrak{D}_a\left(\xi^c\mathfrak{D}_b\xi_c\right) - \mathfrak{D}_a\xi^c\mathfrak{D}_b\xi_c, \\
&= \frac{1}{2}\mathfrak{D}_a\mathfrak{D}_b\tilde{\psi} - \frac{1}{4\tilde{\psi}}\Big(\,\tilde{D}_a\tilde{\psi}\tilde{D}_b\tilde{\psi} + \Omega_a\Omega_b - h_{ab}\Omega_c\Omega^c \\
&\quad + \frac{1}{\tilde{\psi}}\,\xi_a\xi_b\tilde{D}_c\tilde{\psi}\;D^c\tilde{\psi} - 2\xi_{(b}\varepsilon_{a)cde}\xi^c\Omega^dD^e\tilde{\psi}\,\Big).
\end{aligned} \tag{4.20}$$

The left-hand side of this expression is manifestly orthogonal to ξ^a. Hence, it can be projected to S without loss of generality

$$-\mathcal{R}_{\underline{ab}\underline{c}d}\xi^b\xi^d = \frac{1}{2}\tilde{D}_a\tilde{D}_c\tilde{\psi} - \frac{1}{4\tilde{\psi}}\left(\tilde{D}_a\tilde{\psi}\tilde{D}_c\tilde{\psi} + \Omega_a\Omega_c - h_{ac}\Omega_b\Omega^b\right)\,. \tag{4.21}$$

Next, we look at the components $\mathcal{R}_{\underline{abc}d}\xi^d$ which can be obtained from the Killing equation Eq. (4.2) by projecting all the indices. So we have

$$-\mathcal{R}_{\underline{abc}d}\xi^d = \frac{1}{4\tilde{\psi}^{3/2}}\left(\varepsilon_{bcd}\tilde{D}_a\tilde{\psi} + \varepsilon_{cad}\tilde{D}_b\tilde{\psi} + \varepsilon_{abd}\tilde{D}_c\tilde{\psi}\right)\Omega^d - \frac{1}{2\tilde{\psi}^2}\varepsilon_{bcd}\tilde{D}_a\Omega^d\,. \tag{4.22}$$

The final part of the Riemann tensor is the completely projected one. We show by establishing a relation between the covariant derivatives between both spaces that it can be written in

terms of the Riemann tensor from S. We start by considering the term $\tilde{D}_a\tilde{D}_b\alpha_c$ for an one-form α_a in S. Then using Eqs. (4.9), (4.10) and (4.12) yields the relation

$$\begin{aligned}\tilde{D}_a\tilde{D}_b\alpha_c &= \tilde{h}^p{}_a\tilde{h}^q{}_b\tilde{h}^r{}_c\mathfrak{D}_p\left(\tilde{h}^s{}_q\tilde{h}^t{}_r\mathfrak{D}_s\alpha_t\right)\\ &= \tilde{h}^p{}_a\tilde{h}^q{}_b\tilde{h}^t{}_c\mathfrak{D}_p\mathfrak{D}_s\alpha_t - \frac{1}{\tilde{\psi}}\,\tilde{h}^p{}_a\tilde{h}^q{}_b\tilde{h}^r{}_c\,(\mathfrak{D}_p\alpha_q)\,\xi^s\mathfrak{D}_s\alpha_r\\ &\quad -\frac{1}{\tilde{\psi}}\,\tilde{h}^p{}_a\tilde{h}^q{}_b\tilde{h}^r{}_c\,(\mathfrak{D}_p\alpha_r)\,\xi^t\mathfrak{D}_q\alpha_t\,.\end{aligned}$$

Note that we have not used the underlined indices to indicate projection with respect to $\tilde{h}_a{}^b$ because the metric in S do not commute with the covariant derivative operator $\mathfrak{D}$ in M. Now, anti-symmetrizing over the indices a and b we can eliminate the derivatives of α_t on the right-hand side of the equation. In addition, using for the second term Eq. (4.7) and for the third one Eq. (4.8), it is obtained

$$\tilde{D}_{[a}\tilde{D}_{b]}\alpha_c = \mathfrak{D}_{[\underline{a}}\mathfrak{D}_{\underline{b}]}\alpha_{\underline{c}} - \frac{1}{\tilde{\psi}}\left((\mathfrak{D}_{\underline{a}}\alpha_{\underline{b}})(\mathfrak{D}_{\underline{c}}\xi_s)\alpha^s - (\mathfrak{D}_{[\underline{a}|}\alpha_{\underline{c}})(\mathfrak{D}_{|\underline{b}]}\xi_d)\,\alpha^d\right).$$

Using this expression altogether with Eq. (A.4.3), we obtain the relation between the Riemann tensor $\tilde{R}$ in S and the Riemann tensor $\mathcal{R}$ in M given by the following expression

$$-\mathcal{R}_{\underline{abcd}} = -\tilde{R}_{abcd} + \frac{2}{\tilde{\psi}}\Big(\mathfrak{D}_{\underline{a}}\xi_{\underline{b}}\mathfrak{D}_{\underline{c}}\xi_{\underline{d}} + \mathfrak{D}_{\underline{a}}\xi_{\underline{c}}\mathfrak{D}_{\underline{b}}\xi_{\underline{d}} - \mathfrak{D}_{\underline{b}}\xi_{\underline{a}}\mathfrak{D}_{\underline{c}}\xi_{\underline{d}} - \mathfrak{D}_{\underline{b}}\xi_{\underline{c}}\mathfrak{D}_{\underline{a}}\xi_{\underline{d}}\Big). \tag{4.23}$$

Finally, contracting Eqs. (4.20), (4.21), (4.23) and using the relations listed in the last section for ξ^a and Ω_a, we obtain the total decomposition for the Ricci tensor of M in terms of fields in S by

$$-2\xi^a\xi^b\mathcal{R}_{ab} = \frac{1}{2}\tilde{D}^c\tilde{D}_c\tilde{\psi} - \frac{1}{4\tilde{\psi}}\left(\tilde{D}_a\tilde{\psi}D^a\tilde{\psi} - 2\Omega_c\Omega^c\right), \tag{4.24}$$

$$-\xi^b\mathcal{R}_{\underline{ab}} = \frac{1}{2\tilde{\psi}^2}\,\varepsilon_{abc}\tilde{D}^b\Omega^c, \tag{4.25}$$

$$-\mathcal{R}_{\underline{ab}} = -\tilde{R}_{ab} + \frac{1}{2\tilde{\psi}}\tilde{D}_a\tilde{D}_b\tilde{\psi} - \frac{1}{4\tilde{\psi}^2}\left(2\tilde{D}_a\tilde{\psi}\tilde{D}_b\tilde{\psi} - \Omega_a\Omega_b + \tilde{h}_{ab}\Omega_c\Omega^c\right). \tag{4.26}$$

4.4 Geroch-Einstein system

Having expressed the Ricci tensor of M in terms of fields in S, we can "project" the EFE from M to S. To begin with, let us note that Eq. (4.24) and Eq. (4.26) contain second evolution equations for the norm $\tilde{\psi}$ and the metric components $\tilde{h}_{ab}$ respectively. On the other hand Eq. (4.25) (which is equivalent to the twist curl Eq. (4.18)), represents a constraint equation[1]. This equation, altogether with Eq. (4.17), will be the constraints coming from the symmetry reduction. However, for the vacuum case, those constraints turned into a evolution equation for some given scalar field as follows.

By substituting Eq. (2.2) into Eq. (4.18), we obtain that Ω_a is closed form, i.e., it satisfies $\mathrm{d}\Omega = 0$. By virtue of Poincaré's theorem (see for instance [184]), it can be introduced a *twist potential* $\tilde{\omega}$ such that

$$\Omega = \mathrm{d}\tilde{\omega} \quad\Longleftrightarrow\quad \Omega_a = \tilde{D}_a\tilde{\omega}. \tag{4.27}$$

[1] Some authors refer to it as Geroch constraint [166, 168]

Then, replacing the twist potential in Eq. (4.17) and using equations Eqs. (4.24) and (4.26) in the vacuum EFE, the coupled system of evolution equations is obtained

$$\begin{aligned}
\tilde{D}_a\tilde{D}^a\tilde{\psi} &= \frac{1}{2\tilde{\psi}}\tilde{D}^a\tilde{\psi}\tilde{D}_a\tilde{\psi} - \frac{1}{\tilde{\psi}}\tilde{D}^a\tilde{\omega}\tilde{D}_a\tilde{\omega} - 2\Lambda\tilde{\psi},\\
\tilde{D}_a\tilde{D}^a\tilde{\omega} &= \frac{3}{2\tilde{\psi}}\tilde{D}^a\tilde{\psi}\tilde{D}_a\tilde{\omega},\\
\tilde{R}_{ab} &= \frac{1}{2\tilde{\psi}}\tilde{D}_a\tilde{D}_b\tilde{\psi} - \frac{1}{4\tilde{\psi}^2}\tilde{D}_a\tilde{\psi}\tilde{D}_b\tilde{\psi} + \frac{1}{2\tilde{\psi}^2}\left(\tilde{D}_a\tilde{\omega}\tilde{D}_b\tilde{\omega} - \hat{h}_{ab}\tilde{D}_c\tilde{\omega}\tilde{D}^c\tilde{\omega}\right) + \tilde{\psi}\tilde{h}_{ab}\,,
\end{aligned} \tag{4.28}$$

for the variables $\tilde{\psi}, \tilde{\omega}$ and $\tilde{h}_{ab}$. Note that the constraint equations for the one-form Ω_a are implicitly "transported" by the evolution of the variable $\tilde{\omega}$, i.e., $\tilde{\omega}$ evolves such that the constraint equations from the symmetry reduction Eqs. (4.18) and (4.17) are propagated. Unfortunately, written in this way, the above system of evolution equations is not suitable for the numerical scheme that will be introduced in chapter 6. The reason lies in the fact that there are second-order derivatives of the norm $\tilde{\psi}$ in the right-hand side of the third equation which spoils the hyperbolicity of the whole system. We overcome this difficulty is by considering the conformal rescaling

$$\hat{h}_{ab} := \psi\tilde{h}_{ab}. \tag{4.29}$$

Using the conformal transformations listed in Eqs. (A.4.5) and (A.4.7), we can obtain an equivalent system of evolution equations in which there are not second-order derivatives in the right-hand side of the equations. For reasons of hyperbolicity that we shall clarify later in section 6.3.2, this is the suitable form for our numerical implementation. Before writing the resulting system, let us reduce the dimensionality of the equations. As aforementioned, because the map π is smooth, it induces a differentiable structure in S, hence it can be considered as a smooth manifold in three dimensions. Thus, there is a unique smooth Lorentzian metric in S that is pulled back to $\hat{h}_{ab}$ along π. We write this metric in S as h_{ab}. Conversely, there are unique functions ψ and Ω_a, which pull back the norm $\tilde{\psi}$ and twist potential $\tilde{\omega}$ of ξ^a. Then, using the conformal transformations into the system Eqs. (4.28) we obtain the *Geroch-Einstein system* (GES)

$$\begin{aligned}
\nabla_a\nabla^a\psi &= \frac{1}{\psi}\left(\nabla_a\psi\nabla^a\psi - \nabla_a\omega\nabla^a\omega\right) - 2\Lambda,\\
\nabla_a\nabla^a\omega &= \frac{1}{\psi}\nabla^a\psi\nabla_a\omega,\\
R_{ab} &= E_{ab} + \frac{2\Lambda}{\psi}h_{ab}\,,
\end{aligned} \tag{4.30}$$

where

$$E_{ab} = \frac{1}{2\psi^2}\left(\nabla_a\psi\nabla_b\psi + \nabla_a\omega\nabla_b\omega\right), \tag{4.31}$$

and R_{ab} being the three-dimensional Ricci tensor corresponding to the space of orbits S. Note that we have used ∇_a to denote the three-dimensional covariant derivative operator associated with the metric h_{ab}. In addition, using the evolution equation of the scalar fields ψ and ω it can be easily checked that the tensor

$$T_{ab} = E_{ab} - \frac{1}{2}h_{ab}E, \tag{4.32}$$

is divergence free. Thus, it plays the role of the energy momentum tensor given by the coupling between the three-dimensional gravity and two scalar fields ψ and ω. As a result, the GES can be interpreted as 2+1 gravity model coupled to two scalar fields. The corresponding EFE in S takes the form

$$G_{ab} + \frac{\Lambda}{\psi} h_{ab} = T_{ab} \, . \tag{4.33}$$

where G_{ab} is the Einstein tensor in terms of R_{ab}.

4.5 Reconstruction of the four-dimensional Kretschmann scalar

The Kretschmann scalar (Eq. (A.4.4)) is an invariant gauge geometric quantity that will play an important in this work. In order to compute this quantity for the four dimensional manifold M, we need to have full knowing of the four-dimensional Riemann tensor. It can be obtained by using the four-dimensional metric of M, which could be reconstructed following the general procedure that will be described in detail in section 4.6. However, since this way may involves solving some differential equations, it may turn out to be inconvenient from the numerical point of view. A better way to obtain the twenty independent components of the Riemann tensor of M is by means of the projection relations Eqs. (4.21), (4.22), (4.23). In particular, we can obtain the four-dimensional Riemann tensor with respect to the three frame vectors in S after being pulled back to M and the Killing vector ξ^a. This will allow us to obtain the corresponding Kretschmann scalar of M in terms of quantities in S. To begin with, let us write the Riemann tensor of M as

$$\mathcal{R}_{abcd} = (\delta_a{}^p \delta_b{}^q \delta_c{}^r \delta_d{}^s) \mathcal{R}_{pqrs}. \tag{4.34}$$

Then, using Eq. (4.10) we obtain after a straightforward computation that the Riemann tensor be expressed as

$$\begin{aligned} \mathcal{R}_{abcd} \;=\; & \mathcal{R}_{\underline{abcd}} + \frac{1}{\psi}\left(\mathcal{R}_{\underline{abc}p}\xi^p\xi_d - \mathcal{R}_{\underline{abd}p}\xi^p\xi_c + \mathcal{R}_{\underline{apcd}}\xi^p\xi_b - \mathcal{R}_{\underline{bpcd}}\xi^p\xi_a\right) \\ & \frac{1}{\psi^2}\left(\mathcal{R}_{\underline{bpdq}}\xi^p\xi^q\xi_a\xi_c - \mathcal{R}_{\underline{apdq}}\xi^p\xi^q\xi_b\xi_c + \mathcal{R}_{\underline{apcq}}\xi^p\xi^q\xi_b\xi_d - \mathcal{R}_{\underline{bpcq}}\xi^p\xi^q\xi_a\xi_d\right). \end{aligned} \tag{4.35}$$

In order to compute the Kretschmann scalar in M, we contract each covariant term of the right-hand side with respect to its respective contravariant version. Then, using the symmetric and antisymmetric properties of the Riemann tensor listed in Eqs. (A.4.2), the Kretschmann scalar can be expressed as

$$K = \mathcal{R}_{\underline{abcd}}\mathcal{R}^{\underline{abcd}} + \frac{4}{\psi}\mathcal{R}_{\underline{abc}p}\xi^p\mathcal{R}^{\underline{abcd}}\xi_d + \frac{4}{\psi^2}\mathcal{R}_{\underline{apcq}}\xi^p\xi^q\mathcal{R}^{\underline{abcd}}\xi_b\xi_d. \tag{4.36}$$

Clearly, by using the projection relations Eqs. (4.21), (4.22), (4.23) this quantity can be completely expressed in terms of the fields in the space of orbits S. This expression plays an important role in this work; in particular it will be used in chapters 9.4.2 and 10.

4.6 Reconstruction of the four-dimensional metric

It is expected that from the dynamics of S, we will be able to reconstruct the evolution of the four-dimensional manifold M. In what follows, we describe how this task can be carried out. To begin with, let us consider the following two-form in S,

$$\alpha_{ab} := \frac{1}{\psi^2}\varepsilon_{abc}D^c\omega, \tag{4.37}$$

which can be proved to be curl-free, see [92] for details[2]. Thus, there exits a one-form $\hat{\eta}_a$ in S such that

$$\mathrm{d}\eta = \alpha \quad \Longleftrightarrow \quad \nabla_{[a}\eta_{b]} = \alpha_{ab}. \tag{4.38}$$

Note that, in general, it is difficult to find an analytical solution for the expression above. In section 6.5, we discuss how to address numerically this question. By now, let us assume that we are able to solve the above system of equations by whatever means. Using the commutation rule between the pull back and the exterior derivative operator [195], we can pull back Eq. (4.38) to the four-dimensional manifold M such that

$$\mathrm{d}\tilde{\eta} = \tilde{\alpha}, \tag{4.39}$$

where $\tilde{\alpha}_a := \pi^*\alpha_a$ and $\tilde{\eta}_a := \pi^*\eta_a$ are forms in M. Furthermore, by consequence of Eq. (4.4) it follows

$$\tilde{\eta}_a\left(\xi^a\right) = \pi^*\eta_a\left(\xi^a\right) = \eta_a\left(\pi_*\xi^a\right) = 0.$$

Notice that we always can add the gradient of a scalar function to $\tilde{\eta}$ without breaking Eq. (4.39). Hence, we use this freedom for adding the one-form $\mathrm{d}\rho$ such that

$$\tilde{\eta} = \pi^*\eta + \mathrm{d}\rho \quad \Longrightarrow \quad \xi^a\tilde{\eta}_a = 1.$$

Finally, we pull back the metric $\hat{h}_{ab}$ from S to M to obtain another bilinear form $\tilde{h}_{ab}$ orthogonal to ξ^a. Then, the metric in M can be written as

$$g_{ab} = \tilde{h}_{ab} + \tilde{\psi}\tilde{\eta}_a\tilde{\eta}_b. \tag{4.40}$$

Note that ξ^a is a Killing vector of the metric g_{ab} since its coordinates components (by construction) do not depend of the coordinate ρ. The metric g_{ab} does not seem to be unique because we can always add (apart of $\mathrm{d}\rho$) a gradient of some scalar function f to $\tilde{\eta}_a$ such that, the conditions $\xi^a\tilde{\eta}_a = 1$ and Eq. (4.39) holds. However, this freedom only represents a shifting in the coordinate ρ by the function f, hence it does not have any geometrical meaning.

[2] In the original work [92] it was proved that the quantity $\hat{\alpha}_{ab} := \psi^{-3/2}\hat{\varepsilon}_{abc}\hat{D}^c\omega$ is curl-free, where the "hat" indicates that it is given in terms of the reduced metric $\hat{h}_{ab}$. Then, using the conformal transformation Eq. (6.1) we can obtain the curl-free quantity Eq. (4.37) in terms of the evolution metric h_{ab}.

Chapter 5

Generalities of the manifold $\mathbb{S}^2$

As mentioned in chapter 1, in this thesis we will investigate Gowdy spacetimes with spatial topologies $\mathbb{S}^3$ and $\mathbb{S}^1 \times \mathbb{S}^2$. However, based on the symmetry reduction discussed in chapter 4, the analytical and numerical implementation will be carried out (see chapter 6) in the space of orbits S with spatial topology $\mathbb{S}^2$. Hence, due to the important role of this manifold in our approach, we devote the following chapter to discussing some of the most relevant geometric aspects which will be used later along this work. We begin by using the isomorphism between $\mathbb{S}^3$ and SU(2) (see section A.6) in order to find a smooth global vector field on $\mathbb{S}^3$ which, by means of the Hopf map, can be used to define a frame in $\mathbb{S}^2$. Consequently, by introducing the well-known Wigner d-matrices (see for instance [133]), we define the notion of spin-weight of functions on $\mathbb{S}^2$ and introduce a global basis to describe those, namely the spin-weight spherical harmonics. Then, some of their most important properties are listed, including their relation with the raising and lowering differential operators known as eth-operators. Finally, by setting a smooth complex frame on $\mathbb{S}^2$, the components of any tensor field on $\mathbb{S}^2$ are written with a well-defined spin-weight. We base the following presentation on [24,30,80,133,139,172]

5.1 Smooth frame on $\mathbb{S}^3$

In this section we proceed to construct a smooth global manifold on $\mathbb{S}^3$. Let us start defining the manifold $\mathbb{S}^3$ as the sub-manifold of $\mathbb{R}^4$ given by

$$\mathbb{S}^3 := \{ \, (x_1, x_2, x_3, x_4) \in \mathbb{R}^4 \ : \ x_1^2 + x_2^2 + x_3^2 + x_4^2 = 1 \, \} \, . \tag{5.1}$$

Next, consider the group of complex unitary 2×2-matrices with unit determinant SU(2). This group considered as a subset of $\mathbb{R}^4$ obtains a natural smooth manifold structure. Moreover, it is a well-known fact that it is diffeomorphic with $\mathbb{S}^3$ through the map $\Psi : \mathbb{S}^3 \to \mathrm{SU}(2)$ defined by (see [80])

$$\Psi(x_1, x_2, x_3, x_4) := \begin{pmatrix} x_3 + i x_4 & -x_1 + i x_2 \\ x_1 + i x_2 & x_3 - i x_4 \end{pmatrix} \, . \tag{5.2}$$

Since the latter is a smooth Lie group, we can use the map Ψ to endow $\mathbb{S}^3$ with a Lie group structure (see section A.6). Hence, both SU(2) and $\mathbb{S}^3$ can be considered as identical Lie groups via the map Ψ. Henceforth, we will not distinguish any more between $\mathbb{S}^3$ with SU(2). One of the main properties of Lie groups is that they are parallelizable, that is, a smooth global frame can always be constructed at each point. In particular, we can find a smooth

global frame on SU(2) as follows. Let us define for every $u \in \mathrm{SU}(2)$ the left translation map $L_u : \mathrm{SU}(2) \to \mathrm{SU}(2)$ as[1]

$$L_u(v) := uv\,. \tag{5.3}$$

Note that the map L_u is a diffeomorphism from the group to itself for each element u. We choose a basis of the tangent space at the unit element $T_e(\mathrm{SU}(2))$, i.e., a basis $\{\sigma_i\}$ such that satisfies the Lie algebra $[\sigma_i, \sigma_j] = \varepsilon_{ijk}\sigma_k$ for some given functions ϵ_{ijk}. The standard choice for this basis are the *Pauli matrices*

$$\sigma_1 = \frac{1}{2}\begin{pmatrix} 0 & i \\ i & 0 \end{pmatrix}, \quad \sigma_2 = \frac{1}{2}\begin{pmatrix} 0 & -1 \\ 1 & 0 \end{pmatrix}, \quad \sigma_3 = \frac{1}{2}\begin{pmatrix} i & 0 \\ 0 & -i \end{pmatrix}.$$

For all $u \in \mathrm{SU}(2)$, we define the left invariant smooth global frame $\{\chi_i^a\}$ on $\mathbb{S}^3$ as

$$\chi_i^a : u \mapsto (\chi_i)_u := (L_u)_*(\sigma_i).$$

Via Ψ we can consider SU(2) as a sub-manifold of $\mathbb{R}^4$. According to Eq. (5.2), the smooth global frame $\{\chi_i^a\}$ in terms of the standard coordinates (x_1, x_2, x_3, x_4) is written as (see [139])

$$\begin{aligned} 2\chi_1^a &= x_4\partial_{x_1}^a + x_3\partial_{x_2}^a - x_2\partial_{x_3}^a - x_1\partial_{x_4}^a, \\ 2\chi_2^a &= x_3\partial_{x_1}^a - x_4\partial_{x_2}^a - x_1\partial_{x_3}^a + x_2\partial_{x_4}^a, \\ 2\chi_3^a &= -x_2\partial_{x_1}^a + x_1\partial_{x_2}^a - x_4\partial_{x_3}^a + x_3\partial_{x_4}^a. \end{aligned} \tag{5.4}$$

Now, we want to introduce more "suitable" coordinates to describe the above frame. The *Euler coordinates* of $\mathbb{S}^3$ are defined by

$$\begin{aligned} x_1 &= \cos\frac{\theta}{2}\cos\lambda_1, \quad x_2 = \cos\frac{\theta}{2}\sin\lambda_1, \\ x_3 &= \sin\frac{\theta}{2}\cos\lambda_2, \quad x_4 = \sin\frac{\theta}{2}\sin\lambda_2, \end{aligned}$$

where $\theta \in (0, \pi)$ and $\lambda_1, \lambda_2 \in (0, 2\pi)$. Clearly, these coordinates break down at $\theta = 0$ and π. For convenience, we introduce coordinates (θ, ρ, φ) (which are also referred in the literature to Euler coordinates) such that

$$\lambda_1 = (\rho + \varphi)/2, \quad \lambda_2 = (\rho - \varphi)/2, \tag{5.5}$$

where $\rho, \varphi \in (0, 2\pi)$. One of the main reasons to introduce such coordinates is that the vector fields ∂_ρ^a and ∂_φ^a are smooth non-vanish vector fields in $\mathbb{S}^3$, unlike $\partial_{\lambda_1}^a$ and $\partial_{\lambda_2}^a$ which vanish at certain places. When $\theta = 0$, the vector field $\partial_{\lambda_2}^a$ vanishes, while $\partial_{\lambda_1}^a$ vanishes at $\theta = \pi$. On the other hand, the vectors ∂_ρ^a and ∂_φ^a become parallel at the poles ($\theta = 0, \pi$) but never vanish. Finally, using these coordinates, the smooth frame $\{\chi_i^a\}$ can be written as (see [24])

$$\begin{aligned} \chi_1^a &= -\sin\rho\,\partial_\theta^a - \cos\rho\left(\cot\theta\partial_\rho^a - \csc\theta\partial_\varphi^a\right), \\ \chi_2^a &= -\cos\rho\,\partial_\theta^a + \sin\rho\left(\cot\theta\partial_\rho^a - \csc\theta\partial_\varphi^a\right), \\ \chi_3^a &= \partial_\rho^a. \end{aligned} \tag{5.6}$$

In the next section we will use this frame to construct a local smooth frame on $\mathbb{S}^2$.

[1] Also we could have defined the right translation as $R_u(v) := vu$. This translation can generate an equivalent smooth global frame in SU(2) to the one generated by the left transformation.

5.2 Construction of a frame for $\mathbb{S}^2$

Similarly to $\mathbb{S}^3$, the manifold $\mathbb{S}^2$ is defined as the sub-manifold of $\mathbb{R}^3$ satisfying

$$\mathbb{S}^2 := \{\ (y_1, y_2, y_3) \in \mathbb{R}^3\ :\ y_1^2 + y_2^2 + y_3^2 = 1\ \}\,.$$

Now, consider the *Hopf map* $\pi : \mathbb{S}^3 \to \mathbb{S}^2$ defined in Cartesian coordinates by

$$\pi(x_1, x_2, x_3, x_4) = (\ 2(x_1x_3 + x_2x_4),\ 2(x_2x_3 - x_1x_4),\ x_1^2 + x_2^2 - x_3^2 - x_4^2\ ).$$

Using the Euler coordinates (θ, ρ, ϕ), this map can be written as

$$\pi(\theta, \rho, \varphi) = (\sin\theta\cos\varphi, \sin\theta\sin\varphi, \cos\theta).$$

Therefore, writing $y_1 = \sin\theta\cos\varphi$, $y_2 = \sin\theta\sin\varphi$, $y_3 = \cos\theta$, we can introduce polar coordinates (θ, φ) in $\mathbb{S}^2$ for which the Hopf map π obtains the simple representation

$$\pi : (\theta, \rho, \varphi) \mapsto (\theta, \varphi). \tag{5.7}$$

In other words, θ and φ will be understood as representing coordinates in either $\mathbb{S}^3$ or $\mathbb{S}^2$. In order to obtain a smooth frame on $\mathbb{S}^2$, we compute the push forward of the smooth global frame on $\mathbb{S}^3$ (given by Eqs. (5.6)) along π. After a straightforward computation we obtain

$$\begin{aligned}
\pi_*\chi_1^a &= -\sin\rho\,\partial_\theta^a + \cos\rho\csc\theta\,\partial_\varphi^a,\\
\pi_*\chi_2^a &= -\cos\rho\,\partial_\theta^a - \sin\rho\csc\theta\,\partial_\varphi^a,\\
\pi_*\chi_3^a &= 0.
\end{aligned}$$

In particular, note that the push-forward of $\pi_*\chi_3^a$ along π vanishes. Therefore, $\mathbb{S}^3$ can be seen as a principal bundle over $\mathbb{S}^2$ with structure group U(1) generated by the fibers tangential to $\pi_*\chi_3^a$ and projection map π. This is known in the literature as the *Hopf bundle* (see section A.6) and is usually denoted by

$$\mathbb{S}^1 \hookrightarrow \mathbb{S}^3 \to \mathbb{S}^2\,,$$

meaning that the Hopf map projects $\mathbb{S}^3$ onto the base space $\mathbb{S}^2$ with fiber $\mathbb{S}^1$ generated by the group[2] U(1).

Let U be an open subset of $\mathbb{S}^2$. The poles $\theta = 0, \pi$ are assumed to be outside of U so that the representation of the Hopf map given by Eq. (5.7) is well defined and the Euler coordinates cover $\pi^{-1}(U)$. If we restrict ourselves to sufficiently small open subsets, it does not represent a loss of generality since for any sufficiently small choice of the open set U can always be introduced coordinates such that the poles are not in U.

Now, using Eqs. (5.6) let us set the orthonormal frame (e_1^a, e_2^a, e_3^a) on $\mathbb{S}^3$ at some fixed parameter ρ such that

$$e_1^a := \frac{-1}{\sqrt{2}}\,(\chi_2^a + i\chi_1^a)\ ,\quad e_2^a := \overline{e}_1^a\ ,\quad e_3^a := \chi_3^a\,. \tag{5.8}$$

On the other hand, using Eqs. (5.6) we can define a smooth complex frame $(m^a, \overline{m}^a)$ on $\mathbb{S}^2$ as[3] on U by

$$m^a := \frac{-1}{\sqrt{2}}\,(\pi_*\chi_2^a + i\pi_*\chi_1^a)\,|_\rho,$$

[2] $\mathbb{S}^1 := \{(y_1, y_2) \in \mathbb{R}^2\ :\ y_1^2 + y_2^2 = 1\ \}$.

[3] $\overline{m}$ indicates the complex conjugate of m^a.

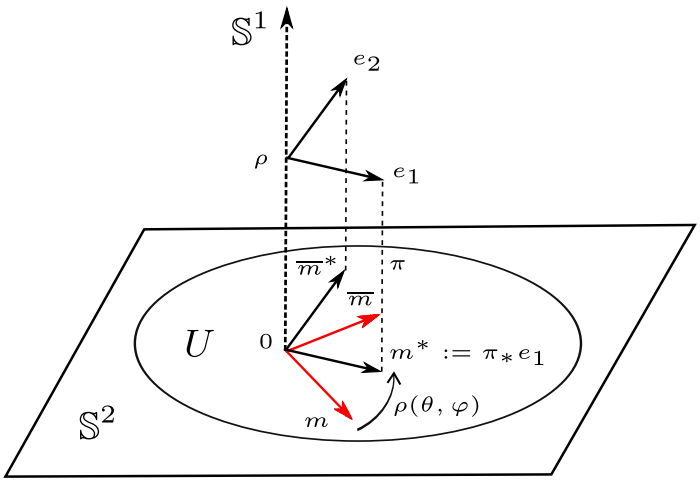

Figure 5.1: *Illustration of the frame projection from $\mathbb{S}^3$ to $\mathbb{S}^2$ using the Hopf map. In order to simplify the figure, abstract indices in the vectors field have been omitted.*

Clearly, any specification of the parameter ρ yields another smooth orthonormal frame on U which corresponds to a rotation of the original frame. The "standard" section, hence the "standard" frame that we shall use without further notice in the following is given by $\rho = 0$, that is,

$$m^a = \frac{1}{\sqrt{2}}\left(\partial_\theta^a - \frac{i}{\sin\theta}\partial_\varphi^a\right).$$

Note that in those coordinates this frame is singular at $\theta = 0$ or $\theta = \pi$. Now, owing to the group action U(1), at any point $p = (\theta, \rho, \varphi) \in \mathbb{S}^3$ the frame (e_1^a, e_2^a, e_3^a) can then be projected to the basis $(e^{i\rho}m^a, e^{-i\rho}\overline{m}^a)$ on $\mathbb{S}^3$ evaluated at the point $\pi(p) \in \mathbb{S}^2$. Further, the local section $\sigma : U \to \pi^{-1}(U)$ specified by any real function $\rho = \rho(\vartheta, \varphi)$ yields a different frame over U which is related to $(m^a, \bar{m}^a)$ by a point-wise rotation

$$m^a \mapsto e^{i\rho(\vartheta,\varphi)}m^a, \quad \overline{m}^a \mapsto e^{-i\rho(\vartheta,\varphi)}\overline{m}^a \tag{5.9}$$

at each point in U. The above is clearly illustrated in Fig. 5.1. Note that we have used ρ to denote the group parameter of U(1), while the rotation function has been denoted by $\rho(\theta, \varphi)$. Clearly, any specification of the function $\rho(\theta, \varphi)$ yields to another smooth orthonormal frame on U which corresponds to a rotation of the original frame. Therefore, it can be interpreted as the smooth local section $U \to \mathbb{S}^3$ defined by $(\theta, \varphi) \mapsto (\theta, \rho, \varphi)$ in the bundle of orthonormal frames, or equivalently in the Hopf bundle. Doing this for every open subset U of $\mathbb{S}^2$ (introducing coordinates such that the poles are not in U as above), the full bundle of orthonormal frames (e_1^a, e_2^a, e_3^a) can be recovered and identified with the Hopf bundle.

Finally, if $f : U \to \mathbb{C}$ is a component of a smooth real tensor field on $\mathbb{S}^2$ with respect to the frame $(m^a, \overline{m}^a)$, the function $e^{is\rho} \cdot (f \circ \pi)$ on $\pi^{-1}(U) \subset \mathbb{S}^3$, which is defined for some integer s called the *spin-weight*, is the corresponding component obtained by any frame rotation above. Any such function f is said to have the *well-defined spin-weight* s.

5.3 The spin-weighted spherical harmonics

Since the *spin-weighted spherical harmonics* (SWSH) play an important role in the representation of functions over $\mathbb{S}^2$, we devote this section to introducing such functions and

summarizing some of their most relevant properties. We start by describing the representation of the three-dimensional rotation group SO(3) as a preparation to introduce the SWSH. The next discussion is based on [71, 132, 133].

5.3.1 Wigner d-functions

Any rotation $\varrho \in \mathrm{SO}(3)$ is uniquely defined in Euler coordinates by $\varrho = (\theta, \rho, \varphi)$. The Wigner d-functions, ${D^l}_{mn}(\varrho)$ with $l \in \mathbb{N}$ and $m, n \in \mathbb{Z}$, satisfying $|m|, |n| \leq l$, are the matrix elements of the irreducible unitary representation of SO(3). Moreover, such matrices form an orthogonal basis on $L^2(\mathrm{SO}(3))$. The Wigner d-functions may be decomposed in terms of the reduced Wigner d-functions by

$$ {D^l}_{mn}(\rho, \theta, \varphi) = e^{-in\rho} {d^l}_{mn}(\theta) e^{-im\varphi} \, . \tag{5.10} $$

The real d- functions are defined by [133]

$$ {d^l}_{mn}(\theta) = \sqrt{\frac{(l+n)(l-n)}{(l+m)(l-m)}} \left(\sin\frac{\theta}{2}\right)^{n-m} \left(\cos\frac{\theta}{2}\right)^{n+m} P_{l-n}^{n-m,n+m}(\cos\theta), \tag{5.11} $$

where $P_{l-n}^{n-m,n+m}(\cos\beta)$ are the Jacobi polynomials. Furthermore, the relation with the Legendre polynomials $P_l^m(\cos\theta)$ is given by the particular case

$$ {d^l}_{m0}(\theta) = \sqrt{\frac{(l-m)}{(l+m)}} P_l^m(\cos\theta) \, . \tag{5.12} $$

These functions satisfy a number of relations. Next, some of their most relevant properties for this work are listed. We start by the symmetry relations

$$ \begin{aligned} {d^l}_{mn}(\theta) &= (-1)^{m-n} {d^l}_{(-m)(-n)}(\theta), \\ {d^l}_{mn}(\pi-\theta) &= (-1)^{l-n} \, {d^l}_{(-m)(n)}(\theta), \\ {d^l}_{mn}(-\theta) &= (-1)^{m-n} {d^l}_{mn}(\theta). \end{aligned} \tag{5.13} $$

In the derivation of the axially symmetric spin spherical harmonic transform in section 7.4.2, we often consider d-functions of the form ${d^l}_{mn}(\pi/2)$ which satisfy

$$ {d^l}_{m0}(\pi/2) = 0, \quad \text{for } l+m = \text{ odd}. \tag{5.14} $$

To finalize this subsection, we want to mention that the Wigner d-matrices can be extended to form a basis for the irreducible unitary representation for $L^2(\mathrm{SU}(2))$ (see for instance [172]). This may allow defining spin-weighted spherical harmonics functions of half integers as well as construct a half spin weight spherical harmonic transform which clearly would deal with spinors fields. We refer the interested reader to the work of Beyer et al. [29] and references therein. Because in this work we shall only consider tensor fields which have integer spin-weights (we will see this in more detail in section 5.4), we will only consider the integer case.

5.3.2 The spin-weighted spherical harmonics

To begin with, let us consider the space of square integrable functions $L^2(\mathbb{S}^2)$ with inner product $<,>$ defined by

$$ < f, g > := \int_{\mathbb{S}^2} f \, \overline{g} \sin\theta \, d\theta \, d\varphi \, , \tag{5.15} $$

for any $f, g \in \mathbb{S}^2$ with $\overline{g}$ denoting the complex conjugation. The spin-weighted spherical harmonics ${}_sY_{lm}(\theta,\varphi)$ constitute an orthogonal basis for the functions in $L^2(\mathbb{S}^2)$ with spin -weight s. They were first developed by Newman and Penrose [143] and were soon realized to be closely related to the Wigner d-functions by Goldberg et al. [96]. He showed that spin-weighted functions may be defined equivalently from the expansion in Wigner d-functions $D^l_{mn}(\varphi,\theta,\rho)$ of a function in $L^2(\mathrm{SO}(3))$ evaluated at $\rho = 0$. The *spin-weighted spherical harmonics* (SWSH) are defined by

$$ {}_sY_{lm}(\theta,\varphi) = (-1)^s \sqrt{\frac{2l+1}{4\pi}} D^l_{m,-s}(0,\varphi,\theta). $$

Noting the decomposition given by Eq. (5.10), the spin spherical harmonics may also be written in terms of the reduced Wigner d-functions as

$$ {}_sY_{lm}(\theta,\varphi) = (-1)^s \sqrt{\frac{2l+1}{4\pi}}\, e^{im\varphi} d^l_{m,-s}(\theta). \tag{5.16} $$

Note that under this form and using the relation Eq. (5.12), we can observe that the standard spherical harmonics correspond to the particular case $s = 0$ of the SWSH. Next, we list some of their most relevant properties. We start by considering the complex conjugation property

$$ {}_s\overline{Y}_{lm}(\theta,\varphi) = (-1)^{s+m}\, {}_{-s}Y_{l,-m}(\theta,\varphi)\,. \tag{5.17} $$

Next, we describe a closed-sum decomposition for products between SWSH. Using Eq. (5.3.2) we can write the product of SWSH in terms of *Wigner d-matrices* as

$$ {}_{s_1}Y_{l_1,m_1}(\theta,\,\varphi)\, {}_{s_2}Y_{l_2,m_2}(\theta,\,\varphi) = \sqrt{\frac{2l_1+1}{4\pi}} D^{l_1}_{s_1 m_1}(0,\,\theta,\,\varphi) \sqrt{\frac{2l_2+1}{4\pi}} D^{l_2}_{s_2 m_2}(0,\,\theta,\,\varphi), \tag{5.18} $$

The product of the right-hand side can be decomposed in the so-called Clebsch-Gordan series which in bracket notation (see [172]) is given by

$$ \begin{aligned} D^{l_1}_{m_1,s_1}(\rho,\,\theta,\,\phi)\, D^{l_2}_{m_2,s_2}(\rho,\,\theta,\,\phi) = \sum_{l\in\Lambda} & \langle l_1,\, l_2;\, m_1,\, m_2 |\, l_1,\, l_2;\, l,\, (m_1+m_2)\rangle \\ & \times \langle l_1,\, l_2;\, s_1,\, s_2 |\, l_1,\, l_2;\, l,\, (s_1+s_2)\rangle \\ & D^l_{(m_1+m_2),(s_1+s_2)}(\rho,\,\theta,\,\phi)\,, \end{aligned} \tag{5.19} $$

where $\Lambda := \{\max(|l_1-l_2|,\, |m_1+m_2|,\, |s_1+s_2|),\, \ldots,\, l_1+l_2\}$. Note that each Clebsch-Gordan coefficient in the series is a real number, i.e., $\langle\cdot,\,\cdot;\,\cdot,\,\cdot|\,\cdot,\,\cdot;\,\cdot,\,\cdot\rangle \in \mathbb{R}$. Defining

$$ \begin{aligned} \mathcal{A}_l(s_1,l_1,m_1;\, s_2,l_2,m_2) := & \sqrt{\frac{(2l_1+1)(2l_2+1)}{4\pi\,(2l+1)}}\, \langle l_1,s_1;l_2,s_2|\, l_1,l_2;l,(s_1+s_2)\rangle \\ & \times \langle l_1,m_1;l_2,m_2|\, l_1,l_2;l,(m_1+m_2)\rangle\,, \end{aligned} \tag{5.20} $$

the Eq. (5.20) together with Eq. (5.19) provides us with the following decomposition of Eq. (5.18)

$$ {}_{s_1}Y_{l_1,m_1}(\theta,\,\varphi)\, {}_{s_2}Y_{l_2,m_2}(\theta,\,\varphi) = \sum_{l\in\Lambda'} \mathcal{A}_l(s_1,l_1,m_1;\, s_2,l_2,m_2)\, {}_{(s_1+s_2)}Y_{l,(m_1+m_2)}(\theta,\,\varphi), \tag{5.21} $$

where $\Lambda' := \{\max(|l_1-l_2|,\, |s_1+s_2|,\, |m_1+m_2|),\, \ldots,\, l_1+l_2\}$. Note that the product of two spin-weighted spherical harmonics is given by a finite linear combination of spin-weighted spherical

harmonics with spin-weight equal to the sum of the original two spin-weights. On the other hand, the orthogonality and completeness of the SWSH follows from the orthogonality of the d-Wigner matrices

$$\int_{\mathbb{S}^2} {}_sY_{l_1m_1}(\theta,\varphi)\ {}_s\overline{Y}_{l_2m_2}(\theta,\varphi)\ d\Omega = \delta_{l_1l_2}\delta_{m_1m_2} \tag{5.22}$$

and

$$\sum_{l=0}^{\infty}\sum_{m=-l}^{l} {}_sY_{lm}(\theta,\varphi){}_s\overline{Y}_{lm}(\theta',\varphi') = \delta(\cos\theta-\cos\theta')\delta(\varphi-\varphi') \tag{5.23}$$

respectively, being δ_{ij} the Kronecker delta and $\delta(x)$ the Dirac delta. Therefore, any square integrable function with spin-weight s defined on $\mathbb{S}^2$ can be represented as

$${}_sf(\theta,\varphi) = \sum_{l=0}^{\infty}\sum_{m=-l}^{l} {}_sa_{lm}\ \ {}_sY_{lm}(\theta,\varphi),$$

where the ${}_sa_{lm}$ are the complex coefficients of the function (also called spectral coefficients). We are assuming the standard convention for coordinates $\theta\in(0,\pi)$ and $\varphi\in(0,2\pi)$. Notice that the standard scalar spherical harmonics are given by $s=0$. Furthermore, from those functions we can obtain any SWSH by using the spin raising and lowering operators known as the *eth-operators* $\eth$ and $\bar{\eth}$ defined by (for simplicity we have written ${}_sf(\theta,\varphi)$ as just f)

$$\eth f := \partial_\theta f - \frac{i}{\sin\theta}\partial_\varphi f - sf\cot\theta, \tag{5.24}$$

$$\bar{\eth} f := \partial_\theta f + \frac{i}{\sin\theta}\partial_\varphi f + sf\cot\theta, \tag{5.25}$$

for any function f on $\mathbb{S}^2$ with spin-weight s. By applying the eth-operators over the SWSH, we obtain the properties of raising and lowering spin-weight

$$\eth\ {}_sY_{lm}(\theta,\varphi) = -\sqrt{(l-s)(l+s+1)}\ {}_{s+1}Y_{lm}(\theta,\varphi), \tag{5.26}$$

$$\bar{\eth}\ {}_sY_{lm}(\theta,\varphi) = \sqrt{(l+s)(l-s+1)}\ {}_{s-1}Y_{lm}(\theta,\varphi). \tag{5.27}$$

Thus, using the properties above it is easy to check that from any function f with spin-weight s, we can get a function with either spin $s+1$ from $\eth$ or spin $s-1$ from $\bar{\eth}$. Thus, they are also known in the literature as the raising and lowering operators [133]. Using the two latter expressions, the commutator between those operators is obtained by

$$[\bar{\eth},\eth]f = 2sf\ . \tag{5.28}$$

Finally, using the above expression and the definitions Eqs. (5.24)- and (5.25), the Laplacian operator in the two-sphere can be written as

$$\Delta_{\mathbb{S}^2}f = \frac{\left(\eth\bar{\eth}+\bar{\eth}\eth\right)}{2}f\ . \tag{5.29}$$

Further, using the commutation relation Eq. (5.28) we obtain the two useful expressions

$$\Delta_{\mathbb{S}^2}f = \eth\bar{\eth}f + sf\ , \tag{5.30}$$

$$\Delta_{\mathbb{S}^2}f = \bar{\eth}\eth f - sf\ . \tag{5.31}$$

5.4 Tensor components in $\mathbb{S}^2$

Finally, we end this chapter by discussing the spin-weight of the tensors components of any tensor over $\mathbb{S}^2$. To begin with, we choose the smooth complex frame $(m^a, \overline{m}^a)$ on $\mathbb{S}^2$ introduced in section 5.2. As mentioned, in these coordinates the frame $(m^a, \overline{m}^a)$ is singular at $\theta = 0$ or $\theta = \pi$. Hence, we will just restrict ourselves to an open subset U of $\mathbb{S}^2$ so that the poles $\theta = 0, \pi$ are outside. Let $(\omega_b, \overline{\omega}_b)$ be the dual coframe of $(m^a, \overline{m}^a)$. Then, the action of U(1) on the inner product $\omega_a^*(m^{*a}) = 1$ implies that the transformation for the coframe should be

$$\omega_a^* = e^{-i\rho(\theta,\varphi)}\omega_a. \tag{5.32}$$

Now, let an arbitrary smooth tensor field $\mathcal{T}$ of type $(p+q, r+s)$ for integers $p, q, r, s \geq 0$ be given on U. Then, its components with respect to the frame $(m^{*a}, \overline{m}^{*a})$ are functions $\mathcal{T} : U \to \mathbb{C}$ given by

$$\mathcal{T}^{*\,a_1\ldots,a_p,b_1\ldots,b_q}{}_{c_1\ldots,c_r,d_1\ldots,d_s} := \mathcal{T}(\underbrace{\omega_{a_1}^*,\ldots}_{p},\underbrace{\overline{\omega}_{b_1}^*,\ldots}_{q},\underbrace{m^{*c_1},\ldots}_{r},\underbrace{\overline{m}^{*d_1},\ldots}_{s}).$$

Using Eqs. (5.9) and (5.32), these functions can be written in terms of the non rotated frame $(m^a, \overline{m}^a)$ and coframe $(\omega_b, \overline{\omega}_b)$ as

$$\begin{aligned}\mathcal{T}^{*\,a_1\ldots,a_p,b_1\ldots,b_q}{}_{c_1\ldots,c_r,d_1\ldots,d_s} &= e^{i(-p+q+r-s)\,\rho(\theta,\varphi)}\,\mathcal{T}(\underbrace{\omega_{a_1},\ldots}_{p},\underbrace{\overline{\omega}_{b_1},\ldots}_{q},\underbrace{m^{c_1},\ldots}_{r},\underbrace{\overline{m}^{d_1},\ldots}_{s}),\\ &= e^{i(-p+q+r-s)\,\rho(\theta,\varphi)}\,\mathcal{T}^{a_1\ldots,a_p,b_1\ldots,b_q}{}_{c_1\ldots,c_r,d_1\ldots,d_s}\,.\end{aligned} \tag{5.33}$$

From the expression above, the spin-weight for the tensor components $\mathcal{T}^{a_1\ldots,a_p,b_1\ldots,b_q}{}_{c_1\ldots,c_r,d_1\ldots,d_s}$ are given by $-p+q+r-s$. Note that due to the transformation rules Eqs. (5.9) and (5.32), the spin-weight will always be an integer number implying that tensor components can be written in terms of SWSH.

Part II

Analytical and numerical infrastructure

Chapter 6

U(1)-symmetric spacetimes with spatial topologies $\mathbb{S}^3$ or $\mathbb{S}^1 \times \mathbb{S}^2$

In this chapter we derive the evolution and constraint equations that we are going to use in our pseudo-spectral implementation. We start by applying the Geroch symmetry reduction introduced in the last chapter to Gowdy spacetimes, to reduce the EFE in four dimensions to the three-dimensional Geroch-Einstein system Eqs. (4.30), which describe a $2+1$-gravity model coupled with two scalar fields. In section 6.3, we discuss the generalized wave map formalism for setting evolution equations that will be used for solving the Cauchy problem in the space orbits S with spatial topology $\mathbb{S}^2$. In particular, we rewrite the system GES given in Eqs. (4.30) as a coupled system of quasilinear wave equations for the metric components with well-defined spin-weights. In other words, there will not be any singular term like $\cot\theta$ floating around in the evolution equations. This implies that we can describe fields in the two-sphere with a single polar coordinate chart and obtain a fully regular evolution. In section 6.4 we briefly discuss the equivalence between the constraints from the generalized wave formalism and the standard Hamiltonian and momentum constraints from the ADM formulation. Additionally, we obtain a representation of the constraint equations in the space of orbits S based on the York-Lichnerowicz conformal decomposition. Finally, in section 6.5 we address the question of how to reconstruct the metric of the four-dimensional manifold M from the three-dimensional metric in the space of orbits S.

6.1 The symmetry reduction for U(1)-symmetric spacetimes

Here, we use many of the mathematical tools introduced in chapter 4. Let us consider $M = \mathbb{R} \times \Sigma$ a time-oriented globally hyperbolic four-dimensional spacetime endowed with a metric g_{ab} of signature $(-,+,+,+)$, a global time-function t and a U(1)- symmetric Cauchy surface Σ. We denote the hypersurfaces given by $t = t_0$ for any constant t_0 by Σ_{t_0}. Each Σ_t is diffeomorphic to Σ. Let ξ^a be a smooth spacelike Killing vector field in M, that is, the generator of the symmetry group U(1) and which is tangent to the hypersurfaces Σ_t. Let the quantities

$$\tilde{\psi} = g_{ab}\xi^a\xi^b, \quad \tilde{\Omega}_a = \epsilon_{abcd}\,\xi^b\mathfrak{D}^c\xi^d,$$

be the *norm* and the *twist* of ξ^a respectively. The operator $\mathfrak{D}_a$ is the covariant derivative compatible with the metric g_{ab}. Let us define the induced metric $\tilde{h}_{ab}$ on S by

$$\tilde{h}_{ab} := g_{ab} - \frac{1}{\tilde{\psi}}\xi_a\xi_b.$$

In order to take advantage of the symmetry induced by ξ^a over M, we introduce the space of orbits S associated to ξ as follows. Consider the map

$$\pi : M \to S,$$

where π maps every $p \in M$ to the (locally) uniquely determined integral curve of ξ^a starting at p. We write the metric on S as $\hat{h}_{ab}$ and denote ψ, Ω_a the fields that pull back to the norm $\tilde{\psi}$ and twist $\tilde{\Omega}_a$ of ξ^a respectively. As mentioned in chapter 4, for vacuum space times (M, g_{ab}) the one-form Ω_a is closed, i.e., $\mathrm{d}\Omega = 0$. Hence, this fact allows us to introduce a twist potential ω so that $\Omega = \mathrm{d}\omega$. Finally, introducing the conformal rescaling

$$h_{ab} := \psi \hat{h}_{ab}, \tag{6.1}$$

the EFE in (M, g_{ab}) can be rewritten as the Geroch-Einstein system[1] described in Eqs. (4.30), which describes a 2+1 gravitational field coupled with two scalar fields. In addition, we point out that there are no second-order derivatives on the right-hand side of the system GES. As we shall explain later in section 6.3.2, this fact makes the system of evolution equations have a suitable form for implementing the generalized wave formalism. In fact, this is the principal reason for introducing the *evolution metric* h_{ab} by Eq. (6.1) and for writing the evolution equations in terms of it instead of the *reduced metric* $\hat{h}_{ab}$. In other words, in terms of the reduced metric $\hat{h}_{ab}$, the third equation contains second derivatives of ψ on the right-hand side See for instance [92]. Hereafter, unless otherwise explicitly stated, we will work with the evolution metric.

6.2 Equations for the cases with spatial topology $\mathbb{S}^3$ or $\mathbb{S}^1 \times \mathbb{S}^2$

In this section, we focus on the case $S := \mathbb{R} \times \mathbb{S}^2$ and the field equations in the form Eq. (4.30). As before let $t : S \to \mathbb{R}$ be a smooth time function on S and

$$\Sigma_t := \{t\} \times \mathbb{S}^2 \simeq \mathbb{S}^2, \quad t \in \mathbb{R}.$$

We introduce coordinates (t, ϑ, φ) on the dense subset $\mathbb{R} \times U$ of S and define $T^a = \partial_t^a$. With the same choice of complex vector field m^a on $U \subset \mathbb{S}^2$ as defined in section 5.2, we introduce the frame $(e_0^a, e_1^a, e_2^a) = (T^a, m^a, \overline{m}^a)$ on $\mathbb{R} \times U$. The spin-weight of any function $f : \mathbb{R} \times U \to \mathbb{C}$ is defined in the same way as in section 5.2, but now with respect to frame transformations of the form

$$T^a \mapsto T^a, \quad m^a \mapsto e^{i\rho(\theta,\varphi)} m^a, \quad \bar{m}^a \mapsto e^{-i\rho(\theta,\varphi)} \overline{m}^a$$

Therefore, the frame vector field T^a has spin-weight 0, m^a spin-weight 1 and $\overline{m}^a$ spin-weight -1. Under the above considerations, we shall choose the dual frame $(\omega_a^0, \omega_a^1, \omega_a^2)$ by

$$\omega_a^0 = \nabla_a t, \quad \omega_a^1 = \frac{1}{\sqrt{2}} \left(\nabla_a \theta + i \sin\theta \, \nabla_a \varphi \right), \quad \omega_a^2 = \overline{\omega}_a^1,$$

with spin-weight of 0, -1 and 1 respectively. Then, the general form of a smooth metric on S is (see for instance [30, 71])

$$h_{ab} = \lambda \, \omega_a^0 \omega_b^0 + 2 \, \omega_{(a}^0 \left(\beta \, \omega_{b)}^1 + \bar{\beta} \, \omega_{b)}^2 \right) + 2\delta \, \omega_{(a}^1 \omega_{b)}^2 + \phi \, \omega_a^1 \omega_b^1 + \bar{\phi} \, \omega_a^2 \omega_b^2. \tag{6.2}$$

[1] We have used ∇_a to denote the three-dimensional covariant derivative operator associated to h_{ab}.

where the metric components are functions depending on (t, θ, φ) with spin-weight of 0 for λ and δ, +1 for β and +2 for[2] ϕ. Since the metric of a sphere of radius r can be written as $g_{\mathbb{S}^2} = 2r\omega^1_{(a}\omega^2_{b)}$, we can interpret the metric component δ as the radius of the $\mathbb{S}^2$-factor. Furthermore, in terms of the SWSH basis, it can be easily proved using Eq. (5.22) that the mode $l = 0$ of function with zero spin-weight represents the mean value of the radius of the $\mathbb{S}^2$-factor. Henceforth, the mode $l = 0$ will be known as the fundamental mode. This interpretation will be used in section 10.6 for analysing the instability of the Nariai spacetime.

In the light of this non-orthonormal frame, the connection coefficients are given by Eq. (A.3.1). After a straightforward computation we find that almost all the structure coefficients (see section A.2) are zero except

$$C^2{}_{12} = C^1{}_{21} = -C^2{}_{21} = -C^1{}_{12} = \frac{-1}{\sqrt{2}}\cot\theta. \tag{6.3}$$

The occurrence of the singular function $\cot\theta$ is a consequence of the fact that the quantities $C^\mu{}_{\nu\rho}$ are not components of a tensor field, hence do not have well-defined spin-weights. The above fact is the reason why in the connection coefficients, and hence in the Ricci tensor (see Eq. (2.13)), there are terms like $\cot\theta$ that diverge at the poles. These sorts of terms cannot be written in terms of SWSH, hence do not have well-defined spin-weights. From now on, we will refer to them as *singular terms*. As we will discuss in the next section, one way to avoid these problematic terms is by writing the frame vectors in terms of the eth-operators introduced in section 5.3. From Eqs. (5.2) and (5.24), the frame vector $(m^a, \overline{m}^a)$ can be written in terms of the eth-operators by

$$m^a(f) = \frac{1}{\sqrt{2}}\left(\eth f + fs\cot\theta\right), \quad \overline{m}^a(f) = \frac{1}{\sqrt{2}}\left(\bar{\eth} f - fs\cot\theta\right), \tag{6.4}$$

for some given function f on $\mathbb{S}^2$ with spin-weight s. We devote the next section to write the evolution equations in a proper way such that all the terms turn out to have well defined spin-weights.

6.3 Evolution equations

Before presenting the evolution equations, let us discuss a bit more about the singular terms contained in Eq. (2.13) due to the structure constants Eqs. (6.3). As we just mentioned, by replacing the derivatives along the frame vectors by the eth-operators, all the singular terms in the evolution equations disappear. This "cancellation" procedure of the singular functions is carried out because all the terms of the evolution equations form the components of the Ricci tensor, which must have a well-defined spin-weight (see [30, 71]). In other words, the frame components of smooth tensor fields in $\mathbb{S}^2$ have well-defined spin-weights so that they can be written in terms of the SWSH, which are globally defined as smooth functions on the two-sphere (even though their coordinate representation may be singular). Therefore, expressing everything with respect to these bases and the spatial derivatives in terms of eth-operators renders the equations manifestly without singular terms.

As was discussed in section 2.5, in most of the literature the related (but not covariant) generalized harmonic formalism is used to set hyperbolic evolution equations for the EFE. However, while this formalism is sufficient for many applications, it is a drawback for us. In fact, for applications with spatial topology $\mathbb{S}^2$ covered by a single singular polar coordinate

[2] Clearly, $\bar{\beta}$ and $\bar{\phi}$ have spin-weight -1 and -2 respectively.

system, it is far more convenient to work with actual covariant quantities (i.e., smooth tensor fields). The reason of this lies in the fact that, as is pointed out in [162, 171], the violation covector $\mathcal{D}_a$ defined in Eq. (2.12) is not a tensor because Γ_a is not a covector. In order to overcome this difficulty, we discuss in what follows the geometric formulation of the wave map gauge.

6.3.1 The wave map gauge

We start by considering a map $\Phi : M \to \bar{M}$ between two general smooth four-dimensional manifolds M and $\bar{M}$ (or open subsets thereof) equipped with Lorentzian metrics[3] h_{ab} and $\bar{h}_{ab}$. The map Φ is called a wave map if it extremizes the functional

$$\mathcal{F}[\Phi] = \int_M \mathrm{tr}_h(\Phi^* \bar{h}) \, \mathrm{Vol}_h.$$

In coordinate charts (x^μ) on M and (y^α) on $\bar{M}$ we obtain the Euler-Lagrange equations (see [195]) for the coordinate representation $y^\alpha = y^\alpha(x^\mu)$ of Φ by

$$\Box_h y^\alpha + \bar{\Gamma}^\alpha{}_{\beta\gamma} h^{\mu\nu} \frac{\partial y^\beta}{\partial x^\mu} \frac{\partial y^\gamma}{\partial x^\nu} = 0. \tag{6.5}$$

Here, $\bar{\Gamma}^\alpha{}_{\beta\gamma}$ are the Christoffel symbols for the metric $\bar{h}_{ab}$ in the coordinate basis on $\bar{M}$, and $\Box_h$ is the wave operator defined for scalar functions defined by h_{ab}. Hereafter we call $\bar{h}_{ab}$ the reference metric. This equation is called the *wave-map equation*. More details about it can be found in [60]. If the manifolds were Riemannian then the analogous equation would characterize a harmonic map between M and $\bar{M}$. Let us point out that the left-hand side of the equation defines a geometric object, namely a section in the pull-back bundle $\Phi^* T\bar{M}$. This is not immediately obvious due to the appearance of the Christoffel symbols in the second term. However, the tensorial character of that term under change of coordinates in $\bar{M}$ is compensated for by the first term which, by itself, is also non-tensorial under such coordinate transformations.

The generalized wave-map equation is the Eq. (6.5) with a non-vanishing, arbitrary right-hand side, a section in $\Phi^* T\bar{M}$ with coordinate representation f^α

$$\Box_h y^\alpha + \bar{\Gamma}^\alpha{}_{\beta\gamma} h^{\mu\nu} \frac{\partial y^\beta}{\partial x^\mu} \frac{\partial y^\gamma}{\partial x^\nu} = -f^\alpha. \tag{6.6}$$

The minus sign appears on the right-hand side by convention. Suppose now that $\bar{M} = M$ and[4] $\Phi = id_M$. Then (x^μ) and (y^α) are two coordinate charts for M and Eq. (6.6) can be read as an equation determining the coordinate system (y^α) for M by imposing a geometrical gauge condition. This equation is a semi-linear wave equation of M which has solutions near any Cauchy surface so that such a coordinate gauge always exists locally.

Choosing the coordinates according to this gauge, i.e., putting $x^\mu = y^\mu$ and expressing the wave operator in these coordinates yields the equation

$$(\bar{\Gamma}^\alpha{}_{\beta\gamma} - \Gamma^\alpha{}_{\beta\gamma}) h^{\beta\gamma} = -f^\alpha,$$

where $\Gamma^\alpha{}_{\beta\gamma}$ are the Christoffel symbols of the metric h on M. In this equation the tensorial character becomes manifest since the left-hand side involves the difference of two connection

[3] All of the following arguments also hold if M and $\bar{M}$ are n-dimensional manifolds for some arbitrary positive integer n and if $\bar{h}_{ab}$ is a general smooth pseudo-Riemannian (not necessary Lorentzian) metric.

[4] id_M denotes the identity map.

coefficients so it gives the components of a vector field in the coordinate basis of the (x^μ). Therefore, this equation holds in any basis on M as long as we interpret the Christoffel symbols as the connection coefficients with the respect to the chosen basis. Note also that this implies that imposing Eq. (6.6) does not constitute a condition on the coordinate system but a condition on the metric components in their dependence on the coordinates.

We define the vector field $\mathcal{D}^a$ with components given by

$$\mathcal{D}^\alpha := (\bar{\Gamma}^\alpha{}_{\beta\gamma} - \Gamma^\alpha{}_{\beta\gamma})h^{\beta\gamma} + f^\alpha. \tag{6.7}$$

where f^α are the components of the vector f^a such that $\mathcal{D}^a = 0$ when Eq. (6.6) is imposed. Note that in the light of our preliminary discussion about the generalized wave map formalism in section 2.5, we are choosing gauge source functions such that

$$F^\alpha = \bar{\Gamma}^\alpha{}_{\beta\gamma}h^{\beta\gamma} + f^\alpha. \tag{6.8}$$

A metric h_{ab} that is restricted by $\mathcal{D}^a = 0$ is said to be in wave gauge with respect to $\bar{h}_{ab}$. We point out that the wave gauge reduces to the widely used generalized harmonic gauge characterized by $\nabla_\nu\nabla^\nu x^\mu = -f^\mu$ on space-times with topology $\mathbb{R}^4$ when the Minkowski metric in Cartesian coordinates x^μ is used as a reference metric. In other words, choosing the reference metric as Minkowski yields $\Gamma^\alpha{}_{\beta\gamma} = 0$, hence $F^\alpha = f^\alpha$. From now on, we proceed similarly as was explained in section 2.5. We define a new tensor field

$$\hat{R}_{ab} := R_{ab} + \nabla_{(a}\mathcal{D}_{b)}, \tag{6.9}$$

where $\mathcal{D}_a = h_{ab}\mathcal{D}^b$. Thus, substituting this expression into Eq. (2.13), the components $R_{\mu\nu}$ of the Ricci tensor R_{ab} with respect to this frame can be written as

$$\hat{R}_{\sigma\rho} = -\frac{1}{2}\, h^{\mu\nu}\partial_\mu\partial_\nu h_{\sigma\rho} + \Upsilon_{\sigma\rho}(h, \partial h) + h_{\alpha(\rho}\nabla_{\sigma)}\bar{\Gamma}^\alpha{}_{\beta\gamma}h^{\beta\gamma} + \nabla_{(\sigma}f_{\rho)}, \tag{6.10}$$

where $\Upsilon_{\mu\nu}(h, \partial h)$ is a symmetric tensor which does not contain any second-order derivatives of the metric[5]. Further, note that $\partial_\nu h_{\sigma\rho}$ represents the derivative of the function $h_{\sigma\rho}$ in the direction of the frame vector field ∂^a_ν. As already explained in section 2.5, the idea of the generalized wave map formalism is to replace the Ricci tensor R_{ab} in the field equation by this new tensor $\hat{R}_{ab}$. We call the resulting equations the "evolution equations" since, under suitable conditions, these have a well-posed initial value problem for any choice of *generalized gauge source functions* f_a and $\bar{h}_{ab}$. Then, the evolution equations in the space of orbits Eqs. (4.30) takes the form

$$\begin{aligned}
\nabla_a\nabla^a\psi &= \frac{1}{\psi}\left(\nabla_a\psi\nabla^a\psi - \nabla_a\omega\nabla^a\omega\right) - 2\Lambda, \\
\nabla_a\nabla^a\omega &= \frac{1}{\psi}\nabla^a\psi\nabla_a\omega, \\
\hat{R}_{ab} &= E_{ab} + \frac{2\Lambda}{\psi}h_{ab},
\end{aligned}$$

with E_{ab} given by Eqs. (4.31). This is manifestly a coupled system of quasilinear wave equations. The evolution equations and the contracted Bianchi identities implies the *subsidiary system*

$$\nabla_b\nabla^b\mathcal{D}_a + \mathcal{D}^b\nabla_{(b}\mathcal{D}_{a)} = 0. \tag{6.11}$$

[5]Note that we write $\Upsilon_{\mu\nu}(h, \partial h)$ to indicate that it only depends of the metric components and its first frame derivatives.

where clearly follows that $\mathcal{D}_a = 0$ if and only if $\mathcal{D}_a = 0$ and $\nabla_a \mathcal{D}_b = 0$ on the initial hypersurface; these conditions therefore constitute *constraints*. Moreover, it can be satisfied for any initial data h_{ab}, ψ and ω by a suitable choice of the free gauge source quantities f_a and $\bar{h}_{ab}$, and is hence referred to as the *gauge constraint*; the constraints

$$\nabla_\mu \mathcal{D}_\nu = 0, \tag{6.12}$$

hold at the initial time if and only if the initial data satisfy the standard Hamiltonian and Momentum constraints (supposing that the gauge constraint and the evolution equations are satisfied). Later in section 6.4 we will explain this relationship in more detail. These are equations that are therefore independent of the generalized gauge source functions. Hence Eq. (6.12) represents the actual "physical constraints" on the initial data for h_{ab}, ψ and ω.

6.3.2 The covariant generalized wave gauge in the case $\mathbb{R} \times \mathbb{S}^2$

Next, we implement the generalized wave gauge introduced in the previous section to the particular case of our interest, that is for $S = \mathbb{R} \times \mathbb{S}^2$. In order to simplify our implementation, we choose as the reference metric $\bar{h}$ of unit two-sphere

$$\bar{h}_{ab} = -\omega^0_a \omega^0_b + 2\, \omega^1_{(a} \omega^2_{b)}. \tag{6.13}$$

This is a smooth metric on S which represents the static cylinder with the standard spatial metric on $\mathbb{S}^2$. Note that all the remaining gauge freedom is then encoded in the vector field f^a. Next we define *the singular and smooth contracted connections coefficients*, respectively

$$\breve{\Gamma}^\mu := h^{\sigma\rho} \bar{\Gamma}^\mu{}_{\sigma\rho}, \tag{6.14}$$

$$\mathring{\Gamma}^\mu := \Gamma^\mu - \breve{\Gamma}^\mu, \tag{6.15}$$

Note that by construction, the $\breve{\Gamma}_a$ terms do not contain any derivatives (but they contain singular terms) since the connections coefficients $\bar{\Gamma}^a{}_{bc}$ are obtained by (see Eq. (A.3.1))

$$\bar{\Gamma}^a{}_{bc} = \frac{\bar{h}^{ad}}{2} \left(C_{dbc} + C_{dcb} - C_{bcd} \right).$$

On the other hand, we point out that all the first-order derivatives of the metric encoded originally in Γ_μ are now in $\mathring{\Gamma}_a$. Therefore, using definitions introduced in Eqs. (6.15), we write the components of the Ricci tensor Eq. (6.10) as

$$\hat{R}_{\mu\nu} = -\frac{1}{2}\, h^{\alpha\beta} \partial_\alpha \partial_\beta h_{\mu\nu} + \nabla_{(\mu} \mathring{\Gamma}_{\nu)} + \mathring{\Upsilon}_{\mu\nu}(h, \partial h, \breve{\Gamma}) + \nabla_{(\mu} \mathcal{D}_{\nu)}, \tag{6.16}$$

where we have defined

$$\mathring{\Upsilon}_{\mu\nu}(h, \partial h, \breve{\Gamma}) := \nabla_{(\mu} \breve{\Gamma}_{\nu)} + \Upsilon_{\mu\nu}(h, \partial h)\,, \tag{6.17}$$

and the violation covector is given by

$$\mathcal{D}_a = f_a - \mathring{\Gamma}_a. \tag{6.18}$$

Finally, using Eqs. (6.11) and Eq. (6.16) we write the generalized wave Geroch-Einstein system (WGES) for the space of orbits as[6]

$$\begin{aligned} h^{\mu\nu}\partial_\mu\partial_\nu\psi - h^{\mu\nu}\Gamma^\rho{}_{\nu\mu}\partial_\rho\psi &= \frac{h^{\rho\sigma}}{\psi}\left(\partial_\rho\psi\partial_\sigma\psi - \partial_\rho\omega\partial_\sigma\omega\right) - 2\Lambda, \\ h^{\mu\nu}\partial_\mu\partial_\nu\omega - h^{\mu\nu}\Gamma^\rho{}_{\nu\mu}\partial_\rho\omega &= \frac{h^{\rho\sigma}}{\psi}\,\partial_\rho\psi\partial_\sigma\omega, \\ h^{\rho\sigma}\partial_\rho\partial_\sigma h_{\mu\nu} - 2\mathring{\Upsilon}_{\mu\nu}(h,\partial h,\breve{\Gamma}) &= 2\nabla_{(\mu}f_{\nu)} - \frac{1}{\psi^2}\left(\partial_\mu\psi\,\partial_\nu\psi + \partial_\mu\omega\,\partial_\nu\omega\right) - \frac{4\Lambda}{\psi}h_{\mu\nu}\,, \end{aligned} \tag{6.19}$$

where we have reduced the GES to a coupled system of quasilinear wave equations for the independent coordinate components. We notice that the first terms on the left-hand side constitute the principal part of this evolution system, i.e., quasilinear wave operators. These terms by themselves are not tensorial, hence give rise to singular terms (terms proportional to $\cot\theta$) which do not have well-defined spin-weights when the frame derivatives are replaced by eth-operators. The second terms on the left-hand sides cancel these problematic terms completely, and consequently, the left-hand sides become tensorial. The right-hand side terms are tensorial already. As a result of this fully tensorial character of all these equations, the system of evolution equations Eq. (6.19) can now be solved by implementing a pseudo-spectral method based on the SWSH. In other words, we have obtained a system of evolution equations whose spatial derivatives can be evaluated at any point by using the eth-operators, hence we have overcome the pole problem for evolution problems on the $\mathbb{S}^2$ topology.

To finalize, recalling our previous discussion at the end of section 2.5, we point out that thanks to the fact that there are no second-order derivatives in right-hand side in any of the equations of GES, we obtain that the WGES is a system of quasi-linear wave equations. This cannot be achieved using the reduced metric $\hat{h}_{ab}$. Therefore, it becomes clear why we decided to write the evolution equations in terms of the evolution metric h_{ab} instead of $\hat{h}_{ab}$.

6.4 Constraint equations

6.4.1 Equivalence between the ADM and GWF constraints

In this part, we discuss the equivalence of the constraints from GWF ($\mathcal{D}_a = 0 = \partial_t\mathcal{D}_b$) with respect to the well-known Hamiltonian and momentum constraints from the ADM formulation. This with the aim to construct initial data for our formulation based on the York-Lichnerowicz conformal decomposition. To start with, we consider the orthogonal the unit vector η^a to the Cauchy surface Σ_t

$$\eta^a := \frac{1}{\alpha}(1,-\beta,-\bar{\beta}), \quad n_a = (-\alpha,0,0)\,, \tag{6.20}$$

where $\beta,\bar{\beta}$ are the components of the *shift vector* B^a and $\alpha = \sqrt{\beta\bar{\beta}-\lambda}$ is the *lapse function* from the ADM formulation (see section 2.2.2)[7]. The induced metric γ_{ab} in the Cauchy surface is given by

$$\gamma_{ab} = h_{ab} + \eta_a\eta_b\,.$$

[6]Note that because ψ is a scalar, $\nabla_\mu\psi = \partial_\mu\psi$. Similarly for ω.

[7]Note that we have used the B^a instead of β^a to denote the shift vector as is usual to avoid confusion with the metric components $\beta,\bar{\beta}$

Next, we define the zero tensor that represents the EFE in the space of orbits Eq. (4.33) as[8]

$$\mathcal{M}^{ab} := G^{ab} + \frac{\Lambda}{\psi} h^{ab} - T^{ab}, \tag{6.21}$$

Because the contraction $G^{ab}n_b$ does not contain second time derivatives of any of the metric components (see for instance [195]), the constraint equations can be represented as the components of the vector $\mathcal{C}^a$

$$\mathcal{C}^a := \mathcal{M}^{ab} n_b \, . \tag{6.22}$$

Furthermore, the standard Hamiltonian and momentum constraints from the ADM formulation can be written respectively as

$$\begin{aligned} \mathcal{H} &:= 2 n_a \mathcal{C}^a, \\ J^a &:= \gamma^b{}_a \mathcal{C}^a. \end{aligned} \tag{6.23}$$

Let us assume by now that we have solved these equations, thus the constraint vector $\mathcal{C}^a$ vanishes. The question that arises now is this: How do we guarantee that the constraints from the GWF are satisfied? Before answering this question, note that we can always choose coordinates such that initially $\mathcal{D}_a = 0$. The real issue is to guarantee that $\partial_0 \mathcal{D}_b = 0$. In order to establish the relationship between the last expression with the standard constraints from the ADM, we substitute R_{ab} by $R_{ab} + \nabla_a \mathcal{D}_b$ into Eq. (6.21) to obtain (see [162])

$$\nabla^{(a}\mathcal{D}^{b)} - \frac{1}{2} h^{ab} \nabla_c \mathcal{D}^c = \mathcal{M}^{ab}.$$

Because of the definition Eq. (6.22), we can obtain the relation with the Hamiltonian and momentum by just computing $\mathcal{M}^{\mu 0}$. In other words, we shall focus in analysing

$$\nabla^{(0}\mathcal{D}^{\mu)} - \frac{1}{2} h^{0\mu} \nabla_\nu \mathcal{D}^\nu = \mathcal{M}^{\mu 0}. \tag{6.24}$$

Using coordinates such that $\mathcal{D}_\nu = 0$ clearly implies that $\nabla_\nu \mathcal{D}_\mu = \partial_\nu \mathcal{D}_\mu$ owing to the second terms $\Gamma^\rho{}_{\nu\mu}\mathcal{D}_\rho$ vanish. Further, any spatial derivative of $\mathcal{D}_\nu$ should vanish as well. Hence, all the terms $\nabla_\nu \mathcal{D}_\mu$ vanish except $\nabla_0 \mathcal{D}_\mu = \partial_0 \mathcal{D}_\mu = \partial_t \mathcal{D}_\mu$. With the above in mind, a straightforward computation of $\mathcal{M}^{\mu 0}$ in terms of Eq. (6.24) yields

$$\begin{aligned} \mathcal{C}^\nu &= -\frac{1}{2}\left(h^{0\mu}h^{\nu\rho} + h^{0\rho}h^{\nu\mu}\right)\nabla_\mu \mathcal{D}_\rho + \frac{1}{2} h^{0\nu} h^{\mu\rho} \nabla_\mu \mathcal{D}_\rho, && (6.25) \\ &= -\frac{1}{2}\left(h^{00}h^{\nu\rho}\partial_0 \mathcal{D}_\rho + h^{0\rho}h^{\nu o}\partial_0 \mathcal{D}_\rho - h^{0\nu}h^{0\rho}\partial_t \mathcal{D}_\rho\right), && (6.26) \\ &= -\frac{1}{2} h^{00} h^{\nu\rho} \partial_0 \mathcal{D}_\rho \, . && (6.27) \end{aligned}$$

Clearly, this equation shows the direct dependence on the time derivatives of $\mathcal{D}_\mu$ and the constraints from ADM. Therefore, it is clear that by solving the standard Hamiltonian and momentum constraints from ADM, we also find suitable initial data for the GWF formulation. s.

[8] The energy momentum tensor T_{ab} is given by Eq. (4.32).

6.4.2 York-Lichnerowicz conformal decomposition on $\mathbb{S}^2$

To this day, the most successful approach to tackle the constraint equations has been the conformal method, also known in the literature as the York-Lichnerowicz conformal decomposition; see [13] and references therein. In this part, we will discuss the implementation of the York-Lichnerowicz conformal decomposition on $\mathbb{S}^2$ for the Hamiltonian and momentum constraint. To begin with, let us use Eqs. (6.23) and the Gauss-Codazzi and Codazzi-Mainardi equations (see [195]) into the Hamiltonian and momentum constraints to obtain

$$\begin{aligned} {}^{(2)}R + \mathcal{K}^2 - \mathcal{K}_{ij}\mathcal{K}^{ij} - \frac{2\Lambda}{\psi} &= 2\rho, \\ D_j(\mathcal{K}^{ji} - \gamma^{ji}\mathcal{K}) &= j^i, \end{aligned} \tag{6.28}$$

where $D_j = \gamma_j{}^\mu \nabla_\mu$, $\rho := n_\mu n_\nu T^{\mu\nu}$ and $j^i := -\gamma^i{}_\nu n_\mu T^{\nu\mu}$ correspond to the energy and momentum density respectively. $\mathcal{K}_{ij}$ is the extrinsic curvature tensor with $\mathcal{K} = \mathcal{K}^i{}_i$. Note that the indices $i, j...$ represent spatial coordinate indices taking values $1, 2$. In order to implement the York-Lichnerowicz conformal decomposition, we proceed to decompose the extrinsic mean curvature tensor into its trace and trace-free part. Because here we are in two dimensions, the extrinsic curvature will have just three degrees of freedom. The decomposition of the extrinsic curvature is given as

$$\mathcal{K}_{ij} = A_{ij} + \frac{1}{2}\mathcal{K}\gamma_{ij}\,, \tag{6.29}$$

where one degree of freedom is left on the trace $\mathcal{K}$ while the other two remain in the trace-free part A_{ij}. Because the topology of the Cauchy surface is $\mathbb{S}^2$, we can guarantee that there exist coordinates such that the induced metric on Σ is conformal to the standard unit two-sphere metric. Hence, we look for initial data such that

$$\gamma_{ij} := \delta \mathring{\gamma}_{ij},$$

where $\mathring{\gamma}_{ij}$ represents the metric for the unit two-sphere in the frame $(m^a, \overline{m}^a)$ given by

$$\mathring{\gamma}_{ij} = \begin{pmatrix} 0 & 1 \\ 1 & 0 \end{pmatrix}.$$

Next, we introduce the conformal transformation for the trace-free part

$$A^{ij} := \delta^{-2}\mathring{A}^{ij},$$

from where, using the standard conformal transformation rules (see section A.4), it follows

$$A_{ij} = \mathring{A}_{ij}, \tag{6.30}$$

$$D_i A^{ij} = \delta^{-2}\mathring{D}_i\mathring{A}^{ij}. \tag{6.31}$$

The covariant trace-free part A_{ij} turned out to be conformally invariant, thus we can use this relation to identify the degrees of freedom of A_{ij}. Because of the trace-free condition for $\mathring{A}_{ij}$, it follows that the off-diagonal components are zero. Further, it is obtained that

$$\mathring{A}^{11} = \mathring{A}_{22}, \quad \mathring{A}^{22} = \mathring{A}_{11}, \quad \mathring{A}_{22} = \bar{\mathring{A}}_{11}. \tag{6.32}$$

As a consequence of the spin-weights from the frame vectors $(m^a, \overline{m}^a)$, the component A_{11} should be a function with spin-weight 2, whereas A_{22} should be with -2. We ended up with one degree of freedom in the tensor A_{ij}. Using all the mentioned properties for A_{ij}, we

proceed to write the Hamiltonian and momentum constraints. We start by considering the term $A_{ij}A^{ij}$. Using Eqs. (6.4.2) and (6.30) we obtain

$$A_{ij}A^{ij} = 2\frac{|\mathring{A}_{11}|^2}{\delta^2}, \tag{6.33}$$

where $|.|$ corresponds to the standard norm for complex functions. On the other hand, using again the conformal transformation formulas Eqs. (A.4.7), we express the two-dimensional Ricci scalar as

$$^{(2)}R = \delta^{-1}\left(\mathring{R} - \mathring{D}_a\mathring{D}^a \ln\delta\right), \tag{6.34}$$

where $\mathring{R} = 2$ since it corresponds to the Ricci scalar of the unit two-sphere. Replacing Eqs. (6.31), (6.33) and (6.34) into Eqs. (6.28) and expressing the frame vectors in terms of eth-operators by means of Eq. (6.4), it can be obtained after a straightforward calculation that the Hamiltonian and momentum constraints take the form [9]

$$\bar{\eth}\eth\,\delta = 2\delta + \delta^2\left(\frac{\mathcal{K}^2}{2} - 2\Lambda^2 - 2\rho\right) + \frac{|\eth\delta|^2}{\delta} - 2|\mathring{A}_{11}|^2, \tag{6.35}$$

$$\bar{\eth}\mathring{A}^{22} = \frac{\delta}{2}\eth\mathcal{K} + \sqrt{2}\delta^2 j^2, \tag{6.36}$$

$$\eth\mathring{A}^{11} = \frac{\delta}{2}\bar{\eth}\mathcal{K} + \sqrt{2}\delta^2 j^1, \tag{6.37}$$

where we have expressed the equations in terms of eth-operators instead of covariant derivatives. Note that because the second equation corresponds to the complex conjugate of the third one, the components of A_{ij} can be totally determined by just solving either Eq. (6.36) or (6.37). Therefore, an additional decomposition such that the conformal transverse or weighted decomposition (see [1]) is not required in contrast to the three-dimensional case. In order to write the constraints as an elliptic system of equations, let us consider a function ϖ with spin-weight $+1$ such that $\mathring{A}_{11} = \eth\varpi$. Then, using Eq. (6.32) and expressing the Laplacian on $\mathbb{S}^2$ in terms of the eth-operators by Eq. (5.30), the constraint equations can be reduced to the system of elliptic equations

$$\Delta_{\mathbb{S}^2}\delta = 2\delta + \delta^2\left(\frac{\mathcal{K}^2}{2} - 2\Lambda^2 - 2\rho\right) + \frac{|\eth\delta|^2}{\delta} - 2|\eth\varpi|^2, \tag{6.38}$$

$$\Delta_{\mathbb{S}^2}\varpi = \frac{\delta}{2}\bar{\eth}\mathcal{K} + \sqrt{2}\delta^2 j + \varpi. \tag{6.39}$$

where we have noted $j = j^2$ (note that $j^1 = \bar{j}$). As a result, we have ended up with a system of two second-order elliptic differential equations depending of $\mathcal{K}, \rho, j$, where the two latter are functions in terms of the scalar fields ψ and ω. In other words, the initial data depend on the three functions $\mathcal{K}, \psi, \omega$.

To finalize this part, we point out that there are several results regarding the existence and uniqueness of solutions of the constraint equations in three-dimensional Cauchy surfaces; see [13] for a review. All of them depend on the prescribed mean curvature which could be assumed to be either constant, near-constant, or far-from-constant. For the first two cases, it is almost completely understood whether or not a solution of the constraint equations exists, in contrast with the latter case for which just a few results are known. Nevertheless, we stress that because all these results are given for three-dimensional Cauchy surfaces or bigger

[9] We have use $\mathcal{K}_{ij}\mathcal{K}^{ij} = A_{ij}A^{ij} + \frac{1}{2}\mathcal{K}^2$.

dimensions, they may not be extended directly to two-dimensional Cauchy surfaces. Hence, in our particular situation, we do not know under what conditions solutions of the elliptic system of equations Eqs. (6.38) and (6.39) exist unless we would solve the constraints in the original manifold. Because this question goes beyond of the scope of this work, we leave it as a future project.

6.4.3 Choosing initial data

After solving the two elliptic equations, the initial data is obtained by replacing Eq. (6.29) into the relation between the mean curvature and the time derivative for the spatial metric (see section 2.2.2) $\partial_t\, \gamma_{ij} = 2\alpha \mathcal{K}_{ij} + D_{(i}B_{j)}$, where $B_i = \delta \mathring{\gamma}_{ij} B^j$, $B^j = (\beta, \bar{\beta})$ and $\alpha = \sqrt{\beta\bar{\beta} - \lambda}$. Thus, the time derivatives for the metric components δ and ϕ are obtained by

$$\partial_t \delta = \sqrt{\beta\bar{\beta} - \lambda}\, \mathcal{K}\delta^2 + \frac{\eth\bar{\beta} + \bar{\eth}\beta}{2\sqrt{2}}, \tag{6.40}$$

$$\partial_t \phi = 2\sqrt{\beta\bar{\beta} - \lambda}\, A_{11} + \frac{\delta\eth\beta - \beta\eth\delta}{\delta\sqrt{2}}. \tag{6.41}$$

Notice that we have the freedom of choosing the functions λ and β, meaning that they fix the gauge. Finally, the appropriate generalized gauge source functions should satisfy $\mathring{\Gamma}_a = f_a$. Writing the explicit form of the $\mathring{\Gamma}_a$ coefficients in terms of the eth-operators by replacing Eq. (6.4) into Eq. (6.15)

$$\begin{aligned}
f_0 = {} & \Big(\sqrt{2}\eth\beta\bar{\beta}^2 + \sqrt{2}\eth\bar{\beta}\left(\delta\lambda - \beta\bar{\beta}\right) - \sqrt{2}\lambda\eth\beta\bar{\phi} + \sqrt{2}\eth\lambda\left(\beta\bar{\phi} - \delta\bar{\beta}\right) - 2\delta\lambda\partial_t\delta + \\
& 2\beta\bar{\beta}\partial_t\delta + \delta^2\partial_t\lambda - \phi\bar{\phi}\partial_t\lambda - \bar{\beta}^2\partial_t\phi + \lambda\bar{\phi}\phi_t - \beta^2\partial_t\bar{\phi} + \lambda\phi\partial_t\bar{\phi} + \sqrt{2}\delta\lambda\bar{\eth}\beta - \sqrt{2}\beta\bar{\beta}\bar{\eth}\beta - \\
& \sqrt{2}\beta\delta\bar{\eth}\lambda + \sqrt{2}\phi\bar{\beta}\bar{\eth}\lambda + \sqrt{2}\beta^2\bar{\eth}\bar{\beta} - \sqrt{2}\lambda\phi\bar{\eth}\bar{\beta}\Big)/ \\
& 2\left(\delta^2\lambda - 2\beta\delta\bar{\beta} + \phi\bar{\beta}^2 + \left(\beta^2 - \lambda\phi\right)\bar{\phi}\right),
\end{aligned}$$

$$\begin{aligned}
f_1 = {} & \Big(-\sqrt{2}\beta^2\eth\bar{\phi} + \sqrt{2}\lambda\phi\eth\bar{\phi} + \sqrt{2}\eth\phi\bar{\beta}^2 + 2\sqrt{2}\eth\bar{\beta}\ \left(\beta\delta - \phi\bar{\beta}\right) - \sqrt{2}\lambda\eth\phi\bar{\phi} + \\
& \sqrt{2}\eth\lambda\left(\phi\bar{\phi} - \delta^2\right) - 4\beta\delta\partial_t\delta + 4\phi\bar{\beta}\partial_t\delta - 4\delta\bar{\beta}\partial_t\phi + 4\beta\bar{\phi}\partial_t\phi + 4\delta^2\partial_t\beta - 4\phi\bar{\phi}\partial_t\beta - \\
& 2\sqrt{2}\beta\delta\bar{\eth}\beta + 2\sqrt{2}\phi\bar{\beta}\bar{\eth}\beta + 2\sqrt{2}\beta^2\bar{\eth}\delta - 2\sqrt{2}\lambda\phi\bar{\eth}\delta + 2\sqrt{2}\delta\lambda\bar{\eth}\phi - 2\sqrt{2}\beta\bar{\beta}\bar{\eth}\phi\Big)/ \\
& \left(\delta^2\lambda - 2\beta\delta\bar{\beta} + \phi\bar{\beta}^2 + \left(\beta^2 - \lambda\phi\right)\bar{\phi}\right),
\end{aligned}$$

$$f_2 = \overline{\mathring{\Gamma}}_1\,. \tag{6.42}$$

Note that under the previous construction, we have assumed the spatial metric γ_{ij} to be diagonal, which implies that $\phi = 0$. However, we have written the general expression because they provide the general expression to monitor the evolution of the constraint violation covector $\mathcal{D}_a$.

We end this section by mentioning that in this work we shall find initial data by analytically solving the constraints for some particular situation. However, for more general cases, we could implement a Richardson's iteration procedure (see [82]) based on the SWSH to solve numerically the constraints equations. We believe that this opens the door to a large number of possible situations that could be studied in future investigations. In section 10.4.2 we provide an description of the algorithm.

6.5 Reconstruction of the four-dimensional metric

To finalize this chapter, we reconstruct the four-dimensional metric from the numerical solution of reduced metric $\hat{h}_{ab}$ obtained from the evolution metric h_{ab}. To begin with, we remark that there is not a general analytic procedure for solving Eq. (4.38).

We start by considering Eq. (4.38), that leads to the following system of equations

$$\begin{aligned} \partial_0\eta_1 - \partial_1\eta_0 &= \alpha_{01}, \\ \partial_2\eta_0 - \partial_0\eta_2 &= \alpha_{20}, \\ \partial_1\eta_2 - \partial_2\eta_1 &= \alpha_{12}. \end{aligned} \tag{6.43}$$

Evidently, the first two equations are evolution equations for the fields η_1 and η_2, while the latter corresponds to a constraint equation that can be written as

$$\mathcal{C} = \partial_1\eta_2 - \partial_2\eta_1 - \alpha_{12}. \tag{6.44}$$

From the curl-free property of α_{ab}, and the two previous evolution equations, it can be obtained[10]

$$\begin{aligned} \partial_0\,\mathcal{C} &= \partial_1(\alpha_{02} + \partial_2\eta_0) - \partial_2(\alpha_{03} + \partial_1\eta_0) - \partial_0\alpha_{12}, \\ &= \partial_1\alpha_{02} + \partial_2\alpha_{10} + \partial_0\alpha_{21} = 0, \end{aligned}$$

This expression shows the propagation of the constraint once it is satisfied at the initial time ($\partial_0 = \partial_t$). Hence, if we would like to solve numerically the system Eqs. (6.43), firstly, we would have to choose initial values for η_0, η_1, η_2 such that the constraint Eq. (6.44) is satisfied, and secondly, we would use the first two evolution equations to integrate numerically the components η_1, η_2. Therefore, the reconstruction of the four-dimensional metric would follow from the discussion given in section 4.6.

[10]Note that n_0 is a real function with spin-weight 0.

Chapter 7

The pseudo-spectral implementation

As explained earlier, we will use a spectral method based on spin-weighted spherical harmonics to approximate spatial derivatives. A basic introduction to spectral methods can be found in books like [73, 78, 192] and references therein. This chapter starts with a brief description of the method of lines, which sets the framework for our numerical approach. The Runge-Kutta-Fehlberg method is used as the temporal discretization (except for the convergence tests for which the explicit 4th-order Runge-Kutta method is used). We shortly discuss these methods in section 7.2. Besides, because the spin-weight spherical transform is based on the standard discrete Fourier transform, we also briefly discuss some of its properties. The core of this chapter is section 7.4, where we discuss the algorithm of complexity $\mathcal{O}(L^3)$, where L is the band limit of the functions on $\mathbb{S}^2$ in terms of the spin-weighted spherical harmonics to compute the spin-weighted spherical harmonic transforms (forward and backward) introduced by Huffenberger and Wandelt [112]. Henceforth, we will refer to this algorithm as HWTs. Then, we introduce an optimized version of this transform for the case of functions on $\mathbb{S}^2$ with spin-weight s that exhibit axial symmetry (i.e., invariant along the coordinate vector field ∂^a_φ). As a result, we obtain an algorithm of complexity $\mathcal{O}(L^2)$ which requires a low memory cost in comparison with that required by HWTs. In this work, we will focus on functions that exhibit axial symmetry, hence our spectral implementation is based on this transform. For details, improvements and applications of the HWTs for general functions in $\mathbb{S}^2$ we refer the reader to [29, 30]. In section 7.5, we discuss our method for choosing the "optimal" grid size in order to keep numerical errors as small as possible and, finally, section 7.6 provides a small discussion about our Python implementation of the AST, which is the acronym adopted to refer to the set of forward and backward transforms.

7.1 Method of lines

The framework of this work to numerically integrate the hyperbolic evolution equations in time is the method of lines (MOL); see [54, 175]. To illustrate the method, let us consider the function $u(t, x^\mu)$ that we will note simply by u, which represents the vector of unknowns. Then, a first-order system of PDEs can be written symbolically as

$$\partial_t u = f(t, u, \partial u),$$

where $f(t, u, \partial u)$ includes all the spatial derivatives. Assuming that the PDEs system is well-posed at certain time t for a given data u, the function $f(t, u, \partial u)$ has been approximately

determined somehow (for example, by implementing the fast Fourier transform) resulting in the discrete function $F(t, U)$, where the unknown u has been approximated, which is called U. This approximation yields a time-dependent system of ordinary differential equations (ODE) for U which can be symbolically written as

$$\partial_t U = F(t, U). \tag{7.1}$$

This system is called the *semi-discrete system* of the original PDE problem because the spatial derivatives have been completely approximated, while the time derivative is still "exact". Then, we solve this semi-discrete system numerically using any technique for solving ODEs. The resulting system is known as the *fully discrete system*. There are many integrators for ODEs discussed in the references above. In particular for this thesis, we choose the explicit 4th-order Runge-Kutta scheme (RK4) which will be used for convergence tests, and the Runge-Kutta-Fehlberg scheme (RKF) for normal evolutions. We devote the next section to briefly discuss their implementation.

7.2 Time integrator and convergence test

The following presentation is mainly based on the standard reference [51]. Consider the semi-discrete system Eq. (7.1) with solution U_n at certain discrete time t_n. Then, the approximate solution U_{n+1} at the next time $t_{n+1} = t_n + h$ is obtained using the RK4 (in 4 stages) as follows;

$$\begin{aligned} k_1 &= F(t_n, U_n), \\ k_2 &= F(t_n + h/2, U_n + k_1/2), \\ k_3 &= F(t_n + h/2, U_n + k_2/2), \\ k_4 &= F(t_{n+1}, U_n + k_3), \\ U_{n+1} &= U_n + (k_1 + 2k_2 + 2k_3 + k_4)/6. \end{aligned}$$

This method has local *truncation error* $\mathcal{O}(h^4)$ provided that the solution u has five continuous derivatives. This means that for sufficiently small values of the step h, there exists a constant $C > 0$ such that the difference between the discretized solution and the exact solution is smaller than Ch^4. A way to improve the accuracy of this method is by varying the time step size whenever it is required. The idea is to adapt the time step to ensure that the truncation error is kept within a specified bound, usually called *tolerance* (TOL). One of the most popular of this type is the Runge-Kutta-Fehlberg Method due to its easy implementation and effectiveness. This uses a 5th-order Runge-Kutta to estimate the local error of a RK4. Owing to the size of the equations, we omit them here. However, they can be found explicitly in [51].

On the other hand it is always essential to carry out a *convergence test*, which is a study of how the numerical solution behaves as the resolution in a discrete implementation is increased. This provides a way to quantify the *total error* in a numerical implementation. The fundamental idea is based on comparing the errors (or relative errors) from the numerical solutions obtained for different resolutions. See for instance [1] for a general discussion about it. In particular, in this thesis, we will carry out convergence tests with the discrete scheme RK4, which is described as follows. Let us assume two numerical solutions obtained with RK4 for different step sizes h_1, h_2, where $2h_2 = h_1$. Thus, the errors in each solution are $E_1 = \mathcal{O}(h_1^4)$ and $E_2 = \mathcal{O}(h_1^4/16)$ respectively. The convergence factor for the $RK4$ is defined

by

$$q := \mathrm{Log}_2\left(\frac{E_1}{E_2}\right) = 4, \tag{7.2}$$

which means that by increasing the resolution by a factor of 2 our numerical solution will approach the "exact solution" at the rate of 2^4, in line with the order of the RK4. Later, in section 8.5, we will use this algorithm to test the convergence of our numerical implementation.

7.3 The discrete Fourier transform

A basic introduction to the fast Fourier transform, its properties and implementation can be found in [73, 78, 192] and references therein. Here, we will restrict ourselves to mention the necessary properties for this work. The one-torus $\mathbb{T}$ is defined by $\mathbb{T} := \mathbb{S}^1$ parametrized by the variable $x \in [0, 2\pi]$. Then, it can be defined $L^2(\mathbb{T})$ as the space of square integrable functions in $\mathbb{T}$ with inner product

$$< f, g >:= \int_{\mathbb{T}} f(x)\overline{g(x)}\, dx\ , \tag{7.3}$$

for any $f, g \in \mathbb{T}$. According to the standard theory of Fourier series, those functions can be written in terms of a convergence series by

$$f(x) := \sum_{n=-\infty}^{\infty} a_k e^{ikx}, \tag{7.4}$$

with Fourier coefficients (also known as frequencies or modes) $a_k \in \mathbb{C}$ given by

$$a_k = \frac{1}{2\pi}\int_{\mathbb{T}} f(x)e^{-ikx}dx, \tag{7.5}$$

which decay exponentially for large values of k. Usually, these are known in the literature as *wave numbers*. Next, let us evaluate the function $f \in L^2(\mathbb{T})$ at a discrete even number of points N regularly distributed by a distance Δx over the interval $[0, 2\pi]$. Then, the *discrete Fourier transform* is defined as

$$a_k := \frac{1}{N}\sum_{m=0}^{N-1} F_m e^{-ix_m k}, \tag{7.6}$$

where k takes integer values from $-N/2 + 1$ to N, and F_m denotes the the numerical values of the function f sampled at the points $x_m = (2\pi/N)m$ for $m \in \{0, 1, ..., N-1\}$. On the other hand, the *inverse discrete Fourier transform* is defined as

$$F_m := \sum_{k=-N/2+1}^{N/2} a_k e^{ix_m k}. \tag{7.7}$$

Hereafter we call the highest frequency $L = N/2$ as the *band limit*. The above equation is known as the *discrete backward Fourier transform*. We have obtained the numerical values of the function $f \in \mathrm{L}^2(\mathbb{T})$. Note that the Fourier series expansion has been truncated at some wave number L. In the light of these transforms, any function $f \in \mathrm{L}^2(\mathbb{T})$ can be expressed either in terms of its sampled values F_m or in terms of the set of modes a_k's . Note that for

an odd number of grid points, the limits in the equation above are modified by $-(N-1)/2$ for the lower limit and $(N-1)/2$ for the maximum (see [46] for details). Clearly, the two sets are related by a square $N \times N$ matrix. Thus, swapping representations requires performing N^2 operations. However, thanks to the algorithm of Cooley-Tukey [68], this computation can be carried out in $\mathcal{O}(N\text{Log}_2 N)$ operations.

Conforming to Eq. (7.4), we require an infinite number of Fourier coefficients to describe a continuous smooth function exactly. However, the Nyquist-Shannon theorem states that for the discrete case, a finite number of Fourier coefficients is enough for sampling function. Further, this number is determined by the size of the grid where the function is sampled. The Nyquist-Shannon theorem states the following:

Theorem 7.3.1 *If $f \in L^2(\mathbb{T})$ is band-limited so that its Fourier coefficients vanish after wave number k, then f can be completely reconstructed from its values sampled at intervals of Δx provided that $1/\Delta x \geq k$.*

The highest frequency k that can be reconstructed is known as the *Nyquist frequency* or the *cut-off wave number* that we shall denote by k_c. The theorem also asserts that if the sampling is chosen such that it fails to satisfy the criterion above, the frequency k outside of the Nyquist frequency band, i.e., $|k| > k_c$, will reappear in the reconstructed function at a frequency $k + mk_c$, where m is an integer such that $|k + mk_c| \leq k_c$. This fact is known as the *aliasing error*. In other words, aliasing error occurs when a high frequency is sampled at discrete intervals and misinterpreted as a low frequency. In addition, aliasing may occur during the computation of products among functions sampled on a finite grid. However, if the Fourier series of both functions above are truncated up to some frequency $k = 2k_c/3$ (and setting the other $1/3$ frequencies equal to zero), then this problem can be avoided. This procedure is known in the literature as the $2/3$-*rule* to prevent aliasing. For a more detailed discussion see for instance [73, 192].

We finalize this section by mentioning the *truncation error*, that is the error coming from the difference between f and its discretization F. As noted in [97], it can be proved that the order of the truncation error for a Fourier series approximation of certain p-differentiable function f that is truncated at wave number k is $\mathcal{O}(1/k^p)$. Therefore, it is well-known that "spectral methods converge exponentially" for smooth functions, hence are expected to be more accurate than finite difference methods (like RK4) that converge polynomially.

7.4 Implementation of the spin-weighted transforms

7.4.1 General description of the HWTs

To begin with, let us consider a square integrable spin-weighted function $f \in L^2(\mathbb{S}^2)$ with spin-weight s. The forward and backward spin-weighted spherical harmonic transformations are defined, respectively, by

$$ {}_s a_{lm} = \int_{\mathbb{S}^2} f(\theta, \varphi)\, {}_s\overline{Y}_{lm}(\theta, \varphi)\, d\Omega, \tag{7.8} $$

$$ {}_s f(\theta, \varphi) = \sum_{l=|s|}^{L} \sum_{m=-l}^{l} {}_s a_{lm}\, {}_s Y_{lm}(\theta, \varphi), \tag{7.9} $$

where the decomposition has been truncated at the maximal mode L. Henceforth, we shall refer to it as the *band limit*. To calculate numerically the integral in Eq. (7.8) over a finite

coordinate grid, a quadrature rule and knowledge of the SWSH over that grid is required. The quadrature rule presented in [112] is based on a smooth non-invertible map where the poles are geometrically expanded as circles on $\mathbb{T}^2$. Once a quadrature rule on equidistant points on $\mathbb{T}^2$ has been specified, we proceed to compute the SWSH which are written in terms of the Wigner d-matrices introduced in section 5.3.2, and which can be calculated using recursion rules given by [191]. Adopting the notation $\Delta^l_{mn} := d^l_{mn}(\frac{\pi}{2})$ the Wigner d-matrices in Eq. (5.16) can be expressed as

$$d^l_{mn}(\theta) = i^{m-n} \sum_{q=-l}^{l} \Delta^l_{qm}\, e^{-iq\theta} \Delta^l_{qn}, \tag{7.10}$$

where n and m take integer values that run from $-l$ to l. Later in section 7.4.2, we explain in detail how to compute the Δ^l_{nm} terms. The expression above allows us to write the *forward* and *backward spin-weighted spherical harmonic transforms* respectively as

$$ {}_sa_{lm} = i^{s-m} \sqrt{\frac{2l+1}{4\pi}} \sum_{q=-l}^{l} \Delta^l_{qm} I_{qm} \Delta^l_{qs}, \tag{7.11}$$

$$ {}_sf(\theta,\varphi) = \sum_{m,n} e^{im\theta} e^{in\varphi} J_{mn}, \tag{7.12}$$

where the matrices I_{mn} and J_{mn} are computed from the standard two-dimensional Fourier transforms (forward and backward respectively) over 2π-periodic extensions of the function ${}_sf(\theta,\varphi)$ into $\mathbb{T}^2$. In general, the complexity of the outlined algorithm is $\mathcal{O}(L^3)$.

7.4.2 Axially symmetric spin-weighted transforms

The axially symmetric spin-weighted forward transform

Let us begin by pointing out that the previous algorithm can be decomposed into two main tasks; namely, computation of the Δ^l_{mn} terms and calculation of the I_{mn} and J_{mn} matrices by means of the two-dimensional forward and backward Fourier transform respectively, acting over some given function $f(\theta,\varphi)$. Next, we discuss in detail how to simplify these tasks for the case of axially symmetric functions, i.e., functions that only depend on the θ coordinate. Let us consider a square integrable axially symmetric spin-weighted function $f(\theta) \in L^2(\mathbb{S}^2)$ with spin-weight s. Because of the φ dependence of the non-zero m modes of SWSH, see Eq. (5.16), we can write the function $f(\theta)$ in terms of ${}_sY_{l0}(\theta,\varphi)$. Hence, the forward spin-weighted spherical harmonic transform Eq. (7.8) can be written in a simple form as

$$ {}_sa_l = \int_{\mathbb{S}^2} f(\theta)\, {}_s\overline{Y}_l(\theta)\, \sin\theta\, d\theta d\varphi,$$

where we have used the notation ${}_sa_l := {}_sa_{l0}$ and ${}_sY_l(\theta) := {}_sY_{l0}(\theta,\varphi)$. Then, we rewrite Eq. (7.11) as

$$ {}_sa_l = i^s \sqrt{\frac{2l+1}{4\pi}} \sum_{n=-l}^{l} \Delta^l_{n0} I_n \Delta^l_{ns}, \tag{7.13}$$

with[1]

$$ I_n := 2\pi \int_0^{\pi} e^{-in\theta}\, f(\theta) \sin\theta\, d\theta. \tag{7.14}$$

[1]The factor 2π comes from the trivial integral over φ.

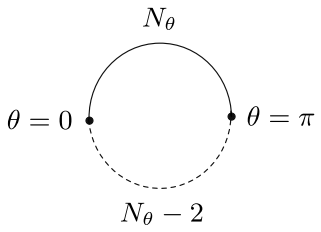

Figure 7.1: *Sampling on* $\mathbb{T}$.

Similarly to the procedure for HWTs [112], the number of computations required to obtain the spectral coefficients ${}_sa_l$ can be reduced by a factor of two by using symmetries associated with the Δ^l_{mn} quantities. In addition, we can introduce another reduction owing to the fact that $\Delta^l_{n0} = 0$ for $l + n = odd$. This allows us to reduce the number of computations by a further factor of 2. Therefore, we define *the axially symmetric spin-weighted forward transform* (ASFT) as

$$ {}_sa_l = i^s \sqrt{\frac{2l+1}{4\pi}} \sum_{n \equiv l (\mathrm{mod} 2)}^{l} \Delta^l_{n0} J_n \Delta^l_{ns} \quad (n+=2), \tag{7.15} $$

where n is a positive integer that increases in steps of two and starts at 0 or 1 depending on whether l is even or odd. The vector J_n is defined by

$$ J_n := \begin{cases} I_n & n = 0, \\ I_n + (-1)^s I_{(-n)} & n > 0. \end{cases} \tag{7.16} $$

The evaluation of I_n can be carried out by extending the function ${}_sf(\theta)$ to $\mathbb{T}$ as a 2π-periodic function. This allows the implementation of the standard one-dimensional Fourier transform in contrast to the general case of HWTs that, because of the φ-dependence, requires a two-dimensional Fourier transform. Now, we define the extended function on $\mathbb{T}$ as

$$ {}_sF(\theta) := \begin{cases} {}_sf(\theta) & \theta \leq \pi, \\ (-1)^s \, {}_sf(2\pi - \theta) & \theta > \pi. \end{cases} $$

Clearly, the vector I_n remains unchanged because ${}_sF(\theta)$ agrees with ${}_sf(\theta)$ on the integration domain in Eq. (7.14). The function ${}_sF(\theta)$ is chosen to be 2π-periodic, hence it can be written as an one-dimensional Fourier sum. However, firstly we need to define the number of sampling points in $\mathbb{T}$. Let us consider Fig. 7.1. In this diagram, the upper part of the circumference represents the number of samples N_θ taken for $0 \leq \theta \leq \pi$, whereas the lower part shows the $N_\theta - 2$ samples for $\pi < \theta < 2\pi$. Clearly, the subtraction by 2 in the lower half of the circumference comes from the extraction of the poles to avoid oversampling. Therefore, to sample a function on $\mathbb{T}$ we proceed as follows. If the desired number of samples for a function ${}_sf(\theta)$ on $\mathbb{S}^2$ is N_θ, then the number of samples for the extended function ${}_sF(\theta)$ on $\mathbb{T}$ should be $N'_\theta = 2(N_\theta - 1)$ and the spatial sampling interval will be $\Delta\theta = 2\pi/N'_\theta$. Therefore, the extended function can be written as a 1-dimensional Fourier sum by

$$ {}_sF(\theta) = \sum_{k=-N'_\theta/2+1}^{N'_\theta/2} F_k e^{ik\theta}. $$

The substitution of this equation into Eq. (7.14) yields

$$I_n = 2\pi \sum_{k=-N'_\theta/2+1}^{N'_\theta/2} F_k w(k-n), \tag{7.17}$$

where $w(p)$ is a function $\mathbb{Z} \to \mathbb{R}$ defined by

$$w(p) = \int_0^\pi e^{ip\theta} \sin\theta \, d\theta = \begin{cases} 2/(1-p^2) & p \text{ even}, \\ 0 & p \text{ odd}, \, p \neq \pm 1, \\ \pm i\pi/2 & p = \pm 1. \end{cases}$$

By comparison with Eq. (7.17) we note that the latter is proportional to a discrete convolution in the spectral space. Therefore, it can be evaluated as a multiplication in the real space such that I_n is the 1-dimensional forward Fourier transform of $2\pi \, {}_sF \, w_r$ as follows

$$I_n = \frac{2\pi}{N'_\theta} \sum_{q'=0}^{N'_\theta-1} \exp\left(-inq\Delta\theta\right) \, {}_sF(q'\Delta\theta) \, w_r\left(q'\Delta\theta\right),$$

where $w_r(q'\Delta\theta)$ is the real-valued quadrature weight in $\mathbb{T}$ given by

$$w_r(q'\Delta\theta) = \sum_{p=-N'_\theta/2+1}^{N'_\theta/2} e^{-ipq'\Delta\theta} \, w(p).$$

Finally, we want to emphasize that even though this way of sampling functions on $\mathbb{T}$ allows us to include the value of the extended function at the poles, it yields an even number of modes in spectral space. Hence, we will not have the same number of positive and negative modes after the implementation of ASFT. Indeed, for the mode $I_{N'_\theta/2}$ (see Eq. (7.16)), the vector $J_{L'}$ cannot be calculated since the term $I_{-N'_\theta/2}$ is not given by the 1-dimensional forward Fourier transform. We avoid this issue by calculating the set of J_n terms up to $n = N'_\theta/2 - 1$. Note that setting $I_{N'_\theta/2}$ to zero does not constitute a loss of information due to the exponential decay of the spectral coefficients of the Fourier transform. In fact, this extra mode is in general numerically negligible, hence it will not affect the accuracy of the ASFT.

Now, in order to satisfy the Nyquist condition [78], the relation between the number of sampling points in $\mathbb{T}$ and the band limit must satisfy the inequality

$$2(N_\theta - 1) \geq (2L+1) + 1,$$

where the last term on the right-hand side comes from counting the extra term without a mirrored partner. As a result, the maximum value of the band limit for which the ASFT is exact is given for

$$L = N_\theta - 2. \tag{7.18}$$

The axially symmetric spin-weighted backward transform

This transform maps the spectral coefficients ${}_sa_l$ back to the corresponding axially symmetric function on $\mathbb{S}^2$. As the inverse transform does not contain integrals, issues of quadrature accuracy do not arise. In a similar way as we implemented the properties of the 3-dimensional

Δ^l_{nm} term to obtain Eq. (7.15), we can write from Eq. (7.12) *the axially symmetric spin-weighted backward transform* (ASBT) as

$$ {}_sf(\theta) = \sum_{n=-N'_\theta/2+1}^{N'_\theta/2} e^{in\theta} G_n, $$

where the vector G_n is given by

$$ G_n := \begin{cases} 0 & \text{if } n = N'_\theta/2, \\ i^s \sum\limits_{l\equiv \mathrm{mod}_2(n)}^{L} \sqrt{\frac{2l+1}{4\pi}}\ \Delta^l_{n(-s)}\ {}_sa_l\ \Delta^l_{n0} & (l\mathrel{+}=2). \end{cases} \tag{7.19} $$

Similar to Eq. (7.15), l increases in steps of two and starts at $l(\mathrm{mod}2)$. We set $G_{N'_\theta/2} = 0$ because in the implementation of the ASFT we chose $I_{N'_\theta/2} = 0$. The evaluation of Eq. (7.19) is carried out by a 1-dimensional inverse Fourier transform that results in a function ${}_sf(\theta)$ sampled on $\mathbb{T}$. So, as we require the function on $\mathbb{S}^2$, we may simply truncate the output at $\theta = \pi$.

Computation of the three-dimensional Δ^l_{nm}

So far, the forward and backward spin-weighted spherical harmonic transforms have been simplified for axially symmetric functions by the implementation of a one-dimensional Fourier transform instead of a two-dimensional one as required in the algorithm HWT. In fact, we can simplify the computation of the Δ^l_{nm} terms even further. This has a significant effect on the efficiency of both ASFT and ASBT, given that such a task takes around half of the execution time in practical situations. Therefore, we devote this section to discussing this issue.

To begin with, we explain how the Δ^l_{nm} terms are computed and we bring up a relevant fact for both ASFT and ASBT. By examination of Eq. (7.15) and Eq. (7.19), we realize that we do not really need to calculate the complete set of Δ^l_{nm} terms[2] to perform the transform. Instead, we just need to compute up to the Δ^l_{ns} term, where s is the spin-weight of the function that is supposed to be transformed. This yields a remarkable speed-up of the algorithm since mostly $s \ll L$. Now, based on this, we proceed to compute the Δ^l_{ns} terms implementing the recursive algorithm introduced by Trapani and Navaza in [191]. The recursive relations are given by the following equations

$$ \begin{aligned} (a) \qquad \Delta^l_{l0} &= \sqrt{\frac{2l-1}{2l}}\Delta^{l-1}_{(l-1)0}, \\ (b) \qquad \Delta^l_{lm} &= \sqrt{\frac{l(2l-1)}{2(l+m)(l+m-1)}}\Delta^{l-1}_{(l-1)(m-1)}, \\ (c) \qquad \Delta^l_{nm} &= \frac{2m}{\sqrt{(l-n)(l+n+1)}}\,\Delta^l_{(n+1)(m)} - \sqrt{\frac{(l-n-1)(l+n+2)}{(l-n)(l+n+1)}}\,\Delta^l_{(n+2)(m)}, \end{aligned} $$

where the letters "a", "b" and "c" denote the sequence in which they should be used. We note that terms with a combination of indices outside of the correct range are set to be 0. One way to visualize the above algorithm is by means of the pyramidal representation of the Δ^l_{ns} terms in Fig. 7.2. The volume of the complete pyramid represents the complete

[2] n and m take integer values from $-l$ to l.

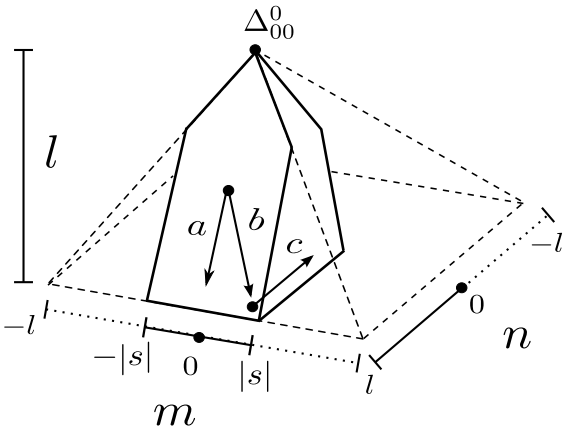

Figure 7.2: *Pyramidal representation for the* $\Delta^l{}_{mn}$ *terms.*

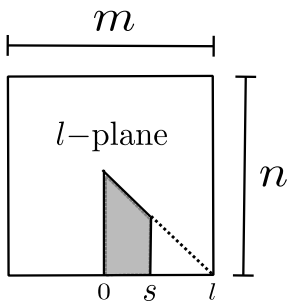

Figure 7.3: *Upper view of the l-plane.*

set of the Δ^l_{nm} terms. Setting the top peak of the pyramid as $\Delta^0_{00} = 1$, we start moving down both in vertical direction using rule (a), and in diagonal direction by (b). Thus, the Δ^l_{ns} terms in the right-hand side in the front face of the pyramid can be found. Then, using rule (c) repeatedly, allows to find the terms behind the front face in order to calculate the right-hand side of the pyramid volume. If we would need to compute the full set of Δ^l_{nm} terms, we would need to repeat this algorithm in order to obtain the complete right-hand side of the pyramid volume. However, we just need to repeat step (b) until we reach the row corresponding to $l = |s|$ (for the given l-level) because we are just interested in computing the first Δ^l_{ns} terms. Moreover, since only the Δ^l_{ns} terms with positive values of n are needed to compute both ASFT and ASBT (see Eqs. (7.15) and (7.19)), we implement rule (c) until we reach the column $n = 0$. The left-hand side of the pyramid volume can be obtained by applying the mirror rule $\Delta^l_{n(-|s|)} = (-1)^{l-n}\Delta^l_{n|s|}$ (see [191]). In Fig. 7.3, we observe a schematic representation of this, where the number of Δ^l_{ns} terms that have to be computed are represented by the gray section. In this illustration we call the collection of the Δ^l_{ns} terms for each l as *l-plane*. Note that the gray section is not a rectangle since we can implement the symmetric transposition rule $\Delta^l_{n|s|} = (-1)^{|s|-n}\Delta^l_{|s|n}$. In short, we will require $\mathcal{O}(L^2)$ operations to compute the Δ^l_{ns} terms needed to implement both ASFT and ASBT, which will allow us to pre-compute the Δ^l_{nm} terms for a low memory cost in comparison with the algorithm for HWTs[3].

Outlook of the transforms

We have presented both the forward and backward spin-weighted spherical harmonic transform for the axial symmetric case by implementing simplifications of the general algorithm HWTs in order to optimize them for axially symmetric functions in $\mathbb{S}^2$. The first main simplification is the replacement of the two-dimensional by an one-dimensional Fourier transform in both the forward and backward transforms. This substitution reduces the number of computations from $\mathcal{O}(L^2 \log_2 L^2)$ to $\mathcal{O}(L \log_2 L)$. The second simplification lies in the fact that for both the forward and backward transforms we do not need to compute the full set of Δ^l_{nm} terms (which are in the general case L^3 terms). The resulting algorithm requires just $\mathcal{O}(L^2)$ operations for each transform. However, if we pre-compute the Wigner coefficients Δ^l_{mn}, as

[3]For $L = 1024$, the memory cost of AST is $\backsim$ 1MB whereas for HWT is $\backsim$ 1 GB.

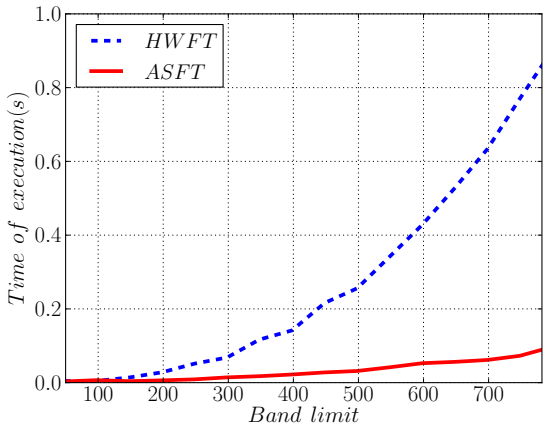

Figure 7.4: *Time performance comparison between HWFT and ASFT.*

we are going to do it in our numerical evolution, the transform only requires $\mathcal{O}(L \log_2 L)$ operations. In what follows, we refer to those as the axial symmetric transforms (AST).

To finalize this outlook of the algorithm, in Fig. 7.4 we contrast the time of execution between the HWFT and ASFT applied to a function f with spin-weight 0. As expected, for lower band limits the time difference between both transforms is not really significant. However, as we increase the band limit the difference becomes significant. In section 7.6 we will provide some details of our Python implementation of those transforms.

7.5 Choosing the optimal grid

Because the axially symmetric transforms are based on the Fourier transform, we expect that spectral coefficients decay exponentially to zero when the band limit tends to infinity. Theoretically speaking, a function is described in spectral space by an infinite number of spectral coefficients. On the other hand, because of the machine rounding error[4], any sufficiently smooth function is described by a finite set of spectral coefficients that contribute numerically to the spectral decomposition. In other words, the spectral coefficients with an order lower than 10^{-15} are negligible numerically, thus unnecessary for an accurate description of functions in the spectral space. Hereafter, we call the l-order to the last mode above the order 10^{-15} as the *optimal band limit*. Consequently, by virtue of Eq. (7.18) the optimal band limit defines the *optimal number of grid points*. Taking a larger number of grid points in comparison than the optimal one will add unnecessary computations in the transform; consequently, the accuracy is reduced instead of enhanced. We refer to this as the sampling error. In our implementation this error in controlled by keeping the number of grid points as close as possible to the optimal case. To this end, we proceed as follows. Initially, we sample the initial data in a large grid. In our case we have chosen $N_\theta = 1025$. Then, we apply the ASFT to each function of the initial data and identify the highest mode, which is just above the threshold 10^{-15}. In other words, we identify the optimal band limit for each function of the system. From all these modes we set the order of the highest mode as the optimal band limit for the initial data. Henceforth, we will refer to this as *the global optimal band*

[4]In this paper, the terms "machine rounding error" and "machine precision" refer to the finite precision such that numbers can be represented in a computer. We always assume that this precision is of order 10^{-15} which corresponds to standard "double precision".

limit. Using Eq. (7.18) we obtain the optimal number of grid points required to sample the functions of the system. Finally, we begin the numerical solution of the system by interpolating the initial data in the optimal grid. Now, we discuss how we keep the optimal grid size during the evolution. For each time step, we check the last mode of each field in order to observe whether they are smaller than some given tolerance. For this implementation, it has been set to 10^{-14}. Then, if some of those modes do not satisfy the mentioned condition, then the number of grid points is not enough for sampling some of the functions of the system. Therefore, we need to interpolate all the functions to a bigger grid. We point out that the new grid should not differ too much from the previous one because, as we mentioned before, it could lead to many unnecessary grid points, hence to larger errors. In this implementation, we decided to increase the grid by four points each time it is required. Using this small increment, we expect to stay close enough to the optimal grid and as a consequence keep a good accuracy.

To finalize this section, we point out that due to non-linearities in our evolution equations, some kind of filtering process is required in order to avoid the so-called aliasing effect. For this we use the 2/3-rule explained in section 7.3.

7.6 Code implementation of the AST

As an outcome of this thesis, we have written a Python module (for Python 2.7) for the implementation of the AST based on the algorithm discussed previously. For a basic introduction to this programming language we recommend [53]. The module allows us to create objects of spin-weighted functions for which we can define an algebra. Hence, the basic operations of sum, subtraction and multiplication among spin-weighted functions can be defined. We devote this last section to explaining the general structure of this module as well as providing a simple example for its use. It is for free distribution and can be found in `http://gravity.otago.ac.nz/wiki/index.php/People/LeonEscobar` at the link `Axial symmetric spin-weighted functions`.

The module is divided into two pieces. The first part contains the implementation of the AST algorithm in C-language. This is with the aim of making the code performance as fast and efficient as possible. The source code for the implementation of the ASFT and ASBT, as well as the eth-operators, are contained in this part. All these functions are compiled in a dynamical C-library called "`libaxial_spin_trans.so`". The source C-code for building up this library, as well as the directions, are included (in a "readme" file) in the directory `c_code`. Hence, even though the entire module has been written with the aim to be used in Python, the C-library can be also implemented independently in another C-code if it is desired. The second part of the module consists of the Python implementation. This part uses the C-library mentioned above to define the Python functions of the module. One of the main features of this module is the possibility for defining objects from the class "functions". These objects will represent the axial symmetric spin-weighted functions that have two attributes. The first one contains the discrete representation of the function at the interval $[0, \pi]$ as a vector (we are assuming functions like $f(\theta)$).

The second attribute is the spin-weight of the function. In addition, we define the basic operations of sum, subtraction and multiplication among spin-weighted functions for the object of this class. The ASFT, ASBT and eths-operator will act only over an object from this class giving as output functions belonging to this class as well. For this reason, this Python module can be seen not only as a set of functions but also as a Python environment to work with axial symmetric SWSH. Here there is a summary of the functions available in

the module (`f` represents an object that belongs to the class `function_in_s2`.)

1. `create_mesh(Ntheta)`: This function creates an appropriate grid based on the number of samples.

2. `function_in_s2(list_of_functions,list_of_spins)`: This function defines functions in $[0, \pi]$ as objects. Each function is an object with two attributes as we have already mentioned. Note that we can define an array of functions with their respective array of spin-weights.

3. `forward(f)`: To compute the forward axial symmetric spin transform of `f`. The output is an object from the class `salm` which contains the spectral representation of the function.

4. `backward(salm)`: To compute the backward axial symmetric spin transform to objects from the class `salm`. The output is an object of the class `function_in_s2`.

5. `ethU(f)`: $\eth$ (raising spin) applied over `f`. The output is another object of the class `function_in_s2`.

6. `ethD(f)`: $\bar{\eth}$ (lowering spin) applied over `f`. The output is another object of the class `function_in_s2`.

7. `C(f)`: To take the complex conjugate of `f`. The output is another object of the class `function_in_s2`.

In order to better illustrate how to use these functions, in what follows we discuss a short example of their implementation. Let us consider the following Python code which shows how to get started with this module.

```
1 import sys
2 import numpy as np
3
4 #To include the path where the is module is to the variable enviroment
5 sys.path.append('/path/to/the/module')
6 from Axial_Spin_Weight_Functions import functions as sf
7
8 #***************Defining grid *****************
9 Ntheta = 64
10 theta = sf.create_mesh( Ntheta )
11
12 #************Defining the functions************
13 fa = np.cos(theta)
14 fb = np.sin(theta)
15 f_on_grid = np.array( [ fa, fb ] )
16 spins    =  np.array( [ 0 , 1  ] )
17 f = sf.function_in_s2( f_on_grid , spins )
18
19 #****** Computing the spectral coefficients******
20 al = sf.forward(f)
21 # Returns all the spectral coefficients of the first function
22 print al[0]
23 #returns from the first set sal, the coefficients with the first spin
24 print al[0,1]
25 # Recovering the function
```

```
26 f2 = sf.backward( al )
27
28 #********* Action of the eths operators *********
29 f3 =   sf.ethU( f2 )
30 print "resulting spin", f3.spin
31 print "checking the function on the grid" ,f3.map
32 f4 =  sf.ethD(  sf.ethU( f3[1] ) )
33 print "resulting spin", f4.spin
34 print "checking the function on the grid" ,f4.map
35
36 #******** Operations between functions **********
37 f5 = f[0] + f[1]
38 print "resulting spin", f5.spin
39 print "checking the function on the grid" ,f5.map
40 f6 = f * f2
41 print "resulting spin", f6.spin
42 print "checking the function on the grid" ,f6.map
43
44 # Error of no allowed operation.
45 print f2 + f4
```

In the first two lines, we load some default Python modules. In lines 5 and 6 we set the environment of variable such that we can load the axial symmetric transform module `Axial_symmetric_spin_weight_functions` in our script. Note that we have loaded the module under the name `sf`. In lines 9 and 10 we define the grid. From line 13 to 17, we define the array of axial symmetric spin-weighted functions composed by the functions `fa` and `fb` (sampled as vectors) with spin-weights listed in the array `spins`. Once we have defined the function`f` we can use the ASFT, ASBT and the eths-operator on it, or in each component by separated. For example, in line 20, we compute the spectral coefficients of the array `f` by using the ASFT. Clearly, we can also recover the array of functions sampled at the grid from the spectral coefficients by using ASBT. From line 29 to 32, we test the action of the eth-operators in `f` while from line 37 to 45, we test the algebra corresponding to SWSH. We want to point out that each component of the array `f` is also an object of the class `function_in_s2`. Hence, we can also treat them as an independent axial symmetric function (with its respective spin-weight) as is shown in lines 32 and 37. We have included this Python script, called `example.py`, in the directory `how_to_use_me`.

Finally, we would like to mention that we have generalized this module to the general SWSH. This module uses the C-library `libcoffee.so` linked with the C-library given by Huffenberger and Wandelt in `spinsfast.so`. The latter can be downloaded at http://www.physics.miami.edu/~huffenbe/research/spinsfast. The generalization of the Python module is straightforward from the axial symmetric case, keeping almost the same structure of the objects and functions. This module can be also found http://gravity.otago.ac.nz/wiki/index.php/People/LeonEscobar at the link General spin weighted functions. Because in this work we are only interested in considering axial functions, we have simply used this module to test the performance of the axial symmetric one, but we did not use it for any of our numerical studies. However, it may be useful for a future research in more general scenarios.

Part III

Applications to Gowdy spacetimes and their analysis

Chapter 8

Testing our implementation on a Gowdy spacetime $\mathbb{R} \times \mathbb{S}^3$

To analyse the consistency, accuracy and feasibility of our numerical infrastructure, this chapter we reproduce an inhomogeneous cosmological solution of the vacuum EFE with spatial topology $\mathbb{S}^3$. In addition, we conduct a detailed numerical analysis to identify the major sources of potential errors and explore the behaviour of the constraints for different gauges by choosing different generalized gauge source functions.

8.1 The class of smooth Gowdy symmetry generalized Taub-NUT solutions

As aforementioned in chapter 3, solutions of the EFE have the property of being uniquely determined (up to isometries) by the Cauchy data on a Cauchy surface, at least locally in time. However, there exist some special cases for which the maximal globally hyperbolic development of the data can be extended in several inequivalent ways. These extensions are not globally hyperbolic, hence there is a *Cauchy horizon* whose topology and smoothness may be, in general, complicated. Furthermore, closed causal curves exist in the extended regions which violate the causality conditions. A well-known example of this sort of solution is the Taub solution [188], which is a two-parametric family of spatially homogeneous cosmological models with spatial topology $\mathbb{S}^3$. This solution can be extended through smooth complete Cauchy horizons with topology $\mathbb{S}^3$ to the Taub-NUT solutions [144].

As a test for our numerical implementation described along this chapter, we reproduce a family of exact inhomogeneous solutions with spatial topology $\mathbb{S}^3$ that belong to the class of *smooth Gowdy-symmetric generalized Taub-NUT solutions* introduced by Beyer et al. in [32] and motivated by the early work of Moncrief [135] about generalizations of the Taub-NUT solution. This class incorporates all Gowdy-symmetric time-oriented maximally extended globally hyperbolic solutions of the EFE in vacuum with zero cosmological constant and spatial topology $\mathbb{S}^3$. To cover the maximal global hyperbolic developments (see [63, 162]), the class is written in terms of some "areal" time function $t \in (0, \pi)$ and the Euler coordinates introduced in section 6.2 for the spatial part. In these coordinates the class of smooth metrics takes the form[1]

$$g_{ab} = e^{M}(-\mathrm{d}t^2 + \mathrm{d}\theta^2) + R_0 \left(\sin^2 t \; e^{u}(\mathrm{d}\rho + Q \; \mathrm{d}\varphi)^2 + \sin^2 \theta \; e^{-u} \; \mathrm{d}\varphi^2\right), \tag{8.1}$$

[1]Note that in order to be consistent with our notation, we have changed the original notation from [32] by $\rho_1 \to \rho$ and $\rho_2 \to \varphi$.

with a positive constant R_0 and smooth functions u, Q and M that depend only on t and θ. A large class of such solutions of the Einstein vacuum equations were constructed in [32] as an application of the Fuchsian method (see [4, 5, 34]).

8.2 The family of exact solutions

Here we discuss a three-parametric family of explicit smooth Gowdy-symmetric generalized Taub-NUT solutions introduced by Beyer et al. in [33] which can be considered as spatially inhomogeneous generalizations of the Taub solution. This family of exact solutions was derived by implementing the so-called soliton methods (see [109]), and it was shown that they are regular in the maximal globally hyperbolic region $0 < t < \pi$. The components of the metric Eq. (8.1) for this family of solutions are given as

$$e^M = \frac{R_0}{64c_1^3}\left(U^2+V^2\right), \quad e^u = \frac{R_0}{64c_1^2}\frac{Ue^{-M}}{1+y},$$
$$Q = x + \frac{c_3}{8}\left(1-x^2\right)\left(7+4y+y^2+\frac{(1-y)V^2}{4c_1^2U}\right),$$

where

$$U := c_3^2\left(1-x^2\right)(1-y)^3 + 4c_1^2(1+y), \quad V := 4c_1\,(1-y)\,(1-c_3x(2+y))\,,$$

with $x=\cos\theta$, $y=\cos t$. Here c_1 and c_3 are real constants that, together with R_0, define a particular solution, thus this is a three-parametric family of exact solutions. Clearly, according to the definition of the Euler coordinates in Eq. (5.5), the coordinate vector fields ∂^a_ρ and ∂^a_φ are non-vanishing Killing vector fields with closed circles as integral curves. This allows us to perform the Geroch reduction with respect to either of the two fields by defining the corresponding projection map π, quotient manifold S, the objects ψ, ω and the projected metric h_{ab} [33]. In this work we perform the Geroch reduction only with respect to the vector field ∂^a_ρ, hence we obtain the smooth orbit manifold $S=\mathbb{R}\times\mathbb{S}^2$. The push-forward of the other vector field along π defined in Eq. (5.7), which we denote by ∂^a_φ, is a smooth Killing field of the $2+1$ metric h_{ab}. Consequently, all the metric components are axial symmetric in the sense defined in section 7.4.2, hence the axial symmetric transform introduced introduced in chapter 7 is the natural choice for our numerical implementation discussed below. After the symmetry reduction procedure we find that

$$\psi = R_0\sin^2 t\; e^u, \tag{8.2}$$
$$\partial_t\omega = -R_0\,\frac{\sin^3 t}{\sin\theta}\,e^{2u}\partial_\theta Q, \tag{8.3}$$
$$\partial_\theta\omega = -R_0\,\frac{\sin^3 t}{\sin\theta}\,e^{2u}\partial_t Q, \tag{8.4}$$
$$h_{ab} = \psi\left(\, e^M(-\mathrm{d}t^2+\mathrm{d}\theta^2) + R_0\sin^2\theta\; e^{-u}\mathrm{d}\varphi^2\,\right),$$

where ψ and ω are the norm and twist associated to ∂^a_ρ and h_{ab} the $2+1$ metric. Now, as described in section 6.3.2, see Eq. (6.2), we write the metric in terms of the frame $(T^a, m^a, \overline{m}^a)$

$$\lambda = R_0\sin^2 t\; e^{M+u}, \tag{8.5}$$
$$\beta = 0, \tag{8.6}$$
$$\delta = R_0\sin^2 t\;\left(e^{M+u}+R_0\right)/2, \tag{8.7}$$
$$\phi = R_0\sin^2 t\;\left(e^{M+u}-R_0\right)/2. \tag{8.8}$$

We notice that the smooth contracted connections coefficients $\mathring{\Gamma}_\mu$ associated with h_{ab} are calculated from Eq. (6.15) by first computing the contracted Christoffel symbols Γ_μ of h_{ab} and then by calculating $\breve{\Gamma}_\mu$ from Eq. (6.14) and the background metric Eq. (6.13). The results are

$$\mathring{\Gamma}_0 = -\cot t, \tag{8.9}$$

$$\mathring{\Gamma}_1 = \mathring{\Gamma}_2 = \sqrt{2}\, c_3^2\, \csc^2 t\, \sin^8 \frac{t}{2}\, \sin 2\theta. \tag{8.10}$$

Henceforth, we refer to h_{ab} as the $2+1$ smooth Gowdy symmetry generalized Taub-NUT solutions (GTN). We point out that this family of solutions contains the well-known Taub-NUT solution [188] as a special case by setting $c_3 = 0$ and writing c_1 and R_0 in terms of arbitrary parameters l and m as

$$c_1 = \frac{1}{l}\left(\sqrt{l^2+m^2}+m\right), \quad R_0 = 2l\sqrt{l^2+m^2}, \tag{8.11}$$

for $l > 0$ and $m \in \mathbb{R}$. This is a spatially homogeneous solution. On the other hand, inhomogeneous solutions are obtained by choosing any non-zero value for c_3 (see [33] for details).

8.3 Choice of the gauge and initial data

As we mentioned in the previous section, a homogeneous solution of the GTN family can be obtained by choosing $c_3 = 0$, whereas inhomogeneous solutions are given for any other value of c_3. Thus, we understand this parameter as a "switch" between homogeneous and inhomogeneous solutions. This fact motivates us to write the metric only in terms of this parameter and choosing $c_1 = 1$, $R_0 = 2$.

For the following it is also convenient to list the values of the metric functions at the time $t = \pi/2$ which we shall use as the initial data for our numerical evolutions. Notice that we cannot use $t = 0$ or $t = \pi$ as initial times because the data are singular there. Thus, evaluating Eqs. (8.5)–(8.8) and time derivatives at $t = \pi/2$, we obtain[2]

$$\lambda_0 = -4 - c_3^2 \sin^2\theta, \qquad \partial_t\lambda_0 = -4c_3^2 \sin^2\theta, \tag{8.12}$$

$$\phi_0 = \frac{c_3^2}{2}\sin^2\theta, \qquad \partial_t\phi_0 = c_3^2 \sin^2\theta, \tag{8.13}$$

$$\delta_0 = 4 + \frac{c_3^2}{2}\sin^2\theta, \qquad \partial_t\delta_0 = c_3^2 \sin^2\theta, \tag{8.14}$$

$$\beta_0 = 0, \qquad \partial_t\beta_0 = 0. \tag{8.15}$$

From Eq. (8.2) and its time derivative we obtain the initial value for ψ_0 and $\partial_t\psi_0$ respectively. Finally, by integrating Eq. (9.8) with respect to θ and setting the irrelevant integration constant to zero we obtain ω_0. By considering Eq. (8.3) we obtain $\partial_t\omega_0$. The explicit form of these functions is

[2] We have used $\partial_t g_0$ to denote the temporal partial derivative of any function g evaluated at the initial time.

$$\omega_0 = \frac{-128(-8+16c_3\cos\theta)}{256+288c_3^2+3c_3^4-512c_3\cos\theta-4c_3^2\left(-56+c_3^2\right)\cos 2\theta+c_3^4\cos 4\theta}\,, \tag{8.16}$$

$$\psi_0 = \frac{8\left(1+\frac{1}{4}c_3^2\sin^2\theta\right)}{(1-2c_3\cos\theta)^2+\left(1+\frac{1}{4}c_3^2\sin^2\theta\right)^2}\,, \tag{8.17}$$

$$\begin{aligned}\partial_t\omega_0 = {} & 128(64+64c_3^2\cos^2\theta-64c_3^3\cos^3\theta-4c_3^4\sin^4\theta \\ & +c_3\cos\theta\left(-128+8c_3^2\sin^2\theta+9c_3^4\sin^4\theta\right))/\,B\,,\end{aligned} \tag{8.18}$$

$$\begin{aligned}\partial_t\psi_0 = {} & -64c_3(128c_3\cos^2\theta-32c_3\sin^2\theta+4c_3^3\sin^4\theta+c_3^5\sin^6\theta \\ & +16\cos\theta\left(-12+5c_3^2\sin^2\theta\right)-24c_3^3\sin^2 2\theta)/\,B\,,\end{aligned} \tag{8.19}$$

where

$$B = \left(32-64c_3\cos\theta+64c_3^2\cos^2\theta+8c_3^2\sin^2\theta+c_3^4\sin^4\theta\right)^2\,.$$

8.4 Possible numerical error sources

The purpose of the following subsections is now to evolve the evolution equations (6.19) for the just discussed initial data numerically. We shall do this for two sets of generalized gauge source functions. Before we go into the details in section 8.5 and 8.6, however, let us discuss possible numerical error sources that we shall focus on in the particular numerical examples below.

Obvious error sources in our numerical evolutions are time and spatial discretization errors. In general it is expected that time discretization errors are larger than spatial ones thanks to the rapid (exponential) convergence of the latter. In order to investigate the presumably more significant time discretization errors we shall use two different time discretization schemes, the (non-adaptive) 4th-order Runge-Kutta scheme and the (adaptive) Runge-Kutta-Fehlberg (RKF) scheme. See [73] for details about adaptive Runge-Kutta methods. Spatial discretizations shall always be based on our adaptive framework discussed in section 7.5. In particular for runs using the adaptive RKF scheme, all discretization errors are therefore expected to be mostly small and well under control.

However, in our numerical experiments we identify further error sources that turn out to be more severe than the previous ones. As discussed in section 7.5, we want to sample each unknown function on an "optimal" grid where the corresponding band limit is given by Eq. (7.18). Since, however, we are required to choose the same band limit for all unknown functions and we have therefore decided to choose the maximum of all these "optimal" band limits as the global band limit, we consequently oversample several of the unknowns. This is not only inefficient numerically, but also leads to numerical noise. The origin of this noise is that the "unnecessary" modes associated with too large band limits are in general not zero numerically. In fact, while they are typically of the order of the machine precision initially, they may grow during the evolution in particular due to the coupling of modes associated with non-linear terms in the equations. Typically, the larger the difference between the optimal band limit of any function and the global band limit is, the larger is this noise. This error is difficult to control in practice and it is quite common that once this noise has started to grow during the evolution it continues to grow faster and faster. We identify this error by looking at the evolution of the highest modes of representative unknowns during the evolution. The only conceivable cure for this problem would be to work with higher machine precisions, which would, however, significantly slow down the numerical runs. Our numerical infrastructure is completely based on "double precision". We have not yet attempted to work with higher

machine precisions such as "quad precision". Further comments on this in the context of a different numerical infrastructure can be found, for example, in [26].

Another severe numerical error is the constraint violation error. Recall that due to Eq. (6.11), the constraints $\mathcal{D}_\mu = 0$ are satisfied identically during evolution if the exact evolution equations hold and if the constraints are satisfied initially. In the numerical case, however, we neither satisfy the evolution equations identically nor are the constraints satisfied identically initially. In order to make some steps to tackle this, one could try to analyse this problem in the situation where the evolution equations are satisfied identically (i.e., we pretend that the numerical evolutions are done with a infinite resolution in space and time and with infinite machine precision), but where the constraints may be violated initially, say, due to rounding errors associated with finite machine precision. Then, Eq. (6.11) describes the exact evolution of the constraint violation quantities $\mathcal{D}_\mu$. The non-zero initial data for these quantities imply that these quantities will in general be non-zero at all times during the evolution and, depending on the particular properties of the evolution system, hence of Eq. (6.11), may in fact grow rapidly during the evolution. If this is the case, the constraint violation error can quickly become very large during the evolution. In particular, it cannot be reduced by a higher numerical resolution because this error is a consequence of a severe instability of the continuum evolution equations. There are two possible cures for these errors. On the one hand, one can introduce constraint damping terms that render the evolution equations stable (at least in practical situations) [31, 47, 103]. This technique has proved to be quite useful for producing stable calculations for asymptotically flat spacetimes (see for instance [150]). However, the analysis may be difficult and, in general, requires approximations that may only hold in certain regimes of the evolution. In this part, we work without constraint damping terms. Another way to improve this error would be to work with higher machine precisions as above.

In principle, the mentioned errors sources cannot always be separated from each other cleanly. In fact, they may depend on each other, or they may be strongly coupled. In any case, for practical purposes it is often useful to think of these as separate independent error sources and analyse the numerical results consequently.

8.5 Numerical evolutions in areal gauge

In this section, we shall fix the gauge freedom for the evolution equations by identifying the generalized gauge source functions with the contracted Christoffel symbols of the exact solution. This is achieved by identifying the generalized gauge source functions f_μ with the quantities $\mathring{\Gamma}_\mu$ of the exact solution given by Eqs. (8.9)–(8.10). As is common in the literature, we refer to this coordinate gauge as *areal gauge*. We want to point out that the same kind of spacetimes in the same coordinates have been constructed numerically with different methods in [108]. However, in contrast to our discussion here, some of the EFE turn out to be formally singular in the "interior" of the Gowdy square in the formulation used there, hence are ignored to avoid serious numerical problems. We shall evolve the evolution equations (6.19) for the initial data given by Eqs. (8.12)–(8.19) at $t = \pi/2$ and these generalized gauge source functions. The resulting numerical solutions are given in the same coordinates as the exact solution and direct comparisons between the exact and the numerical solutions can be performed conveniently by considering the quantity

$$E(t) := \max_{\mu,\nu} \| \, h^{(e)}_{\mu\nu}(t,\theta) - h^{(n)}_{\mu\nu}(t,\theta) \, \|_{L^2(\mathbb{S}^2)} \, ,$$

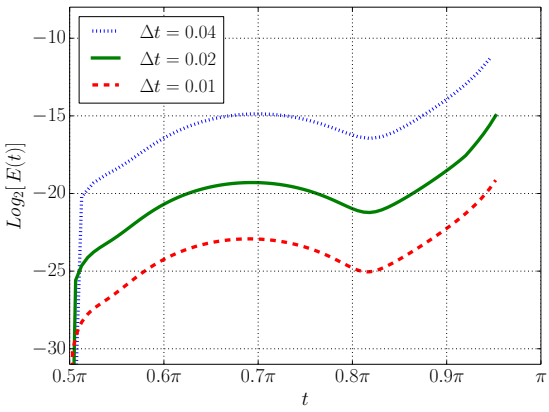

Figure 8.1: *Convergence test,* $c_3 = 0.2$

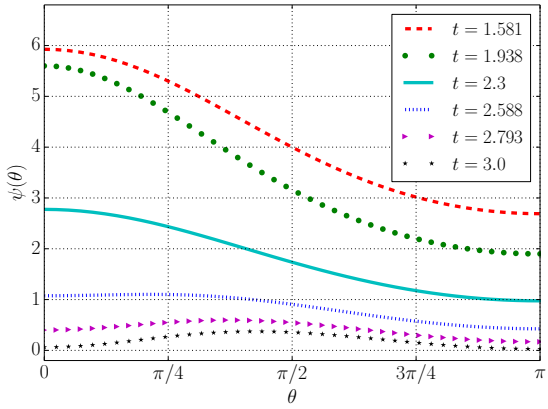

Figure 8.2: *Norm of the Killing vector,* $c_3 = 0.2$

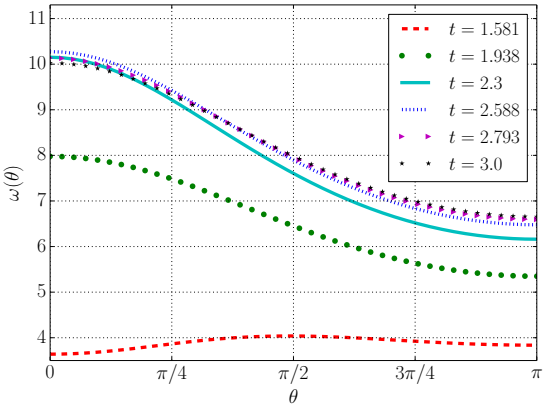

Figure 8.3: *Twist of the Killing vector,* $c_3 = 0.2$

where $h^{(e)}_{\mu\nu}(t,\theta)$ represents a frame component of the *exact* solution for a given t, whereas $h^{(n)}_{\mu\nu}(t,\theta)$ represents the numerical values. The norm $\|\cdot\|_{L^2(\mathbb{S}^2)}$ is approximated by the discrete ℓ^2-norm for functions $d(t,\theta)$ as

$$\| d(t,\theta) \|_{L^2(\mathbb{S}^2)} \approx \sqrt{\frac{2\pi^2}{N} \sum_{i=0}^{N} d(t,\theta_i)^2}\,, \tag{8.20}$$

where N represents the total number of collocation points θ_i where the function is sampled.

As a first test for our numerical implementation we present a convergence test in Fig. 8.1 for $c_3 = 0.2$. The evolution was carried out with the 4th-order Runge-Kutta scheme. The figure shows the expected convergence rate when the time discretization error is dominant. This is not surprising since at each t all the metric components are very smooth functions that can be resolved on the grid with high accuracy so long as t does not get too close to $t = \pi$. The oversampling and constraint violation errors discussed in the previous subsection are expected to be small during the early evolution.

Next, we replace the non-adaptive 4th-order Runge-Kutta scheme by the adaptive RKF method. In Fig. 8.2 and Fig. 8.3 we show the numerical evolutions of the geometric quantities ψ and ω for $c_3 = 0.2$. The numerical error in these calculations are shown in Fig. 8.4 for different values of c_3. The error tolerance Tol of the RKF method is chosen to be 10^{-8}. This

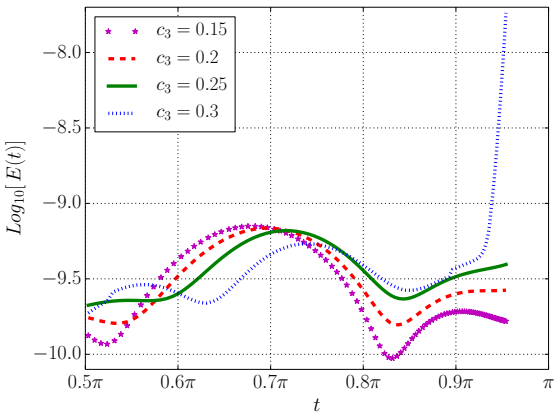

Figure 8.4: *Error propagation for various values of* c_3 *and* $Tol = 10^{-8}$

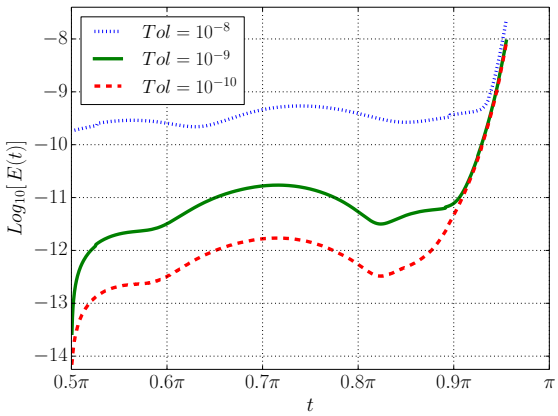

Figure 8.5: *Error propagation for various values of* Tol *and* $c_3 = 0.3$

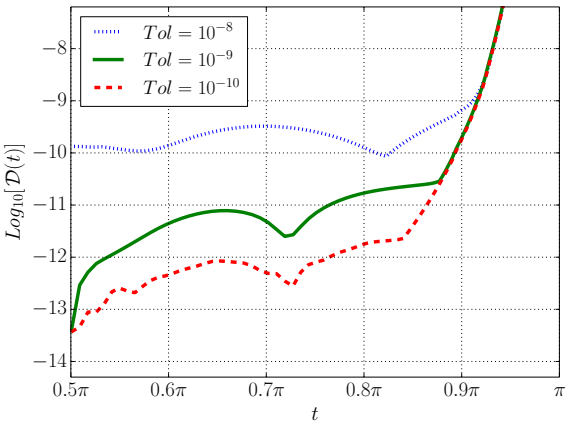

Figure 8.6: *Constraints propagation for various values of* Tol *and* $c_3 = 0.3$

figure suggests that the numerical error is stable during a long period of the evolution and in fact smaller than Tol. The larger c_3 is, however, hence the more inhomogeneous the solution is, the more rapidly the numerical errors grows close to $t = \pi$ as expected. Fig. 8.5 indicates that the behaviour close to $t = \pi$ cannot be improved by decreasing the value of Tol. This suggests that close to $t = \pi$ the numerical error is not dominated by the time discretization error. In fact, one of the other error sources discussed in section 8.4 must become dominant there.

Our experience with this particular system suggests that both errors, i.e., the oversampling error and the constraint violation error dominate at late times, in particular, when the value of the constant c_3 is increased. Regarding the oversampling error, we just point out that due to the particular dependence of the initial data on c_3, the initial oversampling noise is larger the larger c_3 is. This follows directly from Eqs. (8.12)–(8.19). We can check that the optimal band limit of the metric components and their time derivatives are small in comparison with the optimal band limits of ψ_0, ω_0 and the corresponding time derivatives. The larger discrepancy, the larger c_3 is. We then find that the resulting initial oversampling noise grows during the evolution. In order to measure the constraint violation error, we define

the quantity

$$\mathcal{D}(t) := \max_{\mu} \| f_\mu(t,\theta) - \mathring{\Gamma}_\mu(t,\theta) \|_{L^2(\mathbb{S}^2)}.$$

In Fig. 8.6, we show the evolution of this quantity for $c_3 = 0.3$. At late times, the curves look very similar to ones of $E(t)$ in Fig. 8.5. This suggests that the constraint violation error contributes significantly to the total numerical error.

8.6 Numerical evolutions in wave gauge

In this section we describe numerical computations for the same spacetimes as before, but using a different coordinate gauge. To this end, we want to choose the same initial data as before but work with different generalized gauge source functions. Since we do not want to resolve these complicated non-linear PDEs, our strategy is to use exactly the same initial data for the values of the metric components and their first time derivative values, and also exactly the same initial values of the generalized gauge source functions as before. In order to implement a different coordinate gauge, we then apply the following "gauge driver condition" during the evolution whose purpose is to rapidly drive the generalized gauge source functions from their *initial values* fixed by the gauge constraint towards the *target generalized gauge source functions* $\hat{f}_\mu$:

$$f_\mu = (\mathring{\Gamma}_\mu|_{t_0} - \hat{f}_\mu) e^{-q(t-t_0)} + \hat{f}_\mu. \tag{8.21}$$

Here, the parameter q controls how rapidly the gauge is driven towards the target. The quantities $\mathring{\Gamma}_\mu|_{t_0}$ are calculated from the initial data and are understood as functions of the spatial coordinates only. Notice that different gauge drivers for the generalized wave representation of the EFE were considered in [129]. Eq. (8.21) guarantees that the gauge constraint is satisfied at the initial time. As discussed at the end of section 2.5, the physical constraints, even though they pose highly non-trivial restrictions on the choice of the initial data because they are essentially linear combinations of the well-known Hamiltonian and momentum constraints, turn out to *not* be restrictions on the generalized gauge source functions. Hence, it is not necessary to introduce terms in Eq. (8.21) which account for the first time derivative of $\mathring{\Gamma}_\mu$ at $t = t_0$.

We apply this idea to calculate the same spacetimes as before, but now we choose the *wave gauge* as the target gauge, which is defined by the condition $\hat{f}_\mu = 0$. For our numerical tests we choose $q = 10$ in Eq. (8.21). Before we present our numerical results we notice that it is straightforward to derive the formula

$$t_{(w)} = \frac{\pi}{2} + \frac{1}{2} \log\left(\frac{1 - \cos t}{1 + \cos t} \right), \tag{8.22}$$

which for our spacetimes relates the time coordinate t in areal gauge (used in section 8.5) and the time coordinate $t_{(w)}$ in wave map gauge. This formula holds identically even though Eq. (8.21) is strictly speaking not the exact wave map gauge. However, as a consequence of $\mathring{\Gamma}_0|_{t_0=\pi/2} = 0$ that follows from Eq. (8.9), the target gauge source function $\hat{f}_0 = 0$ agrees identically with $f_0 = 0$. Eq. (8.22) is then obtained by solving the exactly homogeneous wave map equation Eq. (6.5) for the wave map time coordinate function with appropriate initial conditions. Eq. (8.22) allows us to make direct comparisons between our results here and the results in the previous section. In particular, it reveals that the wave time slices $t_{(w)} = const$ are the same as the areal time slices $t = const$ (for different constants), and, the "singularities" at $t = 0, \pi$ are shifted to infinity, in particular, $t_{(w)} \to \infty$ for $t \to \pi$. We point out, however, that it is not possible to derive a formula that relates the spatial coordinates

in both gauges. This is true even if q in Eq. (8.21) was so large that we could consider our gauge as the exact wave map gauge. This is a consequence of the fact that the homogeneity of the wave equations for the spatial wave map coordinates is destroyed by terms given by the reference metric Eq. (6.13). In fact, we shall demonstrate below that the spatial coordinates on each time slice are different in areal and wave map coordinates.

In order to obtain a more geometric and detailed comparison of the two gauges, we consider the Eikonal equation as follows (See [81]):

$$\nabla_a \tau \nabla^a \tau = -1. \tag{8.23}$$

Let τ be a smooth solution of the initial value problem of the Eikonal equation with smooth initial data $\tau_0 : \Sigma_0 \to \mathbb{R}$ prescribed freely on any smooth Cauchy surface Σ_0 in any smooth globally hyperbolic spacetime. The method of characteristics applied to this PDE allows us to prove that such a solution indeed always exists at least sufficiently close to the initial hypersurface Σ_0. For definiteness now we restrict ourselves to the case of zero initial data $\tau_0 = 0$ for all of what follows. Fix any point p in the timelike future of Σ_0 in the spacetime and consider any timelike geodesic through p (with unit tangent vector). Any such geodesic must intersect Σ_0 at some point x_0 in the past of p. There is precisely one such timelike geodesic through p with unit tangent vector which intersects Σ_0 perpendicularly in x_0, hence the point x_0 is uniquely determined. The value $\tau(p)$ of the solution τ of the Eikonal equation with zero initial data then represents the proper time along this timelike geodesic from x_0 to p. The quantity τ is therefore a meaningful geometric scalar quantity which can be used to compare our numerical spacetimes, in particular when the same spacetime is calculated in different coordinate gauges. We proceed as follows for initial data parameter $R_0 = 2$, $c_1 = 1$ and $c_3 = 0.1$ (see section 8.2)

Firstly, we calculate the corresponding solution of Einstein's evolution equations in areal gauge (in the same way as in section 8.5) and of the Eikonal equation Eq. (8.23) (with zero initial data) up to $t = 3$. The value of the resulting τ function on the $t = 3$-surface expressed with respect to spatial areal coordinates yields the dashed curve in Fig. 8.7. Secondly, Eq. (8.22) implies that $t = 3$ corresponds to $t_{(w)} \approx 4.217$. For the same initial data parameters as in the first step, we calculate the corresponding solution of Einstein's evolution equations in wave gauge numerically (using the gauge driver condition Eq. (8.21) with $q = 10$) and of the Eikonal equation Eq. (8.23) (with zero initial data) up to $t_{(w)} \approx 4.217$. The value of the resulting τ function on the $t_{(w)} \approx 4.217$-surface expressed with respect to spatial wave map coordinates yields the continuous curve in Fig. 8.7.

Since the $t = 3$-surface and the $t_{(w)} \approx 4.217$-surface represent the same geometric surface in our spacetime and since τ is a geometric scalar quantity, the value of the solution of the Eikonal equation on this surface should be the same function in both steps above. However, since this function is expressed in terms of different spatial coordinates, namely areal coordinates in the first step and wave map coordinates in the second step, the two curves in Fig. 8.7 are slightly different. Hence, Fig. 8.7 can be understood as a representation of the difference of these two sets of spatial coordinates. This difference is emphasized in Fig. 8.8 where the two curves in Fig. 8.7 are subtracted directly. Intuitively, these two sets of spatial coordinates should agree at geometrically distinct points, namely, at the poles and also at the equator as a consequence of a reflection symmetry which is inherent to our particular class of exact solutions. Indeed the difference curve in Fig. 8.8 is zero at the poles $\theta = 0, \pi$ and the equator $\theta = \pi/2$.

Next, we present plots of the constraint violations in both gauges; see Fig. 8.9. The dashed curve has been calculated in areal gauge (in the first step above). The continuous

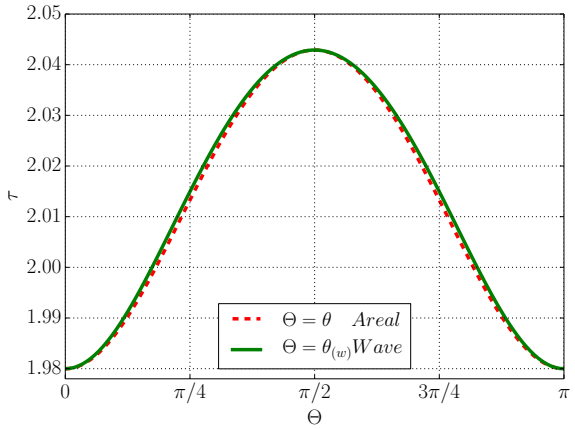

Figure 8.7: *Proper times comparison.*

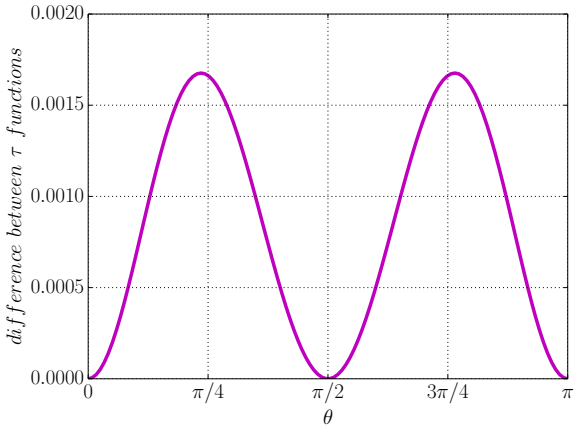

Figure 8.8: *Difference of the proper times.*

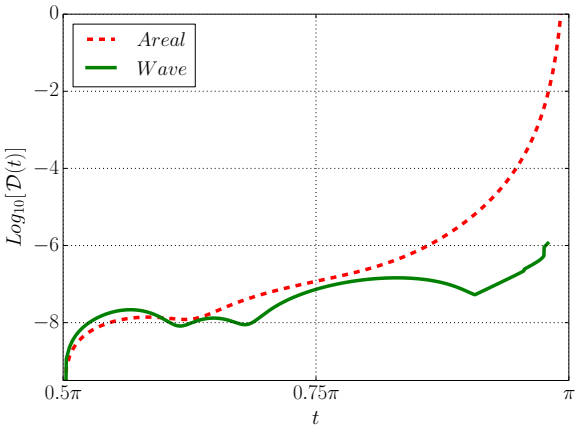

Figure 8.9: *Comparison of the constraint violations.*

curve has been calculated in wave map gauge (in the second step above) but has then been expressed in terms of the areal time function by means of Eq. (8.22). It is interesting to notice that the constraint violations are significantly smaller in wave map gauge than they are in areal gauge towards the end of the numerical evolution.

Finally, we comment on the fact that in wave map gauge the shift quantity β in Eq. (6.2) is a non-trivial non-zero function in contrast to areal gauge; see Eq. (8.6). When β cannot be assumed to be zero identically, the algebraic complexity of the evolution equations is increased dramatically. It is surprising that irrespective of this it appears that we get better numerical results in wave map than in areal gauge.

Chapter 9

Numerical studies of Gowdy spacetimes $\mathbb{R} \times \mathbb{S}^1 \times \mathbb{S}^2$

Motivated by the works of Garfinkle [90] and Ståhl [183], in this chapter we shall numerically explore the behaviour of Gowdy spacetimes $\mathbb{S}^1 \times \mathbb{S}^2$ using our analytical and numerical scheme. In particular, we want to study the behaviour of the Kretschmann scalar, thereby identify whether at the polar regions possible true spikes could emerge. As we mentioned in chapter 1, we expect to cast some light on Ståhl's conjecture that in general this sort of spacetimes should develop spikes at the polar regions at the singularity. We remark that due to smoothness conditions of the topology $\mathbb{S}^1 \times \mathbb{S}^2$ (also $\mathbb{S}^3$), the behaviour at the polar regions of Gowdy solutions of the Einstein equations with such spatial topology is still not well understood. Since only true spikes have geometrical meaning, we will focus on those. According to Rendall and Weaver in [156], true spikes are characterized by a non-uniform spatial divergence of the Kretschmann scalar. Thus, we will focus on determining whether this quantity tends to develop spikes at the poles. As discussed in chapter 6, we stress that our implementation allows us to avoid problematic terms like $\cot\theta$ in the constraints and evolution equations. In particular, the Kretschmann scalar can be evaluated without any problem at the poles using our approach in contrast to the case of using the standard coordinate frame and differential operators. In other words, thanks to our analytical and numerical infrastructure we can compute the actual value of the Kretschmann scalar at the poles, which allows us to have an understanding of the behaviour of this quantity at those particular places.

9.1 The general metric $\mathbb{S}^1 \times \mathbb{S}^2$ in areal gauge

To begin with, let us use the metric for the case $\mathbb{S}^1 \times \mathbb{S}^2$ in areal gauge introduced in section 3.3.3,

$$g_{\mathbb{S}^1\times\mathbb{S}^2} = e^{\lambda-W}\left(-\mathrm{d}t^2+\mathrm{d}\theta^2\right)+e^{W}\left(\mathrm{d}\varphi+Q\mathrm{d}\rho\right)^2+e^{-W}\sin^2 t\sin^2\theta\,\mathrm{d}\rho^2, \tag{9.1}$$

where the metric functions W, λ and Q depend only on t and θ and are subject to the regularity conditions Eqs. (3.8) and (3.9). Recall that ρ is the coordinate on the $\mathbb{S}^1$-factor while (θ,φ) are the coordinates on the $\mathbb{S}^2$-factor. Clearly, the coordinate vectors ∂^a_ρ and ∂^a_φ correspond to the Killing vectors. Similarly to the generalized Gowdy Taub-NUT solution considered in chapter 8, the spacetime singularities ("big bang" and "big crunch") are at $t=0$ and $t=\pi$. In order to obtain a more convenient form for the metric, we introduce the following transformation

$$W := P + 2\log\sin\theta + \log\sin t, \quad \lambda := 2(P+\gamma+\log\sin\theta\,\log\sin t). \tag{9.2}$$

Further, choosing the new time $\tau = -\log\tan(t/2)$, the metric becomes

$$g_{\mathbb{S}^1\times\mathbb{S}^2} = \mathrm{sech}\tau\{e^{P}[e^{2\gamma}\left(-\mathrm{sech}^2\tau \mathrm{d}\tau^2 + \mathrm{d}\theta^2\right) + \sin^2\theta\left(\mathrm{d}\varphi + Q\mathrm{d}\rho\right)^2] + e^{-P}\mathrm{d}\rho^2\}, \tag{9.3}$$

which is the metric form used by Garfinkle in [90]. In his work, he points out that the smoothness of the metric at the axis is satisfied if P, Q and γ are smooth functions of $\cos\theta$ with the two latter vanishing at the points $\theta = 0$ and $\theta = \pi$. As in the $\mathbb{T}^3$ case, the vacuum Einstein field equations yield evolution equations just for the variables P and Q. On the other hand, the variable γ is determined by the constraint equations

$$\partial_\theta\gamma = \frac{\cosh^2\tau\left(A\tanh\tau + B\cot\theta\right)}{\cot^2\theta - \sinh^2\tau}, \tag{9.4}$$

$$\partial_\tau\gamma = \frac{A\cot\theta + B\sinh\tau\cosh\tau}{\cot^2\theta - \sinh^2\tau}, \tag{9.5}$$

where the quantities A and B are given by

$$\begin{aligned} 2A &:= \tanh\tau\,\partial_\theta P + \partial_\tau P\partial_\theta P + e^{2P}\sin^2\theta\,\partial_\tau Q\partial_\theta Q, \\ 4B &:= 2\tanh\tau\,\partial_\tau P + \partial_\tau P^2 + e^{2P}\sin^2\theta\,\partial_\tau Q^2 + \tanh^2\tau \\ &\quad + \mathrm{sech}^2\tau\left(\partial_\theta P^2 + e^{2P}\sin^2\theta\,\partial_\theta Q^2\right) - 4\,. \end{aligned}$$

Thus, for two given functions P and Q we can determine γ (up to some integration constant) by integrating Eq. (9.4) and $\partial_\tau\gamma$ from Eq. (9.5). There are, however, two remaining difficulties with respect to the equations that determine γ. The first one has to do with the fact that the denominator in both equations vanishes. Then, smoothness of the metric requires that the numerators of these equations vanish whenever the denominator does. The second difficulty has to do with the fact that γ must vanish at the poles. Hence, these two requirements place conditions on the choice of P and Q, but once these conditions are satisfied for the initial data, the evolution equations will preserve them. For detail we refer the reader to [90].

9.2 Symmetry reduction and choice of initial data

Next, we conduct the symmetry reduction with respect to the Killing vector $\xi^a = \partial^a_\rho$. Following the symmetry reduction explained in chapter 4 (similar to chapter 8), we obtain

$$\psi = e^{-P}\left(Q^2e^{2P}\sin^2\theta + 1\right)\mathrm{sech}\tau, \tag{9.6}$$

$$\partial_\tau\omega = \mathrm{sech}\tau\sin\theta\left(2Q\partial_\theta P + \partial_\theta Q + 2Q\cot\theta - e^{2P}Q^2\sin^2\theta\partial_\tau Q\right) \tag{9.7}$$

$$\partial_\theta\omega = \mathrm{sech}\tau\sin\theta\left(2Q\partial_\tau P + \partial_\tau Q - e^{2P}Q^2\sin^2\theta\,\partial_\tau Q\right), \tag{9.8}$$

$$h_{ab} = \psi\left(\,\mathrm{sech}\,\tau e^{P+2\gamma}(-\mathrm{sech}^2\tau\,\mathrm{d}\tau^2 + \mathrm{d}\theta^2) + \frac{e^P\sin^2\theta\,\mathrm{sech}\tau}{1 + e^{2P}\sin^2 Q^2}\mathrm{d}\phi^2\,\right), \tag{9.9}$$

where ψ and ω are the norm and twist associated with ∂^a_ρ and the evolution metric h_{ab}. Now, as described in chapter 6, we write the metric in terms of the frame $(T^a, m^a, \overline{m}^a)$ as

$$\lambda = -e^{2\gamma}\text{sech}^4\tau\left(1+e^{2P}Q^2\sin^2\theta\right), \tag{9.10}$$
$$\beta = 0, \tag{9.11}$$
$$\delta = \frac{\text{sech}^2\tau}{2}\left(1+e^{2\gamma}+e^{2(P+\gamma)}Q^2\sin^2\theta\right), \tag{9.12}$$
$$\phi = \frac{\text{sech}^2\tau}{2}\left(-1+e^{2\gamma}+e^{2(P+\gamma)}Q^2\sin^2\theta\right). \tag{9.13}$$

As initial data for our numerical implementation, we could have used the one given by Garfinkle at [90]. However, for the following numerical experiment we use other initial data because they require less grid points in our pseudo-spectral implementation than the one used by Garfinkle. In other words, the spectral decomposition of the metric components Eqs. (9.10)–(9.13) by using similar functions $P, Q, \partial_\tau P$ and $\partial_\tau Q$ as in Garfinkle's work, turns out to be a bit large, hence not very practical for our numerical purposes. Therefore, in order to make numerical evolution as simple as possible, we decided to choose instead $P = 0, \partial_\tau P = 2, Q = 0, \partial_\tau Q = 2\cos\theta$. Using Eq. (9.5) we obtain $\partial_\tau\gamma = 0$ and after integrating Eqs. (9.4), we obtain $\gamma = (\sin^4\theta)/16$ which clearly vanishes at the poles. For the initial time we set $\tau = 0$, which corresponds to $t = \pi/2$ in the coordinate time of Eq. (9.1). Then, evaluating Eqs. (9.10)–(9.13) and their corresponding time derivatives we obtain the projected initial data in the space of orbit S

$$\begin{aligned}
&\lambda_0 = -e^{(\sin^4\theta)/8}, && \partial_\tau\lambda_0 = 0,\\
&\phi_0 = (-1+e^{(\sin^4\theta)/8})/2, && \partial_\tau\phi_0 = 0,\\
&\delta_0 = (1+e^{(\sin^4\theta)/8})/2, && \partial_\tau\delta_0 = 0,\\
&\beta_0 = 0, && \partial_\tau\beta_0 = 0.
\end{aligned}$$

From Eq. (9.6) and its time derivative, ψ_0 and $\partial_t\psi_0$ are obtained, while ω_0 is obtained by integrating Eq. (9.8) (and setting the integration constant to zero). Finally, considering Eq. (9.7) the initial values are

$$\begin{aligned}
&\psi_0 = 1, && \partial_\tau\psi_0 = -2,\\
&\omega_0 = -(\cos^2\theta)/2, && \partial_\tau\omega_0 = 0.
\end{aligned}$$

Note that it was not necessary to use the York-Lichnerowicz conformal decomposition on $\mathbb{S}^2$ introduced in section 6.4.2 for finding initial data in the space of orbits. Instead, we solved the constraints in the original spacetime and projected the solution to the space of orbits.

9.3 Using a gauge driver

Using the initial data above, we obtain that initially the generalized gauge source functions vanish. In this case, we keep $f_0 = 0$ during the evolution. In addition, with the aim of obtaining an expression for the Kretschmann scalar as short as possible (because in the general case this expression is huge and not practical for numerical purposes) we decided to keep $\beta = 0$ during the evolution. To do so, we use the evolution equation from the metric component β to evolve the gauge source function f_1 such that $\beta = 0$. In other words, from

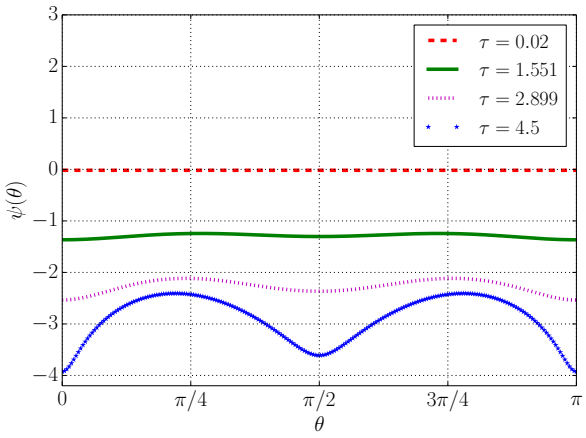

Figure 9.1: *Snapshots of the evolution of ψ.*

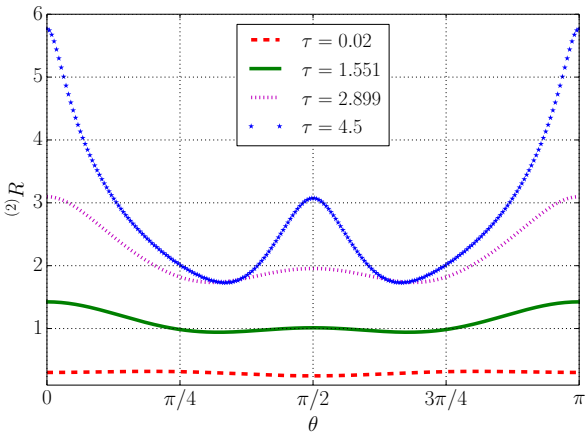

Figure 9.2: *Snapshots of the evolution of $^{(2)}R$.*

the differential equation of β we obtain an evolution equation for f_1 such that it preserves $\beta = 0$. Thus, the evolution equation for f_1 is given by

$$\nabla_{(0} f_{1)} = -\mathring{\Upsilon}_{01}(h, \partial h, \breve{\Gamma}) + \frac{1}{\psi^2}\left(\partial_0\psi\, \partial_1\psi + \partial_0\omega\, \partial_1\omega\right),$$

which is a first-order evolution equation that does not contain any second-order derivatives. Later in section 10.3, we will implement a similar idea to preserve a convenient form of the metric component. Further, we will analyse the hyperbolicity of the resulting system of evolution equations in more detail. This analysis could be extended to the system considered here, although not in a direct manner. Nevertheless, since we obtained stable evolutions in our numerical experiment, we decided not to carry out such analysis for this case.

9.4 Numerical studies

9.4.1 Collapsing behaviour of the factors $\mathbb{S}^1$ and $\mathbb{S}^2$

In this part we describe the behaviour of two geometrical quantities, namely the norm ψ of the Killing vector along the $\mathbb{S}^1$-factor and the Ricci scalar $^{(2)}R$ of the two-dimensional induced metric γ_{ij} (see chapter 6.4.2) of the Cauchy surfaces Σ_τ determined by any constant value of the coordinate time τ. To begin with, in Figs. 9.1 and 9.2 we show some snapshots of the evolution for ψ and $^{(2)}R$ at several times. Note that the final time that is shown is $t = 4.5$, which we believe is enough to draw some conclusions about the future behaviour of this spacetime. However, we have to mention that we carried out the evolution up to this value because some functions become "spiky" at some points during the evolution; consequently, more spectral coefficients were required to describe them. Thus, we incremented of the number of grid points along the evolution in the way described in section 7.5, and as a result, the numerical temporal integration was slowed down owing to the large number of grid points required in each time step. Certainly, this is a disadvantage of our pseudo-spectral method.

Getting back to our discussion, the behaviour of the norm ψ shown in the Fig. 9.1 reveals that the length of the symmetry orbits contract faster near the polar and equatorial regions than anywhere else. This suggests that spikes develop in these regions. On the other hand, we plot in Fig. 9.2 some snapshots of the evolution for $^{(2)}R$. In there, we observe that this quantity grows revealing a contraction of the $\mathbb{S}^2$-factor in time. In both cases, the behaviours

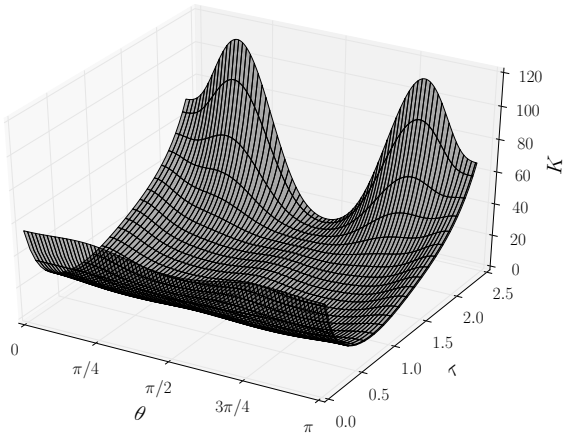

Figure 9.3: *Early evolution of the Kretschmann scalar.*

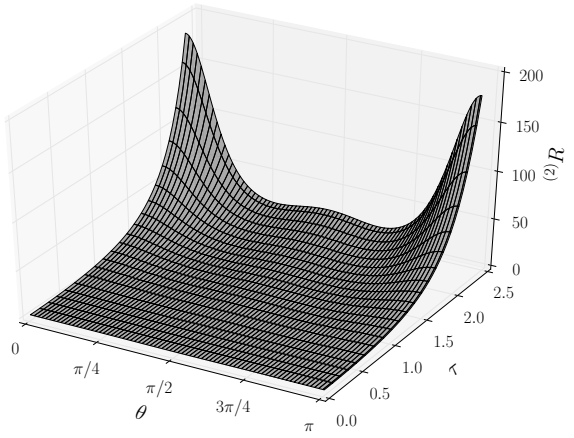

Figure 9.4: *Early evolution of* ${}^{(2)}R$.

of ψ and ${}^{(2)}R$ suggest that the spacetime collapses[1] faster at the poles than anywhere else, hence in the regions around them some spikes may be given.

9.4.2 Behaviour of the Kretschmann scalar

In this part we discuss the behaviour of the Kretschmann scalar of original four-dimensional spacetime. We can find this quantity in terms of fields in the space of orbit S by using Eq. (4.36) obtained in section 4.5. Clearly, $(T^a, m^a, \overline{m}^a, \xi^a)$ is the frame vector set in the four-dimensional manifold that we use to carry out the reconstruction procedure. Let us begin by considering Fig. 9.3 that shows the early behaviour of the Kretschmann scalar. In there, we observe that this quantity does not grow at the beginning as one would expect. Instead, it decreases for some time before increasing. We can interpret this behaviour as a possible expansion of the four-dimensional spacetime before entering the contraction phase due to the future singularity. This behaviour is significantly different from the observed for the geometric quantities ψ and ${}^{(2)}R$ which both decrease and increase in a monotonic manner since the beginning of the evolution. See, for instance, the early behaviour of ${}^{(2)}R$ in Fig. 9.4.

Next, we turn our attention to the behaviour of the Kretschmann scalar close to the final time in our implementation. To start with, let us consider Fig. 9.5, which shows snapshots of the evolution of the Kretschmann scalar. The other half of the figure is given by a reflection about the equator which is preserved during the evolution owing to our choice of initial data. However, for general solutions this symmetry does not holds. The figure shows clearly that the Kretschmann scalar becomes "spiky" near the equator as well as at the poles, suggesting that some possible future spikes could appear at those places. As mentioned before, Garfinkle showed that the behaviour of this spacetime is similar to the $\mathbb{T}^3$ case except at the poles. This implies that we could expect the emergence of spikes at any place. In addition to this, in the region near to the poles some spikes could appear as well. In fact, it seems that the curvature tends to diverge faster near the poles than at any other place. Moreover, it seems that the spikes of the Kretschmann scalar moves toward the poles. This could be a direct consequence of the divergent behaviour of ψ and ${}^{(2)}R$ at those places. Hence, it is reasonable to think that if some spikes arise during the evolution, they should appear first at the poles than anywhere else. We show the late (in our simulation) evolution behaviour of the Kretschmann scalar in

[1] This behaviour is different to the case with positive cosmological constant in section 10.7.1.

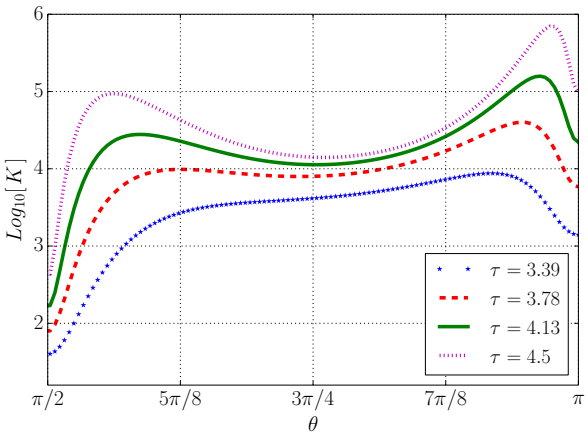

Figure 9.5: *Snapshots of the late evolution of K in half of the spatial domain.*

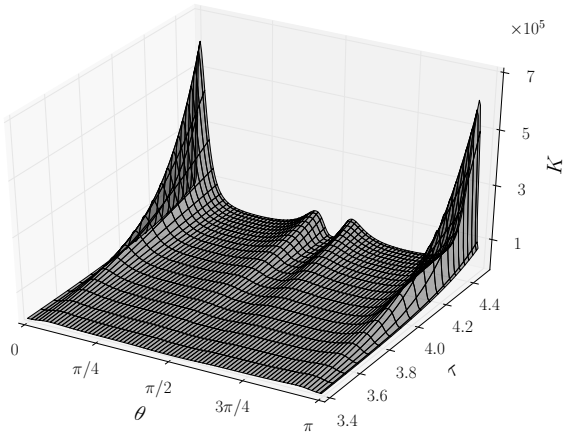

Figure 9.6: *Late evolution of K.*

Fig. 9.6. Clearly, it illustrates how large the spikes are in comparison with the other regions.

To finalize, we want to stress that by means of this numerical experiment, we have provided some numerical evidence that support Ståhl's prediction about that, in general, spikes (true spikes) may be developed at the poles in Gowdy spacetimes $\mathbb{S}^1 \times \mathbb{S}^2$ at the singularity. On the other hand, using a different approach (solving the generalized conformal field equations), Beyer [25] found similar numerical results for a certain family of Gowdy $\mathbb{S}^3$ spacetimes, namely a class of solutions of the Einstein field equations close to the family of λ-Taub-NUT spacetimes. These studies together with our findings provide evidence that supports Ståhl's prediction that suggests that a direct treatment by Fuchsian methods is not possible for studying the behaviour of this sort of Gowdy spacetimes, $\mathbb{S}^1 \times \mathbb{S}^2$ and $\mathbb{S}^3$, at the singularities.

Chapter 10

Studies of Gowdy perturbations of the Nariai spacetime

In this chapter we investigate the mechanism that triggers the non-linear instability of the Nariai spacetime under Gowdy perturbations. This study extends the investigation initialized by Beyer [27,28] which, by means of a series of analytical and numerical techniques, was able to confirm the expected instability of the Nariai solution under this sort of perturbations. However, as was mentioned in chapter 1, the underlying mechanism that causes such instability was not well understood. This is one of the main questions that we address in this chapter.

We begin this chapter by introducing the Nariai spacetime in section 10.1. Then, we define perturbations of the Nariai spacetime in section 10.2. In section 10.4, based on the scheme of the York-Lichnerowicz conformal decomposition for $\mathbb{S}^2$ introduced in section 6.4, we construct both analytically and numerically initial data for perturbations of the Nariai spacetime. Additionally, in section 10.5 we introduce the "Nariai gauge" that allows us to write the evolution equations in a convenient form for the posterior analysis of the perturbations. Further, by means of the use (and analysis) of constraint damping terms into the WGES, we guarantee the stability of the numerical implementation. We devote section 10.6 to the study of the instability of the Nariai spacetime. To do so, we start by introducing constraint damping terms into the evolution equations in order to make our numerical scheme stable. Then, by means of some numerical experiments, we present our discussion of the stability of the Nariai spacetime under homogeneous and inhomogeneous perturbations. Finally, in section 10.7, we explore the asymptotic behaviour of the perturbations of the Nariai spacetime for both when the Kretschmann scalar blows up (the collapsing case) and when it tends to a constant value (the expanding case). In particular, we analyse the second case in the light of the cosmic no-hair conjecture (CNH) discussed in section 3.2.3.

10.1 The Nariai spacetime

Birkhoff's theorem states that every spherically symmetric solution[1] of the vacuum EFE with positive cosmological constant is locally isometric either to the Kottler-Schwarzschild-de Sitter (KSS) solution or to the Nariai solution (see, for instance, [105]). The first of these solutions, found first by Kottler [122], can be interpreted as a black hole immersed in a de Sitter universe, which is the maximally symmetric solution of the vacuum EFE with a

[1] Any spacetime that admits as isometry group the group of rotation $SO(3)$ (see section A.6) is called spherically symmetric.

positive cosmological constant that represents an universe expanding at an exponential rate. The KSS solution is characterized by two parameters, namely the mass of the black hole and the value of the cosmological constant. When the latter vanishes the KSS reduces to the Schwarzschild spacetime (see [101]). On the other hand, when the mass of the black hole is zero, the KSS becomes the de Sitter spacetime.

The second solution was discovered by Nariai [142]. This spacetime has become an object of special interest since Ginsparg and Perry [95] proved that it emerges as the extremal limit of Kottler-Schwarzschild–de Sitter black holes. In other words, it can be interpreted as a de Sitter universe containing a black hole of maximal size, that is, the ratio of the black hole is equal to the cosmological horizon. The Nariai spacetime is the direct product of a two-dimensional de Sitter space with a two-sphere and it admits a six-dimensional group of motion.

Thanks to its geometrical properties, the Nariai spacetime has been used to model several situations. Among them, we find the quantum pair creation of black holes during the inflation epoch carried out by Bousso and Hawking [42–44] and the modelling of the spacetime between two static masses (stars) by Fennen and Giulini [77], just to mention a few. The Nariai spacetime metric can be written in coordinates that cover the maximal analytical extension as

$$g_{Nariai} = \frac{1}{\Lambda}(-\mathrm{d}t^2 + \cosh^2 t\, \mathrm{d}\rho^2 + g_{\mathbb{S}^2}), \tag{10.1}$$

with the standard coordinate ρ in the manifold $\mathbb{S}^1$, the standard metric $g_{\mathbb{S}^2}$ of the two-sphere and the time coordinate $t \in \mathbb{R}$. Clearly, its spatial topology is $\mathbb{S}^1 \times \mathbb{S}^2$ and ∂^a_ρ is a Killing vector along the $\mathbb{S}^1$-factor. Henceforth, we denote this vector as ξ^a. A particular property of the Nariai solution is its time dependence. While the $\mathbb{S}^1$-factor of the spatial slices expands ($t > 0$) or collapses ($t < 0$) in time, the volume of the $\mathbb{S}^2$-factor remains constant. Thus, the expansion of this solution is clearly anisotropic; consequently, the cosmic no-hair picture is not satisfied with respect to these coordinates. Moreover, Beyer in [27] showed that there are no coordinates of the Nariai solution for which the cosmic no-hair picture is attained.

10.2 Perturbations

Next, we address the question of how to define perturbations of the Nariai spacetime. One reasonable way to do it is by means of the standard linearised theory of cosmological perturbations [137]. However, we will not follow this approach because we want to study the effect of the full set of non-linear terms on the behaviour of the perturbations. In fact, it will be shown in section 10.6 that the non-linear terms play a critical role in the behaviour of the perturbed spacetime under inhomogeneous perturbations.

To begin with, the instability of the Nariai spacetime was first addressed (to our knowledge) by Bousso and Hawking [41, 43, 44] in the spherically symmetric case. They considered perturbations of the Nariai spacetime at the slice $t = 0$ such that the two-sphere area is not constant, but instead is given such that the two-sphere size oscillates as a function of the angular variable of the $\mathbb{S}^1$-factor. Then, if the sizes of the two-spheres are smaller than the corresponding to Nariai, then the spacetime collapses in a big crunch. On the other hand, the larger two-spheres will expand exponentially to generate an asymptotic to a de Sitter region. In other words, they claimed that an arbitrary number of cosmological black holes can be constructed, with expanding cosmological regions in between, in the spherically symmetric case.

As mentioned in the previous section, Beyer [27] studied the instability of the Nariai spacetime under general homogeneous perturbations. Later in [28], he studied whether spa-

tially inhomogeneous perturbations of the Nariai spacetime could be exploited in order to construct cosmological black hole solutions with arbitrary combinations of black holes and cosmological regions as was stated in the spherically symmetric case. However, in contrast to the latter, he provided analytical and numerical evidence to suggest that it is not possible to construct cosmological black hole solutions by means of inhomogeneous perturbations of the Nariai solutions.

The basic idea of his approach consists of embedding the Nariai spacetime in a more general class of solutions that shares the same spatial topology $\mathbb{S}^1 \times \mathbb{S}^2$. For the homogeneous case the general class was the *Kantowski-Sachs family* while for the inhomogeneous case it was a *Gowdy symmetric family* of metrics. The perturbations were defined as solutions of the EFE whose initial data on some Cauchy surface are "close" to data in a Cauchy surface of the Nariai solution. The word "close" in this context means that the two data sets (Nariai and its perturbations) should be at a "small distance" with respect to some suitable norm. Using this approach, he provided evidence, analytically for the homogeneous case and numerically for the inhomogeneous case, that confirmed the instability of the Nariai solution. However, in the latter case it was not well understood the source of the instability. As already mentioned at the beginning of this chapter, we will address this question in section 10.6.

We point out that this perturbations introduced by Beyer were defined in the areal gauge, hence they can not be easily translated to another gauge. Furthermore, it may happen that what is a perturbation of the Nariai metric in the areal gauge might not be in another gauge because its distance to the Nariai spacetime (in the new gauge) is no longer "small". In other words, the fact that two metrics are close under some given norm in certain gauge, does not necessarily implies that they are going to remain close in any other gauge. Therefore, in order to overcome this delicate issue, we introduce perturbations of the Nariai spacetime by exploiting the fact that its Kretschmann scalar is constant. After a straightforward calculation, the Kretschmann scalar of the Nariai metric Eq. (10.1) can be expressed as

$$K_{Nariai} = 8\Lambda^2. \tag{10.2}$$

Thus, it is expected that the Kretschmann scalar of any real perturbation of the Nariai metric will be close to this constant value but not equal. The important point here is that if the Kretschmann scalar K of some spacetime is not equal to K_{Nariai}, then it cannot be locally isometric to the Nariai spacetime, hence it can be a perturbation. Therefore, we introduce perturbations of the Nariai spacetime as some Gowdy symmetric metric g with spatial topology $\mathbb{S}^1 \times \mathbb{S}^2$ and Kretschmann scalar K such that the difference

$$K_p := K - K_{Nariai}, \tag{10.3}$$

is small non zero quantity. Hereafter, we will call K_p as *the perturbation of the Kretschmann scalar*. Clearly, by taking any norm for the function[2] K_p, it can be possible to define a gauge invariant distance between the Nariai metric and the perturbation.

10.3 Setting the Nariai gauge

One of the disadvantages of the GWF (to our knowledge) is that there is not a geometric relationship between the generalized gauge source functions and the resulting spacetime coordinates. The most common way to introduce a sort of "criterion" for the choice of those

[2]For instance $\|K_p\|_\infty = \max\{\ |K_p| :\ \theta \in [0, \pi]\ \}$.

functions is by means of the ADM "lapse" and "shift" view of the coordinate freedom. Using this, we can promote the generalized gauge source functions to "system variables" with evolution equations (usually called gauge drivers) depending on some prescribed metric components. Even though this approach has been successful in some complicated situations (see for instance [150, 151]), it may cause some problems for the stability of the numerical implementation for some situations. The reason lies in the fact that the resulting system of equations (including the gauge drivers) may turn out not to be symmetric hyperbolic; then, the setting for the Cauchy problem of the EFE will no longer be well-posed. In order to determine the hyperbolicity of the resulting system, one would have to analyse the resulting system of equations for the particular choice of gauge drivers and metric components. Some other general proposals for gauge drivers that preserve hyperbolicity can be found in [127, 128]. In this work, we will construct gauge drivers by forcing some evolution equations to provide a specific solution of the metric components. In other words, by fixing some metric components we construct the gauge drivers.

To begin with, we recall the form of the Nariai metric components defined in Eq. (10.1). In these coordinates, after the symmetry reduction, the metric components h_{00} and h_{01} (the ones that defined the gauge) satisfy

$$-\lambda = \delta, \quad \beta = \phi = 0.$$

Henceforth, we will refer to this as the *Nariai gauge*. Next, we will find generalized gauge source functions such that the Nariai gauge is preserved during the evolution. This will simplify significantly the analysis of the behaviour of the perturbations in section 10.6. Let us use the evolution equation for λ, δ, β and $\bar{\beta}$ to express the evolution equations for the gauge source function f_0, f_1 and f_2. Hence, they are promoted to evolution variables; consequently, the resulting system may or may not be symmetric hyperbolic. Next, we consider this question for the Nariai gauge following the discussion about hyperbolicity in section 2.3.

Imposing Gowdy symmetry on the metric guarantees that all the functions are real. Hence $f_1 = f_2$ and all the partial derivatives with respect to the coordinate φ vanish. Expanding the covariant derivatives and expressing the frame vectors $(m^a, \overline{m}^a)$ in terms of the coordinate vector ∂_θ in Eq. (6.19), we obtain evolution equations for[3] δ, ϕ, ψ and ω as

$$\partial_{tt}\delta + a\partial_{\theta\theta}\delta + b\partial_\theta f_1 = \dots\,, \tag{10.4}$$
$$\partial_{tt}\phi + a\partial_{\theta\theta}\phi + b\partial_\theta f_1 = \dots\,, \tag{10.5}$$
$$\partial_{tt}\psi + a\partial_{\theta\theta}\psi = \dots\,, \tag{10.6}$$
$$\partial_{tt}\omega + a\partial_{\theta\theta}\omega = \dots\,, \tag{10.7}$$

where $a = h^{11}/h^{00}$ and $b = \sqrt{2}/h^{00}$. The ellipses in the right-hand side of the equations denote the rest of the terms present in the evolution equations that are not relevant for this analysis, that is, terms depending on the generalized gauge source functions, metric components and their first-order derivatives. On the other hand, setting $\lambda = -\delta$ and $\beta = \bar{\beta} = 0$ we obtain evolution equations for the generalized gauge source functions f_0, f_1 as

$$\partial_{tt}\lambda = -\partial_{tt}\delta \implies \partial_t f_0 - \partial_\theta f_1 = \dots\,, \tag{10.8}$$
$$\partial_{tt}\beta = 0 \implies \partial_t f_1 - \partial_\theta f_0 = \dots\,. \tag{10.9}$$

Naturally, these evolution equations, which we call *gauge drivers*, control the behaviour of the generalized gauge source functions so that the Nariai gauge is preserved during the evolution.

[3] We are using ∂_{tt} to denote second time derivative.

Next, in order to analyse the hyperbolicity of the resulting system of evolution equations Eqs. (10.4)–(10.9), we write them using the first-order form as

$$\partial_t u + \Pi\, \partial_\theta u = s(u)\ , \tag{10.10}$$

where we have defined the vector

$$u = (\ \delta, \partial_t\delta, \partial_\theta\delta, \phi, \partial_t\phi, \partial_\theta\phi, \psi, \partial_t\psi, \partial_\theta\psi, \omega, \partial_t\omega, \partial_\theta\omega, f_0, f_1\ )\,, \tag{10.11}$$

and Π is a matrix of dimension 14×14 depending on the quantities[4] a, b. After a straightforward calculation we find the eigenvalues of Π

$$\upsilon_{1,2,3,4} = -\upsilon_{5,6,7,8} = -\sqrt{-a}, \quad \upsilon_{13} = -\upsilon_{14} = -1, \quad \upsilon_{9,10,11,12} = 0.$$

Furthermore, it is obtained that the determinant of the matrix whose columns are the eigenvectors of the matrix V defined in section 2.3 is proportional to a^2. Note that $h^{00}, -h^{11} > 0$ provided that h_{ab} is a Lorentzian metric with signature $(-,+,+)$. Thus, $a < 0$. Further, because V is invertible (its determinant is always different from zero), we can always obtain a complete set of eigenvectors with real eigenvalues that guarantees the strongly hyperbolicity of the system Eq. (10.10). Moreover, recalling the mentioned in section 2.3 that for the case of one spatial dimension the distinction between strongly hyperbolicity and symmetric hyperbolicity does not apply, we can conclude that the first-order system Eq. (10.10) is symmetric hyperbolic.

10.4 Construction of initial data

10.4.1 Analytical initial data

In this part, we introduce a three-parametric family of initial data that allow us to obtain a certain form for K_p (see section 10.2) that is different from zero. This implies that the family of initial data yields perturbations of the Nariai spacetime. Let us begin by identifying the initial data for the Nariai spacetime. According to Eqs. (10.1), the initial data for the Nariai spacetime in the space of orbits S is given by

$$\delta_0 = \psi_0 = 1, \quad \beta_0 = \phi_0 = \omega_0 = f_0 = f_1 = 0, \tag{10.12}$$

$$\partial_t\delta_0 = \partial_t\psi_0 = \partial_t\beta_0 = \partial_t\phi_0 = \partial_t f_1 = 0,\ \partial_t f_0 = -1, \tag{10.13}$$

where for simplicity we have chosen $\Lambda = 1$. Henceforth, we keep this value for the cosmological constant. To find initial data for the perturbations we choose the same metric components, norm and twist, as for the Nariai metric leaving the perturbations totally determined by the time derivatives of those functions. We express the constraint equations in terms of the time derivatives of the metric components, thus their elliptic representation is not required. Using Eqs. (6.40) and (6.41) to express $\mathcal{K}$ and A_{11} in terms of the metric components, and replacing those into the constraint equations Eqs. (6.35)–(6.37) we obtain the following system[5]

$$\begin{aligned} (\partial_t\delta_0)^2 &= (\partial_t\psi_0)^2 + (\partial_t\omega_0)^2 + (\partial_t\phi_0)^2, \\ \eth\,(\partial_t\delta_0) &= \bar{\eth}\,(\partial_t\phi_0). \end{aligned} \tag{10.14}$$

[4] Because of the size of Π we do not write it here explicitly.

[5] We have omitted the complex conjugate of the momentum constraint.

There are an infinite number of functions $(\partial_t\delta_0, \partial_t\phi_0, \partial_t\omega_0, \partial_t\psi_0)$ that satisfy these constraints. In particular, for our numerical experiments we will restrict ourselves to the following family

$$\begin{aligned}
\partial_t\delta_0 &= 2\,\epsilon\sin^2\theta + c_1\ , \\
\partial_t\phi_0 &= \epsilon\sin^2\theta\ , \\
\partial_t\omega_0 &= c_2\ , \\
\partial_t\psi_0 &= \pm\sqrt{(\partial_t\delta_0)^2 - (\partial_t\phi_0)^2 - (\partial_t\omega_0)^2}\ ,
\end{aligned} \tag{10.15}$$

where ϵ, c_1 and c_2 are real constants. Clearly, by substituting the above functions in Eqs. (6.42) we obtain the initial value of the generalized gauge source functions f_0, f_1. Note that because of the square root, the parameters c_1 and c_2 have to be chosen such that $|c_1|\geq|c_2|$, whereas ϵ is totally free. Next, we write the perturbation of the four-dimensional Kretschmann scalar in terms of this family. As explained in section 4.5, using the conformal relation Eq. (6.1) between the evolution and reduced metric, the projection relation of the Riemann tensor Eqs. (4.21), (4.22) and (4.23) (and its symmetric and antisymmetric properties), we can obtain all the components of the four-dimensional Riemann tensor with respect to the frame $(T^a, m^a, \overline{m}^a, \xi^a)$ in terms of fields in the space of orbits S. Note that the Kretschmann scalar contains second time derivatives of the metric components. However, these terms can be removed by using the evolution equation WGES Eq. (6.19). Furthermore, replacing Eqs. (10.12) into (4.36) and using the constraints Eqs. (10.14) the initial Kretschmann scalar can be expressed as

$$\begin{aligned}
K \;=\; & 8 + 2\,(\partial_t\delta_0 - \partial_t\psi_0)\,\partial_t\psi_0\,\big(2\partial_t\delta_0\,\partial_t\psi_0 - (\partial_t\psi_0)^2 - 4\big) - 4\,|\eth(\partial_t\psi_0)|^2 \\
& + (3\,\partial_t\delta_0\,\partial_t\psi_0 + 4(\partial_t\psi_0)^2 - 2)(\partial_t\omega_0)^2 + 9(\partial_t\omega_0)^4/4\ .
\end{aligned} \tag{10.16}$$

From here, we obtain that the second and third terms corresponding to the perturbation K_p of the Kretschmann scalar in terms of [6] $\partial_t\delta_0$, $\partial_t\psi_0$ and $\partial_t\omega_0$ as expected. Evidently, by setting $\epsilon = c_1 = c_2 = 0$, we obtain $K = K_{Nariai}$ and the initial data for the Nariai spacetime.

10.4.2 Numerical initial data

In this part, we provide a numerical solution of the elliptic representation of the constraint equations (see section 6.4.2) in the space of orbits S. We start by fixing part of the initial data in order to simplify the constraints. In particular, we choose the free part of the initial data such that the momentum constraint is automatically satisfied. Thus, we shall only focus in solving the Hamiltonian constraint. However, we point out that the following algorithm could also be used in more complicated situations where the momentum constraint is not trivially satisfied. Following the work of Frauendiener [82], we use Richarson's iteration procedure for solving the Hamiltonian constraint for the axial symmetry case.

Simplifying the constraint equations

To begin with, from the definition of the energy momentum tensor given in Eq. (4.32), we obtain that the energy and momentum density can be written in the Nariai gauge as

$$\begin{aligned}
\rho &= \frac{(\partial_t\psi)^2 + (\partial_t\omega)^2 + \eth\psi\,\bar{\eth}\psi + \eth\omega\,\bar{\eth}\omega}{2\delta^2\psi^2}, \\
j &= \frac{\eth\psi\,\partial_t\psi + \eth\omega\,\partial_t\omega}{\sqrt{2}\,\delta\psi^2},
\end{aligned}$$

[6] The term $\partial_t\phi$ does not appear in this expression because we have used the constraints equations to removed it.

where the norm ψ and twist ω are freely chosen. In order to simplify the equations, we choose $\omega = 1 - \psi$ and $\partial_t \psi = \partial_t \omega$ that yield the cancellation of the momentum densities. Furthermore, by setting the mean curvature $\mathcal{K} = 0$, the equations Eqs. (6.36) and (6.37) are trivially satisfied by choosing $A_{11} = A_{22} = 0$. We recall that $\mathcal{K}$ is the mean curvature of the induced metric in the Cauchy surface obtained from the evolution metric h_{ab} (see section 6.1). Under the above assumptions, the Hamiltonian constraint (Eq. (6.35)) takes the following form in terms of the free functions ψ and $\partial_t \psi$:

$$\Delta_{\mathbb{S}^2}\delta = 2\delta - \frac{2\delta^2}{\psi} - \frac{\delta(\partial_t\psi)^2}{\psi^2} + \frac{|\eth\delta|^2}{\delta} - \frac{\delta|\eth\psi|^2}{\psi^2}. \tag{10.17}$$

Next, we choose $\psi = \delta^2$ in order to obtain an elliptic equation depending on the free function $\partial_t \psi$ as

$$\Delta_{\mathbb{S}^2}\delta = -2 + 2\delta - \frac{\partial_t\psi}{\delta^3} - \frac{3|\eth\delta|^2}{\delta}. \tag{10.18}$$

Note that for $\partial_t \psi = 0$ we obtain the trivial solution $\delta = 1$, that corresponds to the Nariai metric at $t = 0$. Hence, in order to obtain perturbations of the Nariai solution, we have to provide a non-zero function $\partial_t \psi$.

In principle, there is no restriction on the function $\partial_t \psi$, hence we might be able to prescribe it freely and obtain a numerical solution up to some given accuracy. However, we point out that we do not know whether we may or may not be able to find a solution of Eq. (10.18) for some given function $\partial_t \psi$. Certainly, it would be interesting to determine the specific conditions on the function $\partial_t \psi$ in order to guarantee the existence of a solution for Eq. (10.18). However, this question is beyond the scope of this work, thus it is left as an open problem for a future research.

Richardson's iteration procedure

Now, we describe the basic idea for using a spectral implementation based on the SWSH for solving Eq. (10.18). Basically, we follow the approach introduced by Frauendiener in [82] for solving non-linear elliptic equations. For more information about these kind of methods, the interested reader is referred to [78,145] and references therein. Let us start by identifying the right-hand side of Eq. (10.18) as a non-linear function $f(\delta, \eth\delta)$ with spin-weight 0. Additionally, in order to use the AST, we assume the function f is axial symmetric. This assumption allows us to write f as

$$f(t,\theta) = \sum_{l=0}^{N} a_l(t)\, {}_0Y_l(\theta),$$

where we have used the notation introduced in chapter 7. The variable N represents the total number of collocation points where the function is sampled. We construct a Richardson's iteration procedure by writing a numerical solution of Eq. (10.18) after $n+1$ steps by $\delta_{n+1} = \delta_n + \zeta$, where ζ will be called the *correction factor*. Next, linearising the function f at the step $n+1$ (written as f_{n+1}) around the previous step n (f_n) and replacing it into Eq. (10.18), we obtain the linearised equation for ζ as [7]

$$\Delta_{\mathbb{S}^2}\,\zeta - \left(\frac{\partial f}{\partial\delta}\right)_n \zeta - \left(\frac{\partial f}{\partial\,\eth\delta}\right)_n \eth\,\zeta = -\left(\Delta_{\mathbb{S}^2}\delta_n - f_n\right). \tag{10.19}$$

[7] We have noted $\left(\frac{\partial f}{\partial\delta}\right)_n$ as the partial derivative of f with respect to δ evaluated at the step n.

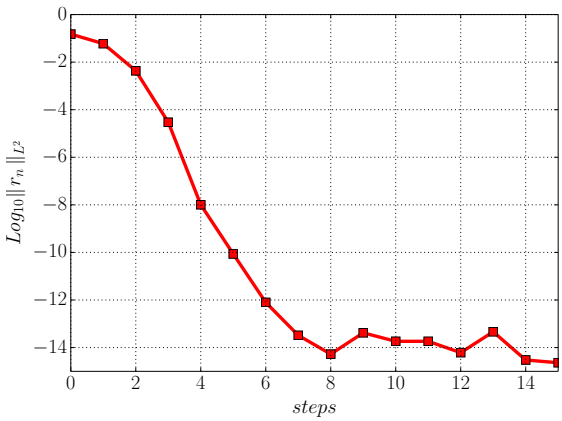

Figure 10.1: *Decay of the norm of the residual error.*

The right-hand side of this equation is known as the residual r_n, that represents the failure of δ_n to satisfy the elliptic equation at the step n. Due to the spatial topology of the domain, we write the correction factor and the residual in terms of the SWSH. Using the properties of the eth-operators Eq. (5.26), the linearised equation yields a system of equations for the N coefficients of ζ written on the SWSH basis. Introducing suitable collocation points $\theta_1, ..., \theta_N$, and forcing the approximate solution to satisfy Eq. (10.19) at those points, we obtain a system of N equations for the N coefficients of ζ, i.e., we obtain a system of $N \times N$ equations that can be solved numerically. At this point, we want to point out that the matrix in the right-hand side of Eq. (10.19) is invertible, consequently the equation has a unique solution if the term $(\partial f/\partial\delta)_n$ is different from an eigenvalue of the Laplacian $\Delta_{\mathbb{S}^2}$, namely $-l(l+1)$. As long as this condition is satisfied, we can find a numerical solution of Eq. (10.19).

Once we have found the coefficients from the correction factor, we update the function δ for the $n+1$ step and repeat the procedure above until reach $r_n \sim 0$. For later use, and as an illustrative example, we solve the Hamiltonian constraint for the initial function

$$\partial_t\psi = \epsilon\, {}_0Y_3(\vartheta). \tag{10.20}$$

where the value of ϵ controls the order of the perturbation. In Fig. 10.1 we show the behaviour of the norm $\|r_n\|_{L^2(\mathbb{S}^2)}$ (see section 8.20) obtained for the choice of $\epsilon = 10^{-4}$ (note that we have plotted the logarithm of the absolute value of that quantity). In the figure we observe that the norm of r_n decays until it reaches a satisfactory order of $\mathcal{O}(10^{-14})$. Once we have obtained the function δ, we obtain the other fields as

$$\begin{aligned} \phi_0 = \partial_t\phi_0 = \partial_t\delta_0 = f_0 = 0, \quad \partial_t\omega = \partial_t\psi, \\ \psi = \delta^2, \quad \omega = 1-\delta^2, \quad f_1 = \mathring{\Gamma}_1. \end{aligned} \tag{10.21}$$

Note that for $\partial_t\psi$ we obtain $\delta = 1$, then we recover the Nariai initial data. Later, in the discussion about inhomogeneous perturbations, we will use this initial data. Finally, similarly as it was done with the analytical initial data family, the function K_p can also be expressed in terms of the initial data. However, because the equation turns out to be very large in this case, we do not write it here.

10.5 Setting a stable evolution

10.5.1 Evolution variables

In the coordinates used to write the Nariai spacetime Eq. (10.1) the variable ψ grows exponentially. This behaviour is also observed for perturbations of the Nariai metric in the Nariai gauge. Such exponential growth is very problematic from the numerical point of view because the time derivatives will diverge in a short time crashing our numerical implementation. In order to overcome this situation, let us consider the following transformations:

$$\psi \to e^{\psi_*}, \quad \delta \to e^{\psi_*}\delta_*, \quad \phi \to e^{\psi_*}\phi_*, \quad \omega \to e^{\psi_*}\omega_*. \tag{10.22}$$

We rewrite the first-order system Eqs. (10.10) in terms of new variables $(\delta_*, \psi_*, \omega_*)$ which will be called *evolution variables*. To show that this change of variables does not affect the symmetric hyperbolicity of the resulting first-order system, let us first consider the original second-order system WGEF Eq. (6.19). The principal part of the wave equation for δ in terms of the new variable δ_* is

$$h^{ab}\partial_a\partial_b(e^{\psi_*}\delta_*) = h^{ab}\left(e^{\psi_*}\partial_a\partial_b\delta_* + 2e^{\psi_*}\partial_a\delta_*\partial_a\psi_* + \delta_*\partial_a\partial_b e^{\psi_*}\right),$$

where the last term $\partial_a\partial_b e^{\psi_*}$ can be written as the wave operator of ψ in terms of the new variable ψ_*. Replacing the wave equation for ψ_* obtained from the evolution equation for ψ in the expression above, we obtain that the principal factor of the wave equation for δ_* becomes

$$h^{ab}e^{\psi_*}\partial_a\partial_b\delta_*,$$

which just corresponds to a rescaling by a positive factor of the principal term in the evolution equation. A similar result is obtained for the principal part of the evolution equations for ϕ_* and ω_*. Next, defining the vector u_* in similar manner as u was defined (see Eq. (10.11)), we end up with the following first-order system

$$\partial_t u_* + \Pi_*\ \partial_\theta u_* = s(u_*)\,. \tag{10.23}$$

By a straightforward calculation it can be proved that Π_* has the same set of eigenvalues and eigenvectors as the characteristic matrix Π corresponding to the system u; hence, the symmetric hyperbolicity of the new system follows.

10.5.2 Constraint damping terms

Unfortunately, the proposed change of variables is not enough to make our numerical implementation stable. The reason lies in the fact that the constraint equations can be solved just up to some truncation error and this (from our experience) may trigger a growth of the violation covector components $\mathcal{D}_\mu$. One way to deal with this problem, is by adding *constraint damping terms* to the evolution equations WGES (see Eqs. (6.19)) in the way explained in section 2.5.2. To start with, we assume that the violation covector components as time-dependent functions. In other words,

$$\mathcal{D}_\mu(t,\theta) \simeq \mathcal{D}_\mu(t). \tag{10.24}$$

However, since $\mathcal{D}_\mu$ is a covector, the projection of its spatial components $\mathcal{D}_1, \mathcal{D}_2$ to the frame $(m^a, \overline{m}^a)$ have spin-weight 1 and -1, which directly implies that $\mathcal{D}_1 = \mathcal{D}_2 = 0$ under the above assumption because only a function with spin-weight 0 can have a mode of $l = 0$

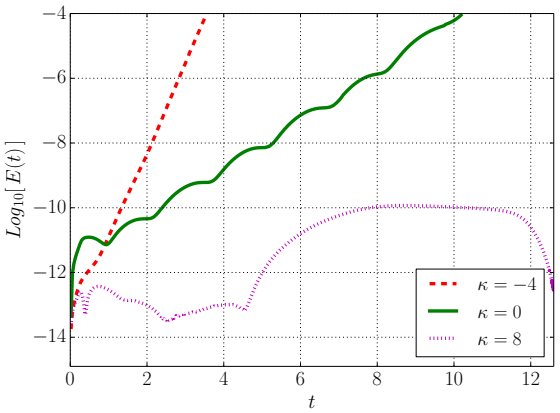

Figure 10.2: *Evolution of $E(t)$ using RKF with $Tol = 10^{-9}$ and different values of κ.*

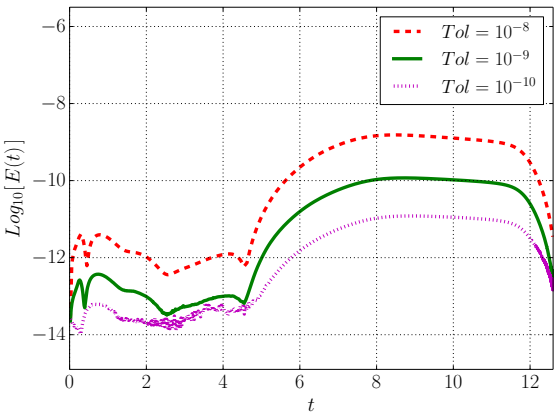

Figure 10.3: *Evolution of $E(t)$ with $\kappa = 8$ using RKF with different tolerances.*

(which is spatially independent). On the other hand, because the perturbed metrics will be "close" to the Nariai metric during the initial part of the evolution, we can use it as the background metric for writing the subsidiary equation that rules the evolution of $\mathcal{D}_0$. Thus, replacing the Nariai metric in Eq. (2.15) with $\eta_a = (-1, 0, 0)$ we obtain the evolution equation that govern the behaviour of $\mathcal{D}_0(t)$ as

$$\partial_{tt}\mathcal{D}_0(t) + (1 + 2\kappa)\partial_t\mathcal{D}_0(t) = 0,$$

for some constant κ. Evidently, the solution of this equation is

$$\mathcal{D}_0(t) = Ae^{\varrho} + B, \tag{10.25}$$

where $\varrho = -(1+2\kappa)$ with A being a real constant. An exponential decay for $\mathcal{D}_0(t)$ is obtained for $\kappa > -1/2$. Note that the function $\mathcal{D}_0(t)$ will never tend to zero. Instead, it will approach the constant value B which is fixed for the initial value $\mathcal{D}_1(0)$. This, however, does not represent a serious issue for our numerical calculations as long as we provide initial data such that B is small enough. Thus, to control the growth of $\mathcal{D}_0(t)$ we have to choose a suitable value for the constant κ.

In order to check numerically the validity of the above statement we proceed as follows. We define the *constraint error* for our implementation as[8]

$$E(t) := \sqrt{\| \mathcal{D}_0(t,\theta) \|^2_{L^2(\mathbb{S}^2)} + \| \mathcal{D}_1(t,\theta) \|^2_{L^2(\mathbb{S}^2)}}\,,$$

where the norm $\| \, . \, \|_{L^2(\mathbb{S}^2)}$ is numerically computed by using Eq. (8.20). Fig. 10.2 shows the error obtained for different values of the constant κ. Here, we have used the initial data family described in section 10.4 with $c_1 = c_2 = 0$ and $\epsilon = -0.5 \times 10^{-5}$. These data will be used in section 10.7 to discuss the asymptotic behaviour of the Nariai spacetime. The evolution was carried out implementing the pseudo-spectral method described in chapter 7 with the RKF method as time integrator.

As we expected, the error for $\kappa = -4$ grows exponentially whereas for $\kappa = 8$ it can be controlled. At this stage, we want to point out that according to Eq. (10.25), for $\kappa = 0$ we should obtain a damped solution for $\mathcal{D}_0(t)$. However, such behaviour is not observed because the numerical error coming from the time discretization grows rapidly due to the non-linear

[8] We have excluded $\mathcal{D}_2(t)$ from this definition because $\mathcal{D}_1(t,\theta) = \overline{\mathcal{D}_2(t,\theta)} = \mathcal{D}_2(t,\theta)$ in Gowdy symmetry.

terms present in the evolution equations. Hence, the choice of some positive value for κ may be required. From our experience, the value $\kappa = 8$ provides a good behaviour; hence, from now on, we will use it in all that follows.

To finalize this section, Fig. 10.2 shows that the error behaviour can be controlled along the evolution even though the perturbed metric moves away from the Nariai spacetime. Since the previous analysis is not valid for the late behaviour, it is not expected that the proposed constraint damping terms can control the error in that situation. However, as is also observed in Fig. 10.3, the constraint damping terms improve the accuracy of our implementation. Note that the error is always below the established error tolerance. Nevertheless, the price that we pay for such accuracy is that the "time step" becomes smaller and smaller during the evolution[9] and eventually this "freezes" the evolution of the system. One could overcome this issue by setting a lower bound for the time step value, with the drawback that the error will start to grow rapidly after a minimum time step than the lower bound is required. However, for the purposes of this work, it would be enough to do all the numerical experiments in the range of time that we can "cover" satisfactorily without losing accuracy.

10.6 Perturbations of the Nariai spacetime

In this section we proceed with the analysis of the instability of the Nariai spacetime. For simplicity, we have divided the perturbations into two types: homogeneous and inhomogeneous perturbations, which will be discussed separately. As mentioned in section 10.2, a detailed analysis of the first case has been already done by Beyer in [27]. However, in this section we revisit this case as a preparation for the analysis in the inhomogeneous case.

10.6.1 Homogeneous perturbations

Let us consider the case for which the analytical initial data family introduced in section 10.4.1 yields a constant value of K_p, that is given by choosing the initial values of the time derivatives of the metric components to be spatially independent. Furthermore, since the perturbations g are in this case manifestly homogeneous spacetimes, they should belong to a Kantowski-Sachs family of metrics similar to the homogeneous perturbations in [27]. Therefore, from now on, we refer to homogeneous perturbations for the case when the perturbation of the Kretschmann scalar K_p does not depend on the spatial coordinate θ. However, we point out that this definition of homogeneous perturbations is not general since it refers to a particular initial data family.

To obtain the initial data for this case from the initial data family given in Eqs. (10.15), we choose $\epsilon = 0$ and take the negative root for $\partial_t\psi_0$. The perturbations are given in terms of the constants c_1 and c_2. Thus, all the variables can be expressed in terms of the fundamental mode ${}_0Y_0(\theta)$ which is spatially independent. Henceforth, we shall understand that any homogeneous perturbation is written only in terms of the fundamental modes.

We start this analysis by assuming that the initial perturbations are small, i.e., $c_1^2 = c_2^2 \approx 0$. Hence, all the terms proportional to these will be negligible in the evolution equations *only* for the following heuristic discussion. Henceforth, we will refer to them as second-order

[9] In the cases shown in the figures the time step was in the order of 10^{-7}.

perturbations. As a result, all the second-order derivatives in the WGES vanish except[10]

$$\begin{aligned} \partial_{tt}\psi_* &\approx 2\Lambda. \\ \partial_t f_1 &\approx -1, \end{aligned} \tag{10.26}$$

where $\Lambda = 1$. We do not replace the value of Λ in the equation yet because we want to show that its positive value is the cause of the initial growth of the variable ψ_*. The variable $\partial_t\psi_*$ grows until it reaches a certain order; consequently, the contributions of the non-linear terms in the evolution equations that involve this quantity are no longer negligible. In other words, non-linear terms like $\partial_t\delta_*\,\partial_t\psi_*$ become first-order perturbations, namely terms proportional to either c_1 or c_2. Then, the system of equations turns into

$$\begin{aligned} \partial_{tt}\delta_* &\approx (\partial_t\delta_*\,\partial_t\psi_*)/2 + (\partial_t\psi_*)^2/2 + \partial_t\psi_* f_1, \\ \partial_{tt}\psi_* &\approx 2 - (\partial_t\delta_*\,\partial_t\psi_*)/2 - (\partial_t\psi_*)^2/2, \\ \partial_{tt}\omega_* &\approx (\partial_t\omega_*\,\partial_t\psi_*)/2, \\ \partial_t f_1 &\approx -1 + (\partial_t\psi_*)^2/2. \end{aligned} \tag{10.27}$$

This is the point where the evolution of the perturbed spacetime starts to be different from the Nariai spacetime. Note that for the Nariai initial data $\partial_t\delta_* = 0$ and just $\partial_t\psi_*$ changes in time, i.e., for the Nariai initial data the variable δ_*, which we can interpret as the mean radius of the $\mathbb{S}^2$-factor (see section 6.2), does not change during the evolution. On the other hand, the perturbed initial data $\partial_t\delta_* \neq 0$ causes the change of δ_* in time. To illustrate the above, we numerically solve the full system of evolution equations given in Eqs. (6.19) for the initial data with parameters $c_1 = -c_2 = 10^{-6}$. Let us start by considering Fig. 10.4 which shows the evolution of the variable $\partial_t\psi_*$. In the figure is observed an early rapid growth of this variable. On the other hand, we plot the behaviour of $\partial_t\delta_*$ and K_p in Fig. 10.5. In there, we observe that both quantities move away from zero which is their corresponding Nariai value. Clearly, the increment of δ_* is due to $\partial_t\delta_* > 0$ for the chosen initial data. Since this sign never changes, it is expected that δ_* grows indefinitely, i.e., the $\mathbb{S}^2$-factor expands. Additionally, this initial data make that $K_p < 0$ (see Eq. (10.16)). Similarly, setting initially $c_1 = 10^{-6}$ and $c_2 = 0$ we obtain $\partial_t\delta_* < 0$, which yields the monotonic decrease of δ_* (the $\mathbb{S}^2$-factor collapses) and the growth of K_p.

In short, we conclude that the $\mathbb{S}^2$-factor exhibits a *collapsing behaviour* for initial data such that $\partial_t\delta_* > 0$, whereas for $\partial_t\delta_* < 0$ it exhibits an *expanding behaviour*. For the particular case when $\partial_t\delta_* = K_p = 0$, the Nariai case, the $\mathbb{S}^2$-factor does not change. Note that this clearly shows that the fundamental mode of δ_* is unstable, consequently yielding the instability of the Nariai under this sort of perturbation.

The consistency of our analysis with respect to the results given by Beyer [27] becomes evident if we consider the initial mean curvature, which according to [27] we denote by $H_*^{(0)}$, associated with the induced metric in the Cauchy surface in the space of orbits S, obtained from the reduced metric $\hat{h}_{ab}$ (see section 6.1). This curvature in terms of the evolution variables is given by[11]

$$H_*^{(0)} = \partial_t\delta_*.$$

This clearly relates the initial mean curvature of the $\mathbb{S}^2$-factor from the reduced metric $\hat{h}_{ab}$ (the metric that is obtained from the symmetry reduction of the four-dimensional metric;

[10] For the numerical experiments, however, it will be used for the numerical computation the full system of equations.

[11] This notation change for inhomogeneous perturbations where H_2 is used instead of $H_*^{(0)}$ according to [28].

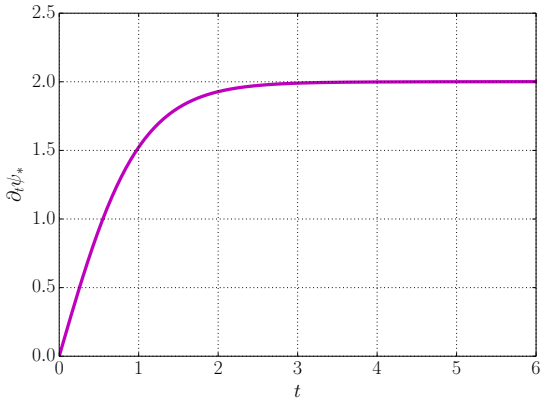

Figure 10.4: *Evolution of* $\partial_t\psi_*$.

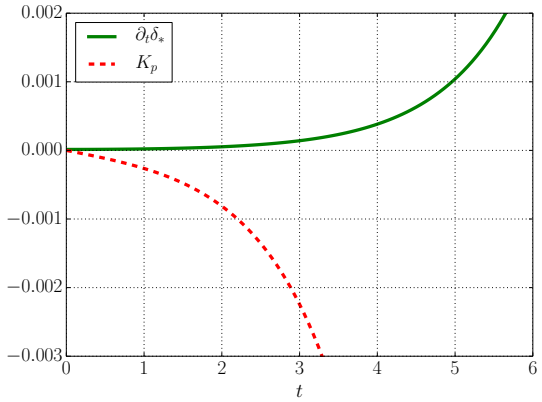

Figure 10.5: *Evolution of* $\partial_t\delta_*$ *and* K_p.

see, for instance, section 6.1) with the initial value of $\partial_t\delta_*$. Using a different approach, Beyer showed that homogeneous perturbations with initial mean curvature $H_*^{(0)} > 0$ produce an expansion of the $\mathbb{S}^2$-factor, whereas the opposite behaviour (collapsing) is given for $H_*^{(0)} < 0$. The Nariai spacetime is obtained for $H_*^{(0)} = 0$, that corresponds to $\partial_t\delta_* = 0$ in our setting.

10.6.2 Inhomogeneous perturbations

In this part, we shall focus on studying the mechanism that "triggers" the instability of the Nariai spacetime under inhomogeneous perturbations. Similarly, as was carried out in the previous section, we will concentrate on evolution equations of the variable δ_* and the initial value of $\partial_t\delta_*$. To obtain this kind of perturbations, we provide initial data such that K_p is spatially dependent. This corresponds to setting $\epsilon \neq 0$ in the initial data family. Henceforth, we will refer to any mode different from the fundamental as *harmonic modes* or simply *harmonics*.

Next, we will focus on discussing the effect of the non-linear terms like $\partial_t\delta_*\partial_t\psi_*$ in the evolution equations, in order to illustrate how they may contribute to the triggering mechanism that causes the expanding or collapsing behaviour of the $\mathbb{S}^2$-factor. Naturally, the following discussion also holds for other non-linear terms. Let us begin by writing both functions in terms of the SWSH basis as

$$\partial_t\delta_* = \sum_{l_1=0}^{\infty} a_{l_1}\,{}_0Y_{l_1}(\theta), \tag{10.28}$$

$$\partial_t\psi_* = \sum_{l_2=0}^{\infty} b_{l_2}\,{}_0Y_{l_2}(\theta). \tag{10.29}$$

Note that we have used the axial symmetric notation introduced in chapter 7. The multiplication between those terms can be carried out by following the multiplication formula for SWSH given in Eq. (5.21). In principle, this kind of product provides several harmonics which will contribute to the evolution equations. However, just under certain conditions, this product will produce contributions to the fundamental modes of the evolution equations. These are of particular importance here because, as we already discussed in the previous section, they trigger the expanding or collapsing behaviour of the $\mathbb{S}^2$-factor. In order to identify how these fundamental modes are generated, let us consider the multiplication between two terms from Eqs. (10.28) and (10.29) for some fixed l_1 and l_2 respectively. Using Eq. (5.21)

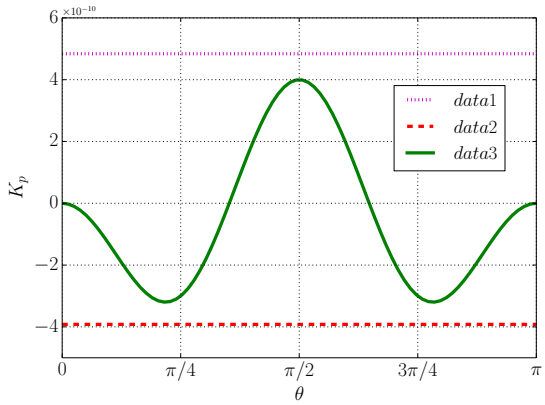

Figure 10.6: *K_p for different sets of initial data.*

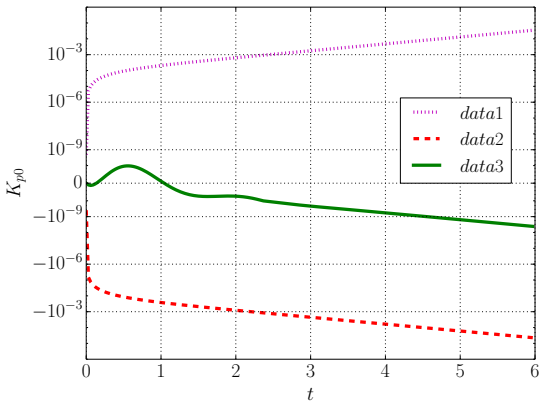

Figure 10.7: *Evolution of the fundamental mode of K_p for different sets of initial data in semi-logarithmic scale.*

we obtain

$$a_{l_1}\,{}_0Y_{l_1}(\theta)\,b_{l_2}\,{}_0Y_{l_2}(\theta) = \sum_{l\in\Theta} A_l(0,l_1,0:0,l_2,0)\,{}_0Y_l(\theta), \tag{10.30}$$

where $\Theta := \max\{|l_1-l_2|,...,l_1+l_2\}$ and A_l is a constant value obtained from the multiplication between Clebsch-Gordan coefficients given by Eq. (5.20). To conduct the analysis of the above product, we consider separately the following two situations.

Situation 1

When $\partial_t\delta_*$ and $\partial_t\psi_*$ have a non-zero fundamental mode. In this case the product between those terms will produce contributions to the fundamental modes of the system of equations. In particular, these contributions will trigger the changing in time of the fundamental mode of δ_* which, as mentioned in the previous section, controls the expanding or collapsing behaviour of the $\mathbb{S}^2$-factor. In other words, according to the last section, the contributions to the fundamental mode in the evolution equation of δ_* causes that the $\mathbb{S}^2$-factor experiences either an expanding or collapsing behaviour. Next, by using the analytical initial data family, we provide numerical evidence that illustrates the above.

Let us consider the analytical initial data introduced in section 10.4.1 where $\epsilon = 0.5\times 10^{-5}, c_1 = 4.47210022, c_2 = 0$ and $\partial_t\psi$ is given by the positive root. From the initial data Eq. (10.16) and using the evolution variables Eq. (10.22), it is obtained that the fundamental mode of K_p is numerically zero (to the order of 10^{-14}) while for $\partial_t\delta_*$ it is positive (to the order of 10^{-11}). Henceforth, we refer to this as[12] *data*3. In Fig. 10.6 we plot the behaviour of K_p for this initial data together with two others corresponding to *data*1 and *data*2, which describe homogeneous perturbations with $c_1 = 0.5\times 10^{-5}, c_2 = 0$ and $c_1 = c_2 = 1.4\times 10^{-5}$. Note that for *data*1 the fundamental mode of $\partial_t\delta_*$ is negative while for *data*2 is positive. Next, let us consider Fig. 10.7 in which the vertical axis is shown in semi-logarithmic scale for a better appreciation of the temporal change of the order of magnitude of the fundamental mode of K_p. Since *data*1 yields $K_p > 0 > \partial_t\delta_*$, we obtain that the resulting $\mathbb{S}^2$-factor exhibits a collapsing behaviour. On the other hand, for *data*2 we have initially $K_p < 0 < \partial_t\delta_*$, then the $\mathbb{S}^2$-factor undergoes an expanding behaviour as expected. For *data*3, where the fundamental mode of K_p was chosen numerically zero, we observe that the behaviour of K_p is initially

[12]Choosing $\epsilon = 0.5\times 10^{-5}$ and $c_2 = 0$ the value of c_1 can be found.

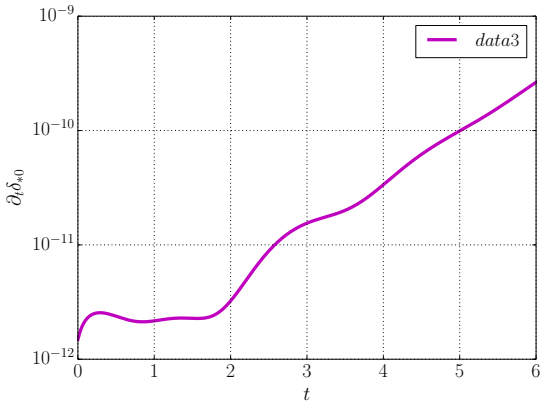

Figure 10.8: *Evolution of the fundamental mode of $\partial_t\delta_*$ for data3 in logarithmic scale.*

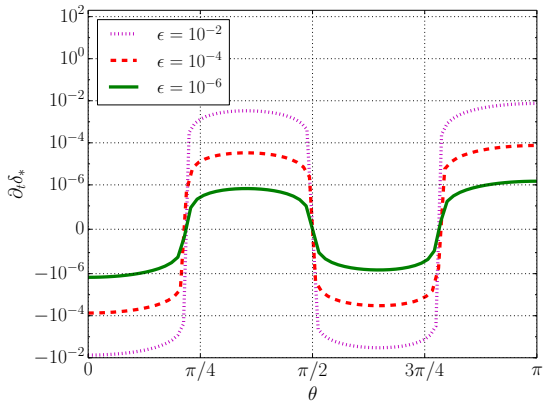

Figure 10.9: *Initial $\partial_t\delta_*$ obtained numerically for different values of ϵ in logarithmic scale.*

oscillatory but later becomes monotonic because of the growth of $\partial_t\delta_*$, which is illustrated in Fig. 10.8. The figure shows that regardless the oscillation of K_p, if the variable $\partial_t\delta_*$ stays positive, eventually the homogeneous perturbations become dominant and trigger the expansion of the $\mathbb{S}^2$-factor.

Situation 2

Now, let us consider the case when one of the functions $\partial_t\delta_*$ or $\partial_t\psi_*$ have a fundamental mode different from zero. In this case, one might think that the product between these two functions do not produce any fundamental mode. However, considering Eq. (10.30), we clearly see that those can be produced when $l_1 = l_2$. Thus, we can say that homogeneous perturbations are generated by the non-linear contributions of the inhomogeneous perturbations. Furthermore, as we will confirm in the following numerical experiments, they will become dominant and eventually trigger the expanding or collapsing behaviour of the $\mathbb{S}^2$-factor. In order to determine whether inhomogeneous perturbations develop an expanding or collapsing behaviour of the $\mathbb{S}^2$-factor, we have to look at the resulting sign of the fundamental mode of $\partial_{tt}\delta_*$ when the homogeneous perturbation become dominant. According to our previous discussion on homogeneous perturbations, if the fundamental mode of $\partial_{tt}\delta_*$ becomes positive when the homogeneous perturbations become dominant, the $\mathbb{S}^2$-factor would experience a collapsing behaviour. On the other hand, it would undergo an expansion if $\partial_{tt}\delta_*$ turns negative. Note that this behaviour is given because of the instability of the fundamental mode of δ_* discussed in our analysis of homogeneous perturbations. In what follows, by using the numerical initial data, we provide numerical evidence that supports the above discussion.

Let us consider the numerical initial data as introduced in section 10.4.2. Following the algorithm based on Richardson's iteration, we solve numerically the Hamiltonian constraint for $\epsilon = 10^{-2}, 10^{-4}$ and 10^{-6} respectively. In all the cases, we obtained that the initial fundamental mode of $\partial_t\delta_*$ ($\partial_t\delta_{*0}$) is numerically zero (of order $\mathcal{O}(10^{-14})$). This is clearly illustrated in 10.9, which shows that its mean value is approximately zero. On the other hand, Fig. 10.10 shows the initial perturbation of the Kretschmann scalar for the three cases, which confirms that the three sets of initial data generate perturbations of the Nariai metric.

The evolution of the fundamental mode of $\partial_t\delta_*$ is shown in Fig. 10.11. In this plot, we observe that this mode is initially zero. However, because of the contribution from all the non-linear terms present in the evolution equation of $\partial_{tt}\delta_*$, this mode quickly starts to oscillate. Eventually, this mode becomes dominant turning monotonic the behaviour of $\partial_t\delta_*$.

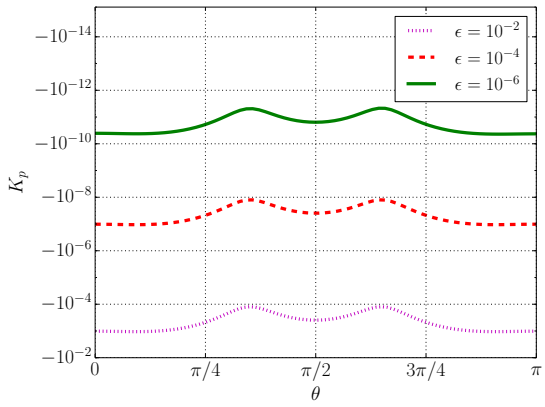

Figure 10.10: *Initial K_p obtained numerically for different values of ϵ in logarithmic scale.*

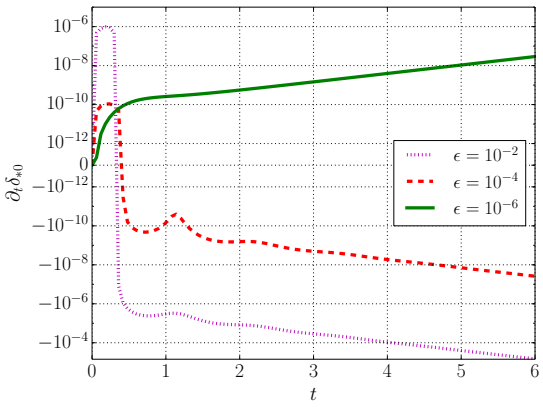

Figure 10.11: *Evolution of the fundamental mode of $\partial_t \delta$ for different values of ϵ in logarithmic scale.*

Comparison with known results

Similarly to the case of homogeneous perturbations, let us consider the initial mean curvature associated with the induced metric in the Cauchy surface obtained from the reduced metric $\hat{h}_{ab}$ and denoted in this case by H_2. For the numerical experiment carried out in [28], H_2 is chosen as a spatially depended function which is shifted up or down by the tuning of some given parameter. When the mean value of H_2 is above zero, an expansion of the $\mathbb{S}^2$-factor is obtained while a collapsing behaviour is obtained for a mean value lower than zero. On the other hand, in the "critical case", when the mean value of H_2 is zero (zero fundamental mode), the behaviour was not understood. As was pointed out by Beyer, at some stage during the evolution, the $\mathbb{S}^2$-factor "makes a decision" about whether to expand or to collapse. In our analysis, this "decision" is clearly explained by the contributions of the non-linear terms to the fundamental mode of $\partial_{tt}\delta_*$ as explained above, i.e., if the fundamental mode of $\partial_{tt}\delta_*$ becomes negative when the fundamental mode becomes dominant, the $\mathbb{S}^2$-factor would experience a collapsing behaviour in contrast to the expanding behaviour if such a mode was initially positive.

We point out that in [28], the numerical experiments were conducted about the "critical case" for "small" inhomogeneous perturbations. That is, perturbations given for an amplitude of the function H_2 in the order 10^{-4}. For large perturbations (bigger than 10^{-4}) it was posed the question on whether it might be observed different behaviours, such as the formation of multiple collapsing and expanding regions as it is claimed in [41] that can be given for the spherically symmetric case. However, our analysis suggests that such a behaviour cannot occur. This is clearly illustrated in the numerical experiment shown above that uses the numerical initial data for 10^{-2}, 10^{-4} and 10^{-6}. In terms of the evolution variables, the mean curvature H_2 can be written as

$$H_2 = \partial_t \delta_* \, \delta_*^{-3/2}.$$

Similarly for $\partial_t \delta_*$, it is found that the initial fundamental mode (which corresponds to its mean value) of H_2 in all the cases is zero. In Fig. 10.12 we show the initial value of this function for each amplitude (Note the similarity of the initial functions of H_2 to $\partial_t \delta_*$). Recalling Fig. 10.11, the evolution of the variable $\partial_t \delta_*$ shows that by increasing the order of the inhomogeneous perturbations, we enlarge the initial contribution to the fundamental mode of $\partial_{tt}\delta_*$ that yields a faster expansion or collapse of the $\mathbb{S}^2$-factor than if we were using a smaller value of ϵ.

To finalize this section, we point out that all the above analysis provides evidence of

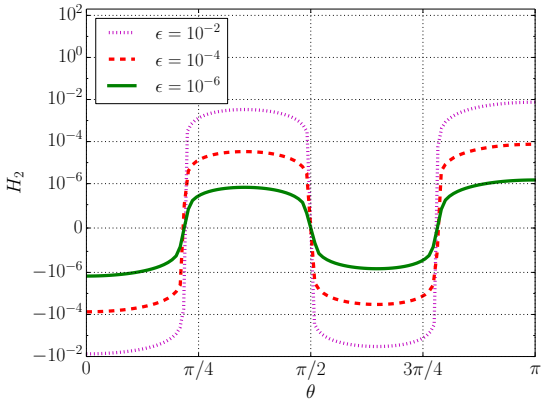

Figure 10.12: *Initial H_2 obtained numerically for different values of ϵ in logarithmic scale.*

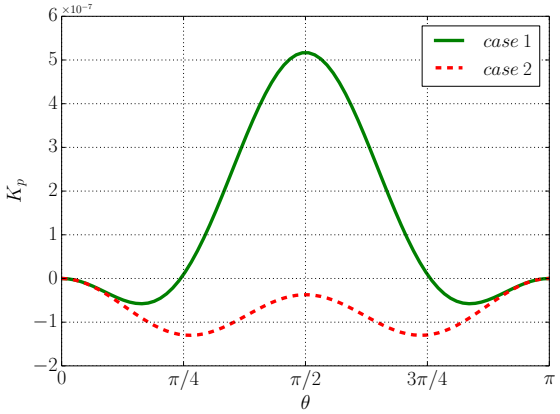

Figure 10.13: *Initial K_p for both the expanding and collapsing case.*

the non-linear instability of the Nariai spacetime under inhomogeneous perturbations and that our approach to this issue constitutes a significant progress in the understanding of the underlying mechanism.

10.7 Studies of the asymptotic behaviour

We devote this section to the study of the asymptotic behaviour of the Kretschmann scalar of the perturbations for when $K < K_{Nariai}$ and $K > K_{Nariai}$, that we identify as the *expanding* and *collapsing* cases respectively. The names comes from the fact that for the first case K stays bounded whereas for the second one it blows up.

For the following numerical experiments, we will use the analytical initial data family such that $c_1 = c_2 = 0$. We obtain the collapsing case by setting $\epsilon = 0.5 \times 10^{-5}$ which makes the fundamental mode of K_p positive. On the other hand, the expanding case is given by $\epsilon = -0.5 \times 10^{-5}$, where the fundamental mode of K_p is negative. Intuitively, the fundamental mode of K_p can be interpreted as its mean value over the spatial domain. This is illustrated in Fig. 10.13 where we observe that the K_p corresponding to the collapsing case, named *case* 1, has a positive mean value. Evidently, in the expanding case, *case* 2, we also confirm the statement above since the fundamental mode for K_p is negative. We start our analysis by firstly discussing the collapsing case and secondly the expanding case.

10.7.1 Collapsing case

Before presenting the evolution of the Kretschmann scalar, we describe briefly the behaviour of the variables ψ_* and the spatial Ricci scalar of the $\mathbb{S}^2$-factor. The evolution of these two important geometric quantities is shown in Fig. 10.14. We observe that the fundamental modes of both quantities blow up. Recalling that $\psi = e^{\psi_*}$ represents the norm of the Killing vector along the $\mathbb{S}^1$-factor and ${}^{(2)}R$ corresponds to the Ricci scalar of the $\mathbb{S}^2$-factor, we can infer that while the length of all the individual symmetry orbits along the $\mathbb{S}^1$-factor expand, the $\mathbb{S}^2$-factor collapses because its curvature diverges. This behaviour was also observed by Beyer in [28]. He identified such phenomenon as evidence that the perturbed spacetime evolves towards a "cigar singularity". This behaviour is significantly different from that observed in Gowdy symmetric $\mathbb{S}^1 \times \mathbb{S}^2$ spacetimes with zero cosmological constant discussed in chapter 8. However, it may be the case that this type of singularity is due to some kind

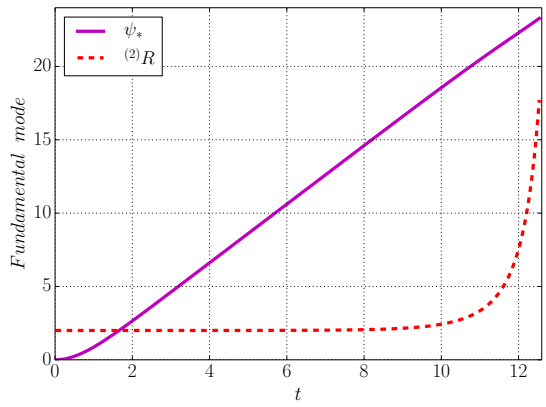

Figure 10.14: *Evolution of ψ_* and $^{(2)}R$ in the collapsing case.*

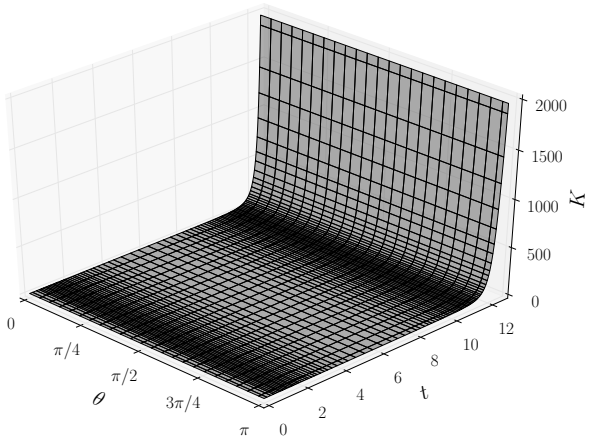

Figure 10.15: *Evolution of K in the collapsing case.*

of geometric effect due to the chosen gauge or initial data family. This question goes beyond the scope of this work and hence we leave it for a future research.

Now, we turn our attention to the behaviour of the Kretschmann scalar. When the spacetime evolves towards the singularity this quantity blows up. This is clearly shown in[13] Fig. 10.15. However, what is not quite clear is how the harmonics will behave in this case. To shed some light on this query, we plot some snapshots for the harmonics evolution in Fig. 10.16. For a better appreciation of the different order of magnitude we show the vertical axis in a semi-logarithmic scale. In this figure, we do not plot each mode separately; instead, we just remove the fundamental mode from the Kretschmann scalar and plot the resulting function composed of all the harmonics. Henceforth, we will refer to this function, denoted by K_l, as oscillations of the Kretschmann scalar. In order to avoid any possible misunderstanding, we want to clarify that the "steep" behaviour of the oscillations near $\pi/4$ and $3\pi/4$ in Fig. 10.16 corresponds to an effect of the semi-logarithmic scale, hence the figure does not describe the real way how the oscillations are.

In the figure, we observe that the oscillations of the Kretschmann scalar are amplified when the spacetime approaches the singularity. However, apart of this, we do not observe any particular region where a possible spike could emerge, in contrast to the case without cosmological constant discussed in section 9.4.2, that is, the oscillations seem to remain smooth along the evolution. Fig. 10.17 shows the evolution of K_l. Of course, it is also possible that we observe this behaviour because the spacetime is still far away from the singularity, hence any true spike has not yet emerged. Certainly, it is very difficult to answer this question; it requires a more extensive analysis from both the analytical and numerical points of view. This question goes beyond the scope of this work, thus we leave it as an open problem.

10.7.2 Expanding case

Finally, we discuss the expanding behaviour of the perturbations of the Nariai spacetime. Since this analysis is carried out in the light of the cosmic no-hair conjecture[14] (CNH), we

[13] The difference between dark and light regions in the figure is due to the adaptive time integration RKF. The darker a region is, the smaller the time step.

[14] See section 3.2.3 for a discussion of this conjecture.

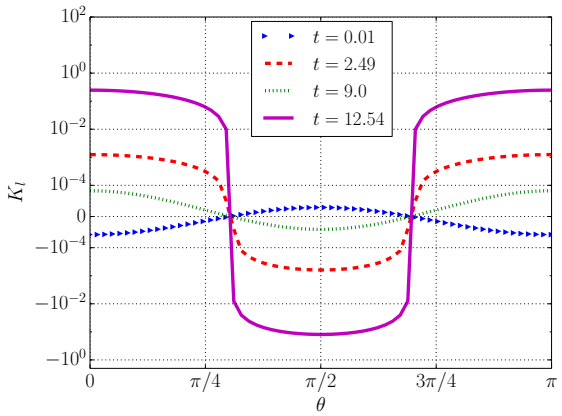

Figure 10.16: *Snapshots of the evolution of K_l in semi-logarithmic scale in the collapsing case.*

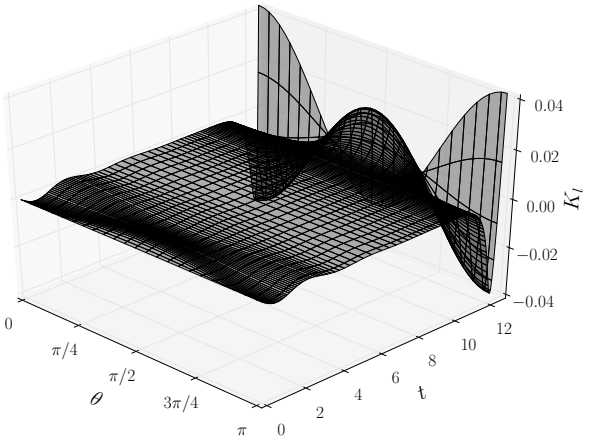

Figure 10.17: *Evolution of K_l in the collapsing case.*

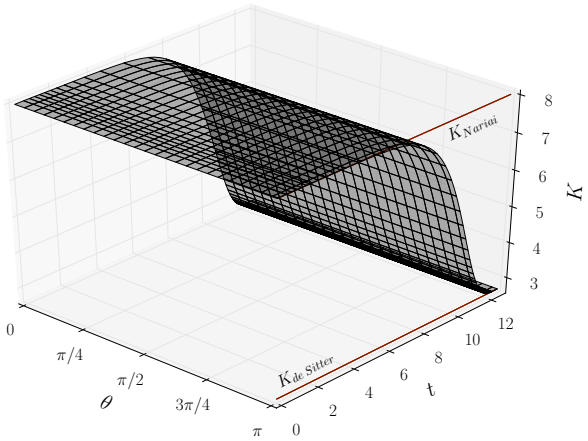

Figure 10.18: *Evolution of K in the expanding case.*

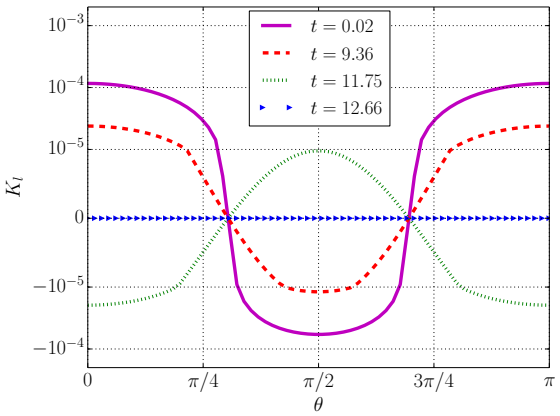

Figure 10.19: *Snapshots of the evolution of K_l in semi-logarithmic scale in the expanding case.*

start by identifying the Kretschmann scalar of the de Sitter spacetime. It is well-known (see, for instance, [113]) that this quantity is a constant value given by

$$K_{de\ Sitter} = \frac{8\Lambda^2}{3}. \tag{10.31}$$

According to the CNH, if perturbations of the Nariai spacetime develop an expanding behaviour ($K < K_{Nariai}$), they should evolve towards a spacetime locally isometric to the de Sitter spacetime. For simplicity, hereafter we will omit to say locally isometric and just say that a spacetime times evolves towards the de Sitter spacetime. Therefore, it is expected that their corresponding Kretschmann scalar should evolve asymptotically to $K_{de\ Sitter}$. This is precisely shown in Fig. 10.18 where we have plotted the evolution of K. Notice that we have added two lines to indicate the reference values of the Kretschmann scalars corresponding to the Nariai and de Sitter spacetimes respectively. The figure shows that starting from a value close to K_{Nariai}, the Kretschmann scalar evolves towards the de Sitter value $K_{de\ Sitter}$. However, this plot cannot show how close K is from $K_{de\ Sitter}$. To address this question,

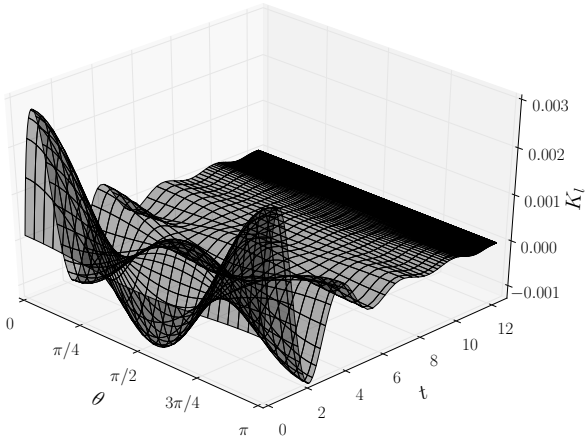

Figure 10.20: *Evolution of K_l in the expanding case.*

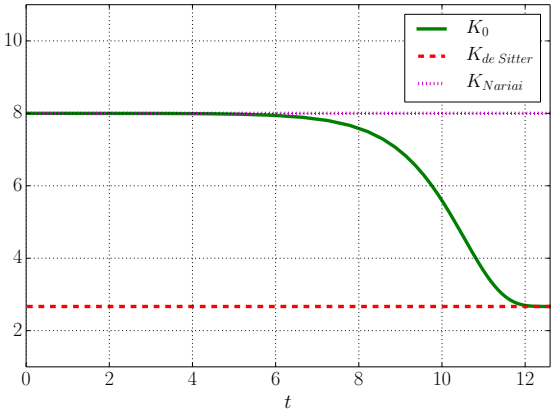

Figure 10.21: *Evolution of the fundamental mode of K (K_0) and the reference values K_{Nariai} and $K_{de\ Sitter}$.*

we plot some snapshots of the evolution of K_l in Fig. 10.19 using the semi-logarithmic scale in the vertical axis. In the figure, we observe that the oscillations of the Kretschmann scalar are damped during the evolution. We show a continuous illustration of this process in Fig. 10.20. Those pictures make evident the fact that K becomes homogeneous during the evolution, i.e., the fundamental mode becomes the only one that rules the evolution of K. Finally, Fig. 10.21 shows the evolution of this mode to confirm that it reaches the constant value $K_{de\ Sitter}$. Naturally, this behaviour is also given in the homogeneous case. Clearly, the above suggests that perturbations of the Nariai spacetime that exhibit an expanding behaviour evolves towards the de Sitter spacetime. However, at this point we certainly cannot ensure that those perturbations evolve towards the de Sitter spacetime as suggested by the CNH. In order to study this question in more detail we analyse the behaviour of the $\mathbb{S}^2$-factor. Particularly, we focus on studying the behaviour of its corresponding Ricci scalar.

It is well-known that in two dimensions the Riemann tensor ${}^{(2)}R_{abcd}$ is given by the following expression (see [123])

$$ {}^{(2)}R_{abcd} = \frac{{}^{(2)}R}{2}(\gamma_{ac}\gamma_{bd} - \gamma_{ad}\gamma_{bc}), $$

where γ_{ab} represents the two-dimensional metric in $\mathbb{S}^2$. Thus, it is clear that all the geometric information in the manifold $\mathbb{S}^2$ is encoded in the Ricci scalar. In the particular case where ${}^{(2)}R$ is constant, the metric γ_{ab} describes a two-sphere of constant radius; consequently, the $\mathbb{S}^2$-factor turned out to be spherically symmetric. Further, it can be argued that the four-dimensional spacetime turns homogeneous, then, if its Kretschmann scalar coincides with $K_{de\ Sitter}$, yields that it is locally isometric to de Sitter spacetime. Therefore, in our particular case, showing that the perturbations of the Nariai spacetime become spherically symmetric during the evolution will be enough evidence to assert that the de Sitter spacetime acts as a future attractor for those.

Following the argument above, we analyse the evolution of ${}^{(2)}R$. Fig. 10.22 shows the behaviour of the oscillations of this quantity. In there we observe that the amplitude of the oscillations decay very rapidly during the evolution, implying (as expected) that the quantity ${}^{(2)}R$ tends to be spatially independent. In fact, as is shown in Fig. 10.23, the amplitude of the oscillations reach the order of machine accuracy which can be numerically considered

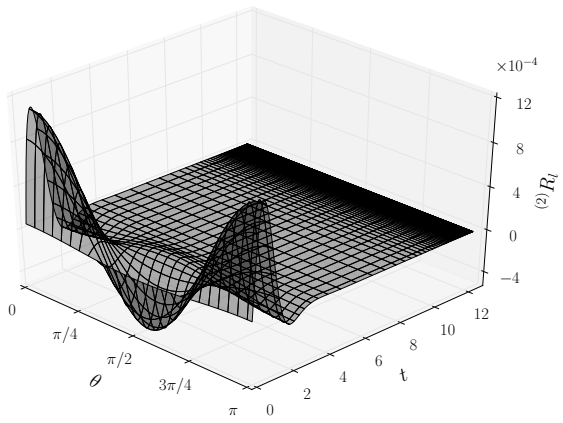

Figure 10.22: *Evolution of* ${}^{(2)}R$ *in the expanding case.*

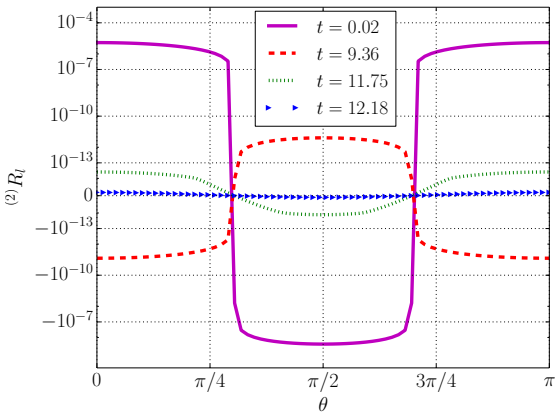

Figure 10.23: *Snapshots of the evolution of* ${}^{(2)}R_l$ *in semi-logarithmic scale in the expanding case.*

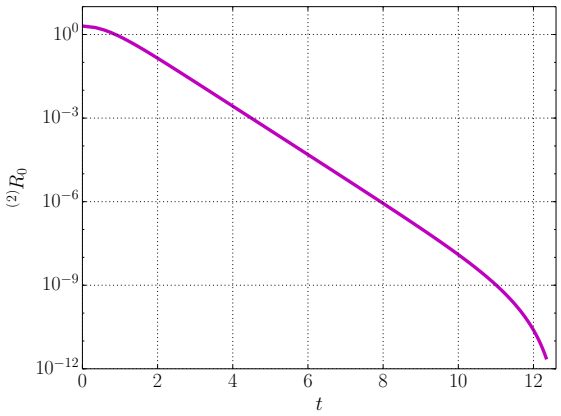

Figure 10.24: *Evolution of the fundamental mode of* ${}^{(2)}R$ *in logarithmic scale.*

as zero. Hence, this fact allow us to infer that the $\mathbb{S}^2$-factor turns (asymptotically) into a two-sphere which entails the spherical symmetry of the perturbed spacetime. Additionally, the evolution of the fundamental mode of this quantity is represented in Fig. 10.24. It can be interpreted as an expansion of the mentioned sphere (as expected) when the perturbed spacetime approaches towards the de Sitter spacetime.

We end this chapter by remarking that the above discussion provides enough evidence to conclude that perturbations of the Nariai spacetimes become spherically symmetric. Moreover, considering the fact that the Kretschmann scalar corresponds to the $K_{de\,Sitter}$, we conclude that these perturbations turn into homogeneous spacetime locally isometric to the de Sitter spacetime as suggested by the CNH.

Chapter 11

Discussion and future projects

Having described the ideas in which is based our analytic and numerical infrastructure in Part II, and its applications to Gowdy spacetimes in Part III, we now summarize and discuss the major results of this work. This chapter ends with a short review of some other possible applications that we may consider as future projects.

11.1 Discussion of the analytical infrastructure

The purpose of this work was to introduce an analytic and numerical approach to the treatment of the Cauchy problem of the vacuum EFE for spacetimes with spatial topologies $\mathbb{S}^3$ or $\mathbb{S}^1 \times \mathbb{S}^2$ and symmetry group U(1). The general idea consisted of taking advantage of the action of the symmetry group U(1) on those spacetimes and writing them as a principal fiber bundle, which is trivial for $\mathbb{S}^1 \times \mathbb{S}^2$ but not for $\mathbb{S}^3$. Thus, the Cauchy problem in a four-dimensional problem was reduced to a three-dimensional initial value problem for a manifold with spatial topology $\mathbb{S}^2$. Expressing all the fields in terms of the SWSH, it was possible to avoid coordinate representations that suffer from coordinate singularities this kind of manifold. We implemented the generalized wave map formalism to reduce the GES in the space of orbits $S = \mathbb{R} \times \mathbb{S}^2$ to a system of quasilinear wave equations in terms of the generalized gauge source functions with well-defined spin-weights. As a result, thanks to the fully tensorial character of these equations, the system of evolution equations WGES given in Eq. (6.19) could be solved by using a $2+1$-pseudo-spectral method based on the SWSH. However, in this thesis, we have applied our infrastructure for studying Gowdy symmetric spacetimes, where thanks to the symmetry group $\mathrm{U}(1) \times \mathrm{U}(1)$, the vacuum EFE can be reduced to a $1+1$-system of partial differential equations.

There are several results regarding the existence and uniqueness of solutions of the constraint equations in three-dimensional Cauchy surfaces; see [13] and references therein. All of them depend on a prescribed mean curvature which is assumed to be either constant, near-constant, or far-from-constant. For the first two cases, it is almost completely understood under what conditions a solution of the constraint equations exists or not. In contrast, for the latter case only a few results are known. Unfortunately, in our case, where we deal with two-dimensional initial Cauchy surfaces, these results may not be extended directly. In other words, even though we have obtained an elliptic representation of the constraints in the space of orbits S based in the standard York-Lichnerowicz conformal decomposition, none of the mentioned results in three-dimensions apply unless we solve the constraints in the original spacetime and project the solution to the space of orbits. We have followed this approach in chapter 9 (see also [35]). Therefore, in general, we do not know under what conditions the

solutions of the system of two elliptic equations Eqs. (6.38) and (6.39) exist. Certainly, this question goes beyond of the scope of this work, hence we leave it as a future project.

Nevertheless, it may happen that, in some situations, solving the system of elliptic equations in the space of orbits may be easier than solving the traditional constraints in the original spacetime. Particularly in this work, specifically in section 10.4.2, we were able to solve the constraint equations analytically in the space of orbits to find perturbations of the Nariai spacetime. To do so, following the work of Frauendiener [82], we introduced a spectral method based on the Richarson's iteration method and the SWSH for solving the constraints in the axial symmetry case. Nevertheless, we emphasize that this algorithm can be easily extended to the more general case of U(1) symmetric spacetimes, which clearly opens the door to a large number of possible situations that could be studied using this approach.

In general, we conclude that our approach should be of interest to researchers working on problems where spherical coordinates are a natural choice, since it yields a simple and unified description of tensor fields without the undue complexity of the traditional vector and tensor harmonics [1]. Furthermore, since the generalized wave map formalism provides an elegant covariant way to write evolution equations over $\mathbb{S}^2$ keeping the gauge freedom, we believe that it could be easily adapted to standard pseudo-spectral approaches (see, for instance, [49,186]) for studying more complicated scenarios in $3+1$-dimensions that implicitly contains this topology. In other words, we believe that this work clearly illustrates how numerical relativity could greatly benefit from this approach since it provides a natural way to treat tensor fields over $\mathbb{S}^2$.

11.2 Discussion of the numerical infrastructure

The numerical implementation for solving the WGES on $\mathbb{R}\times\mathbb{S}^2$ was based on the method of lines. Our choice to conduct the temporal integration was the Runge-Kutta-Fehlberg method (except for convergence test). Because in this work we restricted ourselves to applications of Gowdy symmetric spacetimes, the spatial derivatives over $\mathbb{S}^2$ were calculated by using the AST (after expressing the frame derivatives in terms of the eth-operators) which provided an efficient treatment of axially symmetric functions by reducing the complexity of the general algorithm of the HWTs $\mathcal{O}(L^3)$ (where L is the band limit of the functions on $\mathbb{S}^2$ in terms of the spin weight spherical harmonics) to $\mathcal{O}(L^2)$. Furthermore, because of the low memory cost of the AST, we only had to compute the Wigner coefficients Δ^l_{mn} only when the grid resolution changes which reduced the number of operations per transform to just $\mathcal{O}(L\log_2 L)$.

Clearly, one of the advantages of our implementation is that the spatial derivatives are straightforward computed in our pseudo-spectral method (PS) in contrast to how they would have been calculated by using a finite differencing method (FD). Thus, as discussed in chapter 7, the PDE system of equations yielded by the vacuum EFE is reduced to an ODE system which can be solved it numerically by using any time integrator. However, in situations where the functions develop spikes, i.e., regions where functions are not smooth, our implementation dramatically loses accuracy with respect to a FD. In the context of numerical relativity, the above implies that our numerical implementation is not suitable for studying extreme situations, like singularities or Cauchy horizons, where the spatial derivatives are not smooth. On the other hand, our pseudo-spectral approach is most convenient for studying situations where the gravity acts "smoothly" as for expansion of cosmological models or propagation of gravitational waves, just to mention a few, because the spatial derivatives remain smooth all the times.

The most natural way to enhance our implementation would be by using a multi-domain

PS method; see, for instance, [45, 72] and references therein. The general idea will consist of dividing the computational region into subdomains, each of them with its own set basis functions and collocation points. Thus, it may be possible to make a multi-domain PS method for treating not smooth functions. In addition, technical tricks to control the accuracy, such as special forms of spectral filtering or more sophisticate "constraints damping terms", could be introduced to improve the implementation.

An important technical result of this work was the development of a module, written in Python 2.7, for the implementation of the AST. It can be freely downloaded under the GNU General Public License (GPL) at gravity.otago.ac.nz/wiki/uploads/People/Axial_Spin_Weight_Functions.zip. This module allows objects to be defined that represent spin-weighted functions and that follow the basic operations among them. Hence, it can be seen not only as a set of functions but also as a Python environment for working with axial symmetric SWSH. Additionally, keeping in mind possible future projects that will be mentioned later, we have generalized this module for the general SWSH.

11.3 Discussion of the applications

To analyse the consistency, accuracy and feasibility of our numerical infrastructure, in chapter 8 we reproduced an inhomogeneous cosmological solution of the vacuum EFE with spatial topology $\mathbb{S}^3$. In there, we conducted a detailed numerical analysis to identify the major sources of potential errors. Further, we explored the behaviour of the constraints for different gauges by choosing different generalized gauge source functions.

Later in chapter 9, motivated by the works of Garfinkle [90] and Ståhl [183], we numerically explored the behaviour of Gowdy $\mathbb{S}^1 \times \mathbb{S}^2$ spacetimes using our infrastructure. In particular, studying the behaviour of the Kretschmann scalar and other geometrical quantities, we observed that spikes could emerge at the polar regions. Since our numerical implementation avoids problematic terms like $\cot\theta$ in the evolution equations, we were able to compute the Kretschmann scalar without any problem at the poles in contrast to the standard approach based on coordinate frames. This advantage allows us to carefully explore the behaviour of this quantity near to the poles. In fact, we found that the curvature associated with the $\mathbb{S}^2$-factor diverges near the poles faster than in any other place (including the equator). Moreover, the maxima of the Kretschmann scalar move towards the poles which leads us to think that if some spikes develop during this evolution, they should appear first at the poles. Following a different approach, Beyer [25] found similar numerical results for a certain family of Gowdy $\mathbb{S}^3$ spacetimes, namely a class of solutions of the vacuum EFE close to the family of λ-Taub-NUT spacetimes. These studies together with our findings provide evidence that support Ståhl's prediction about the general raising of spikes (true spikes) at the polar regions, which suggests that Fuchsian methods are not enough for studying the behaviour of this sort of Gowdy spacetimes at the singularities. Therefore, we believe that more numerical and analytical work is required in order to fully understand the behaviour of Gowdy spacetimes with spatial topologies $\mathbb{S}^1 \times \mathbb{S}^2$ and $\mathbb{S}^3$, as has been already done in the last decades for the $\mathbb{T}^3$ case.

As another application, based on the previous works [27, 28], we investigated the underlying mechanism that causes the non-linear instability of the Nariai spacetime and explored the asymptotic behaviour of its perturbations. We introduced Gowdy perturbations of the Nariai spacetime in terms of the Kretschmann scalar value and constructed initial data (analytically and numerically) based on the scheme of the York-Lichnerowicz conformal decomposition for $\mathbb{S}^2$ introduced in section 6.4. Additionally, we introduced the Nariai gauge that allowed us

to write the evolution equations in a convenient form for the posterior analysis of the perturbations. By means of the implementation (and analysis) of constraint damping terms into the WGES it was possible to achieve stable numerical computations that allow us to draw conclusions about the asymptotic behaviour of the perturbations.

One of the more important findings from our analysis was that in contrast to homogeneous perturbations (spatially independent), the non-linear terms in the inhomogeneous perturbations (spatially independent) play a fundamental role in the "triggering" mechanism of the expanding or collapsing behaviours. The reason lies in the fact that inhomogeneous perturbations can develop an expanding or collapsing behaviour of the $\mathbb{S}^2$-factor of because the contributions of the non-linear terms to the fundamental modes of the metric components. In order to determine whether inhomogeneous perturbations develop an expanding or collapsing behaviour, we just have to look at the resulting sign of the fundamental mode of the perturbation of the Kretschmann scalar with respect to the SWSH basis. If initially it was positive, the perturbed spacetime would experience a collapsing behaviour, whereas it would undergo an expanding behaviour if it was negative. For the particular case where the fundamental mode is initially zero, we found that all the contributions from the non-linear terms to the fundamental mode will generate homogeneous perturbations of the Kretschmann scalar whose that will eventually trigger the expanding or collapsing behaviour of the $\mathbb{S}^2$-factor. In other words, our analysis lead us to conclude that the Nariai spacetime is unstable and this finding accords with the previous works of [27,28]. Therefore, we believe that our approach to this issue constitutes a significant progress for better understanding of the underlying mechanism. In addition to this, our approach also allowed us to cast lights in the question posed by Beyer in [28] about the formation of multiple cosmological black holes for large perturbations. After a systematic analytical and numerical analysis, we provided strong evidence suggesting that such behaviour is not possible.

On the other hand, we studied the asymptotic behaviour of perturbations for the case when the Kretschmann scalar blows up (the collapsing case) and when it tends to a constant value (the expanding case). For the former case, we found that while the length of the symmetry orbits along the $\mathbb{S}^1$-factor expands, the $\mathbb{S}^2$-factor collapses. This suggests that the four-dimensional manifold with local topology $\mathbb{S}^1 \times \mathbb{S}^2$ collapses in an inhomogeneous way. This behaviour, also observed by Beyer in [28], can be identified as evidence that the perturbed spacetime evolves towards a "cigar singularity", in contrast to that observed for Gowdy symmetric $\mathbb{S}^1 \times \mathbb{S}^2$ spacetimes with zero cosmological constant in chapter 9. However, it may be the case that this type of singularity is due to some kind of geometric effect because of the chosen gauge or initial data family. We leave this question for a future research. Regarding the behaviour of the Kretschmann scalar, we did not observe any particular region where possible spikes could emerge. We observed that the oscillations of the Kretschmann scalar remain smooth during the evolution. However, it is highly likely that this behaviour is observed because the spacetime is still far away from the singularity, hence it is natural not observe any spike. Unfortunately, we are unable to answer this question since a more extensive analysis from both the analytical and numerical points of view is required. Thus, we also leave this other question as an open problem for a future project.

Finally, the expanding case was analysed in the light of the CNH. By means of numerical experiments, we found evidence that suggests that any perturbation of the Nariai spacetime that exhibits an expanding behaviour evolves towards the de Sitter spacetime. This was obtained, firstly, by realizing that the numerical value of the Kretschmann scalar of perturbations reach the corresponding value of the de Sitter spacetime, and, secondly, by studying the evolution of curvature of the $\mathbb{S}^2$-factor which revealed that those perturbations become spherically symmetric. Thus, we found that perturbations of the Nariai spacetime turn

asymptotically homogeneous and locally isometric to the de Sitter spacetime as suggested by the CNH.

11.4 Future projects

Next, we shall summarize some future research projects that were either left open as open questions in this thesis or that emerge as an immediate application of our infrastructure. However, before proceeding, we want to stress once again that we have built an analytical and numerical infrastructure for treating the Cauchy problem for spacetimes with spatial topologies $\mathbb{S}^3$ or $\mathbb{S}^1 \times \mathbb{S}^2$ and symmetry group U(1). Hence, since we have only used this infrastructure to study Gowdy symmetric spacetimes, the first immediate future project that we have in mind is to consider more general scenarios with only U(1) as symmetry group. For this reason, we have generalized the Python module for the general SWSH, i.e., no axial symmetry, that uses a C-library linked with the original C-code given by Huffenberger and Wandelt. As we already mentioned in section 7.6, this module can also be freely downloaded at http://gravity.otago.ac.nz/wiki/index.php/People/Spin_Weight_Functions.zip. All the following are some future projects that could be using either this module or the AST.

Inhomogeneous scalar field perturbations of the Nariai spacetime

The satisfactory results presented in chapter 10 suggest the suitability of the approach proposed in this thesis to construct more general (inhomogeneous) cosmological models with spatial topologies $\mathbb{S}^3$ and $\mathbb{S}^1 \times \mathbb{S}^2$. Therefore, the main goal is to apply this infrastructure to study more realistic cosmological models, thereby studying more systematically the collapsing and expanding behaviour of these. We believe that this research will lead us to a better understanding of the properties of solutions of the EFE, hence it will yield new insights regarding the important questions about the origin, evolution and future of the universe.

In this work, it was possible to construct initial data for cosmological models from inhomogeneous perturbations of the Nariai spacetime. However, the vacuum assumption is too restrictive for considering those models as realistic. In fact, current measurements [121] suggest that the early universe should be better described by a hot plasma, composed mainly of certain scalar field known in the literature as dark energy. Thus, as a future project, we propose to generalize the inhomogeneous perturbations to the case of cosmological models filled with *dark energy*. In particular, motivated by the mentioned work of Bousso and Hawking [42–44], we will explore the behaviour of the Nariai spacetime under perturbations caused by some scalar field. The crucial point here is to realize that the cosmological constant plays the same role as the potential function associated with the scalar field[1]. Moreover, it will be promising to explore the relationship between different kinds of potentials and the CNH as it has been extensively done for homogeneous spacetimes (see, for instance, [31, 165]).

Cosmological models in the Einstein-Vlasov setting

The next natural step in a systematic construction of more realistic (inhomogeneous) cosmological models is to consider the *Einstein-Vlasov system*. The well-known Vlasov equation [185] arises in kinetic theory to provide a statistical description of a set of particles. It differs from other equations of kinetic theory because there is no direct interaction between particles. In particular, no collisions among the particles are included in the model. Instead,

[1] Note that if we assume a constant scalar field with potential function equal to the cosmological constant, then we retrieve the Nariai solution

their interaction is mediated by the geometry of space time, thus the particles will be moving freely along the geodesics ruled by the EFE. This yields the so-called *Einstein-Vlasov system* (see [8, 153]). This system equations have been successfully implemented in the context of both stellar dynamics and cosmological models. However, in many other situations (depending on the symmetries of the spacetimes and particles considered) an analytical treatment of these equations is too complicated or virtually impossible, thus numerical infrastructures dealing with such systems are required. Therefore, as a future project, we are interested in applying our infrastructure to study the behaviour Gowdy symmetric (with spatial topology $\mathbb{S}^1 \times \mathbb{S}^2$ or $\mathbb{S}^3$) cosmological models in the Einstein-Vlasov setting.

Explorations in U(1)-symmetric cosmological spacetimes

As mentioned in section 3.1, thanks to the numerical evidence provided by [23], it has been conjectured that polarized U(1)-symmetric spacetimes are in fact AVTD at the singularity. However, it has to be pointed out that such numerical experiments were conducted for the $\mathbb{T}^3$ spatial topology. Hence, it is reasonable to explore this issue for other topologies, such as $\mathbb{S}^3$ or $\mathbb{S}^1 \times \mathbb{S}^2$, and determine whether similar behaviour near the singularity is found. Similarly as in the polarized case, the oscillatory behaviour of generic U(1)-symmetric spacetimes at the singularity only has been numerically explored for the $\mathbb{T}^3$ case (see for example [91]), which encourages us to implement our infrastructure to these sorts of scenario. However, as already mentioned, this study will be only possible after a technical enhancing of our infrastructure by using a multi-domain PS method. In fact, as was shown in [111], multi-domain methods have proven to make a significant improvement in the study of singularities, a fact that motivates us even more to implement it.

Simulations of binary black hole systems

The binary black hole system is well-known to be the prime source of gravitational waves. At large distances from compact sources, the wave fronts of any radiation field become spherical, a fact that naturally leads to any numerical simulation to spherical coordinate system. In fact, spherical coordinates and spherical harmonics are standard analytic tools in the description of radiation (see for example [1]). Nevertheless, as was shown along this work, the use of spherical coordinates in numerical work yields the vexing problem of coordinate singularities at the poles. FD approximations are mainly affected because they have no natural way of enforcing the correct boundary conditions on their solutions, i.e., the polar singularities have to be regularized by means of standard tricks (see, for instance, [45, 149]). Therefore, we believe that our infrastructure could be implemented in order to improve current approaches like the Spectral Einstein Code (SpEC) [117], widely used (and developed) by the research community in this subject.

The Ricci flow on $\mathbb{S}^3$

We finalize this discussion by mentioning that our implementation can also be used to study the Ricci flow in manifolds with topology $\mathbb{S}^3$. We are strongly convinced that it is a fascinating area of research since the understanding Ricci flow was crucial for proving the so-called *Thurston's geometrization conjecture* [189]. The question that we would like to address here is whether the Ricci Flow can be visualized by using numerical methods. For instance, it can be shown that any metric with topology $\mathbb{S}^2$ converges to the round metric under Ricci flow (normalized). However, the situation is unclear in higher dimensions. In particular, there are many intriguing questions about the behaviour of the Ricci flow for manifolds with topology

$\mathbb{S}^3$. For instance, to determine whether the flow evolves for infinite time without developing singularities or not (see for instance [169]) is one of the major issues. In addition, from the view point of the physics, the Ricci flow has been also used to find inequalities in general relativity regarding the evolution of the surface area and the enclosed Hawking mass [173]. For a compilation of possible applications of the Ricci flow in physics, see [198] and references therein. In short, we certainly believe that our infrastructure could serve to cast some light on some of these questions.

Appendices

Appendix A

Tools of differential geometry

The theory of General Relativity is written in the language of differential geometry. Since the aim of this document is to be as self-contained as possible, in this part we briefly introduce the mathematical concepts in differential geometry that we will use in this thesis. However, we remark that our purpose here is just to briefly review some fundamental definitions, notations and conventions that are necessary for this work, and not to provide a detailed presentation in formal differential geometry. For the reader interested in a more detailed and formal discussion of such matter, we recommend [139, 184, 195] and references therein. We shall base the following presentation on those books.

A.1 Differentiable manifolds

Let us start by defining a topological space. Let X be any set and τ denoting a certain collection of subsets of X. The pair (X, τ) is a topological space if τ satisfies the following requirements:

(i) The union of an arbitrary (maybe infinite) collection of subsets in τ is contained in τ, including both the empty set $\emptyset$ and X.

(ii) The intersection of a finite number of subsets from τ is contained τ.

Each element of τ is called an *open set*. Further, τ is said to be a *topology* on X. Now, let us consider A an open set of X. Then, a collection of open sets B in τ is said to be an *open cover* of A if the union of these sets contains A. A subcollection of B which also cover A is referred to as a *subcover*. Finaly, the set A it is said to be *compact* if every open cover of A has a finite subcover, i.e., a subcover consisting of only a finite number of sets.

first Now, we define a manifold M as a topological space satisfying the following two properties. First, that there is a family of open neighbourhoods U_i together with continuous one-to-one mappings $f_i : U_i \longmapsto \mathbb{R}^n$ (with a continuous inverse). Second, the family of open neighbourhoods covers M, i.e., $\cup_{i=1} U_i = M$. According to the definition of a manifold M there exist mappings $\phi : U \to \mathbb{R}^n$, where U is an open region in M. If p is a point in M , then $\phi(p) = (x^1, ..., x^n)$ will be a vector in $\mathbb{R}^n$. Such mapping is represented by $\{x^\mu\}$, where $\mu = 1, ..., n$, is called a coordinate system. If two regions U and V have a non-empty intersection $U \cap V = \emptyset$, with coordinates x^μ and $\tilde{x}^\mu$, then we can define an invertible coordinate transformation $x^\mu = \tilde{x}^\mu(x^\nu)$ in $U \cap V$. Unless otherwise explicitly stated, we will assume that such coordinate transformations can be differentiated an arbitrary number of times. Such coordinate transformations will be called *smooth*. If a manifold has smooth

coordinate mappings, then the manifold is called a *smooth manifold*. Furthermore, a manifold is called *compact* if it is compact in the topological sense.

A.2 Tensors, notation and conventions

A smooth curve $\gamma(t)$ in M is defined as a map in an interval of the real line into M as $\gamma(t) : t \in \mathbb{R} \to M$. A tangent vector u at certain point $p \in M$ is a linear operator, which assigns to each scalar function $f : M \to \mathbb{R}$ a real number denoted by $u(f)$. It can be viewed as a directional derivative along a curve $\gamma(t)$ through p. Furthermore, the directional derivatives along the coordinate lines at p form a basis of n-dimensional vectors which are the tangent vectors at p. This space is called the *tangent space* T_p. We can construct a vector field $u(p)$ in M by assigning to each point $p \in M$ a tangent vector $u \in T_p$ so that the components of u at p are differentiable functions of the local coordinates x^μ.

A general *basis* (or *frame*) ∂_μ is formed by $\mu = 0, ...n$ linearly independent vectors such that any vector $u \in T_p$ is a linear combination of these basis vectors. Symbolically, the above can be written as $u = u^\mu \partial_\mu$ using the Einstein summation convention. Henceforth, we will write either u or u^a (or any Latin index instead of a) to denote a general vector, i.e., not referred to a basis. On the other hand, we shall use u^μ to denote its components with respect to a certain frame which can be written as ∂_μ or ∂^a_μ. The *commutator* $[u, v]$ between two vector fields u and v is defined by $[u, v](f) = u(v(f)) - v(u(f))$ for any differentiable scalar function f. For a given frame ∂^a_μ the commutator

$$[\partial_\mu, \partial_\nu]^a = C^\sigma{}_{\mu\nu} \partial^a_\sigma, \tag{A.2.1}$$

defines the *structure coefficients* $C^\sigma_{\mu\nu}$. We say that the frame ∂^a_μ is a coordinate when all the $C^\sigma_{\mu\nu}$ vanish. A one-form α, which we also denote by α_a, acts on a vector u^a and gives a real number $\alpha(u) = \alpha_a(u^a)$. In order to write a form in component-form, we define a one-form basis. We will denote the one-form basis by ω^μ_a with $\mu = 0, ...n$, defined by $\omega^\mu_a \partial^a_\nu = \delta^\mu_\nu$, where δ^μ_ν is the Kronecker-symbol. The vectorial space expanded by ω^μ_a is called the dual space T^*_p of the tangent space T_p. Then, any one-form $\sigma \in T^*_p$ is a linear combination of the dual basis as $\sigma_a = \sigma_\mu \omega^\mu_a$. Besides, the action (contraction) of σ on some vector $u^a \in T_p$ can be expressed in terms of their respective components with respect to the basis $\omega^\mu_a, \partial^a_\mu$ as $\sigma_a u^a = \sigma_\mu u^\mu$.

Next, we define a *tensor* $\mathcal{T}$ of type (p, q) that we write as $\mathcal{T}^{a_1 ... a_p}{}_{b_1 ... b_q}$, as the multilinear function that maps p one-forms and q vectors into $\mathbb{R}$ at certain point of M. It can be expressed by components of the basis of elements for vectors and one-forms as follows

$$\mathcal{T}^{a_1 ... a_p}{}_{b_1 ... b_q} := \mathcal{T}^{\mu ... \nu}{}_{\rho ... \delta} \; \partial^{a_1}_\mu \otimes ... \otimes \partial^{a_p}_\nu \otimes \omega^\rho_{b_1} \otimes ... \otimes \omega^\delta_{b_q} \; ,$$

where $\mathcal{T}^{\mu ... \nu}{}_{\rho ... \delta}$ correspond to the components of the tensor with respect to the frame $\{\partial^a_\mu\}$ and coframe $\{\omega^\mu_a\}$ respectively. The symbol $\otimes$ is known in the literature as the *tensor product*. Hereafter, we will say that this tensor is p times *contravariant* and q times *covariant*. Besides, we will refer to the Latin indices as *abstract indices* because they simply represent the number of "slots" that a general tensor has, while the Greek indices will be called as *component indices*. The *symmetric part* of a contravariant tensor of rank p is defined as

$$\mathcal{T}_{(a_1 ... a_p)} := \frac{1}{p!} \sum_\pi \mathcal{T}_{a_{\pi(1)} ... a_{\pi(p)}},$$

and the antisymmetric part by

$$\mathcal{T}_{[a_1 ... a_p]} := \frac{1}{p!} \sum_\pi \delta_\pi \mathcal{T}_{a_{\pi(1)} ... a_{\pi(p)}},$$

where the sum is taken over all the permutations, π, of $1,,...p$ and δ_π is $+1$ for even permutations and -1 for odd. A totally antisymmetric contravariant tensor of type p, is called a p-form. Finalliy, an assigment of a tensor for each point p in the manifold M is called a *tensor field*.

A.3 The metric tensor and the connection coefficients

The scalar product between two vectors u^a and v^b in M, denoted by $\langle u^a\ ,\ v^b\rangle$, is defined in terms of a symmetric 2-covariant tensor, which for every pair of vectors gives a scalar. This tensor is called *the metric tensor* in the manifold M and is defined as

$$\langle v^a, u^b\rangle = \langle u^b, v^a\rangle := g_{ab}\ u^a v^b = g_{\nu\mu}\ u^\nu v^\mu\ .$$

In the framework of the general relativity a vector v^a is said to be *timelike* if $g_{ab}v^a v^b < 0$, *null* if $g_{ab}v^a v^b = 0$ and *spacelike* if $g_{ab}v^a v^b > 0$. Furthermore, the number of timelike and spacelike frame vectors is independent of the choice of the frame. Hence, the number of timelike and spacelike frame vectors is called the *signature* of the metric. For the particular case when the signature of the metric is such that the number of timelike frame vectors is one and the rest are spacelike the metric is called *Lorentzian metric*.

The contravariant components $g^{\mu\nu}$ of the inverse of metric tensor g^{ab} are defined such that $g^{\mu\nu}g_{\nu\rho} = \delta^\nu_\rho$. Further, it is defined the *lowering* or *raising* of indices as $v_a = g_{ab}v^b$ and $v^a = g^{ab}v_b$ respectively, which correspond to a change of one-form for its respective vector and vice-versa.

The covariant derivative $\mathfrak{D}_{v^a}$ in the direction of the vector v^a at a point p, maps an arbitrary tensor into a tensor of the same type. If v^a is unspecified, the covariant derivative $\mathfrak{D}$ generates a tensor of type $(r, s+1)$ from a tensor of type (r, s). If we have a set of basis vectors, $\{\partial^a_\mu\}$ we will denote $\mathfrak{D}_{\partial_\mu}$ by $\mathfrak{D}_\mu$. The *connection coefficients* are defined as the components of the directional derivative of the basis vectors as (see [184])

$$\mathfrak{D}_\nu \partial^a_\mu := \Gamma^\alpha{}_{\nu\mu}\partial^a_\alpha.$$

Hence, the connection coefficients $\Gamma^\alpha_{\mu\nu}$ represent the α-component of the rate of change of ∂^a_μ by a "displacement" in the direction of ∂^a_ν. Then, if we have a vector field $u^a = u^\mu\partial^a_\mu$ and a one-form $v_a = v_\mu\omega^\mu_a$ using the Leibniz rule the equation above yields

$$\begin{aligned}\mathfrak{D}_\nu u^a &= (\partial^a_\nu u^\mu + \Gamma^\mu{}_{\rho\nu}u^\rho)\partial^a_\mu\ ,\\ \mathfrak{D}_\nu v_b &= (\omega^\nu_b v_\mu - \Gamma^\rho{}_{\mu\nu}v_\rho)\omega^\mu_b\ .\end{aligned}$$

Naturallly, this operator can be generalized to tensors of type (q, r); see, for instance, [184]. Using the compatible metric condition $\mathfrak{D}_\nu g_{\mu\alpha} = 0$, the general form of the connection coefficients in any frame can be obtained by

$$\Gamma^\alpha{}_{\beta\gamma} = \frac{1}{2}g^{\alpha\sigma}(\partial_\gamma g_{\sigma\beta} + \partial_\beta g_{\sigma\gamma} - \partial_\sigma g_{\beta\gamma} + C_{\gamma\sigma\beta} + C_{\beta\sigma\gamma} - C_{\sigma\beta\gamma}), \tag{A.3.1}$$

where we have used $C_{\rho\mu\nu} := g^{\rho\alpha}C^\alpha{}_{\mu\nu}$. Further, the connection coefficients are related to the structure coefficients by $C^\alpha{}_{\mu\nu} = 2\Gamma^\alpha{}_{[\nu\mu]}$. Note that just in the special case of the coordinate frame the structure coefficients vanish and the connection coefficients are symmetric in their lower indices.

A.4 The Riemann and Ricci tensors

The *Riemann tensor* is a tensor of type $(1,3)$ that maps a one-form and three vectors into a real number. The components of this tensor respect to some general frame are given by

$$\mathcal{R}^{\mu}{}_{\nu\alpha\beta} = \partial_\alpha \Gamma^{\mu}{}_{\nu\beta} - \partial_\beta \Gamma^{\mu}{}_{\nu\alpha} + \Gamma^{\rho}{}_{\nu\beta}\Gamma^{\mu}{}_{\rho\alpha} - \Gamma^{\rho}{}_{\nu\alpha}\Gamma^{\mu}{}_{\rho\beta} - C^{\rho}{}_{\alpha\beta}\Gamma^{\mu}{}_{\nu\rho} \,. \tag{A.4.1}$$

This tensor satisfies the following symmetry relations

$$\mathcal{R}_{abcd} = -\mathcal{R}_{abdc}, \quad \mathcal{R}_{a[bcd]} = 0, \quad \mathfrak{D}_{[a}\mathcal{R}_{eb]cd} = 0. \tag{A.4.2}$$

where the last two are known in the literature as the *Bianchi identities*. In addition, the action on a one-form α_a can be written as

$$\mathcal{R}_{abc}{}^{d}\alpha_d = \mathfrak{D}_a\mathfrak{D}_b\alpha_c - \mathfrak{D}_b\mathfrak{D}_a\alpha_c \,. \tag{A.4.3}$$

The *Ricci tensor* is defined by $\mathcal{R}_{bd} := \mathcal{R}^{a}{}_{bad}$. Further, the *Ricci scalar* is defined by $\mathcal{R} := \mathcal{R}^{a}{}_{a}$ and represents a measure of the curvature of the manifold M where it is referred. An interesting geometric invariant quantity which will play an important role in this work is the *Kretschmann scalar* defined by

$$K := \mathcal{R}_{abcd}\mathcal{R}^{abcd}. \tag{A.4.4}$$

Finally, we list the conformal transformation formulas for the Ricci tensor and Ricci scalar. Let us assume a 4-dimensional manifold M endowed with a metric g_{ab} and a scalar function Ω such that we can define a new metric in M as $\tilde{g}_{ab} = \Omega^2 g_{ab}$ ($\tilde{g}^{ab} = \Omega^{-2} g^{ab}$). Then, we say that we have defined a *conformal rescaling* between the two metrics. The explicit relation between the two respective covariant derivatives $\tilde{\mathfrak{D}}_a$ and $\mathfrak{D}_a$ is

$$\tilde{\mathfrak{D}}_b\omega_a = \mathfrak{D}_b\omega_a - W^{c}{}_{ab}\omega_c, \tag{A.4.5}$$

where

$$W^{c}{}_{ab} = \frac{1}{\Omega}\left(2\delta^{c}{}_{(a}\mathfrak{D}_{b)}\Omega - g_{ab}g^{cd}\mathfrak{D}_d\Omega\right) \,. \tag{A.4.6}$$

Using this equation in Eq. (A.4.3), the relation between Ricci tensors can be obtained by (see [195])

$$\begin{aligned}\tilde{\mathcal{R}}_{ab} \;=\; & \mathcal{R}_{ab} - (n-2)\mathfrak{D}_a\mathfrak{D}_b\ln\Omega - g_{ab}g^{cd}\mathfrak{D}_c\mathfrak{D}_d\ln\Omega \\ & + (n-2)(\mathfrak{D}_a\ln\Omega)(\mathfrak{D}_b\ln\Omega) - (n-2)g_{ab}g^{cd}(\mathfrak{D}_c\ln\Omega)(\mathfrak{D}_d\ln\Omega) \,.\end{aligned} \tag{A.4.7}$$

Further, from where the relation between Ricci scalars is obtained

$$\tilde{\mathcal{R}} = \frac{1}{\Omega}\left(\mathcal{R} + 2(n-1)\,\mathfrak{D}^a\mathfrak{D}_a\,\ln\Omega - (n-2)(n-1)g^{ac}(\mathfrak{D}_a\ln\Omega)(\mathfrak{D}_c\ln\Omega)\,\right). \tag{A.4.8}$$

A.5 Lie derivative and isometries

Let us consider that M and N are two smooth manifolds and let f be a smooth map such that $f : M \to N$. This map induces the smooth map $f_* : T_pM \to T_{f(p)}N$ for a given $p \in M$, called *push forward*, which is defined by

$$f_*u^a(g) := u^a(g \circ f),$$

for $u^a \in T_pM$ and g a scalar function $g : N \to \mathbb{R}$. In addition, it is also induced the *pull back* $f^* : T^*_{f(p)}N \to T^*_pM$ defined by

$$\langle f^*\alpha_a, u^a\rangle := \langle \alpha, f_* u^a\rangle,$$

for any $\alpha_a \in T^*_f(p)N$. Next, let us consider a vector field $u = u^\mu e^a_\mu$ which induces the infinitesimal parameter transformation ϕ_t defined by $\tilde{x}^\mu = \phi_t(x^\mu) = x^\mu + tu^\mu$ for t being a small parameter. The *Lie derivative* of the covariant tensor $\mathcal{T}$ along the vector u^a is written as[1]

$$\mathcal{L}_u\mathcal{T} = \lim_{t\to 0}\frac{1}{t}(\phi_t^*\mathcal{T} - \mathcal{T}).$$

A useful relation is the Lie derivative for a two-covariant tensor (like the metric tensor) along some vector u^a that components are given by

$$\mathcal{L}_u\mathcal{T}_{\mu\nu} = \mathfrak{D}_\alpha T_{\mu\nu}u^\alpha + T_{\alpha\nu}\mathfrak{D}_\mu u^\alpha + T_{\mu\alpha}\mathfrak{D}_\nu u^\alpha\,. \tag{A.5.1}$$

In the following, we define a relevant concept to this work, the Killing vectors. Let us consider a manifold endowed with a metric g_{ab}, and let ϕ_t be a one-parameter transformation defined as above. Then, ϕ_t is an *isometry* if and only if $\phi_t^* g_{ab} = g_{ab}$. We call the vector field ξ^a that generates the isometry ϕ_t as *Killing vector*. Furthermore, it can be proved that

$$\mathcal{L}_\xi g_{ab} = 0. \tag{A.5.2}$$

In addition, it can be easily proved that $\xi_a = g_{ab}\xi^b$ satisfies the so-called *Killing equation*

$$\mathfrak{D}_{(a}\xi_{b)} = 0. \tag{A.5.3}$$

Clearly, the number of isometries correspond to the number of linearly independent Killing vectors. The maximum number of Killing vectors in a n-dimensional manifold is $(n+1)n/2$. Thus, in the particular case where $n = 4$, there may be up to ten of those vectors. A metric corresponding to a manifold that admits the maximum number of Killing vectors is said to be *maximally symmetric*.

Finally, we introduce the well-known totally antisymmetric *Levi-Civita tensor* associated with the metric g_{ab} of dimension n by

$$\epsilon_{a_1\,\ldots a_n} := \sqrt{|\det(g)|}\,\omega_{a_1}\wedge\ldots\wedge\omega_{a_n} \tag{A.5.4}$$

where $\det(g)$ denotes the determinant of the metric g_{ab} and $\wedge$ represents the antisymmetric tensorial product (or exterior product) given by $\alpha_b \wedge \beta_a := \alpha_{[b}\otimes\beta_{a]}$. Because this tensor is usually used to define integration in manifolds (see [195]), it also receives the name of *volume element* and is denoted by $\mathrm{Vol}_g := \epsilon_{a_1\,\ldots a_n}$.

A.6 Lie groups, Lie algebras and fiber bundles

A *Lie group* G is a differentiable manifold endowed with a group structure (in the usual sense of the algebra) such that the group operations are differentiable. The dimension of a Lie group G is defined to be the dimension of the manifold. Of particular interest in physical applications are the matrix groups. Those are subgroups of the general linear group, denoted by $GL(n,\mathbb{C})$, formed by the set of all non-singular linear transformations in $\mathbb{C}^n$. The elements

[1] In particular, for the spacial case where T^a, $\mathcal{L}_u T^a = [u, T]^a$.

of this group are represented by $n \times n$ non-singular matrices with complex entries. The group operation is the matrix multiplication, and the inverses of each element are given by the inverse matrices. Some important subgroups of $GL(n, \mathbb{C})$ (which are also Lie groups) for this work are the unitary group $\mathrm{U}(n)$, the special group of rotations $\mathrm{SO}(n)$ and the special linear group and the special unitary group $\mathrm{SU}(n)$. They are defined respectively as follows (see [139]);

$$\mathrm{U}(n) := \{A \in GL(n, \mathbb{C}) \mid AA^\dagger = A^\dagger A = I\}, \tag{A.6.1}$$

$$\mathrm{SO}(n) := \{A \in GL(n, \mathbb{R}) \mid \det A = 1 \quad and \quad AA^T = A^T A = I\}, \tag{A.6.2}$$

$$\mathrm{SU}(n) := \{A \in \mathrm{U}(n) \mid \det A = 1\}, \tag{A.6.3}$$

where $\dagger$ represents the Hermitian conjugation. Next, we define the *action* of a Lie group G on a manifold M by the map $\sigma : G \times M \to M; (g, p) \to gp$, which satisfies the following two conditions: $\sigma(e, p) = p$ for e being the identity of G, and $\sigma(g_1, \sigma(g_2, p)) = \sigma(g_1 g_2, p)$. The group action σ is said to be *transitive* if for any $p_1, p_2 \in M$ there exists an element $g \in G$ such that $\sigma(g, p_1) = p_2$. Furthermore, it is said to be *free* if every element different from the identity of G has no fixed points in M, i.e., if there exists an element $p \in M$ such that $\sigma(g, p) = p$, then g must be the unit element e. The action is said to be *effective* if the unit element $e \in G$ is the only element that defines the trivial action on M. In other words, if $\sigma(g, p) = p$ for all $p \in M$ then g must be the unit element e. Additionally, G is called an *isometry group* or *group of motion*, if the pull back σ^* preserves the metric g defined in M at any point p, i.e., $\sigma^* g = g$. Finally, the *orbit* of p under the action σ is the subset of M defined by

$$G_p = \{\sigma(g, p) | g \in G\}. \tag{A.6.4}$$

If the action of G on M is transitive, the orbit of any $p \in M$ is M itself. Now, we define Lie algebra associated with a Lie group. Let a and g elements of the Lie group G. The *right-translation* $R_a : G \to G$ and the *left-translation* $L_a : G \to G$ of g by a are defined by $R_a g := ga$ and $L_a g = ag$ respectively. By definition, R_a and L_a are manifestly diffeomorphism in G. Clearly, these maps induce $L_{a*} : T_g G \to T_{ag} G$ and $R_{a*} : T_g G \to T_{ag} G$. Since these translations lead to equivalent results, we will consider only the left-translation in the following. Let u be a vector field on a Lie group G at the element g. Then, u is said to be a *left-invariant vector field* if for any $a \in G$

$$L_{a*} u(p) = u(ag). \tag{A.6.5}$$

Let us denote the set of left-invariant vector fields on G by $\mathfrak{g}$. Further, T_e will be the tangent space defined at the identity of G. Thus, it can defined the map $H : \mathfrak{g} \to T_e$ by $H(u) = u(e)$ which is an isomorphism. It follows that the set of left-invariant vector fields is a vector space isomorphic to $T_e G$. The Lie bracket is a bilinear map $\mathfrak{g} \times \mathfrak{g} \to \mathfrak{g}$ that satisfies the following properties for all $X, Y, Z \in \mathfrak{g}$,

(i) $[X, X] = 0$,

(ii) $[X, [Y, Z]] + [Y, [Z, X]] + [Z, [X, Y]] = 0$.

The set of left-invariant vector fields endowed with the Lie bracket is called the *Lie algebra* of a Lie group G. In particular, it can be proved that each element ξ^a of the Lie algebra corresponds to the vector fields generated by the effective action of the isometry group (or group of motion) that are, as we already mentioned before, the Killing vector (KVF).

We finalize this section by briefly discussing the idea of fiber bundles. A simple idea of a *fiber bundle* E over a manifold M (called the base manifold) can be obtained by imagining another manifold F, the *fiber*, to be attached to each point of M in such a way that for suitable regions where the coordinates x^ν are given on M and ξ on the fiber, the fiber bundle has coordinates (x^ν, ξ^a), i.e., E is locally $M \times F$. On regions where two coordinate systems in M apply, the corresponding coordinate transformations on E are given by the usual coordinate transformations in M together with the fiber transformations $\tilde{\xi}^b = \tilde{\xi}^b(\xi^a)$ for each $p \in M$. These fiber transformations belong to a group of transformations on F called the *structure group of the bundle*. This group denoted by G is a Lie group. For the particular case when the structure group and the fiber can be identified as $F \cong G$ the bundle is known as a *principal fiber bundle*. The map $\pi : E \to M;\ (p, f) \to p$ is called a *projection* onto the *base manifold* M. A map $\sigma : M \to E$ such that for each point p in M gives a unique point $\sigma(p) \in \pi^{-1}(p)$ is called a *section*. All the maps involved in the definitions must of course be suitably smooth. If F is a vector space, the bundle is called a *vector bundle*. Finally, a *frame bundle* $F(M)$ for a base manifold M sets of all the possible bases of $T_p(M)$ such that, the structure group is the group of non-singular linear transformations $GL(n, \mathbb{R})$.

Appendix A. Tools of differential geometry

Bibliography

[1] M. Alcubierre. *Introduction to 3+1 Numerical Relativity*. Oxford Science Publications, 2008. (Cited on pages 9, 12, 13, 54, 58, 112, and 116.)

[2] M. Alcubierre, G. Allen, B. Brügmann, E. Seidel, and W. M. Suen. Towards an understanding of the stability properties of the 3+1 evolution equations in general relativity. *Physical Review D*, 62(12):124011, 2000. (Cited on page 14.)

[3] D. Alic, W. Kastaun, and L. Rezzolla. Constraint damping of the conformal and covariant formulation of the Z4 system in simulations of binary neutron stars. *Physical Review D*, 88(6):064049, 2013. (Cited on page 17.)

[4] E. Ames, F. Beyer, J. Isenberg, and P. G. LeFloch. Quasilinear hyperbolic fuchsian systems and AVTD behaviour in $\mathbb{T}^2$-symmetric vacuum spacetimes. *Annales Henri Poincaré*, 14(6):1445–1523, 2013. (Cited on page 74.)

[5] E. Ames, F. Beyer, J. Isenberg, and P. G. LeFloch. Quasilinear symmetric hyperbolic fuchsian systems in several space dimensions. In M. Agranovsky, M. Ben-Artzi, G. J. Galloway, L. Karp, V. Maz'ya, S. Reich, D. Shoikhet, G. Weinstein, and L. Zalcman, editors, *Complex Analysis and Dynamical Systems V*. American Mathematical Society, Providence, Rhode Island, 2013. (Cited on page 74.)

[6] L. Andersson. The global existence problem in general relativity. In *The Einstein Equations and the Large Scale behaviour of Gravitational Fields*, pages 71–120. Springer, 2004. (Cited on pages 19 and 20.)

[7] L. Andersson and A. D. Rendall. Quiescent cosmological singularities. *Communications in Mathematical Physics*, 218(3):479–511, 2001. (Cited on page 21.)

[8] H. Andréasson. The Einstein-Vlasov system/kinetic theory. *Living Reviews in Relativity*, 8(2), 2005. (Cited on page 116.)

[9] H. Andréasson and H. Ringström. Proof of the cosmic no-hair conjecture in the $\mathbb{T}^3$-gowdy symmetric Einstein-Vlasov setting. *arXiv:1306.6223*, 2013. (Cited on page 23.)

[10] P. Anninos, D. Bernstein, S. Brandt, J. Libson, J. Masso, E. Seidel, L. Smarr, W. M. Suen, and P. Walker. Dynamics of apparent and event horizons. *Physical Review Letters*, 74(5):630, 1995. (Cited on page 13.)

[11] R. Arnowitt, S. Deser, and C. W. Misner. Dynamical structure and definition of energy in general relativity. *Physical Review*, 116(5):1322, 1959. (Cited on page 13.)

[12] H. Bantilan, F. Pretorius, and S. S. Gubser. Simulation of asymptotically AdS5 spacetimes with a generalized harmonic evolution scheme. *Physical Review D*, 85(8):084038, 2012. (Cited on page 10.)

[13] R. Bartnik and J. Isenberg. The constraint equations. In *The Einstein equations and the large scale behaviour of gravitational fields*, pages 1–38. Springer, 2004. (Cited on pages 53, 54, and 111.)

[14] T. W. Baumgarte and S. L. Shapiro. Numerical integration of Einstein's field equations. *Physical Review D*, 59(2):024007, 1998. (Cited on page 13.)

[15] T. W. Baumgarte and S. L. Shapiro. Numerical relativity and compact binaries. *Physics Reports*, 376(2):41–131, 2003. (Cited on page 9.)

[16] T. W. Baumgarte and S. L. Shapiro. *Numerical Relativity: Solving Einstein's Equations on the Computer*. Cambridge University Press, 2010. (Cited on pages 9 and 17.)

[17] V. A. Belinskii, I. M. Khalatnikov, and E. M. Lifshitz. Oscillatory approach to a singular point in the relativistic cosmology. *Advances in Physics*, 19(80):525–573, 1970. (Cited on page 22.)

[18] V. A. Belinskii, I. M. Khalatnikov, and E. M. Lifshitz. A general solution of the Einstein equations with a time singularity. *Advances in Physics*, 31(6):639–667, 1982. (Cited on page 22.)

[19] B. K. Berger and D. Garfinkle. Phenomenology of the Gowdy universe on $\mathbb{T}^3 \times \mathbb{R}$. *Journal of Mathematical Physics*, 57(8):4767–4777, 1998. (Cited on page 25.)

[20] B. K. Berger, D. Garfinkle, J. Isenberg, V. Moncrief, and M. Weaver. The singularity in generic gravitational collapse is spacelike, local, and oscillatory. *Modern Physics Letters A*, pages 1565–1574, 1998. (Cited on page 22.)

[21] B. K. Berger, D. Garfinkle, and V. Moncrief. Comment on"the Gowdy $\mathbb{T}^3$ cosmologies revisited". *arXiv preprint gr-qc/9708050*, 1997. (Cited on page 25.)

[22] B. K. Berger and V. Moncrief. Numerical investigation of cosmological singularities. *Journal of Mathematical Physics*, 48:4676–4687, 1993. (Cited on page 25.)

[23] B. K. Berger and V. Moncrief. Numerical evidence that the singularity in polarized U(1) symmetric cosmologies on $\mathbb{T}^3 \times \mathbb{R}$ is velocity dominated. *Journal of Mathematical Physics*, 57(12):7235–7240, 1998. (Cited on page 116.)

[24] F. Beyer. *Asymptotics and singularities in cosmological models with positive cosmological constant*. PhD thesis, University of Potsdam, Potsdam, 2007. (Cited on pages 19, 26, 35, and 36.)

[25] F. Beyer. Investigations of solutions of einstein's field equations close to λ-Taub–NUT. *Classical and Quantum Gravity*, 25(23):235005, 2008. (Cited on pages 88 and 113.)

[26] F. Beyer. A spectral solver for evolution problems with spatial $\mathbb{S}^3$-topology. *Journal of Computational Physics*, 228(17):6496–6513, 2009. (Cited on pages 2 and 77.)

[27] F. Beyer. Non-genericity of the Nariai solutions: I. Asymptotics and spatially homogeneous perturbations. *Classical and Quantum Gravity*, 26(23):235015, 2009. (Cited on pages iii, 5, 6, 22, 89, 90, 99, 100, 113, and 114.)

[28] F. Beyer. Non-genericity of the Nariai solutions: II. Investigations within the Gowdy class. *Classical and Quantum Gravity*, 26:235016, 2009. (Cited on pages iii, 5, 6, 89, 90, 100, 104, 105, 113, and 114.)

[29] F. Beyer, B. Daszuta, and J. Frauendiener. A spectral method for half-integer spin fields based on spin-weighted spherical harmonics. *Classical and Quantum Gravity*, 32(17):175013, 2015. (Cited on pages 2, 4, 39, and 57.)

[30] F. Beyer, B. Daszuta, J. Frauendiener, and B. Whale. Numerical evolutions of fields on the 2-sphere using a spectral method based on spin-weighted spherical harmonics. *Classical and Quantum Gravity*, 31(7):075019, 2014. (Cited on pages iii, 2, 3, 4, 35, 46, 47, and 57.)

[31] F. Beyer and L. Escobar. Graceful exit from inflation for minimally coupled Bianchi A scalar field models. *Classical and Quantum Gravity*, 30(19):195020, 2013. (Cited on pages 77 and 115.)

[32] F. Beyer and J. Hennig. Smooth Gowdy-symmetric generalized Taub–NUT solutions. *Classical and Quantum Gravity*, 29(24):245017, 2012. (Cited on pages 2, 4, 26, 73, and 74.)

[33] F. Beyer and J. Hennig. An exact smooth Gowdy-symmetric generalized Taub–NUT solution. *Classical and Quantum Gravity*, 31(9):095010, 2014. (Cited on pages 2, 26, 74, and 75.)

[34] F. Beyer and P. G. LeFloch. Second-order hyperbolic Fuchsian systems and applications. *Classical and Quantum Gravity*, 27(24):245012, 2010. (Cited on page 74.)

[35] P. Bizoń, S. Pletka, and W. Simon. Initial data for rotating cosmologies. *Classical and Quantum Gravity*, 32(17):175015, 2015. (Cited on page 111.)

[36] C. Bona, T. Ledvinka, C. Palenzuela, and M. Žáček. General-covariant evolution formalism for numerical relativity. *Physical Review D*, 67(10):104005, 2003. (Cited on page 16.)

[37] C. Bona, T. Ledvinka, C. Palenzuela, and M. Žáček. Symmetry-breaking mechanism for the Z4 general-covariant evolution system. *Physical Review D*, 69(6):064036, 2004. (Cited on page 16.)

[38] C. Bona and J. Massó. Hyperbolic evolution system for numerical relativity. *Physical Review Letters*, 68(8):1097, 1992. (Cited on page 14.)

[39] C. Bona, J. Massó, E. Seidel, and J. Stela. New formalism for numerical relativity. *Physical Review Letters*, 75:600–603, Jul 1995. (Cited on pages 14 and 17.)

[40] C. Bona, J. Massó, E. Seidel, and J. Stela. First order hyperbolic formalism for numerical relativity. *Physical Review D*, 56(6):3405, 1997. (Cited on page 14.)

[41] R. Bousso. Adventures in de Sitter space. In *The Future of Theoretical Physics and Cosmology*. Cambridge University Press, 2003. (Cited on pages 90 and 104.)

[42] R. Bousso and S. W. Hawking. Probability for primordial black holes. *Physical Review D*, 52(10):5659, 1995. (Cited on pages 5, 90, and 115.)

[43] R. Bousso and S. W. Hawking. Pair creation of black holes during inflation. *Physical Review D*, 54(10):6312, 1996. (Cited on pages 5, 90, and 115.)

[44] R. Bousso and S. W. Hawking. (Anti-) evaporation of Schwarzschild–de Sitter black holes. *Physical Review D*, 57(4):2436, 1998. (Cited on pages 5, 90, and 115.)

[45] M. Boyle, L. Lindblom, H. P. Pfeiffer, M. A. Scheel, and L. E. Kidder. Testing the accuracy and stability of spectral methods in numerical relativity. *Physical Review D*, 75(2):024006, 2007. (Cited on pages 113 and 116.)

[46] W. L. Briggs et al. *The DFT: An Owners Manual for the Discrete Fourier Transform*. Siam, 1995. (Cited on page 60.)

[47] O. Brodbeck, S. Frittelli, P. Hübner, and O. A. Reula. Einstein's equations with asymptotically stable constraint propagation. *Journal of Mathematical Physics*, 40(2):909, 1999. (Cited on pages 16 and 77.)

[48] T. Buchert. On average properties of inhomogeneous fluids in general relativity: Perfect fluid cosmologies. *General Relativity and Gravitation*, 33(8):1381–1405, 2001. (Cited on page 1.)

[49] L. T. Buchman, H. P. Pfeiffer, M. A. Scheel, and B. Szilágyi. Simulations of unequal-mass black hole binaries with spectral methods. *Physical Review D*, 86(8):084033, 2012. (Cited on page 112.)

[50] A. B. Burd and J. D. Barrow. Inflationary models with exponential potentials. *Nuclear Physics B*, 308(4):929–945, 1988. (Cited on page 23.)

[51] R. L. Burden and J. D. Faires. Numerical Analysis. *Brooks/Cole, USA*, 2001. (Cited on page 58.)

[52] G. Calabrese. A remedy for constraint growth in numerical relativity: the Maxwell case. *Classical and Quantum Gravity*, 21(17):4025, 2004. (Cited on page 15.)

[53] J. Campbell, P. Gries, J. Montojo, and G. Wilson. *Practical Programming: an Introduction to Computer Science Using Python*. Pragmatic Bookshelf, 2009. (Cited on page 67.)

[54] C. Canuto, M. Y. Hussaini, A. Quarteroni, and T. A. Zang. *Spectral Methods in Fluid Dynamics*. 1988. (Cited on page 57.)

[55] B. Carr. Primordial Black Holes: Do They Exist and Are They Useful? In H. Suzuki, K. Sato, Y. Suto, and J. Yokoyama, editors, *Inflating Horizon of Particle Astrophysics and Cosmology*, 2005. (Cited on page 1.)

[56] S. Chakraborty and B. Paul. Inflation in Bianchi models and the cosmic no-hair theorem. *Journal of Mathematical Physics*, 64(12), 2001. (Cited on page 23.)

[57] M. W. Choptuik. Universality and scaling in gravitational collapse of a massless scalar field. *Physical Review Letters*, 70(1):9, 1993. (Cited on page 13.)

[58] M. W. Choptuik, E. W. Hirschmann, S. L. Liebling, and F. Pretorius. An axisymmetric gravitational collapse code. *Classical and Quantum Gravity*, 20(9):1857, 2003. (Cited on pages 2 and 27.)

[59] Y. Choquet-Bruhat. Théorème global d'unicité pour les solutions des équations d'Einstein. *Bulletin de la Société Mathématique de France*, 96:181–192, 1968. (Cited on page 12.)

[60] Y. Choquet-Bruhat. *General Relativity and the Einstein Equations*. Oxford mathematical monographs. Oxford University Press, Oxford, New York, 2008. (Cited on page 48.)

[61] Y. Choquet-Bruhat and R. P. Geroch. Global aspects of the Cauchy problem in general relativity. *Communications in Mathematical Physics*, 14(4):329–335, 1969. (Cited on page 12.)

[62] D. Christodoulou. The instability of naked singularities in the gravitational collapse of a scalar field. *Annals of Mathematics-Second Series*, 149(1):183–218, 1999. (Cited on page 21.)

[63] P. T. Chruściel. On space-times with U(1)× U(1) symmetric compact Cauchy surfaces. *Annals of Physics*, 202:100–150, 1990. (Cited on pages 20, 24, and 73.)

[64] P. T. Chruściel. *On Uniqueness in the Large of Solutions of Einsteins Equations (Strong Cosmic Censorship)*, volume 27 of *Proceedings of the Centre for Mathematics and its Applications*. The Australian National University, 1991. (Cited on page 21.)

[65] P. T. Chruściel. Conformal boundary extensions of Lorentzian manifolds. *Journal of Differential Geometry*, 84(1):19–44, 2010. (Cited on page 21.)

[66] P. T. Chruściel, J. Isenberg, and V. Moncrief. Strong cosmic censorship in polarised Gowdy spacetimes. *Classical and Quantum Gravity*, 7(10):1671–1680, 1990. (Cited on pages 21 and 25.)

[67] C. Collins. Global structure of the "Kantowski–Sachs" cosmological models. *Journal of Mathematical Physics*, 18(11):2116–2124, 1977. (Cited on page 20.)

[68] J. W. Cooley and J. W. Tukey. An algorithm for the machine calculation of complex fourier series. *Mathematics of Computation*, 19(90):297–301, 1965. (Cited on page 60.)

[69] J. Curtis and D. Garfinkle. Numerical simulations of stiff fluid gravitational singularities. *Physical Review D*, 72(6):064003, 2005. (Cited on pages 21 and 22.)

[70] T. Damour, M. Henneaux, A. D. Rendall, and M. Weaver. Kasner-like behaviour for subcritical Einstein-matter systems. *Annales Henri Poincaré*, 3(6):1049–1111, 2002. (Cited on page 22.)

[71] G. F. T. Del Castillo. *3-D Spinors, Spin-Weighted Functions and their Applications*. Springer Science, Boston, MA, 2012. (Cited on pages 39, 46, and 47.)

[72] M. D. Duez, F. Foucart, L. E. Kidder, H. P. Pfeiffer, M. A. Scheel, and S. A. Teukolsky. Evolving black hole-neutron star binaries in general relativity using pseudospectral and finite difference methods. *Physical Review D*, 78(10):104015, 2008. (Cited on page 113.)

[73] D. R. Durran. *Numerical Methods for Fluid Dynamics*, volume 32 of *Texts in Applied Mathematics*. Springer, New York, NY, 2010. (Cited on pages 57, 59, 60, and 76.)

[74] D. M. Eardley, E. Liang, and R. K. Sachs. Velocity-Dominated Singularities in Irrotational Dust Cosmologies. *Journal of Mathematical Physics*, 13(1):99, 1972. (Cited on page 22.)

[75] K. Eppley. Evolution of time-symmetric gravitational waves: Initial data and apparent horizons. *Physical Review D*, 16(6):1609, 1977. (Cited on page 9.)

[76] J. Erickson, D. Wesley, P. Steinhardt, and N. Turok. Kasner and mixmaster behaviour in universes with equation of state w$\geq$ 1. *Journal of Mathematical Physics*, 69(6), 2004. (Cited on page 22.)

[77] M. Fennen and D. Giulini. An exact static two-mass solution using Nariai spacetime. *arXiv:1408.2713*, 2014. (Cited on page 90.)

[78] B. Fornberg. *A Practical Guide to Pseudospectral Methods*. Cambridge University Press, 1998. (Cited on pages 57, 59, 63, and 95.)

[79] Y. Fourès-Bruhat. Théorème d'existence pour certains systèmes d'équations aux dérivées partielles non linéaires. *Acta Mathematica*, 88(1):141–225, 1952. (Cited on pages 3, 9, and 14.)

[80] T. Frankel. *The Geometry of Physics: An Introduction*. Cambridge University Press, 2011. (Cited on page 35.)

[81] J. Frauendiener. Numerical treatment of the hyperboloidal initial value problem for the vacuum Einstein equations. II. The evolution equations. *Journal of Mathematical Physics*, 58(6):064003, 1998. (Cited on page 81.)

[82] J. Frauendiener. Calculating initial data for the conformal Einstein equations by pseudo-spectral methods. *Journal of Computational and Applied Mathematics*, 109(1):475–491, 1999. (Cited on pages 55, 94, 95, and 112.)

[83] J. Frauendiener. Conformal infinity. *Living Reviews in Relativity*, 7, 2004. http://www.livingreviews.org/lrr-2004-1. (Cited on page 14.)

[84] J. Frauendiener. *Generate Solutions of Einstein's Equations*. Unpublished Notes, University of Otago. (Cited on page 27.)

[85] H. Friedrich. On the hyperbolicity of Einstein's and other gauge field equations. *Communications in Mathematical Physics*, 100(4):525–543, 1985. (Cited on pages 14 and 15.)

[86] H. Friedrich. On the existence of n-geodesically complete or future complete solutions of Einstein's field equations with smooth asymptotic structure. *Communications in Mathematical Physics*, 107(4):587–609, 1986. (Cited on pages 20 and 23.)

[87] H. Friedrich. On the global existence and the asymptotic behaviour of solutions to the Einstein-Maxwell-Yang-Mills equations. *Journal of Differential Geometry*, 34:275–345, 1991. (Cited on pages 2, 3, 9, and 14.)

[88] H. Friedrich. Is general relativity "essentially" understood? *Annals of Physics*, 15(1-2):84–108, 2006. (Cited on page 14.)

[89] S. Frittelli and O. A. Reula. First-order symmetric hyperbolic Einstein equations with arbitrary fixed gauge. *Physical Review Letters*, 76(25):4667, 1996. (Cited on page 14.)

[90] D. Garfinkle. Numerical simulations of Gowdy spacetimes on $\mathbb{S}^2 \times \mathbb{S}^1 \times \mathbb{R}$. *Journal of Mathematical Physics*, 60(10):104010, 1999. (Cited on pages iii, 2, 4, 26, 83, 84, 85, and 113.)

[91] D. Garfinkle. Numerical simulations of generic singularities. *Physical Review Letters*, 93(16), 2004. (Cited on pages 21, 22, and 116.)

[92] R. P. Geroch. A method for generating solutions of Einstein's equations. *Journal of Mathematical Physics*, 12(6):918, 1971. (Cited on pages 2, 27, 34, and 46.)

[93] R. P. Geroch. A Method for Generating New Solutions of Einstein's Equation. II. *Journal of Mathematical Physics*, 13(3):394, 1972. (Cited on page 23.)

[94] G. W. Gibbons and S. W. Hawking. Cosmological event horizons, thermodynamics, and particle creation. *Journal of Mathematical Physics*, 15(10):2738–2751, 1977. (Cited on page 5.)

[95] P. Ginsparg and M. J. Perry. Semiclassical perdurance of de Sitter space. *Nuclear Physics B*, 222(2):245–268, 1983. (Cited on pages 5 and 90.)

[96] J. Goldberg, A. Macfarlane, E. T. Newman, F. Rohrlich, and E. Sudarshan. Spin-s spherical harmonics and ð. *Journal of Mathematical Physics*, 8(11):2155–2161, 1967. (Cited on page 40.)

[97] D. Gottlieb and S. A. Orszag. *Numerical Analysis of Spectral Methods: Theory and Applications*. Society for Industrial and Applied Mathematics, 1983. (Cited on page 60.)

[98] E. Gourgoulhon. *3+1 Formalism in General Relativity: Bases of Numerical Relativity*, volume 846. Springer Science & Business Media, 2012. (Cited on page 10.)

[99] R. H. Gowdy. Vacuum spacetimes with two-parameter spacelike isometry groups and compact invariant hypersurfaces: Topologies and boundary conditions. *Annals of Physics*, 83(1):203–241, 1974. (Cited on pages 19, 20, and 23.)

[100] S. R. Green and R. M. Wald. New framework for analyzing the effects of small scale inhomogeneities in cosmology. *Journal of Mathematical Physics*, 83(8):084020, 2011. (Cited on page 1.)

[101] J. B. Griffiths and J. Podolskỳ. *Exact Space-Times in Einstein's General Relativity*. Cambridge University Press, 2009. (Cited on pages 2 and 90.)

[102] Ø. Grøn and S. Hervik. *Einstein's General Theory of Telativity: With Modern Applications in Cosmology*. Springer Science & Business Media, 2007. (Cited on page 20.)

[103] C. Gundlach, J. Martín-García, G. Calabrese, and I. Hinder. Constraint damping in the Z4 formulation and harmonic gauge. *Classical and Quantum Gravity*, 22:3767–3774, 2005. (Cited on pages 16 and 77.)

[104] S. G. Hahn and R. W. Lindquist. The two-body problem in geometrodynamics. *Annals of Physics*, 29(2):304–331, 1964. (Cited on page 9.)

[105] S. W. Hawking and G. Ellis. *The Large Scale Structure of Space-Time*. Cambridge Monographs, 1973. (Cited on pages 21 and 89.)

[106] S. W. Hawking and I. L. Moss. Supercooled phase transitions in the very early universe. *Physics Letters B*, 110(1):35–38, 1982. (Cited on pages 5 and 22.)

[107] J. M. Heinzle, C. Uggla, and N. Röhr. The cosmological billiard attractor. *Advances in Theoretical and Mathematical Physics*, 13:293–407, 2009. (Cited on page 22.)

[108] J. Hennig. Fully pseudospectral time evolution and its application to $1+1$ dimensional physical problems. *Journal of Computational Physics*, 235:322–333, 2013. (Cited on page 77.)

[109] J. Hennig and M. Ansorg. The inner Cauchy horizon of axisymmetric and stationary black holes with surrounding matter in Einstein–Maxwell theory: study in terms of soliton methods. *Annales Henri Poincaré*, 10(6):1075–1095, 2009. (Cited on pages 26 and 74.)

[110] J. Hennig and M. Ansorg. Regularity of Cauchy horizons in $\mathbb{S}^1 \times \mathbb{S}^2$ Gowdy spacetimes. *Classical and Quantum Gravity*, 27:065010, 2010. (Cited on page 26.)

[111] S. D. Hern. Numerical relativity and inhomogeneous cosmologies. *arXiv preprint gr-qc/0004036*, 2000. (Cited on page 116.)

[112] K. M. Huffenberger and B. D. Wandelt. Fast and exact spin-s spherical harmonic transforms. *The Astrophysical Journal Supplement Series*, 189(2):255–260, 2010. (Cited on pages iii, 3, 57, 61, and 62.)

[113] N. Ibohal. Nonstationary de Sitter cosmological models. *International Journal of Modern Physics D*, 18(05):853–863, 2009. (Cited on page 107.)

[114] J. Isenberg and V. Moncrief. Asymptotic behaviour of the gravitational field and the nature of singularities in Gowdy spacetimes. *Annals of Physics*, 199(1):84–122, 1990. (Cited on pages 22, 25, and 26.)

[115] R. Kantowski and R. K. Sachs. Some spatially homogeneous anisotropic relativistic cosmological models. *Journal of Mathematical Physics*, 7(3):443, 1966. (Cited on page 20.)

[116] S. Kichenassamy and A. D. Rendall. Analytic description of singularities in Gowdy spacetimes. *Classical and Quantum Gravity*, 15(5):1339–1355, 1999. (Cited on pages 5, 22, and 26.)

[117] L. Kidder, H. Pfeiffer, and M. Scheel. Spectral Einstein Code. `https://www.black-holes.org/SpEC.html`. (Cited on page 116.)

[118] L. E. Kidder, M. A. Scheel, and S. A. Teukolsky. Extending the lifetime of 3d black hole computations with a new hyperbolic system of evolution equations. *Journal of Mathematical Physics*, 64:064017, Aug 2001. (Cited on page 14.)

[119] Y. Kitada and K. Maeda. Cosmic no-hair theorem in power-law inflation. *Journal of Mathematical Physics*, 45(4):1416–1419, 1992. (Cited on page 23.)

[120] Y. Kitada and K. Maeda. Cosmic no-hair theorem in homogeneous spacetimes. I. Bianchi models. *Classical and Quantum Gravity*, 10(4):703–734, 1993. (Cited on pages 5 and 23.)

[121] E. Komatsu, J. Dunkley, M. R. Nolta, C. L. Bennett, B. Gold, G. Hinshaw, N. Jarosik, D. Larson, M. Limon, L. Page, D. N. Spergel, M. Halpern, R. S. Hill, A. Kogut, S. S. Meyer, G. S. Tucker, J. L. Weiland, E. Wollack, and E. L. Wright. Five-rear Wilkinson microwave anisotropy probeobservations: Cosmological interpretation. *The Astrophysical Journal Supplement Series*, 180(2):330–376, 2009. (Cited on pages 1, 19, and 115.)

[122] F. Kottler. The physical basis of Einstein's theory of gravitation. *Annals of Physics(Leipzig)*, 56:401, 1918. (Cited on pages 5 and 89.)

[123] D. Kramer, H. Stephani, M. MacCallum, and E. Herlt. *Exact Solutions of the Einstein Equations*. VEB Deutscher Verlag der Wissenschaften, Berlin, GDR, 1980. (Cited on page 108.)

[124] L. Lehner. Numerical relativity: A review. *Classical and Quantum Gravity*, 18(17):R25, 2001. (Cited on page 9.)

[125] L. Lehner and F. Pretorius. Numerical relativity and astrophysics. *arXiv:1405.4840*, 2014. (Cited on page 9.)

[126] E. M. Lifshitz and I. M. Khalatnikov. Investigations in relativistic cosmology. *Advances in Physics*, 12(46):185–249, 1963. (Cited on page 22.)

[127] L. Lindblom, K. D. Matthews, O. Rinne, and M. A. Scheel. Gauge drivers for the generalized harmonic Einstein equations. *Physical Review D*, 77(8):084001, 2008. (Cited on pages 10, 16, and 92.)

[128] L. Lindblom and B. Szilágyi. Improved gauge driver for the generalized harmonic Einstein system. *Physical Review D*, 80(8):084019, 2009. (Cited on pages 16 and 92.)

[129] L. Lindblom and B. Szilagyi. Improved gauge driver for the generalized harmonic Einstein system. *Journal of Mathematical Physics*, 80(8):084019, 2009. (Cited on page 80.)

[130] M. MacCallum. The mathematics of anisotropic spatially-homogeneous cosmologies. In *Physics of the Expanding Universe*, pages 1–59. Springer, 1979. (Cited on page 19.)

[131] K.-i. Maeda, M. Sasaki, T. Nakamura, and S. Miyama. A new formalism of the Einstein equations for relativistic rotating systems. *Progress of Theoretical Physics*, 63(2):719–721, 1980. (Cited on pages 2 and 27.)

[132] J. D. McEwen. Fast, exact (but unstable) spin spherical harmonic transforms. *The all results journals*, 1(1):4–18, 2011. (Cited on page 39.)

[133] J. D. McEwen and Y. Wiaux. A novel sampling theorem on the sphere. *IEEE Transactions on Signal Processing*, 59(12):5876–5887, 2011. (Cited on pages 35, 39, and 41.)

[134] V. Moncrief. Global properties of Gowdy spacetimes with $\mathbb{T}^3 \times \mathbb{R}$ topology. *Annals of Physics*, 132(1):87–107, 1981. (Cited on pages 21 and 24.)

[135] V. Moncrief. The space of (generalized) Taub-NUT spacetimes. *Journal of Geometry and Physics*, 1(1):107–130, 1984. (Cited on pages 4, 21, and 73.)

[136] V. Moncrief. Reduction of Einstein's equations for vacuum space-times with spacelike U(1) isometry groups. *Annals of Physics*, 167(1):118–142, 1986. (Cited on page 2.)

[137] V. Mukhanov. *Physical foundations of cosmology*. Cambridge University Press, 2005. (Cited on pages 1 and 90.)

[138] G. Nagy, O. E. Ortiz, and O. A. Reula. Strongly hyperbolic second order Einstein's evolution equations. *Physical Review D*, 70(4):044012, 2004. (Cited on page 14.)

[139] M. Nakahara. *Geometry, Topology and Physics*. CRC Press, 2003. (Cited on pages 35, 36, 121, and 126.)

[140] T. Nakamura. General relativistic collapse of axially symmetric stars leading to the formation of rotating black holes. *Progress of Theoretical Physics*, 65(6):1876–1890, 1981. (Cited on pages 2 and 27.)

[141] T. Nakamura, K. Oohara, and Y. Kojima. General relativistic collapse to black holes and gravitational waves from black holes. *Progress of Theoretical Physics Supplement*, 90:1–218, 1987. (Cited on page 13.)

[142] H. Nariai. On a new cosmological solution of Einstein's field equations of gravitation. *The Science Reports of the Tohoku University Series*, 35(1):46–57, 1951. (Cited on pages 5 and 90.)

[143] E. T. Newman and R. Penrose. Note on the bondi-metzner-sachs group. *Journal of Mathematical Physics*, 7(5):863–870, 1966. (Cited on page 40.)

[144] E. T. Newman, L. Tamburino, and T. Unti. Empty-Space Generalization of the Schwarzschild Metric. *Journal of Mathematical Physics*, 4:915, 1963. (Cited on pages 10 and 73.)

[145] S. A. Orszag. Spectral methods for problems in complex geometries. *Journal of Computational Physics*, 37(1):70–92, 1980. (Cited on page 95.)

[146] P. Parsons and J. D. Barrow. Generalized scalar field potentials and inflation. *Journal of Mathematical Physics*, 51(12):6757–6763, 1995. (Cited on page 23.)

[147] R. Penrose. Gravitational Collapse: The Role of General Relativity. *La Rivista del Nuovo Cimento*, 1:252–276, 1969. (Cited on page 21.)

[148] R. Penrose and W. Rindler. *Two-Spinor Calculus and Relativistic Fields*, volume 1 of *Spinors and Space-Time*. Cambridge University Press, 1984. (Cited on pages 2 and 3.)

[149] H. P. Pfeiffer, L. E. Kidder, M. A. Scheel, and S. A. Teukolsky. A multidomain spectral method for solving elliptic equations. *Computer Physics Communications*, 152(3):253–273, 2003. (Cited on page 116.)

[150] F. Pretorius. Evolution of binary black-hole spacetimes. *Physical Review Letters*, 95:121101, 2005. (Cited on pages 3, 14, 16, 77, and 92.)

[151] F. Pretorius. Numerical relativity using a generalized harmonic decomposition. *Classical and Quantum Gravity*, 22(2):425, 2005. (Cited on pages 10, 16, and 92.)

[152] F. Pretorius. Simulation of binary black hole spacetimes with a harmonic evolution scheme. *Classical and Quantum Gravity*, 23(16):S529, 2006. (Cited on pages 10 and 15.)

[153] A. D. Rendall. An introduction to the Einstein-Vlasov system. *arXiv:gr-qc/9604001*, 1996. (Cited on page 116.)

[154] A. D. Rendall. Accelerated cosmological expansion due to a scalar field whose potential has a positive lower bound. *Classical and Quantum Gravity*, 21(9):2445–2454, 2004. (Cited on page 23.)

[155] A. D. Rendall. *Partial Differential Equations in General Relativity*. Oxford Graduate Texts in Mathematics. Oxford University Press, 2008. (Cited on pages 19 and 22.)

[156] A. D. Rendall and M. Weaver. Manufacture of Gowdy spacetimes with spikes. *Classical and Quantum Gravity*, 18(15):2959–2975, 2001. (Cited on pages 25 and 83.)

[157] O. A. Reula. Hyperbolic methods for Einstein's equations. *Living Reviews in Relativity*, 1:37, 1998. (Cited on page 12.)

[158] H. Ringström. On a wave map equation arising in general relativity. *Communications on Pure and Applied Mathematics*, 57(5):657–703, 2004. (Cited on page 25.)

[159] H. Ringström. Existence of an asymptotic velocity and implications for the asymptotic behaviour in the direction of the singularity in $\mathbb{T}^3$-Gowdy. *Communications on Pure and Applied Mathematics*, 59(7):977–1041, 2006. (Cited on page 25.)

[160] H. Ringström. Future stability of the Einstein-non-linear scalar field system. *Inventiones Mathematicae*, 173(1):123–208, 2008. (Cited on pages 5 and 20.)

[161] H. Ringström. Strong cosmic censorship in $\mathbb{T}^3$-Gowdy spacetimes. *Annals of Mathematics*, 170(3):1181–1240, 2009. (Cited on page 25.)

[162] H. Ringström. *The Cauchy Problem in General Relativity*. ESI Lectures in Mathematics and Physics. European Mathematical Society, Zürich, Switzerland, 2009. (Cited on pages 15, 21, 48, 52, and 73.)

[163] H. Ringström. Cosmic censorship for Gowdy spacetimes. *Living Reviews in Relativity*, 13(2), 2010. (Cited on pages 19 and 24.)

[164] H. Ringström. *On the Topology and Future Stability of the Universe*. Oxford Mathematical Monographs. Oxford University Press, 2013. (Cited on page 20.)

[165] H. Ringström. Proof of the cosmic no-hair conjecture in the T^3-Gowdy symmetric Einstein-Vlasov setting. *arXiv.org*, 2013. (Cited on page 115.)

[166] O. Rinne. *Axisymmetric numerical relativity*. PhD thesis, Trinity Collegue, Cambridge, 2005. (Cited on pages 27 and 31.)

[167] O. Rinne. An axisymmetric evolution code for the Einstein equations on hyperboloidal slices. *Classical and Quantum Gravity*, 27(3):035014, 2010. (Cited on page 2.)

[168] O. Rinne and J. M. Stewart. A strongly hyperbolic and regular reduction of Einstein's equations for axisymmetric spacetimes. *Classical and Quantum Gravity*, 22(6):1143, 2005. (Cited on pages 2 and 31.)

[169] J. H. Rubinstein and R. Sinclair. Visualizing Ricci flow of manifolds of revolution. *Experimental Mathematics*, 14(3):285–298, 2005. (Cited on page 117.)

[170] M. Ruiz, D. Hilditch, and S. Bernuzzi. Constraint preserving boundary conditions for the Z4c formulation of general relativity. *Physical Review D*, 83(2):024025, 2011. (Cited on page 17.)

[171] M. Ruiz, O. Rinne, and O. Sarbach. Outer boundary conditions for Einstein's field equations in harmonic coordinates. *Classical and Quantum Gravity*, 24(24):6349, 2007. (Cited on page 48.)

[172] J. Sakurai and J. Napolitano. *Modern Quantum Mechanics*. Addison-Wesley, 2011. (Cited on pages 35, 39, and 40.)

[173] J. Samuel and S. R. Chowdhury. Energy, entropy and the Ricci flow. *Classical and Quantum Gravity*, 25(3):035012, 2008. (Cited on page 117.)

[174] O. Sarbach, G. Calabrese, J. Pullin, and M. Tiglio. Hyperbolicity of the Baumgarte-Shapiro-Shibata-Nakamura system of Einstein evolution equations. *Physical Review D*, 66(6):064002, 2002. (Cited on page 14.)

[175] W. E. Schiesser. *The Numerical Method of Lines*. Academic Press, 1991. (Cited on page 57.)

[176] U. Seljak, A. Slosar, and P. McDonald. Cosmological parameters from combining the lyman-α forest with CMB, galaxy clustering and SN constraints. *Journal of Cosmology and Astroparticle Physics*, 2006(10):014, 2006. (Cited on page 1.)

[177] S. L. Shapiro and S. A. Teukolsky. Formation of naked singularities: the violation of cosmic censorship. *Physical Review Letters*, 66(8):994, 1991. (Cited on page 13.)

[178] M. Shibata and T. Nakamura. Evolution of three-dimensional gravitational waves: Harmonic slicing case. *Physical Review D*, 52(10):5428, 1995. (Cited on page 13.)

[179] H. Shinkai. Formulations of the Einstein equations for numerical simulations. *Journal of the Korean Physical Society*, 54:2513–2528, 2009. (Cited on page 15.)

[180] L. Smarr, A. Čadež, B. DeWitt, and K. Eppley. Collision of two black holes: Theoretical framework. *Physical Review D*, 14(10):2443, 1976. (Cited on page 9.)

[181] L. Smarr and J. W. York Jr. Kinematical conditions in the construction of spacetime. *Physical Review D*, 17(10):2529, 1978. (Cited on page 13.)

[182] L. L. Smarr. *Sources of Gravitational Radiation: Proceedings of the Battelle Seattle, Workshop, July 24-August 4, 1978*. CUP Archive, 1979. (Cited on page 13.)

[183] F. Ståhl. Fuchsian analysis of $\mathbb{S}^1 \times \mathbb{S}^2$ and $\mathbb{S}^3$ Gowdy spacetimes. *Classical and Quantum Gravity*, 19(17):4483–4504, 2002. (Cited on pages iii, 5, 26, 83, and 113.)

[184] H. Stephani, D. Kramer, M. A. H. MacCallum, C. Hoenselaers, and E. Herlt. *Exact Solutions of Einstein's Field Equations*. Cambridge University Press, second edition, 2003. (Cited on pages 2, 14, 31, 121, and 123.)

[185] D. G. Swanson. *Plasma Waves*. Elsevier, 2012. (Cited on page 115.)

[186] N. Tacik, F. Foucart, and H. Pfeiffer. Binary neutron stars with arbitrary spins in numerical relativity. In *APS Meeting Abstracts*, volume 1, page 14007, 2013. (Cited on page 112.)

[187] M. Tanimoto. Locally U(1)× U(1) symmetric cosmological models: topology and dynamics. *Classical and Quantum Gravity*, 18(3):479, 2001. (Cited on page 20.)

[188] A. H. Taub. Empty space-times admitting a three parameter group of motions. *Annals of Mathematics*, 53(3):472–490, 1951. (Cited on pages 4, 21, 73, and 75.)

[189] W. P. Thurston and S. Levy. *Three-Dimensional Geometry and Topology*, volume 1. Princeton university press, 1997. (Cited on page 116.)

[190] M. Tiglio. Dynamical control of the constraints growth in free evolutions of Einstein's equations. *arXiv:gr-qc/0304062*, 2003. (Cited on page 15.)

[191] S. Trapani and J. Navaza. Calculation of spherical harmonics and Wigner d-functions by FFT. Applications to fast rotational matching in molecular replacement and implementation into AMoRe. *Acta Crystallographica Section A*, 62(4):262–269, 2006. (Cited on pages 61, 64, and 65.)

[192] A. Vretblad. *Fourier Analysis and Its Applications*. Springer, 2006. (Cited on pages 57, 59, and 60.)

[193] J. Wainwright and G. Ellis. *Dynamical Systems in Cosmology*. Cambridge University Press, 1997. (Cited on pages 19 and 20.)

[194] R. M. Wald. Asymptotic behaviour of homogeneous cosmological models in the presence of a positive cosmological constant. *Journal of Mathematical Physics*, 28(8):2118–2120, 1983. (Cited on pages 5 and 23.)

[195] R. M. Wald. *General relativity*. University of Chicago Press, 1984. (Cited on pages 11, 12, 23, 27, 29, 34, 48, 52, 53, 121, 124, and 125.)

[196] E. Weber. Global qualitative study of bianchi universes in the presence of a cosmological constant. *Journal of Mathematical Physics*, 28(7):1658–1666, 1987. (Cited on page 23.)

[197] A. Weyhausen, S. Bernuzzi, and D. Hilditch. Constraint damping for the Z4c formulation of general relativity. *Physical Review D*, 85(2):024038, 2012. (Cited on page 17.)

[198] E. Woolgar. Some applications of Ricci flow in physics. *Canadian Journal of Physics*, 86(4):645–651, 2008. (Cited on page 117.)